Investigating influenza A virus pleomorphy

by Kieran Dee

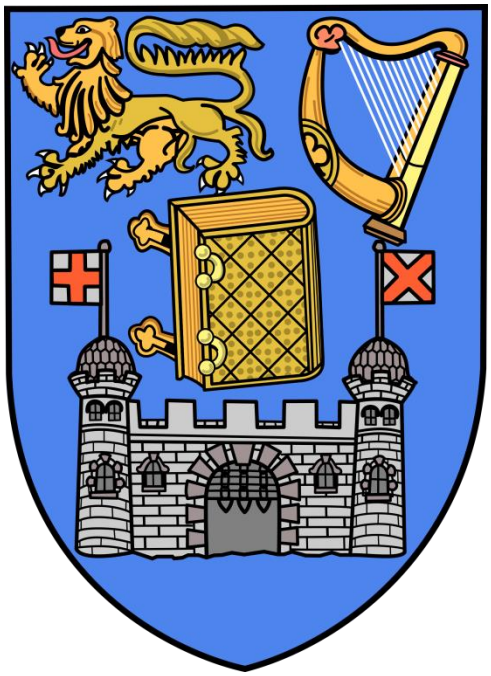

A thesis submitted to Trinity College Dublin for the degree of doctor of philosophy

Supervised by Dr. Kim Roberts

Department of microbiology

Trinity College Dublin

March 2017.

Statutory Declaration

I declare that this thesis has not been submitted as an exercise for a degree at this or any other university and it is entirely my own work, except where it is duly acknowledged in the text.

I agree to deposit this thesis in the University's open access institutional repository or allow the library to do so on my behalf, subject to Irish Copyright Legislation and Trinity College Library conditions of use and acknowledgement.

_____ _____

Summary

Influenza A virus particles display distinct morphologies depending on their source. Most strains that undergo serial passage in laboratory substrates have a uniform, spherical morphology, where the diameter of viral particles is typically 100-150 nm. Strains that have been recently isolated from naturally-infected hosts typically display a pleomorphic, or filamentous morphology. The sizes of these particles are not uniform. The particles exist as a population of differently sized particles that can range in length from 100 nm up to extended filamentous particles that extend ≥ 10 µm in length. These particles maintain a relatively uniform diameter of 55-100 nm. Because of the efficiency displayed by viral pathogens in adapting to the hosts in which they infect, it is widely hypothesised that there must be some biological significance to the production of filamentous particles and that this evolutionary pressure is removed when viruses are propagated in laboratory substrates. The main question that was addressed within this scope of work was to discern what the biological significance of a filamentous morphological phenotype.

Our approach to address this question was to generate morphologically distinct viruses using a reverse genetics system. The concept was to make as few mutations as possible while still generating morphologically distinct viruses. This was achieved by whole gene segment swap reassortant mutations and by single amino acid mutations. The result of these muations was the generation of isogenic viruses that displayed either a spherical-only phenotype or a filamentous-particle-producing phenotype. These viruses were then compared in a range of assays in an attempt to discern the impact of morphology on the behaviour of the virus.

We first investigated the relative growth capacities of either virus in immortalised cell lines, and in agreement with previous observations found a correlation between viruses that produced spherical virions and increased replication kinetics in multi-cycle growth curves in infected immortalised cell lines. This was true of full gene swap and single point mutant viruses. It was also demonstrated that the reduced replication capacity for viruses with a filamentous phenotype was not due to the production of large, extended cell-associated filamentous particles. We speculate that the increased replicative capacity for viruses with a spherical phenotype was due to increased

efficiency of the M1 protein at some stage of the replicative cycle in immortalised cells and that this can be mapped to residue 41 of the M1 protein.

We demonstrated that filamentous virus particles were more resistant to inhibition by polyclonal antisera directed against the viral receptor binding protein. We speculate that this was due to the increased size of filamentous particles. We also demonstrated that filamentous particles were more resistant to inhibition by respiratory mucus derived from primary respiratory epithelial cells. It was demonstrated that the presence of filamentous particles in a given stock of virus is a predictor for resistance to respiratory mucus and that this is dependent on the activity of the neuraminidase enzyme. We investigated if filamentous particles would be better adapted to replicating in primary respiratory epithelial cells by virtue of being less sensitive to the inhibitory effect of respiratory mucus, but found no difference in the replicative capacity of filamentous- or spherical-producing viruses in infected respiratory epithelial cultures. Interestingly, we found that the morphology of cell-associated and released viral particles in these cultures did not match the morphologies of the viruses when they were grown in immortalised cells.

Using a novel piece of equipment, the in vitro transmission system, we investigated the effect on infectivity of spherical and filamentous virus particles when they were carried in aerosolised droplets. We found that viruses with a filamentous phenotype retained greater levels of infectivity when carried in aerosolised droplets, and that this was dependent on the buffer in which the viruses were diluted. It was then demonstrated that viruses with a filamentous phenotype had greater thermal and pH stability compared to spherical particles. Finally, it is demonstrated that virion composition, rather than virion morphology is what determined the thermal and pH stability data recorded for filamentous and spherical viruses.

Acknowledgements

I would first like to thank my supervisor, Dr. Kim Roberts. For her guidance and support while carrying out the work outlined within.

I would like to thank Neal Leddy, Dr. Gavin McManus, and Barry Moran for technical assistance.

I would like to thank our collaborators, Prof. Wendy Barclay and Dr. Ruth Elderfield, for the opportunity to work with their group and for the training and guidance with using the in vitro transmission system.

I would like to thank the Microbiology Society for the award of a travel grant that allowed me to travel to London to work within Prof. Barclay's research group.

I would like to thank Dr. Alastair Fleming and Dr. Joan Geoghegan for their support and in their capacity as members of my thesis committee.

I would also like to thank the administrative and technical support staff in the department of microbiology.

Finally I would like to thank Betty. Without whom I would have never been able to undertake this project.

Contents

List of tables

List of figures

Abbreviation list

^{o}C	Degrees Celcius
BALF	Bronchoalveolar lavage fluid
ESCRT	Endosomal sorting complex required for transport
CEF	Chicken embryo fibroblasts
CPE	Cytopathic effect
CRAC	Cholesterol recognition amino acid consensus
cRNA	Complementary ribonucleic acid
DAPI	4',6-diamidino-2-phenylindole
DEF	Duck embryo fibroblasts
DMEM	Dulbecco modified eagle medium
dNTPs	Deoxyribonucleotide triphosphate
dsDNA	Double stranded deoxyribonucleic acid
dsRNA	Double stranded ribonucleic acid
DTT	1,4-Dithiothreitol
ECE	Embryonated chicken eggs
FSC-A	Forward scatter area
HA	Haemagglutinin
HAE	Human airway epithelium
HIV	Human immunodeficiency virus
hpi	Hours post infection
HNE	Human nasal epithelial
HPAI	Highly pathogenic avian influenza

HTBE	Human tracheobronchial cells
IAV	Influenza A virus
IgA	Immunoglobulin A
IgG	Immunoglobulin G
ID_{50}	50% infectious dose
IRF3	Interferon regulatory factor 3
IVT	In vitro transmission
LIR	LC3 interacting region
LRT	Lower respiratory tract
M	Matrix
MDCK	Madin Darby canine kidney
MES	2-(N-Morpholino)ethanesulfonic acid sodium salt, 4-Morpholineethanesulfonic acid sodium
MOI	Multiplicity of infection
mRNA	Messenger ribonucleic acid
NA	Neuraminidase
NaCl	Sodium chloride
NEP	Nuclear export protein
NHBE	Normal human bronchial epithelial
NIP	Non infectious particle
NLS	Nuclear localisation signal
nm	nanometre
NS	Non-structural
NP	Nucleoprotein

ORF	Open reading frame
PA	Polyacidic protein
PAMPS	Pathogen associated molecular patterns
PolyA	Polyadenylated
PBS	Phosphate buffered saline
pH	Potential hydrogen
pH1N1	Pandemic H1N1
Pfu	Plaque forming units
PB1	Polybasic protein 1
PB2	Polybasic protein 2
PRR	Pathogen recognition receptor
qPCR	Quantitative polymerase chain reaction
RBS	Receptor binding site
RCF	Relative centrifugal force
RdRp	RNA dependent RNA polymerase
RH	Relative humidity
RT	Reverse transcriptase
SF DMEM	Serum free dulbecco modified eagle medium
siRNA	Silencing ribonucleic acid
SP-D	Surfactant protein D
SSC-A	Side scatter area
ssRNA	Single stranded ribonucleic acid
$TCID_{50}$	50% tissue culture infectious dose

TEM	Transmission electron microscopy
TGN	Trans golgi network
URT	Upper respiratory tract
UV	Ultraviolet
Vic75	A/Victoria/3/1975
VLP	Virus like particle
vRNA	Viral ribonucleic acid
vRNP	Viral ribonucleoprotein
WT	Wild type

1. Introduction

Influenza A virus (IAV) is a member of the orthomyxovidae and has a segmented, single stranded negative sense RNA genome. Other influenza genera include influenza B, C and D which also infect humans.

1.1 Global health impact of Influenza A virus

IAV is predominantly maintained in nature through endemic infection of aquatic fowl around the globe. IAV is capable of infecting a wide range of different host species, such as birds, bats, humans, dogs and horses (Forrest and Webster, 2010). IAV is categorised into subtypes based on the sequence and structure of the two major surface glycoproteins that are expressed on the surfaces of virions, haemagglutinin (HA) and neuraminidase (NA). There are currently 18 HA subtypes and 11 NA subtypes that are known. Viruses from the subtypes: H17N10 and H18N11 have only been observed in bats, while the remaining subtypes circulate among wild birds (Webster *et al.*, 1992; Munster *et al.*, 2007; Tong *et al.*, 2012). Fewer subtypes still are known to infect humans. The four pandemics of human IAV for which we have data have been caused by only 3 HA subtypes: H1, H2 and H3, and 2 NA subtypes: N1 and N2 (Chang, 1969; Taubenberger *et al.*, 2012). The HAs of all characterised pandemic strains have ultimately originated from avian strains (Garten *et al.*, 2009).

It has been estimated that millions of people died either directly or indirectly, from secondary infections, in the 1918 IAV H1N1 pandemic (Shanks, 2015). These figures most likely under-represent the total IAV related mortality. They also don't take into account IAV related morbidity or the economic burden sustained as a result of each of these pandemics.

1.1.1 Seasonal epidemics

In addition to sporadic pandemics, IAV causes annual seasonal epidemics in humans during winter months in both hemispheres of the globe. While it is difficult to attribute specific morbidity and mortality with IAV disease without laboratory-confirmed positive results, estimations can be made about the disease burden caused by the virus. For instance, in the years between 1979-2001 the estimated annual number of IAV

hospitalisations was between 55,000 and 431,000 per annual epidemic in the United States (Thompson *et al.*, 2004). Also, one study estimated that the economic impact of seasonal IAV in the United States was $16.3 billion annually (Molinari *et al.*, 2007).

IAV is maintained within the human population due to antigenic malleability and escape of the surface glycoproteins HA and NA of seasonal IAV strains from neutralisation by antibodies, through a process called antigenic drift. This process drives the evolution of IAV, causing the creation of new clades of antigenically distinct virus strains through accumulations of mutations in the epitopes that are presented by the virus (Carrat and Flahault, 2007).

1.1.2 Global pandemics

Since the beginning of the 20th century, there have been 4 IAV pandemics. They occurred in: 1918-1919, 1957-1958, 1968-1969 and 2009-2010. The most noteworthy of these was the 1918-1919 pandemic, where some estimates claim that it resulted in the deaths of tens of millions of people (Shanks, 2015). This is in comparison to the 2009 pandemic which one study estimated the loss of life as being almost 300, 000 associated deaths with the pandemic IAV, with 80% of deaths being in people younger than 65 years old, which is atypical as the elderly are normally the ones to succumb to infection (Dawood *et al.*, 2012). The subsequent pandemics also caused markedly increased levels of mortality worldwide, but the 1918 pandemic remains the greatest cause of IAV mortality ever recorded (Nguyen-Van-Tam and Hampson, 2003; Dawood *et al.*, 2012). Pandemics that affect humans occur when two criteria are met: the generation of virus with novel antigenicity and the capacity for sustained human-to-human transmission. Novel antigenicity can also occur through a process called antigenic shift, in which novel constellations of viral genes are expressed. A novel virus strain can arise when a reassortant event occurs. This is where two or more strains co-infect a cell and are free to exchange genetic material. This is of particular concern when a strain that has been circulating in mammals and thus has the requisite genome to have maximum replicative efficiency in that specific host mixes with an avian strain, which would typically have novel antigenicity. Antigenic shift is the main mechanism through which pandemic strains of IAV arise. This can only occur in instances of “super-infection” where a cell is

infected with more than one different strains of IAV simultaneously. This process allows the emergence of new strains of IAV with novel genetic constellations.

The most likely initial infection event that could initiate a pandemic would be a zoonotic infection. For example, the strain that caused the 2009 pandemic was most closely related to a strain that had been circulating in pigs (Itoh *et al.*, 2009a)and was a chimera of three "parent" strains. Two segments originated from a Eurasian swine genetic lineage, three genetic segments came from a classical swine lineage, and all three of the segments encoding polymerase proteins were from a swine "triple reassortant" lineage (Garten *et al.*, 2009).

It is clear that the emergence of an antigenically novel virus has the capacity to cause severe disease burdens to humans. Novel antigenicity is not the only requirement for the establishment of an IAV pandemic. While this is a necessary first step in the establishment of an IAV pandemic, the virus needs to be replication competent and readily transmissible between humans to have pandemic potential. The pandemic potential of H7N9 viruses that are currently circulating among birds in Asia (Hui, Lee and Chan, 2017) is currently a concern for its pandemic potential because of its novel antigenicity to humans, and capacity to cause severe disease. The reason why H7N9, and other IAV subtypes that circulate in non-human hosts, have not yet established a pandemic is due to replication competency and transmissibility in human hosts. There are sporadic infections of humans with avian-derived H7N9 viruses in China, typically in poultry markets, but no sustained human to human transmission. One study found that over the course of one month, four humans were identified as being positive for H7N9 infection. All of the patients had had contact with poultry 3-8 days prior to symptom onset (Chen *et al.*, 2013). The human samples were sequenced and epidemiologically linked to a market, were one chicken was positive for H7N9 viral infection. This shows that initial zoonotic transmissions occur, but are not sufficient for establishment of a pandemic, or even an epidemic. For this to occur, a number of mutations are necessary to facilitate efficient replication and transmission of avian-origin viruses in mammalian hosts (Herfst *et al.*, 2012; Imai *et al.*, 2012). Therefore the transmissibility of a strain of IAV is a key determinant of its pandemic potential, and judicious surveillance of circulating strains is the key method of preventing the next pandemic.

1.2 IAV genome and virion structure

1.2.1 IAV genome

The genome for IAV consists of eight genetic segments of negative sense, single stranded ribonucleic acid (ssRNA). Each genome segment forms a viral ribonucleoprotein complex (vRNP) that consist of viral RNA (vRNA) complexed with nucleoprotein (NP) and the viral RNA dependant RNA polymerase (RdRp) complex. The RdRp consists of the three polymerase proteins, polybasic protein 2 (PB2), polybasic protein 1 (PB1) and polyacidic protein (PA). The other genetic segments are: HA, NA, matrix (M) and non-structural (NS). Some of the gene segments only encode one viral protein whilst other segments encode several viral proteins. The relative sizes of each of the genetic segments, the proteins that are encoded by them, and a brief outline of the protein function are illustrated in Table 1.1.

Gene Segment	Gene	Nucleotide Length (kb)	Protein	Protein length (amino acid)	Function
1	PB2	2,341	PB2	759	Polymerase complex, cap binding subunit
2	PB1	2,341	PB1	757	Polymerase complex, catalytic subunit
			PB1-F2*	87	Induces apoptosis
			PB1-N40*	718	Maintain balance between PB1 and PB1-F2 expression.
3	PA	2,233	PA	716	Polymerase complex, endonuclease subunit
			PA-N155*	562	?
			PA-N182*	535	?
			PA-X*	252	Host antiviral response control.
4	HA	1,760	HA	552	Envelope protein, binds receptor
5	NP	1,565	NP	497	vRNP complex, binds viral RNA
6	NA	1,466	NA	446	Envelope protein, cleaves HA/receptor interaction
7	M	1,027	M1	252	Virion structural protein
			M2	97	Envelope protein, ion channel
			M42*	99	M2 homolog
8	NS	890	NS1	230	Innate immune modulator
			NEP	121	Export of vRNPs from nucleus

Table 1.1: Summary of the IAV genome, genes, proteins and primary functions of proteins. * denotes accessory proteins that are not essential for viral replication. NEP: nuclear export protein. Reviewed by (Vasin *et al.*, 2014).

1.2.2 Virion structure

A representation of an IAV virion is shown in figure 1.1 (A). At the core of IAV virions are the genomic vRNPs. The vRNPs are surrounded by an M1 lattice that bridges the interior with both the lipid bilayer, derived from host cells, and viral surface glycoproteins HA and NA. The ion channel M2, which bridges the interior and exterior of the virion, is present but in low abundance (Hutchinson *et al.*, 2014). Other viral proteins can be found in virions, but are not essential and are at low levels (Hutchinson *et al.*, 2014). Numerous cellular proteins have been found in mature viral particles (Shaw *et al.*, 2008; Hutchinson *et al.*, 2014). The extent to which packaged cellular proteins affects infectivity is unclear, but one study found that a cellular factor, Annexin V, was specifically packaged into virions and that its presence in infecting virions was able to dampen interferon (IFN) γ- induced signalling in mice (Berri *et al.*, 2014).

Depending on the strain, populations of IAV virions can range in size, from spherical virions that are 120 nm in diameter to particles that can exceed 10 µm in length while maintaining constant width (Roberts, Lamb and Compans, 1998; Bourmakina and García-Sastre, 2003; Harris *et al.*, 2006). Filamentous particles are slightly more narrow than spherical particles and are approximately 80 nm in diameter (Calder *et al.*, 2010; Vijayakrishnan *et al.*, 2013; Dadonaite *et al.*, 2016) which potentially arises from differential curvature of M1-M1 polymerization in the matrix lattice (Calder *et al.*, 2010). There is no difference in the capacity of either filamentous or spherical particles within a population to generate plaque forming units (pfu) (Roberts, Lamb and Compans, 1998). A cryoelectron tomogram of spherical and filamentous particles are shown in figure 1.1 B and are adapted from Calder *et al.*, 2010. Regardless of virion length, infectious virions contain only one set of vRNPs (Noda *et al.*, 2006; Calder *et al.*, 2010; J. S. Rossman *et al.*, 2010). In spherical particles, the vRNPs are condensed in the centre of the virion and on the surface, have NA molecules on one distinct polar end of the particle. For filamentous particles, the vRNPs are always observed at one end of the particle and NA molecules observed at the opposite end (Harris *et al.*, 2006; Calder *et al.*, 2010).

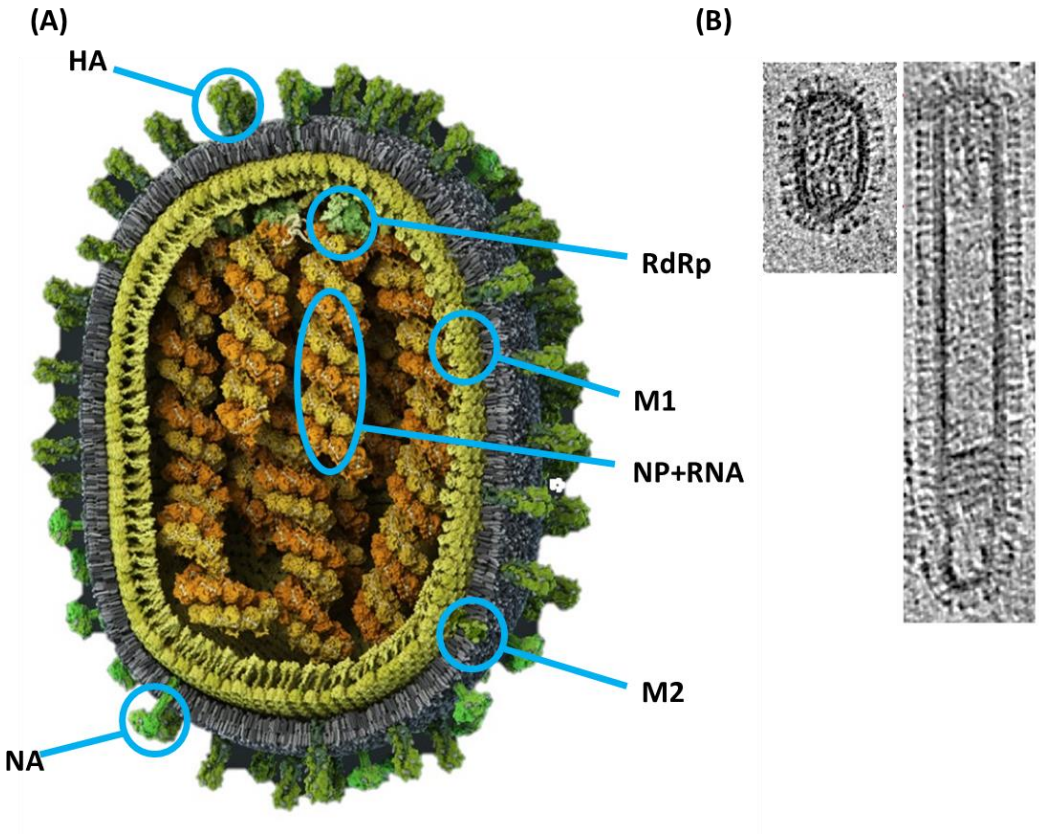

Figure 1.1: Virion structure. (A) Representation of an IAV virion. All of the major structural features of an IAV virion are shown. Dark blue represents the lipid bilayer. NEP and cellular proteins are not shown. Adapted from visual-science.com. (B) Cryoelectron tomogram of a spherical and filamentous particle. Adapted from (Calder *et al.*, 2010).

1.3 IAV replication cycle

One complete replicative cycle for IAV can be defined as the step-wise process of events that begins with the attachment of a viral particle to a permissive host cell and ends with the release of nascent virions capable of continuing the cycle of infection. Figure 1.2 is a diagram that highlights the important stages of an IAV replication cycle, which are discussed in detail in the following subsections.

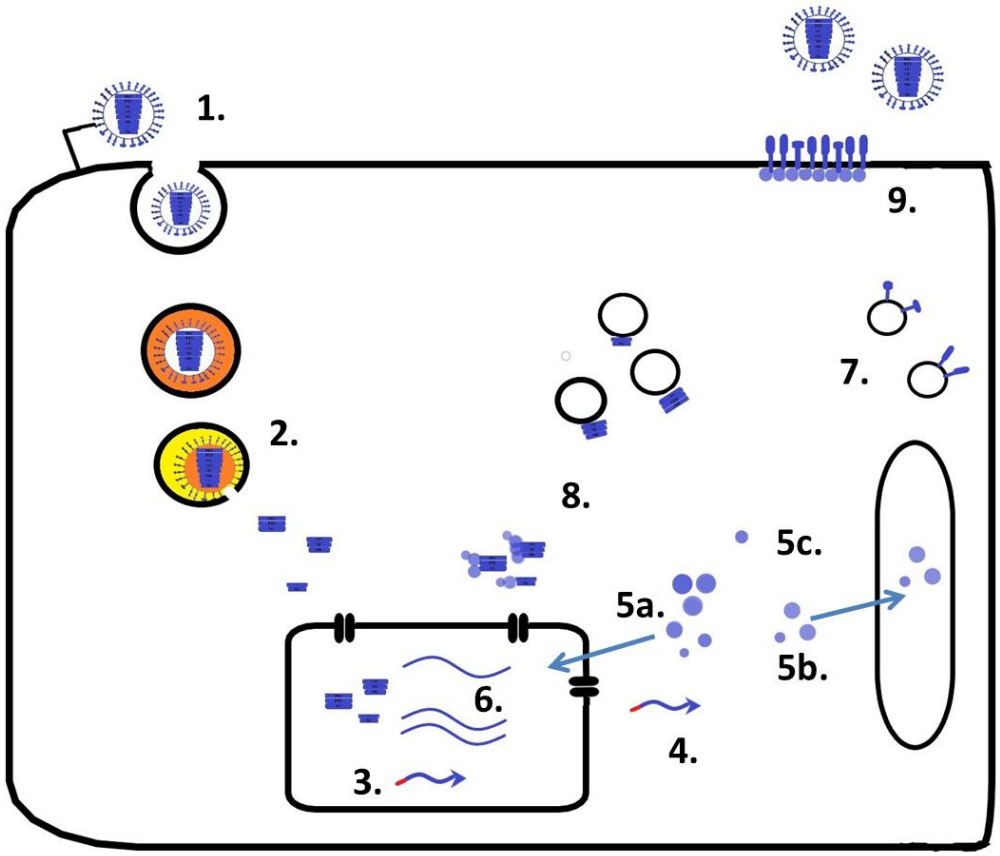

Figure 1.2: Representation of important steps in IAV replication cycle in a permissive host cell. 1. Attachment and entry. 2. Acidification of endosome, genome release and translocation of vRNPs to nucleus. Orange-yellow colouring indicates decreasing pH. 3. mRNA transcription. 4. Protein translation. 5a. Translocation of PB2, PB1, PA, NP, M1 and NEP to nucleus. 5b. Sorting of HA, NA and M2 through endoplasmic reticulum and TGN. 5c. NS1 in the cytoplasm. 6. vRNA and cRNA replication. 7. Transport of HA and NA to the plasma membrane. 8. Transport of vRNPs to the plasma membrane. 9. Assembly and budding. Adapted from (Salomon and Webster, 2009)

1.3.1 Binding and entry (Figure 1.2 (1))

IAV binds via its receptor binding protein, HA, to terminally linked sialic acid ligands that are present on glycoproteins and glycolipids on the surface of host cells. The conformation of how the sialic acid is linked to the penultimate galactose on the glycan molecule is an important factor that determines host-specificity of the virus (Shinya *et al.*, 2006; Nicholls *et al.*, 2007). The epithelial cells of avian intestines are typically rich in sialic acids whose linkage to the penultimate galactose is between the 2^{nd} and 3^{rd} carbons of the sugar bases and is deemed an α2-3 sialic acid (Ito and Kawaoka, 2000). Avian-adapted IAV preferentially binds to these ligands. The epithelial cells of the upper respiratory tracts (URT) of humans are predominantly covered in α2-6 linked sialic acids (Matrosovich *et al.*, 2004) and are preferentially infected by viruses that have evolved to bind that type of sialic acid (Matrosovich *et al.*, 2000). Once a virus has bound to the surface receptor, it can then be engulfed into the cell by either clathrin-/caveolin-dependent or clathrin-independent mediated endocytosis (Mercer and Helenius, 2009; Rossman, Leser and Lamb, 2012).Larger, filamentous particles are thought to use macropinocytosis to enter cells (Sieczkarski and Whittaker, 2005; Rossman, Leser and Lamb, 2012).

1.3.2 Fusion, uncoating, and translocation to the nucleus (Figure 1.2 (2))

Regardless of whichever mechanism used to engulf the virus particle, the pH of the vacuole carrying the virus needs to be lowered to initiate fusion of the viral and cellular membranes (Stegmann, White and Helenius, 1990; Rossman, Leser and Lamb, 2012). As endosomes mature as they travel from the cell surface to the cell interior, they are acidifed by a vacuolar H^+ ATPase which lowers the pH of the lumen of the endosome (Fuchs, Schmid and Mellman, 1989). Depending on the strain of IAV, the pH at which the fusion conformation of HA is triggered can vary (Galloway *et al.*, 2013). At neutral pH, the fusion peptide is buried in the core of the HA trimer. Once triggered by lowered pH, the HA undergoes an irreversible conformational change that causes the extrusion of hydrophobic fusion peptide into the host membrane (Galloway *et al.*, 2013). This conformational change brings the viral membrane and vesicle membrane close together, facilitating fusion of the two membranes.

As well as mediating fusion of viral and cellular membranes, the pH of the interior of the virus particle is concomitantly lowered alongside the pH of the late endosome. This is mediated by the transmembrane tetramer, M2, which is present in low abundance in viral particles (Wang, Lamb and Pinto, 1995; Hutchinson *et al.*, 2014) and functions as a proton pump which acidifies the interior of the virion. At neutral pH and low salt concentrations, M1 binds tightly to vRNPs (Zhirnov, 1992; Ye *et al.*, 1999; Liu, Muller and Ye, 2002). Acidification of the virion causes disassociation of the M1 protein and the vRNP complex (Bui, Whittaker and Helenius, 1996). This is a crucial step, because if the M1-vRNP complex is intact, the vRNPs are unable to translocate to the nucleus (Martin and Helenius, 1991). Once the viral and cellular membranes have fused, the freed vRNPs are released into the cytoplasm of the host cell, where they are translocated individually to the nucleus by means of a nuclear localisation sequence (NLS) present on the NP protein (Cros, García-Sastre and Palese, 2005; Chou *et al.*, 2013). This is most likely mediated by cellular importin-α proteins (Gabriel, Herwig and Klenk, 2008; Gabriel *et al.*, 2011).

1.3.3 Transcription (Figure 1.2 (3))

Once the vRNP complexes enter the nucleus, messenger RNA (mRNA) is generated from each genome segment through the action of the viral RdRp complex. The IAV RdRp utilises a process called “cap-snatching”, whereby 10-15 nucleotides, including the 7-methylguanylate cap, are cleaved by the viral endonuclease PA, from the 5’ end of host cell pre-mRNAs (Dias *et al.*, 2009; Reich *et al.*, 2014). This short host-derived nucleotide sequence acts as a primer for mRNA transcription. At the 3’ end of the mRNA a polyadenylated (polyA) tail is generated by stuttering of the viral RdRp at a site on the vRNA with a string of 5-7 uracil residues near the 5’ end (Pritlove *et al.*, 1998). Both of these processes, cap-snatching and polyA stuttering, are necessary and translation of viral proteins would not be possible without either the 5’ cap or the 3’ polyA tail.

Two of the eight genome segments, 7 and 8, contain two ORFs that are transcribed by subverting host pre-mRNA splicing machinery. This is achieved by the genetic segments bearing similarities to canonical eukaryotic splicing related signals in the viral mRNA (Lamb, Lai and Choppin, 1981; Dubois *et al.*, 2014). The two mRNAs generated this way are M2 and NEP and both are necessary for infectivity. The ten viral mRNAs that are

produced during infection appear to differentially rely on cellular export pathways from the nucleus to the cytoplasm. Silencing ribonucleic acid (siRNA) depletion of different cellular factors involved in host mRNA export were found to differentially knock-down protein expression of each of the ten mRNA species expressed by the virus (Read and Digard, 2010). The cellular proteins NXF1 and UAP56 were found to have the greatest effect in diminishing viral protein production. HA, and spliced and unspliced segment 7 transcripts were found to be the most reliant on expression of NXF1 compared to the other viral mRNAs.

1.3.4 Translation of viral proteins (Figure 1.2 (3))

Because viral mRNAs possess both a 5'-cap, that is derived from host mRNAs, and a polyA tail, viral transcripts subvert normal host protein synthesis. Several novel viral proteins have been discovered whose expression occurs at this stage in the replication cycle. PB1-F2 was originally identified as being a second polypeptide product of the PB1 mRNA and was found to control apoptosis induction (Chen *et al.*, 2001). This polypeptide is expressed in the +1 reading frame of the PB1 mRNA and occurs via leaky ribosome scanning. Subsequent polypeptides from the PB1 mRNA were found to be expressed that were in-frame with PB1, but translation is initiated at a start codon further downstream of the initial start codon, generating amino-terminal truncated forms of PB1 (Zamarin, Ortigoza and Palese, 2006; Wise *et al.*, 2009). Alternative polypeptides are also produced from the PA mRNA. PA-X was identified as being generated as the result of ribosomal frame-shifting, and this protein was found to modulate virulence of the virus in mice (Jagger *et al.*, 2012). Further novel polypeptides that are generated from the PA mRNA, have been identified (Muramoto *et al.*, 2013). It should be noted that not all strains of IAV will express these accessory proteins, and that they are not essential for replication of the virus.

1.3.5 Proteins that are translocated back to the nucleus (Figure 1.2 (5a.))

All of the polymerase proteins: PB2, PB1, PA and NP are translocated back to the nucleus once translated. This is achieved by each protein bearing its own NLS, via different host factors for each protein (Hutchinson and Fodor, 2013). The polymerase proteins are required to continue and amplify the generation of mRNA. M1, NS1 and NEP are also translocated to the nucleus following translation. M1 retention in the nucleus is

dependent on phosphorylation, where if the protein is hyperphosphorylated, it is retained in the nucleus (Bui, Whittaker and Helenius, 1996). Similarly, M1 export is temperature dependent, and it has been shown that at 41^{o}C M1 remains localised in the nucleus and is unable to form a complex with vRNPs (Sakaguchi *et al.*, 2003). All of these proteins are needed in the nucleus as they can begin the cycle of: mRNA generation, further translation of viral proteins, cRNA and then genomic vRNA production.

1.3.6 HA, NA and M2 proteins (Figure 1.2 (5b))

Following translation, the transmembrane proteins HA, NA and M2 are trafficked through the endoplasmic reticulum and to the golgi apparatus. HA molecules that are derived from H5 or H7 subtypes require M2 while being trafficked through the late golgi (Takeuchi and Lamb, 1994; Harvey *et al.*, 2004). The reason for this is that for these subtypes, the HA_0 precursor is cleaved in the trans-golgi network by furin proteases (Stieneke-Gröber *et al.*, 1992). For other HA subtypes, cleavage occurs after the HAs are expressed at the cell surface, but in some cases can be cleaved within the cell as well (Bottcher-Friebertshauser *et al.*, 2010). Premature cleavage of the HA_0 precursor molecule for H5 and H7 subtypes while still inside the golgi presents an issue for the virus. It opens the possibility for the switching of a receptor binding conformation to a fusion conformation due to the decreased pH in the lumen of the late golgi. If this happens then the HA molecule will be unable to bind to cells and any virion bearing HAs with this conformation will be non-infectious. Thus, to overcome this, the M2 ion channel is able to increase the pH of the late golgi by pumping H^+ ions out of the lumen and stabilises the cleaved, receptor binding conformed HA trimer.

1.3.7 NS1 (Figure 1.2 (5c))

NS1 has numerous functions in the replication cycle of IAV, in both the cytoplasm and nucleus of infected cells. In the nucleus it has been shown to regulate the synthesis of viral RNA (Falcon *et al.*, 2004; Wang *et al.*, 2010; Zheng *et al.*, 2015). Arguably though, the most important function of the NS1 protein is in the antagonism of the IFN response to infection. One of the mechanisms by which this is achieved is that NS1 acts as an agonist for the cellular pathogen recognition receptor (PRR) RIG-I (Mibayashi *et al.*, 2007; Rehwinkel *et al.*, 2010). RIG-I recognizes both blunt ended double stranded RNA (dsRNA) as well as dsRNA with a 5’ triphosphate, both of which are typical of viral

infections (Lu *et al.*, 2010). Without the antagonistic action of NS1, RIG-I would sense these viral pathogen associated molecular patterns (PAMPS) and would trigger an IFN-mediated response to infection, inducing an antiviral state in the infected and neighbouring cells.

1.3.8 cRNA, vRNA and vRNP production (Figure 1.2 (6))

Once the translated proteins are translocated back to the nucleus, the vRNPs present from the initial infecting virus particle can be used as templates to generate further mRNA and then switch to generating cRNA and vRNA. Initially, mRNA is produced to provide adequate amounts of viral protein. At a later stage in infection, a switch from transcription-focused generation to a replication-focused production of cRNA and vRNA, where cRNA is produced to be used as a template to generate genomic vRNA (Shapiro and Krug, 1988). M1 has been found to inhibit transcription *in vitro* and mutant M1 proteins that lack the ability to bind to vRNP complexes are incapable of inhibiting transcription (Ye *et al.*, 1987; Baudin *et al.*, 2001). This observation lead to the hypothesis that M1 could potentially mediate the switch from using genomic vRNA as a template for mRNA synthesis and initiate the export of vRNPs from the nucleus to the sites of assembly and budding. However, a more likely mechanism that mediates the switch from transcription to replication has been described, where the RdRp either acting in *cis* or *trans* will direct transcription or replication respectively. cRNA and mRNA have the same sequence in 5'-3' direction but importantly, cRNA lacks a 5' cap or polyA tail. Thus, the synthesis of cRNA must be distinct to that of the synthesis of viral mRNA. One prevailing theory for a mechanism that facilitates this is that mRNA synthesis is performed in *cis*, where mRNA is produced by the polymerase complex that is part of the vRNP. Replication occurs in *trans*, where the polymerase complexes that are not associated with vRNPs generate cRNA (Jorba, Coloma and Ortín, 2009; Moeller *et al.*, 2012). Replication of the genome occurs in a primer-independent manner using cRNA as a template (Vreede, Gifford and Brownlee, 2008; Reich *et al.*, 2014).

1.3.9 Transport of HA and NA to the cell surface (Figure 1.2 (7))

Trafficking of the HA and NA proteins to the apical cell surface is dependent on specific residues in the transmembrane domain of either protein (Kundu *et al.*, 1996; Lin *et al.*, 1998) and cellular factors. Depletion of factors involved with the host vesicular transport

complex, COP1 was shown to inhibit surface expression of HA at the cell surface (Brass *et al.*, 2009). This complex is normally involved in both intra-golgi and golgi-endoplasmic reticulum transport (Cai, Reinisch and Ferro-Novick, 2007), so it is a likely candidate for the transport of HA molecules to the cell surface. Similarly, the sphingomyelin biosynthetic pathway was found to important for the amount of HA and NA expressed on the surface of infected cells (Tafesse *et al.*, 2013).

1.3.10 Export of vRNPs from the nucleus and transportation to the cell surface (Figure 1.2 (8))

Export of vRNPs from the nucleus is dependent on M1 and NEP, where a complex of M1-NEP-vRNP is formed and exported from the nucleus via nuclear pore complexes (Iwatsuki-horimoto *et al.*, 2004; Boulo *et al.*, 2007; Mänz *et al.*, 2012). This is dependent on host factors such as: hsc70 and CRM1 (Neumann *et al.*, 2000; Watanabe *et al.*, 2014). The vRNPs are translocated individually (Chou *et al.*, 2013). Once the vRNPs have exited the nucleus, the M1-NEP-vRNP complex disassociates and the vRNPs associate with Rab11 proteins, most likely in a Rab11-PB2 interaction, at the pericentriolar recycling endosomal compartment and it is here that they are concentrated and the individual segments colocalise with one another (Bruce, Digard and Stuart, 2010; Chou *et al.*, 2013). From here, the vRNPs are transported to the cell periphery by association of Rab11 with vesicles that are transported along microtubules (Momose *et al.*, 2007; Amorim *et al.*, 2011; Eisfeld *et al.*, 2011). It is interesting to note that M1 is not seen to colocalise with the vRNPs shortly after exiting the nucleus, which implies that M1 utilises a different mechanism to reach the cell surface (Amorim *et al.*, 2011).

1.3.11 Assembly and budding (Figure 1.2 (9))

Formation of virions occurs at the plasma membrane. Consensus among the field states that the lipid rafts are the preferred sites of assembly and budding of nascent viral particles (Barman *et al.*, 2001; Nayak, Hui and Barman, 2004; Leser and Lamb, 2005). However, a recent study has questioned this where the authors found no association of viral proteins and hallmark molecules typically found in lipid rafts such as sphingolipids and cholesterol (Wilson *et al.*, 2015). Similarly, a study found that by disrupting lipid rafts by depleting cholesterol, the amount of virus particles released from infected cells

was increased (Barman and Nayak, 2007), but their stability was reduced, suggesting that lipid rafts are not essential for budding, but may be important for virion stability.

M1 is capable of association with the cellular membrane by its self, but this association is significantly strengthened by interaction with the cytoplasmic tails of the M2, HA and NA proteins that are embedded in the cytoplasm (Jin *et al.*, 1997; Baudin *et al.*, 2001; Nayak, Hui and Barman, 2004; Chen *et al.*, 2008; Hilsch *et al.*, 2014). The current step-wise model of assembly is as follows: HA, NA and M2 localise to the cell surface first, where HA and NA group in lipid rafts while M2 is excluded to the edge of the rafts (Leser and Lamb, 2005; Chen *et al.*, 2007; Rossman *et al.*, 2010a); M1 localises to the membrane where it interacts with the cytoplasmic tails of the glycoproteins already present. Viruses lacking either HA or NA cytoplasmic tails are defective in budding and produce particles with significant reductions in M1 and NP proteins (Jin *et al.*, 1997; Zhang *et al.*, 2000). Finally, vRNPs in a 7+1 orientation, 7 segments surrounding a central segment (Noda *et al.*, 2006), are delivered to the areas of the membrane that are enriched in viral protein (Muramoto *et al.*, 2006; Chou *et al.*, 2013).

It is hypothesised that the interaction of the vRNPs with the M1 matrix layer is the initiation step that begins the budding process (Rossman and Lamb, 2011). One vital step in this process is the association of M1 and the cytoplasmic tail of M2. When the cytoplasmic tail of M2 was mutated, a significant reduction in the association between M1-M2 was seen by co-immunoprecipitation and in the membrane of infected cells. The M2 mutant had severely reduced replication capacity in Madin Darby canine kidney (MDCK) cells (Chen *et al.*, 2008).

The mechanistic process by which budding is achieved is unclear. Expression of HA and NA is sufficient to induce curvature in the membrane and cause the budding and release of virus like particles (VLPs) (Chen *et al.*, 2007). Another study refined this observation where they found that expression of HA and NA either together or separately, was sufficient for VLP release through non-specific membrane curvature. The authors also found that expression of M1 and M2 with HA and NA resulted in organised clustering of the glycoproteins into particles that more closely resembled virus particles. These particles were released by constriction of the base of the budding particle (Chlanda *et al.*, 2015), which is the current model for virion release (Rossman *et al.*, 2010). It has

been shown that IAV utilises a budding pathway that is independent of the host endosomal sorting complex required for transport (ESCRT) (Rossman *et al.*, 2010b). Other viruses, such as human immunodeficiency virus (HIV) and ebola virus subvert this host pathway to achieve membrane scission and release of progeny virions (Chen and Lamb, 2008). IAV achieves scission of the membrane and release of nascent viral particles through the action of the M2 protein, where the M2 protein causes membrane curvature and localises to the neck of budding virus particles where it effects the final scission step of the viral and cellular membranes (Rossman *et al.*, 2010).

1.3.12 Production of non-infectious particles (NIPs)

Errors can arise in the replication cycle that result in the production of NIPs. NIPs are particles that resemble mature virions, but are incapable of completing a round of replication alone. An infectious particle can be defined as: a virus particle that is capable of completing a full round of replication in the absence of a co-infecting virus. There are different categories of NIPs. One such example would be a semi-infectious particle, which is a virus particle that has fewer than the full eight genetic segments that constitute the IAV genome. Semi-infectious particles are incapable of completing the viral life cycle in the absence of complementation, which is when there is co-infection with another virus particle that has delivered the lacking segment or segments. Another example of NIPs are defective interfering particles. These are virus particles that deliver one or more defective RNA segments into an infected cell. Similar to semi-infectious particles, defective interfering are incapable of completing the viral life cycle in the absence of complementation. An example of a type of defective interfering particle would be particles that lack an NS segment. If these particles infect a cell, a robust anti-viral IFN response will be induced that can make neighbouring cells refractory to infection. Another example of an NIP is an empty virion. vRNPs are not required for budding events to occur (Gómez-Puertas *et al.*, 2000). VLPs that contain surface glycoproteins and resemble true virions but lack vRNPs are capable of budding from cells (Chen *et al.*, 2007; Chlanda *et al.*, 2015).

The production of NIPs can be simultaneously detrimental and beneficial for the continued spread of the virus in the host. They can be detrimental if the particles begin a doomed replication cycle in cells and are unable to supress the host IFN response

(Frensing *et al.*, 2014). NIPs can be beneficial for the virus by acting as decoys, where innate and adaptive immune responses targeted against extracellular virions would be competitively bound by NIPs, allowing infectious particles to continue the spread of infection. Depending on the strain of virus, and multiple other factors, the ratio of NIPs can be 10:1 (Donald and Isaacs, 1954; Marcus, Ngunjiri and Sekellick, 2009; Brooke *et al.*, 2013)

1.4 Morphology of IAV particles

Viral particles from low passage clinical strains of IAV typically have a filamentous morphology (Choppin, 1960; Shortridge *et al.*, 1998; Itoh *et al.*, 2009b; Elton *et al.*, 2013; Seladi-Schulman *et al.*, 2013). The filamentous morphological phenotype is typically lost when viruses are passaged multiple times in immortalised cells or embryonated chicken eggs (ECEs) (Choppin, 1960; Seladi-Schulman *et al.*, 2013). A switch from a spherical to a filamentous morphological phenotype has been observed when a laboratory-adapted strain was passaged *in vivo* in guinea pigs (Seladi-Schulman, Steel and Lowen, 2013). The morphological phenotype switch, in either direction, is not observed for all strains (Seladi-Schulman *et al*, 2013). Even certain strains which have undergone extensive passage in laboratory substrates have retained a highly filamentous phenotype (Bourmakina and García-Sastre, 2003; Elleman and Barclay, 2004). For certain strains, the cell-associated filamentous particles typically occur as bundles of several particles held closely together, most likely through HA-HA interactions (Bourmakina and García-Sastre, 2003; Elton *et al.*, 2013; Campbell *et al.*, 2014a). Filamentous virus particles have been recorded for Influenza C virus strains and other orthomyxoviruses such as infectious salmon anaemia virus (Koren and Nylund, 1997; Nakatsu *et al.*, 2018).

Filamentous and spherical virions differ in some characteristics. Filamentous particles have increased NA activity, presumably due to their increased size leading to greater levels of protein incorporation, but this remains untested (Campbell *et al.*, 2014b; Seladi-Schulman *et al.*, 2014). Filamentous particles are more efficient at agglutinating red blood cells and that the haemagglutination efficiency is increased when the particles are broken-up (Donald and Isaacs, 1954). However, the difference in the relative haemagglutination capacities of spherical or filamentous particles was not seen in a later study (Roberts *et al.*, 1998). Filamentous particles have higher ratios of M1 and HA

proteins relative to NP (Roberts, Lamb and Compans, 1998). Spherical populations of viruses have been shown to be more sensitive to inactivation by ultraviolet (UV) radiation (Smirnov *et al.*, 1991). The authors of this study postulate that this could be a result of filamentous virus particles harbouring more than one complement of genetic segments, however no difference was noted for the relative amounts of RNA for spherical and filamentous fractions from a sucrose gradient. Later studies have demonstrated that both filamentous and spherical particles contain a single genome when visualised by cyro-electon tomography (Calder *et al.*, 2010; Noda *et al.*, 2012).

Low pH causes the fragmentation of filamentous particles (Calder *et al.*, 2010; Fontana *et al.*, 2012; Rossman, Leser and Lamb, 2012) and this is dependent on the activity of the M2 ion channel (Rossman *et al.*, 2010a). Spherical particles have also been shown to be distorted when incubated at low pHs (Shangguan *et al.*, 1998; Calder *et al.*, 2010; Zhirnov *et al.*, 2016) where for both particle types, the M1 lattice is shown to dissociate from the viral membrane which presumably leads to the particle's distortion as the structural lattice has been lost.

1.4.1 Viral determinants of morphology

There are numerous viral factors that influence morphology, with the majority being mapped to segment 7 of the genome, reviewed in (Dadonaite *et al.*, 2016). The cytoplasmic tails of the M2, HA, NA proteins as well as NP have all been shown to affect virus morphology (Mitnaul *et al.*, 1996; Jin *et al.*, 1997; Iwatsuki-Horimoto *et al.*, 2006; Rossman *et al.*, 2010b; Bialas *et al.*, 2014). In a VLP system, HA and NA expression alone was sufficient to allow the budding and release of spherical VLPs. When M1 and M2 were expressed alongside HA and NA, structured filamentous protrusions similar to budding virions were observed. When M1 and M2 were expressed in the absence of HA and NA, no protrusions were noted and M1 was not visualised at the cell membrane (Chlanda *et al.*, 2015). Binding avidity between vRNPs and M1 has also been shown to correlate with virion morphology, where spherical viruses express M1 and vRNPs that disassociate less readily in high salt concentrations or low pHs (Liu, *et al.*, 2002).

It is a common observation that segment 7 of a given strain is the main arbiter of virion morphology (Roberts, Lamb and Compans, 1998; Bourmakina and García-Sastre, 2003;

Elleman and Barclay, 2004; Campbell *et al.*, 2014a). Similarly, a spherical phenotype has been found to correlate with increased replicative capacity in immortalised cells or embryonated chicken eggs (ECEs) (Yasuda, Bucher and Ishihama, 1994; Bialas, Desmet and Takimoto, 2012; Seladi-Schulman *et al*, 2013; Pu *et al.*, 2017). The inverse has been observed, where a correlation between a filamentous morphology and increased replicative capacity in guinea pigs was recorded (Seladi-Schulman *et al.*, 2013).

There are two proteins that are essential for viral fitness that are expressed from segment 7 of the IAV genome, M1 and M2. M1 is generated from a full length mRNA generated from the vRNA. M2 is generated from a spliced version of the full length mRNA. The ratio of mRNA in infected cells for a given strain of these two is 60:40 for M1 and M2 respectively (Wise *et al.*, 2012). The amount of M1 protein present in a mature virion can outnumber M2 by several hundred fold (Hutchinson *et al.*, 2014). The cytoplasmic tail and transmembrane domain of the M2 protein have been implicated in affecting viral morphology (Roberts, Lamb and Compans, 1998; Iwatsuki-Horimoto *et al.*, 2006; Rossman *et al.*, 2010b; Roberts *et al.*, 2013). The cytoplasmic tail of M2 is also necessary for correct virion formation and certain mutations to it result in highly attenuated viruses. Interestingly, the impact of these mutations is dependent on interactions of the M2 cytoplasmic tail with M1 and this impact differs for M1 proteins from spherical- and filamentous-producing virus strains (McCown and Pekosz, 2006; Grantham *et al.*, 2010). This is further evidence to show that the factors governing morphogenesis are multi-faceted, and dependent on viral protein-protein interactions. A LC3-interacting region (LIR) motif on the carboxy terminus of the IAV M2 protein has been shown to affect the extent of filamentous virus budding (Beale *et al.*, 2014). While it does not abrogate the formation of filamentous virus particles, mutating the LIR motif of the M2 protein reduces the size and prevalence of filamentous bundles that are normally produced from wild type- (WT) infected cells.

Several amino acids in the M1 protein have been shown to affect virion morphology (Table 1.2). Interestingly, certain amino acid substitutions have been shown to affect morphology when expressed in a certain genetic constellation, while the same mutations show no affect in other ones. Initial studies that investigated the amino acids responsible for virion morphology compared the sequences of filamentous-producing

and spherical-producing strains. Differences in the sequences were identified and using reverse genetics, mutant viruses were made. One study investigated the expression of amino acids that matched the spherical strain at positions 95 and 204 in M1. These were found to abrogate filamentous virion production when introduced into the segment 7 of a filamentous-producing virus and expressed with the other 7 segments of a spherical-producing virus (Bourmakina and García-Sastre, 2003). Conversely, another study found that expression of a valine at residue 41, a residue commonly seen in spherical strains, of M1 was sufficient to confer a spherical phenotype to a filamentous-producing strain, A/Victoria/3/1975 (Vic75), while the residue 95 mutation did not cause any phenotypic change (Elleman and Barclay, 2004), seemingly disagreeing with the observation made by Bourmakina and García-Sastre, 2003.

M1 amino acid residue mutation	Phenotype	Genetic constellation	Reference
S30D	Spherical to filamentous	Cal04	(Bialas, Desmet and Takimoto, 2012)
A41V	Filamentous to spherical	Vic75/Udorn	(Roberts, Lamb and Compans, 1998; Elleman and Barclay, 2004)
A41P	Increases filament length and frequency	NL602	(Campbell *et al.*, 2014b)
S85N (+N231D)	Filamentous to spherical	PR8:Nkt 11	(Elton *et al.*, 2013)
N85S (+D231N)	Spherical to filamentous	PR8:Miami	(Elton *et al.*, 2013)
N87S	Spherical to filamentous	PR8	(Seladi-Schulman *et al.*, 2013)
N92S	Spherical to filamentous	PR8	(Seladi-Schulman *et al.*, 2013)
R95K	Filamentous to spherical	WSN:M1Ud	(Bourmakina and García-Sastre, 2003)
R101G	Spherical to filamentous	PR8	(Seladi-Schulman *et al.*, 2013)
K102A	Spherical to filamentous	WSN	(Burleigh *et al.*, 2005)
T169I	Filamentous to spherical	NL602	(Seladi-Schulman *et al.*, 2013)
S183A	Spherical to filamentous	WSN	(Zhang *et al.*, 2015)
T185A	Spherical to filamentous	WSN	(Zhang *et al.*, 2015)
Q198K	Filamentous to spherical	NL602	(Seladi-Schulman *et al.*, 2013)
E204D	Filamentous to spherical	WSN:M1Ud	(Bourmakina and García-Sastre, 2003)
T218A (+V41A+K95R)	Spherical to filamentous	WSN	(Elleman and Barclay, 2004)

Table 1.2: A list of M1 amino acid residues involved in morphogenesis. Abbreviations: Cal04, A/California/04/2009; Nkt11, A/Equine/Newmarket/11/2003; NL602, A/Netherlands/602/2009; Miami, A/Equine/Miami/1963; Udorn, A/Udorn/1972; WSN, A/WSN/1933.

The mechanism by which morphology is governed by protein interactions is unclear. The factors governing the morphology of virus particles are multi-faceted. The amino acids that influence morphology are located all over the M1 protein (Table 1.2) and their bearing on morphogenesis is unknown. Similarly, the observation that the same mutations don't cause a morphological phenotype switch depending on the context in which they are expressed (Bourmakina and García-Sastre, 2003; Elleman and Barclay, 2004) suggests subtle interactions between M1-M1, other viral proteins and cellular factors all of which contribute to morphology in varying capacities. The crystal structure of full length M1 has yet to be solved. So far, only the amino-terminus of M1 has been solved (Sha and Luo, 1997; Arzt *et al.*, 2001). The crystal structure of the matrix protein of a related virus, ISAV, has been solved (Zhang *et al.*, 2017). Differential oligomerisation of M1 has been implicated in the morphology of IAV (Zhang *et al.*, 2015).

Treatment of filamentous particles with an antibody directed against the ectodomain of the M2 protein has been found to disrupt the morphology of the particles (Roberts, Lamb and Compans, 1998; Rossman *et al.*, 2010b). When a filamentous-producing strain was grown in the presence of this antibody it resulted in the evolution of a spherical-producing virus (Roberts, Lamb and Compans, 1998). This phenotype switch was mapped to a single amino acid substitution on the M1 open reading frame (ORF), A41V. The expression of a valine at this position was sufficient to completely abrogate the formation of both cell-associated and released filamentous particles (Roberts, Lamb and Compans, 1998). It is interesting to consider the impact of this mutation when taken in context with a finding from a later study that identified that the locus from which residue 41 of M1 is expressed doubles as a splice donor site (Wise *et al.*, 2012). The authors found that by altering the splice donor site so that the sequence was more homologous to a canonical eukaryotic splice donor site, a homolog of the M2 protein could be expressed. This homolog, M42, differs to M2 by only the ectodomain and was found to be a functional homolog of the ion channel protein. Thus, it is likely that this mutation conferred resistance to the antibody directed against the ectodomain of M2 as the ectodomain of M42 has a different amino acid sequence. It is even more interesting to consider the effect that this may have on morphology. M2 induces the scission event that releases budding virus particles from the cell surface (Rossman *et al.*, 2010b), so it is

possible that M42 may affect this phenotype and possibly the morphology of budding particles.

1.4.2 Cellular determinants of morphology

Cell type and level of polarisation can affect the formation of filamentous virus particles (Roberts and Compans, 1998). Al-Mubarak *et al.*, 2015 found that infection of either chicken embryo fibroblasts (CEF) or duck embryo fibroblasts (DEF) yielded differences in morphological phenotypes. They found that when infected with the same strains of IAV from the H2N3 subtype, CEF cells produced predominantly spherical viral particles and DEF cells produced filamentous particles. Infected CEF cells produced approximately 5-7 fold more virus at 24 and 48 hours post infection. There were similar levels of segment 7 copy numbers and M1 protein levels at 8 and 24 hours post infection in either cell type, which suggests the mechanism that causes the difference in released titres is downstream of transcription and translation of viral proteins. The cause of the difference in titres generated by either cell type is unclear.

An intact actin network is necessary for the generation of filamentous viral particles but not for spherical ones. By inhibiting the formation of filamentous actin by treating cells with cytochalasin D, the production of filamentous virus particles was inhibited (Roberts and Compans, 1998; Simpson-Holley *et al.*, 2002). Despite completely abrogating the production of filamentous particles in infected cells, disruption of the actin network did not greatly affect the titre of released virus particles in a range of different cell types. Filament production was not affected by disrupting the microtubule network by treating infected cells with nocodazole (Roberts and Compans, 1998). Another study found that disruption of the microtubule network resulted in a five-fold loss of infectious titre, but no loss in the amount of released protein (Amorim *et al.*, 2011).

A GTPase that is involved in protein and vesicle trafficking has been identified as crucial in both the budding of IAV and the formation of filamentous particles (Bruce *et al*., 2010). This protein, Rab11, has a range of functions in cells. It is involved in trafficking between the trans-golgi network (TGN), recycling endosomes and the plasma membrane, as well as being involved in remodelling of the actin cytoskeleton (Urbé *et al*., 1993; Ullrich and Molecular, 1996; Chen, W.; Feng, Y.; Chen and Wandinger-Ness,

1998; Riggs *et al.*, 2003). By silencing expression of Rab11a, the formation of filamentous particles was completely abrogated and depending on cell type that was infected, up to a ten-fold reduction in titres was seen (Bruce, Digard and Stuart, 2010). In addition, by silencing a protein that normally modulates the function of Rab11, FIP3, the length of filamentous particles was greatly reduced (Bruce, Digard and Stuart, 2010; Eisfeld *et al.*, 2011). Silencing of Rab11 proteins, but not FIP3, resulted in a ten-fold reduction in viral titres from infected cells (Bruce, Digard and Stuart, 2010), a trend that was matched in another study (Eisfeld *et al.*, 2011). The authors of this study noted that by knocking-down the expression of FIP3 in infected cells, a simultaneous reduction in filament length and reduction in titre compared to cells with intact FIP3 was observed. With two filament-producing strains of IAV, approximately 80% of infectious virus was generated from FIP3 knockdown cells (Bruce *et al*., 2010). This suggests that FIP3 specifically affected the generation of infectious filaments that are extended in length, and that this process is exclusive to the generation of filamentous particles. In IAV infection, Rab11 appears to be necessary for late-stage budding events by delivering vRNPs to sites of virion assembly (Bruce, Digard and Stuart, 2010; Amorim *et al.*, 2011). The authors of these two studies offer a mechanism by which vRNPs first accumulate at the pericentriolar recycling endosomal compartment following translocation from the nucleus. A similar observation was made in a later study (Chou *et al.*, 2013). At the pericentriolar recycling compartment, the vRNPs are organised through speculated interactions between Rab11 and PB2. Then the vRNPs are trafficked to the cell surface through their interaction with Rab11, which is associated with vesicles that are being trafficked.

Cholesterol is necessary for the production of filamentous particles. By depleting cells of cholesterol, the production of cell-associated filamentous particles was abolished (Rossman *et al.*, 2010a). This study also noted that the cytoplasmic tail of M2 binds to cholesterol and the authors speculate that this binding is necessary for filamentous particle formation. Another study noted the importance of putative M1-cholesterol binding sites (Tsfasman *et al.*, 2015). Using *in silico* modelling, the authors of this study identified putative cholesterol recognition amino acid consensus (CRAC) motifs in the M1 protein of the WSN strain. They found that three mutations, F32Y, W45Y, Y100S,

introduced individually were sufficient to induce a filamentous phenotype to the otherwise spherical-producing strain. The authors observed that these particles had defects, such as having a "beads on a string" appearance where there was a chain of connected spherical particles, suggesting that they were defective particles. Similarly, the diameters of these chains were approximately 100 nm, which is marginally larger than has been seen for other filamentous particles (Calder *et al.*, 2010; Vijayakrishnan *et al.*, 2013). The authors also noted that two of the three mutants were less thermally stable than the spherical WT, again suggesting that they were defective particles as opposed to "true" filamentous particles, as spherical and filamentous particles have been shown to be equally thermally stable (Seladi-Schulman *et al.*, 2014).

Overall, the processes that govern IAV morphology are multi-faceted. The factors that determine whether or not filamentous particles will be produced depend on viral protein-protein interactions, viral-cellular protein interactions, and also the type of cell that is infected. Even when "filament-permissive" cells are infected with strains that produce filamentous particles, only a fraction of infected cells will generate the pleomorphic virions (Roberts *et al*., 1998; Bourmakina and García-Sastre, 2003; Elleman and Barclay, 2004). It is still unclear what determines this effect, but could be due to several influencing factors such as IFN signalling, number of infecting particles or degrees of cellular polarisation.

1.5 Innate and adaptive barriers to infection

1.5.1 Respiratory mucus

The target tissue tropism for human IAV is the URT. The epithelium of the URT consists of ciliated, non-ciliated and goblet cells. Non-cilliated cells are thought the be the main cell type to express the human IAV receptor α2,6-linked sialic acid (M. N. Matrosovich *et al.*, 2004; Thompson *et al.*, 2006). Goblet cells are the main producers of respiratory mucus that forms the glycocalyx mucus layer, which is the first host barrier to infection that IAV must overcome (Figure 1.3 A). Mucus consists of approximately a 1% sodium chloride (NaCl) solution and contains 1-2% proteins, with the rest being made up of various glycolipids and carbohydrates (Antunes and Cohen, 2007). Apart from posing as

a physical barrier blocking cells, mucus contains specific inhibitors to infection. One such mediator of inhibition is presentation of sialic acids on glycoproteins that mimic cellular receptors for IAV (Matrosovich and Klenk, 2003). These decoy receptors competitively bind the viral receptor binding protein, HA, which blocks subsequent binding of virus to cells. The main proteins that mediate this effect are called mucins (Figure 1.3 B).

Mucins are the main protein constituents of mucus and are heavily glycosylated and rich in sialic acid ligands (Thornton, Rousseau and McGuckin, 2008). The mucin that is predominantly expressed from goblet cells in tracheal epithelia is MUC5AC (Hovenberg, Davies and Carlstedt, 1996). Overexpression of Muc5ac mRNA in a mouse model was found to significantly increase MUC5AC expression. This correlated with increased resistance to infection when mice were challenged with virus. Bronchoalveolar lavage fluid (BALF) from mice that had increased expression of MUC5AC significantly inhibited IAV *in* vitro more than BALF from WT mice (Ehre *et al.*, 2012). Exosome-like vesicles that were released from human tracheobronchial ciliated epithelium were also found to inhibit IAV infection, and this was dependent on the presence of sialic acids on the vesicles (M Kesimer *et al.*, 2009). The method of presentation of inhibitor is different, but the mode of inactivation is the same.

IAV can counteract the inhibitory effect posed by these decoy receptors through the activity of the NA enzyme (Mikhail N Matrosovich *et al.*, 2004; Cohen *et al.*, 2013), which catalyses the hydrolysis of the glycosidic bond between the final and penultimate monosaccharide neuraminic acid. Through this mechanism NA can release viruses that have bound to decoy receptors, freeing the virions and facilitating the establishment of infection.

Another group of IAV inhibitors present in the glycocalyx and lectins, which are molecules that bind sugars through a defined carbohydrate recognition domain. Lectins are able to bind to and inhibit IAV particles through interaction with glycosylated HA or NA on the virion surface in a calcium ion-dependent manner. An example of one such lectin is surfactant protein D (SP-D) (Madsen *et al.*, 2000). The degree to which lectins that are present in mucus can bind to and inhibit virions depends on the degree of glycosylation on either HA or NA. When treated with ferret BALF sialic acid-mediated inhibition of IAV was greater than SP-D-mediated inhibition (Job *et al.*, 2016). When

BALF was treated with bacterial sialidases the increase in infectivity was greater than when treated with mannan, which would competitively bind the SP-D lectin (Job *et al.*, 2016). Thus, in ferret BALF, sialic acid decoy receptors are the primary mode of innate IAV inhibition.

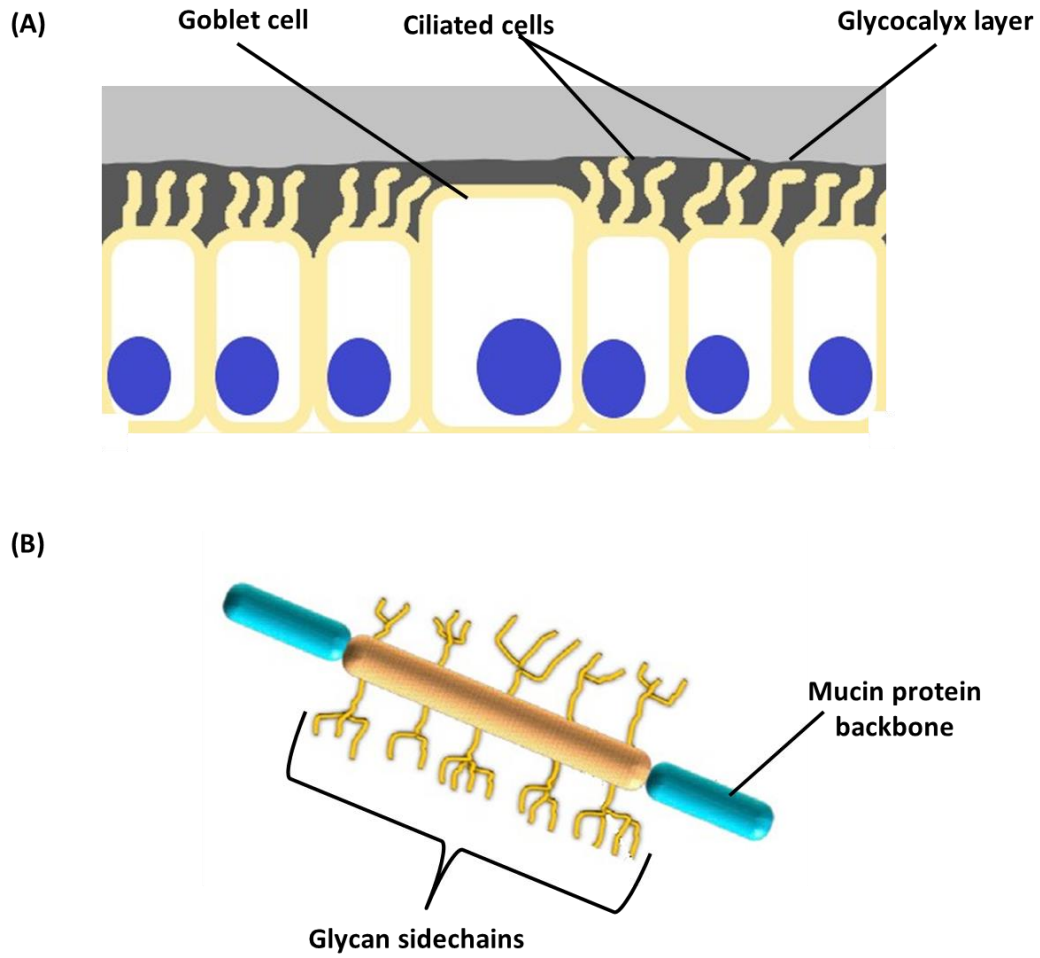

Figure 1.3: Representation of the respiratory epithelium, glycocalyx layer and mucin protein. (A) Respiratory epithelial cells covered by a glycocalyx layer. Mucus-producing goblet cells, ciliated cells and the mucus, glycoclayx layer are shown. (B) Typical mucin protein. Glycosylated side chains from the mucin protein backbone are shown. These

side chains are rich in sialic acids which will act as decoy receptors for IAV. Mucin cartoon adapted from (Zanin *et al.*, 2016).

1.5.2 IFN signalling in response to infection

The type I IFN response plays a major role in the host response to infection. This is induced by cellular receptors, PRRs sensing viral signals and inducing the expression of type I IFNs, IFN-α and –β. One of the main cellular sensors to IAV infection is a helicase called RIG-I (Kato *et al.*, 2006). RIG-I senses IAV RNA through recognition a 5' triphosphate, which is typical of RNA viruses (Hornung *et al.*, 2006). This signal is not typical of cellular cytoplasmic RNAs, and thus allows for recognition by the cell of self and non-self (Takahasi *et al.*, 2008; Lu *et al.*, 2010). Once RIG-I binds this, a signal transduction pathway is induced that ends with the activation of interferon regulatory factor 3 (IRF3) and NF-κB, which leads to the expression of type 1 IFNs reviewed in (García-Sastre, 2011). Once IFN-α and –β are expressed, they are translocated to the outside of the cell. Here they can induce further IFN signalling by binding to cell surface receptors, this is called autocrine signalling or induce antiviral states in neighbouring cells, paracrine signalling. Once the cell surface receptors have been activated through the JAK-STAT pathway, a signal transduction cascade is initiated which results in the up-regulation of hundreds of IFN-stimulated genes (Samuel, 2001).

One example of an IFN-stimulated gene product is viperin. Viperin is highly inducible by type I IFN signalling (Chin and Cresswell, 2001). Viperin has been found to inhibit IAV replication by perturbing lipid rafts, the sites of IAV assembly and budding (Wang, Hinson and Cresswell, 2007). It is interesting to note that this study was performed using spherical strains of IAV, to our knowledge, the effect of viperin on morphology has not been investigated. One study found that viperin knock-out mice had no difference in viral load or lung damage scores, suggesting that its effect *in vivo* might be more nuanced (Tan *et al.*, 2012). Another IFN-induced protein, tetherin, inhibits the release of a retrovirus from infected cells (Neil, Zang and Bieniasz, 2008). Tetherin has also been found to interfere with the release of IAV and this was dependent on the specific HA and NA being expressed by the viruses tested (Gnirß *et al.*, 2015). Another study found that sensitivity to inhibition by tetherin expression was independent of viral morphology (Bruce *et al.*, 2012).

1.5.3 Antibody-mediated immunity

Serum immunoglobulin G (IgG) antibodies directed against the HA of a given strain correlates with vaccine efficacy and reduced viral replication and disease *in vivo*. This is typically measured by the capability of serum antibodies to block haemagglutination of red blood cells by a set amount of virus (Han *et al.*, 2012; Chen *et al.*, 2013; DiazGranados *et al.*, 2014). Serum IgG is not likely the effector of virus inhibition, this is most likely achieved by immunoglobulin A (IgA) which is present in the mucosa (de Silva *et al.*, 2017). In vaccinated individuals, the levels of IgG and IgA antibody secreting B cells are comparable, thus serum IgG can be used as an indicator of levels of mucosal IgA (Sasaki *et al.*, 2008). As well as direct binding to and halting of invading viruses, antibodies are capable of mounting a directed B and T-cell response to infection which are far more efficient at clearing infection (Wrammert *et al.*, 2011; Wilkinson *et al.*, 2012). Unfortunately, due to antigenic drift and the highly variable nature of the antigenicity of IAV, cross-reactivity of antibodies directed against one virus may not bind avidly to another strain, even if they are in the same subtype (Hancock *et al.*, 2009).

1.6 Transmission of IAV

Transmission efficiency is one of the most important factors when assessing the disease burden that a pathogen presents. The relative transmissibility of a given strain of IAV is one determinant of its pandemic potential, the others being novel antigenicity and replication capacity in humans. A transmission event is where infection is successfully transferred from host to another. In the case of IAV, a transmission event can occur as either direct inhalation of aerosolised respiratory droplets containing infectious virus particles, or by interaction with fomites that have settled from the air, e.g. sputum (Mubareka *et al.*, 2009). There are two animal models for investigating transmission of IAV in a laboratory setting, contact and aerosol transmission. Contact transmission models involve co-housed animals which are free to physically interact with one another. Aerosol transmission models do not allow for direct contact between animals, the animals are separately housed and the only potential for transmission is via aerosolised respiratory droplets. Of these two, the aerosol transmission model is considered to be the more stringent. As well as this, it has been suggested that aerosol

transmission is the predominant mode of transmission for IAV (Cowling *et al.*, 2013), with the majority of viral RNA found in droplets ≤5 µm (Milton *et al.*, 2013).

1.6.1 Animal models for IAV transmission

Animal models are the most common method of investigating the complex sequence of events that can lead to transmission of infectious disease from one host to another. Many considerations have to be made when choosing which animal model best suits the hypothesis being tested. While IAV is capable of infecting various species, certain caveats have to be considered when relating infection profiles to human models. For instance, human clinical isolates are avirulent in mice but after serial passage accrue a number of mutations, typically in HA, M, and polymerase gene segments that confer virulence and increase in viral titres (Smeenk *et al.*, 1996; Brown *et al.*, 2001; Ilyushina *et al.*, 2010; Sakabe *et al.*, 2011). Mouse transmission models have been established but they are virus strain specific (Schulman and Kilbourne, 1963; Edenborough, Gilbertson and Brown, 2012). Even viruses which have been adapted to mice and grow to high titres fail to transmit to other mice in direct contact models (Edenborough, Gilbertson and Brown, 2012). Guinea pigs are another animal model that is commonly used to investigate IAV transmission. Unadapted human IAV are capable of infecting guinea pigs at low titres and are readily transmissible from guinea pig to guinea pig in both contact and aerosol transmission models (Lowen *et al.*, 2006). However, guinea pigs do not present with symptoms when infected with IAV, even when infected with highly pathogenic avian influenza (HPAI) strains (Govorkova *et al.*, 2005; Maines *et al.*, 2005; Van Hoeven *et al.*, 2009; Bouvier, 2015). Ferrets are currently considered to be the "gold standard" for modelling IAV infection as they are readily infected by strains that cause disease in humans as well as avian strains that are of significant concern for human health, they also display clinical symptoms that are comparable to humans (Itoh *et al.*, 2009a; Maines *et al.*, 2009; Roberts *et al.*, 2012; Blumenkrantz *et al.*, 2013; Bouvier, 2015).

1.6.2 Role of HA in transmission

The receptor binding protein is arguably one of the most important factors in IAV transmission. It is one of the main determinants of the tropism of a given strain of IAV (Scull *et al.*, 2009). Avian strains of IAV will preferentially bind to α2-3 terminally linked

sialic acids present on cellular glycoproteins (Suzuki *et al.*, 2000) which are the most common linkage found in avian species. α2-6 terminally linked sialic acids are more common in humans with α2-6 linked sialic acids are more predominant in the URT with more α2-3 ligands expressed in the lower respiratory tract (LRT) (Shinya *et al.*, 2006; Nicholls *et al.*, 2007). Amino acid changes in the receptor binding site (RBS) of the HA protein are significant determinants of the transmissibility of IAV (Neumann and Kawaoka, 2015). A switch in preferential binding to α2-3 linked sialic acids to α2-6 linked sialic acids confers increased infectivity from avian to mammalian hosts respectively (Herfst *et al.*, 2012; Imai *et al.*, 2012; Linster *et al.*, 2014). These studies demonstrated that a switch from avian to mammalian RBS binding preference increased transmissibility of H5N1 virus in ferrets. It has been noted that the stability of the H5 HA can be compromised by switching the RBS to preferentially bind α2-6 linked sialic acids but stability can be restored by introduction of further amino acid substitutions to the stalk of the protein and that these mutations further increase transmissibility (Imai *et al.*, 2012; de Vries *et al.*, 2014; Linster *et al.*, 2014). The switch from an avian to a human preference in receptor binding of an avian HA is of particular concern, because it facilitates transmissibility as well as being antigenically novel. All recorded IAV strains that have caused pandemics have had avian origin HAs (Garten *et al.*, 2009).

The HA protein is expressed as a monomer from viral mRNA. Monomers oligomerise in the endoplasmic reticulum to form homo-trimers. Three distinct conformations of HA trimers have been characterised: uncleaved HA_0, receptor-binding HA_1+HA_2 and fusion HA_2 (Kielian and Rey, 2006; White *et al.*, 2008; Harrison, 2009; Gamblin and Skehel, 2010). HA_0 is initially generated during the replication cycle. It requires proteolytic cleavage to HA_1+HA_2 which are linked by a disulphide bond to activate infectivity potential (Steinhauer, 1999). This cleavage is vital for the infectivity of IAV as without cleavage, the HA molecule will be unable to adopt the low pH induced conformational change that induces fusion of the viral and endosomal membranes (Section 1.3.2) (Galloway *et al.*, 2013).

The typical range of fusion pHs of viruses that infect humans can be: 5.0-5.8 (Galloway *et al.*, 2013), with avian-derived viruses having higher fusion pH values (Galloway *et al.*, 2013; Shelton *et al.*, 2013). If fusion is triggered prior to the virus entering the cell, the

HA will no longer be capable of binding to cells due to losing the proper receptor binding conformation. Viruses with higher fusion pHs, the pH at which fusion is triggered, are less transmissible than those with lower pHs (Shelton *et al.*, 2013). Similarly, it has been found that a mutation that increased fusion peptide stability, and lowers fusion pH, was one of the accrued mutations that facilitated aerosol transmission of a previously non-transmissible virus (Linster *et al.*, 2014).

The conformational change that is induced by a low pH can also be induced by increased temperature, this potentially occurs through a mechanism that raises the fusion pH as temperature increases (Huang *et al.*, 2002). Imai *et al*., (2012) demonstrated that one of the adapted mutations in the HA of a H5N1 virus from an avian isolate was a compensatory mutation that increased both temperature and pH stability of HA. They found that a single amino acid substitution conferred both increased temperature stability and lowered the fusion pH, making the HA more stable. They also found that changes in the receptor binding site of an avian strain of virus simultaneously increased receptor binding capability of the virus, but reduced the pH and temperature stability. The stability was rescued by expression of amino acid which resulted in the loss of a glycosylation site in the HA.

pH stability has been shown to correlate with virulence, persistence and stability in the environments (Reed *et al.*, 2010). This study found that a single amino acid in the fusion peptide pocket of a H5 HA lowered the fusion pH and was calculated to persist at 28^{o}C for longer than the WT virus. They also found greater levels of infectious virus in the drinking water of infected ducks compared to WT, which shows that fusion pH affects environmental stability. Another amino acid substitution lowered the fusion pH compared to WT, persisted for longer than WT, but did not transmit as efficiently as WT or the other fusion mutant. An H5N1 virus harbouring a mutant HA with a lowered fusion pH replicated to higher titres in the URT of infected ferrets compared to WT. It had similar virulence as WT but neither virus was transmissible (Zaraket *et al.*, 2013). Acid stability of the HA protein has also been found to influence H5N1 Influenza Virus Pathogenicity (DuBois *et al.*, 2011). It has been noted that the stability of the H5 HA can be compromised by switching the RBS to preferentially bind α2-6 linked sialic acids but stability can be restored by introduction of further amino acid substitutions to the stalk

of the protein and that these mutations further increase transmissibility (Imai *et al.*, 2012; de Vries *et al.*, 2014; Linster *et al.*, 2014).

Stability of the HA protein is typically tested by either determining the thermal stability of viruses, or at what pH fusion is triggered. It stands to reason that viruses which are more thermally stable are more transmissible as they can persist for longer in the environment. Similarly, viruses that have lower fusion pHs are more stable because they have the double benefit of not undergoing premature conformational change in environments with lowered pHs, like human nostrils (England *et al.*, 1999) and fusion events will be initiated later in the maturation of the endosome (Fuchs, Schmid and Mellman, 1989; Skehel and Wiley, 2000), so that fusion occurs closer to the nucleus and RNPs are more easily trafficked to the nucleus following translocation to the cytoplasm.

1.6.3 Role of NA in transmission

One of the main roles of the NA in the IAV replication cycle is to facilitate efficient release of virus from infected cells, continuing the spread of infection. NA is an enzyme that cleaves sialic acids from sialyloligosacchardies. By removing the ligand bound by the HA, newly formed viruses won't be anchored to the cell surface. Another function of the NA is to cleave sialic acids present on proteins found in respiratory mucus (Section 1.5.1). NA is also necessary to curb self-aggregation of IAV particles. In certain strains, both HA and NA are glycosylated (Vigerust *et al.*, 2007; Matsuoka *et al.*, 2009), which can present terminally linked sialic acids that can be bound by other virion HAs causing aggregation and reducing the total number of infectious particles.

As mentioned in section 1.5.1, respiratory mucus contains proteins with the capacity to inhibit IAV infection. Respiratory mucus has been shown to negatively affect infectivity of IAV (Matrosovich *et al.*, 2004a; Ehre *et al.*, 2012). In a recent study, IAV particles have been tracked as they move through a mucus layer (Yang *et al.*, 2014). The capacity of the viruses to move through the mucus was diminished by inactivating the NA and increased with the addition of exogenous NA (Yang *et al.*, 2014). Low NA activity has been shown to affect both contact and aerosol transmission (Zanin *et al.*, 2015). The authors of this paper demonstrated that viruses with lower NA activities were far less transmissible than those with increased NA activity. They did not report any difference in *in vitro*

growth kinetics. They also reported that viruses with lowered NA activity were far more sensitive to inhibition by respiratory mucus and had greatly reduced replication kinetics in normal human bronchial epithelial cells (NHBE) when the cells were allowed to accumulate mucus.

Proper balance of HA and NA is required for efficient replication and transmission of IAV (Mitnaul *et al.*, 2000; Yen *et al.*, 2011; Xu *et al.*, 2012; Zanin *et al.*, 2015). If the HA binds too strongly, compared to the NA activity, nascent budding viruses would likely be unable to detach due to interactions of HA and host receptor. This inhibits the virus from spreading. Similarly, if the NA is too active, it could inhibit attachment and uptake of virus to host cells by cleaving recently formed bonds of HA and receptor. Interestingly, one of the pandemic H1N1 strains proves an exception to this model. A/Netherlands/602/2009 was shown to have comparably strong HA-binding, but weak NA activity (Xu *et al.*, 2012), yet this strain was demonstrably transmissible in both ferrets and guinea pigs (Munster *et al.*, 2009; Campbel *et al.*, 2014a; Campbell *et al.*, 2014b).

1.6.5 Role of segment 7 and morphology in transmission

Segment 7 of the IAV genome encodes 2 proteins, M1 and M2. Released virions comprise of approximately 500 fold more M1 than M2 (Hutchinson *et al.*, 2014). M1 is the most abundant protein in mature virions (Hutchinson *et al.*, 2014). Recent studies have demonstrated that the segment 7 of a transmissible virus can confer transmissibility to a reassortant virus that is otherwise incapable of transmission (Chou *et al.*, 2011; Lakdawala *et al.*, 2011; Ma *et al.*, 2012; Campbell *et al.*, 2014b). Some of these studies demonstrated a correlation between virion morphology and transmissibility (Lakdawala *et al.*, 2011; Campbell *et al.*, 2014a). One study demonstrated that segment 7 conferred transmissibility to an otherwise non-transmissible virus by swapping the segment of a strain from the 2009 H1N1 pandemic (pH1N1) with the segment 7 of a lab-adapted, spherical virus. These studies found that segment 7 conferred a change in morphology of virus produced in MDCK cells. A correlation was seen between the expression of segment 7 from pH1N1 and an increase in a filamentous morphological phenotype. Expression of pH1N1 segment 7 also correlated with increased transmissibility in ferrets and guinea pigs (Lakdawala *et al.*,

2011; Campbell *et al.*, 2014a). These studies offered a convincing correlation between morphology and increased transmissibility, but they did not offer a mechanism by which this is achieved. It has been reported that when normalised to infectious units, filamentous viruses have increased NA activity compared to spherical counterparts (Campbell *et al.*, 2014b; Seladi-Schulman *et al.*, 2014). It is unclear why viruses with a filamentous morphology have increased levels of NA activity, but it is assumed it is due to their increased size facilitating increased amounts of enzyme incorporation. It has been speculated that the increased NA activity of filamentous viruses could contribute to transmission by increased resistance to inhibition by respiratory mucus.

Seladi-Schulman *et al.*, 2013 demonstrated that serial passage in either ECEs or MDCK cells resulted in a switch from strains that produced predominantly filamentous particles to mostly spherical particles. This was dependent on viral strain and the substrate in which they were grown. It was also demonstrated that serial passage of a spherical producing strain in guinea pigs yielded progeny virus that produced filamentous particles. From this they identified single amino acid substitutions in the M1 protein of pH1N1 that switched the morphology of virions from filamentous to spherical.

The filamentous-to-spherical mutants shed overall lower titres in infected guinea pigs, and had delayed peak titres and transmission events. The spherical-to-filamentous mutant failed to transmit, despite having similar replication kinetics in guinea pigs to the spherical WT. The transmission data for the filamentous-to-spherical virus would seem to suggest that the delay in transmission was a result from lowered viral titres in the donor animals, suggesting that strains that produce filamentous particles are better adapted to replicating *in vivo*. This has an obvious effect on transmissibility of the virus, as increased amounts of virus shed by donors increases the possibility of transmission events. However, this hypothesis is undermined by the spherical-to-filamentous data. They found that despite growing to similar titres in donor animals, the spherical WT or filamentous mutant failed to transmit. They did find that the virus isolated from the twelfth passage in guinea pigs, which was a spherical-to-filamentous mutant, grew to higher titres and successfully transmitted. While this virus did display a filamentous morphology, the impact of other accumulated mutations that did not contribute to morphology cannot be discounted.

Morphology alone isn't sufficient for transmission (Campbell *et al.*, 2014b). Using single amino acid substitution experiments the authors were able to generate viruses that had increased or decreased levels of filamentous particles. The trend that they recorded in this study was that while a proline expressed at residue 41 of M1 does increase the amount of filamentous particles budding from cells, it does not correlate with increased transmission. The data suggested that this virus may have been defective in replication which in turn would reduce transmissibility. This study highlights the intricate nature of factors that influence transmission, where if a factor that can increase transmissibility, such as increased filamentous morphology, occurs at the expense of another factor, like replication capacity, then the virus will not transmit.

1.7 Stages of transmission

In order to transmit from an infected host, a minimum amount of virus needs to be shed by the infected person (Figure 1.4 A) to allow enough viral particles to survive in the environment (Figure 1.4 B) to be transferred to an uninfected individual (Figure 1.4 C). The virus needs to be efficient at replication so that it will not be overcome by innate, or adaptive host responses to infection. If a virus has reduced avidity to binding to host cellular receptors then fewer cells will become infected. If a virus is perfectly evolved to infect a host, fewer than 10 pfu are required to establish an infection (Roberts *et al.*, 2011; Frise *et al.*, 2016). If it is not suitably matched to the host it is infecting, then higher titres than possible may be required to establish infection (Roberts *et al.*, 2011).

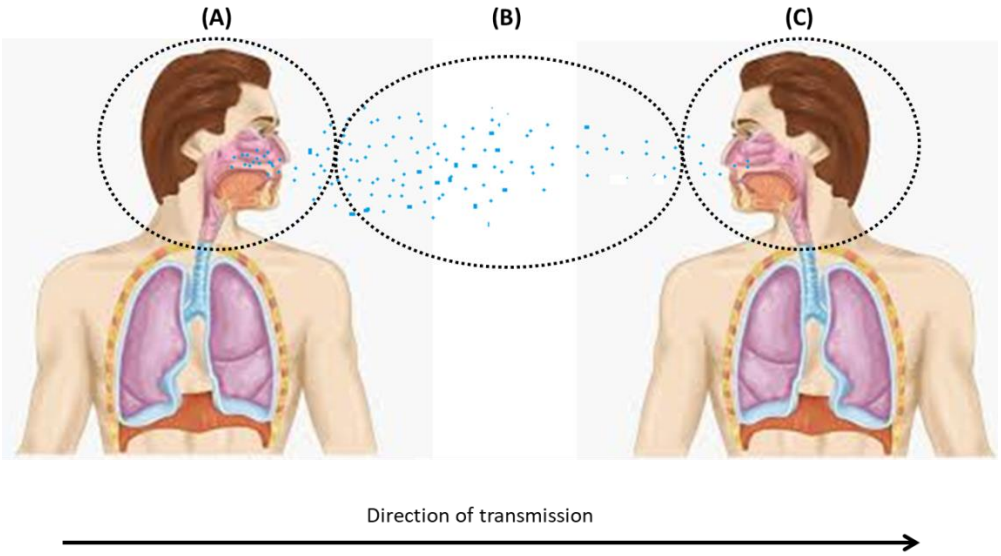

Figure 1.4: Stages affecting viral infectivity in an aerosol transmission event. (A) Shedding titres. A minimum amount of virus needs to be shed to be transmitted. (B) Stability of viruses in the environment. Environmental factors can influence the infectivity of viruses carried within aerosolised droplets. (C) Establishing infection. Viruses need to be adequately suited to infecting a naïve host to successfully establish infection.

1.7.1 Transmitting virus

Inoculum dose corresponds with whether or not infection will occur (Lowen *et al.*, 2006). Inoculum dose also correlates with shed titres (Roberts *et al.*, 2011). Thus, increased shedding titres from a donor increases the likelihood of transmitting infection, up to a replication threshold. The 50% infectious dose (ID_{50}) is a metric that

approximates how many plaque forming units (pfu) will be required as an inoculum dose to infect 50% of exposed animals. Viruses that are adapted to the naïve host will have low ID_{50} values, while viruses that are not will have high ID_{50} values. A virus that is deficient in replication in a given host will result in a lower amount of virus being shed. For example, a study found that despite having a relatively large inoculum dose of $1x10^6$ pfu, a virus with inadequate HA receptor binding and stability grew to significantly lower titres at three days post infection (Imai *et al.*, 2012). This shows that infection can be initiated in hosts, but may be so replication incompetent that only a small number of pfu will be shed. This highlights the difference between ID_{50} and titre shed both of which are important for sustained transmission. Another study demonstrated that while the ID_{50} of two viruses was different, once a sufficiently high inoculum titre was used to infect animals, comparable growth kinetics were observed (Roberts *et al.*, 2011). To be able to successfully transmit from host to the next, a minimum amount of virus will have to be shed from the donor animal. The higher the shed titre, the more probable it is that transmission will occur. One study found that ferrets infected with highly transmissible strains of IAV shed more infectious virus in exhaled aerosols compared to less transmissible strains (Gustin *et al.*, 2013). Another study found a correlation between transmissibility and increased levels of viral RNA in sampled air (Lakdawala *et al.*, 2011)

1.7.2 Environmental effects

Ambient temperature and humidity affect aerosol transmissibility of IAV (Lowen *et al.*, 2007). Using a guinea pig model of transmission, they found that low relative humidity (RH) (20%) was the most efficient condition for aerosol transmission at 20^oC. Transmission was reduced at 50% RH, but interestingly increased at a slightly higher relative humidity (RH), 65%. They found that RH had less of an effect when the ambient temperature was 5^oC. Transmission was completely abrogated at 80% RH. Similarly, no transmission occurred at 30^oC. The authors found that greater levels of virus were shed when the animals were housed at 5^oC than when they were housed at 20^oC, and they speculated that this was the reason for increased transmission seen at this temperature. They also observed no difference in antiviral and pro-inflammatory signalling responses in animals housed at either temperature (Lowen *et al.*, 2007). The authors speculate that the abrogation of transmission at high RH is due to respiratory droplets taking on more

water and promptly settled from the air more quickly, while smaller droplets remained suspended for longer which would lead to increased probability of transmission by inhalation. Another study investigated the effect of RH and temperature for two H3N2 subtype strains of IAV and noted similar levels of transmission, with the most efficient temperature and RH being 23^{o}C and 30% (Gustin *et al.*, 2015).

1.7.3 Establishing infection

From the available evidence, it is likely that natural infection by IAV is only initiated by a small number of virus particles (section 1.7 and 1.7.1). There is some evidence that infected individuals breathe out low titres of virus (as opposed to concentrated levels of virus collected by nasal wash during animal experiments). A study that sampled the air of a health centre with infected individuals estimated that over one hour the inhalation dose would be 30±18 median 50% tissue culture infectious dose ($TCID_{50}$), which is approximately 21 pfu (Yang *et al.*, 2011). Another study found that by quantifying the amount of RNA shed by infected individuals, between 3.2 and 20 copies were exhaled every minute (Fabian *et al.*, 2008). Interestingly, it has been reported that there was a very weak correlation between viral titre as determined by nasopharyngeal swab compared to exhaled virus from infected individuals, where the swab method had orders of magnitude higher level of infectious virus quantified (Milton *et al.*, 2013). Because infected individuals shed such low levels of virus, the ID_{50} of a successful infection will be quite low. Thus, for a virus to be transmissible, it needs to be as fit as possible.

1.8 Summary and project plan

The main question that I will attempt to address within the scope of this thesis will be: what is the biological significance of IAV filamentous particles.

The main themes tested within this thesis are:

1) Filamentous and spherical particles are equally infectious *in vitro* (Roberts, Lamb and Compans, 1998). Similarly, both filamentous and spherical particles only bear one genome set (Calder *et al.*, 2010; Noda *et al.*, 2012). Filamentous viral particles can be ≥10 µm in length, while spherical particles are typically 100-150 nm in diameter. Thus, per infectious unit, filamentous particles are a far greater

drain on cellular and viral resources. The most plausible reason for the adoption of a spherical morphology *in vitro* is due to the sole production of spherical-only particles without unnecessary diversion of resources to the generation of ≥10 µm long filamentous particles, especially when there is no evolutionary pressure driving the selection of that phenotype (Chapter 3).

2) Due to their increased size, filamentous particles may be more resistant to inhibition by inhibitors directed against the viruses. Immune-directed responses are lacking *in vitro*, thus this evolutionary pressure is lacking when viruses are grown in laboratory substrates, which could lead to the spherical morphology (Chapter 4). A correlation between viruses that generate filamentous viral particles and increased transmission has been observed (Lakdawala *et al.*, 2011; Campbell *et al.*, 2014a). Thus, we hypothesise that filamentous particles have some bearing on the transmissibility of IAV. Similarly, it is interesting to note that filamentous particles display increased NA activities (Campbell *et al*., 2014b; Seladi-Schulman *et al*., 2014), thus it is possible that they might be less susceptible to inhibition by decoy receptors present in mucus. This seems likely as the evolutionary pressure of transmission from host-to-host is abolished in a laboratory setting. One of the aims of this project was to attempt to discern at which stage in a transmission event filamentous particles may have a fitness advantage compared to spherical particles, release of virus and survival in the environment (Chapter 6) or infection of a new host (Chapter 5).

Chapter 2: Materials and Methods

2.1 Materials

2.1.1 Plasmids

Plasmid name	Description	Source
pCl-Vic-PB2	"Helper" plasmid: Vic75 PB2 protein	Prof. Wendy Barclay
pCl-Vic-PB1	"Helper" plasmid: Vic75 PB1 protein	Prof. Wendy Barclay
pCl-Vic-PA	"Helper" plasmid: Vic75 PA protein	Prof. Wendy Barclay
pCl-Vic-NP	"Helper" plasmid: Vic75 NP protein	Prof. Wendy Barclay
pPol1-Vic-PB2	"Rescue" plasmid for Vic75 Segment 1	Prof. Wendy Barclay
pPol1-Vic-PB1	"Rescue" plasmid for Vic75 Segment 2	Prof. Wendy Barclay
pPol1-Vic-PA	"Rescue" plasmid for Vic75 Segment 3	Prof. Wendy Barclay
pPol1-Vic-HA	"Rescue" plasmid for Vic75 Segment 4	Prof. Wendy Barclay
pPol1-Vic-NP	"Rescue" plasmid for Vic75 Segment 5	Prof. Wendy Barclay
pPol1-Vic-NA	"Rescue" plasmid for Vic75 Segment 6	Prof. Wendy Barclay
pPol1-Vic-M	"Rescue" plasmid for Vic75 Segment 7	Prof. Wendy Barclay
pPol1-Vic-NS	"Rescue" plasmid for Vic75 Segment 8	Prof. Wendy Barclay
pPol1-PR8-M	"Rescue" plasmid for PR8 WT Segment 7	Prof. Wendy Barclay

Table 2.1: List of plasmids used for research presented within this thesis. "Helper" plasmids contain a human polymerase II promotor sequence and express mRNA that gets translated into indicated protein. "Rescue" plasmids contain a human polymerase I promotor sequence and express negative sense vRNA (Pleschka *et al.*, 1996).

2.1.2 Viruses

Virus name	Description	Stock generation
Vic75 WT	A/H3N2/Victoria/3/1975	P: 3. MOI: 10^{-8} MDCK
Vic:PR8M	Vic75 expressing A/H1N1/Puerto Rico/3/1934 segment 7	P: 3. MOI: 10^{-8} MDCK
Vic75 41V	Vic75 M1 A41V point mutant	P: 3. MOI: 10^{-8} MDCK
Vic75 40E 41V	Vic75 M1 E40E A41V one silent and one point mutant.	P: 3. MOI: 10^{-8} MDCK
Vic75 WT NIP	Vic75 with increased level of NIPs	P: 4. MOI: 10^{-1} MDCK
Vic:PR8M NIP	Vic:PR8M with increased level of NIPs	P: 4. MOI: 10^{-1} MDCK
HNE Vic75 WT	Vic75 grown in HNE cultures	P: 4. MOI: 10^{-2} HNE
HNE Vic:PR8M	Vic:PR8M grown in HNE cultures	P: 4. MOI: 10^{-2} HNE

Table 2.2: List of viruses used in experiments outlined in this thesis. P: passage number. All stocks were made initially from plasmids outlined in table 2.1 using a reverse genetics system (Section 2.2.7). Passage number indicates how many passages in cells viruses have undergone, where the initial rescue was P:1. All passages were performed in MDCK cells.

2.1.3 Cells

Cell types used in this these were:

MDCK cells, A549 cells and human embryonic kidney (HEK) 293T cells were all kind gifts from Prof. Wendy Barclay.

Human Nasal Epithelia (HNE) cultures, were sourced from Epithelix-Sarl, Switzerland. These are primary respiratory epithelial cells that have been obtained from willing volunteers undergoing surgery. The primary cells are isolated and grown to confluence. Once confluent they are seeded onto transwells containing porous membranes. Media was supplied to both basal and apical layers of the cells until confluence was reached. Once this was done media was only supplied from the basal layer. Cells were grown at an air liquid interface until they became fully stratified and differentiated. Once differentiated, the cells were shipped from the supplier and experiments were performed within a month of receipt.

2.1.4 Primers

Primer name	Purpose	Sequence
Vic75 M 300R	Sequencing	5'- CCC ATG GAA TGT TAT CTC CC-3'
Vic75 M 60F	Sequencing	5'- CTC TCT ATC GTT CCG TCA GGC-3'
Universal 1 F	Virus rescue	5'- ACG CGT GAT CAG CAA AAG CAG G-3'
Universal 2 F	Virus rescue	5'- ACG CGT GAT CAG CGA AAG CAG G-3'
Universal 1 R	Virus rescue	5'- ACG CGT GAT CAG TAG AAA CAA GG-3'
M1 444 F	qPCR	5'- ACA GCT AAG GCT ATG GAG CA-3'
M1 690 R	qPCR	5'-ACC AGC ACT GGA GCT AGG AT-3'
M2 F	qPCR	5'-CGA GGT CGA AAC GCC TAT CA-3'
M42 F	qPCR	5'-GAA CAC AGA TCT TGA GGC CTA T-3'
M2/M42 R	qPCR	5'-AAG GCC CTC TTT TCA GAC CG-3'
Vic75 M1 A41V F	Mutagenesis	5'-AAG AAC ACA GAT CTT GAG GTT CTC ATG GAA TGG CTA AAG-3'
Vic75 M1 A41V R	Mutagenesis	5'-CTT TAG CCA TTC CAT GAG AAC CTC AAG ATC TGT GTT CTT-3'
Vic75 M1 E40E A41V F	Mutagenesis	5'-GAA CAC AGA TCT TGA AGT TCT CAT GGA ATG GC-3'
Vic75 M1 E40E A41V R	Mutagenesis	5'-GCC ATT CCA TGA GAA CTT CAA GAT GAT CTG TGT TC-3'
Vic75 PB2 F	qPCR	5'-TGA GTG ATG CCG GGT CAG AT-3'
Vic75 PB2 R	qPCR	5'-AGT ATC CTG GCC CCC ACT TC-3'
Vic75 PB1 F	qPCR	5'-AAT GCC AGC TCA TGG TCC AG-3'
Vic75 PB1 R	qPCR	5'-ATC AAT CCG GGC CCT AGA CA-3'
Vic75 PA F	qPCR	5'-CAG AGG TGT CCC ATT GCA GA-3'
Vic75 PA R	qPCR	5'-AGT CTC GGG TCA GTG AGA GA-3'
Vic75 HA F	qPCR	5'-CCT TTT CGT TGA ACG CAG CA-3'
Vic75 HA R	qPCR	5'-GCA TGG TCA CGT TTT GCA CT-3'
Vic75 NA F	qPCR	5'-AGC CCA TTG TCA GGA AGT GC-3'
Vic75 NA R	qPCR	5'-TTT CCA TCG TCA AAG GCC CA-3'
Vic75 NS F	qPCR	5'-GAG GGA GCA ATT GTT GGC GA-3'
Vic75 NS R	qPCR	5'-GGA GTA AGT GGA GGT CCC CC-3'

Table 2.3 List of primers used for research carried-out within the scope of this thesis. qPCR: Quantitative polymerase chain reaction.

2.1.5 Immunofluorescence reagents

Antibody name	Description	Source
Anti-Vic75 HA	Polyclonal goat antisera raised against Vic75 HA. Primary.	National institute for biological standards and controls. (76/547)
Anti-Vic75	Polyclonal ferret antisera raised against Vic75 WT. Primary.	(Roberts *et al.*, 2011)
Anti-β tubulin IV	Monoclonal mouse anti sera raised against β tubulin. Primary.	Sigma (T941)
Anti-mouse IgG	Goat polyclonal anti-mouse IgG Alexa fluor 594 conjugate	Abcam (150116)
Protein A- Alexa Fluor™ 488 conjugate	Protein A derived from *Staphylococcus aureus* with an Alexa Fluor™ 488 conjugate	Thermo-Fischer (P11047)

Table 2.4: List of immunofluorescence reagents used for experiments outlined in this thesis.

2.1.6 Reagents (including kits)

Reagent	Purpose	Supplier
Agarose	Plaque assay overlay	Oxoid (LP0028)
AlexaFluor™ Phalloidin	Immunofluorescence (IF)	Thermo-scientific (A22287)
Ampicillin	Positive selection of plasmids	Sigma
Bovine serum albumin fraction V	Overlay media	Thermo-Fischer (1560037)
Calcium Chloride ($CaCl_2$)	Buffer constituent	Sigma (449709)
Dextran DEAE	Overlay media	Sigma (D9885)
Distilled water (dH_2O)	Diluent	N/A
Dulbeccos minimum essential media (DMEM)	Cell maintenance	Life technologies (41965-039)
Dpn-1	Digest plasmid DNA	Thermo-scientific (FD1703)
Ethanol	Sterilisation; RNA extraction	VWR
Fetal bovine serum (FBS)	Cell maintenance	Life technologies
4% Formaldehyde	Immunofluorescence	VWR (9713.1000)
4-(2-hydroxyethyl)-1-piperazineethanesulfonic acid (HEPES) 1M	Overlay media	Life Technologies (15630080)
KOD hotstart DNA polymerase	Plasmid mutagenesis	Merck-millipore (71086)
L-glutamine (200mM)	Overlay media	Life Technologies (25030024)
Luria Bertani broth	E.coli growth	Sigma (L7275)
Magnesium Chloride (MgCl)	Buffer	Sigma (M8266)
Mercaptoethanol	RNA extraction	Sigma (M6250)
2-(N-Morpholino) ethanesulfonic acid sodium salt, 4-Morpholineethanesulfonic acid sodium (MES) salt	NA activity	Sigma (71119-23-8)
20-(4-methylumbelliferyl)-a-D-N-acetylneuraminic acid (MUNANA)	NA activity determination	Sigma (M8639)
Minimum essential media (MEM) 10X	Overlay media	Life Technologies (21430020)
MucilAir™ Culture	Culture medium for HNE	Epithelix

medium	cultures.	
Neuraminidase from		
One-step reverse transcriptase quantitative polymerase chain reaction (RT-qPCR) kit	RNA quantification	New England Biolabs (E3005G)
Oseltamivir carboxylate	NA inhibition	Roche
Penicillin/streptomycin 5,000 U/ml	Cell maintenance	Life technologies (15140122)
Phosphate buffered saline (PBS)	Cell maintenance	Lonza (BE17-516Q)
Polyplus transfection reagent	Transfection	Polyplus-transfection SA.
PureYield™ Plasmid Miniprep System	Plasmid extraction	Promega
RNeasy RNA extraction Kit	RNA extraction	QIAGEN (74104)
Sodium Bicarbonate 7.5%	Overlay media	Life technologies (25080094)
Sodium Chloride (NaCl)	Buffer	VWR (27810.262)
Sodium Hydroxide (NaOH)	Buffer	VWR (31627.290)
Triton-X	Immunofluorescence	Sigma (T8787)
2.5% Trypsin (10X)	Cell maintenance	Life technologies (15090-046)
Trypsin L-(tosylamido-2-phenyl) ethyl chloromethyl ketone (TPCK)	Viral infection assays	Worthington biochemical corporation

Table 2.5: List of reagents used

2.1.7 Solutions and buffers

Solution Name	Ingredients	Purpose
Blocking buffer	5% FBS diluted in PBS	Immunofluorescence
Growth media	DMEM, 10% FBS, 1X NEAA	Cell propagation
MES buffer for NA assay	32.5 mM MES, 4mM $CaCl_2$, dH_2O, pH to 6,5 with NaOH.	NA activity
MES buffer for pH plaque reduction assay	100 mM MES, 120 mM NaCl, 0.9 mM $CaCl_2$, 0.5 mM $MgCl_2$.	pH plaque reduction assay
Overlay media	1X MEM, 0.21% BSA fraction V, 1mM L-Glutamine, 0.15% Sodium bicarbonate, 10mM HEPES, 50 U/ml Penicillin/streptomycin, 0.01% Dextran DEAE, 2 µg/ml Trypsin TPCK.	Plaque assay
Infection media (IM)	Serum free (SF) DMEM with 0.21% BSA fraction V and 2 µg/ml Trypsin TPCK.	Virus growth
SF DMEM	DMEM without FBS added	Virus growth

Table 2.6: Solutions and buffers prepared for general use

2.2 Methods

2.2.1 Plasmid mutagenesis

Mutagenesis primers were designed and are outlined in section 2.1.3. Using a KOD hotstart polymerase kit, reactions were set up as follows: 5 µl of 10X reaction buffer, 5 µl of 2 mM deoxyribonucleotide triphosphate (dNTP) mix, 1.5 µl of 10 µM forward and reverse primers, 10 ng of plasmid deoxyribonucleic acid (DNA), 1 µl of KOD DNA polymerase, 15 µl of dH_2O. PCR reactions were performed with the following parameters: 95^oC for 2 minutes, 25 cycles of 95^oC for 20 seconds, 54^oC for 10 seconds, and 70^oC for 250 seconds. PCR products were digested with Dpn-1 for 5 minutes at 37^oC. Plasmids were then transformed into *Eschericia coli*-X31 (E.coli-X31) cells.

2.2.2 Bacteria transformation

Competent E. coli-X31 cells were thawed on ice. 500 ng of plasmid DNA was diluted 1:10. The diluted DNA was added to 100 µl of E.coli-X31 cells and incubated on ice for twenty five minutes. The cells were heat-shocked at 42^oC for 2 minutes, the incubated on ice for one minute. Cells were added to 1 ml of Luria-Bertani broth and incubated at 37^oC for one hour. 100 µl was added to Luria-Bertani agar plates with 0.1 mg of ampicillin. Plates were incubated overnight at 37^oC.

2.2.3 Plasmid miniprep

Single colonies of transformed E.Coli-X-31 cells were added to 2 ml of Luria-Bertani broth containing 0.1 mg ampicillin and incubated at 37^oC for 22 hours. Cultures were centrifuged at 4,000 RCF for one minute. Cell pellets were resuspended in 650 µl of dH_2O. Plasmid extraction was carried-out using the PureYield^{TM} Plasmid Miniprep system. Cell suspensions were lysed with 100 µl of lysis buffer. 350 µl of neutralization buffer was added and the centrifuged for 3 minutes at 4,000 relative centrifugal force (RCF) units. The supernatant was added to ion exchange columns and centrifuged for 20 seconds at 4,000 RCF. The column was washed with 200 µl of endotoxin removal buffer and centrifuged. The column was washed with 400 µl of column wash buffer and centrifuged. 30 µl of dH_2O was added to the column and incubated for two minutes at room temperature, then centrifuged for 20 seconds at 4,000 RCF. Plasmid

concentrations were determined using a Nanodrop spectrophotometer and stored at -20^{o}C.

2.2.4 Immortalised cell line propagation.

Cells were stored at -80^{o}C. To resuscitate, vials were thawed and added to pre-warmed growth media. When cells were 100% confluent, cells were washed with PBS and had trypsin added disassociate cells from the surface of the tissue culture flask. Once cells were detached, they were resuspended in growth media.

2.2.5 IAV propagation.

MDCK cells were seeded from a confluent flask at a seeding density of 1x10^{5} cells/ml 48 hours prior to infection. Depending on which stock was being generated, cells were infected at an multiplicity of infection (MOI) of either 10^{-8} or 10^{-1} (Table 2.2). Virus stocks were harvested when there was observable cytopathic effect (CPE). Supernatant was centrifuged at 1,000 RCF for 10 minutes at 4^{o}C. The clarified supernatant was aliquoted and stored at -80^{o}C.

2.2.6 Virus rescue using reverse genetics.

Viral genetic segments were encoded on plasmids outlined in table 2.1. When HEK 293T cells were approximately 80% confluent they were transfected. Transfection mixtures consisted of 500 ng of DNA of each rescue plasmid and of the PB2 and PB1 helper plasmids. 250 ng and 1000 ng of PA and NP plasmid were used respectively. Using the Polyplus transfection system (Polyplus-transfection SA), the 12 plasmid mixture was added to 250 µl of the Jetprime® buffer. This mixture was vortexed and incubated at room temperature for 10 minutes. 12 µl of the jetprime® reagent was added to the buffer/plasmid mixture, vortexed and incubated for a further 10 minutes. Without changing the growth media, the transfection mixture was added to the HEK 293T cells and incubated at 37^{o}C for approximately 14 hours. MDCK cells were trypsinised and diluted to a concentration of 5x10^{5} cells/ml. The transfected HEK 293T cells were put into suspension with the MDCK cells. The co-culture of cells was incubated for 8 hours. Growth media was removed, cells washed once and replaced with IM. Cells were monitored and once viral-induced CPE was apparent, stocks were harvested as outlined in section 2.2.5.

2.2.7 Plaque assay.

MDCK cells were seeded from a confluent flask at a seeding density of $1x10^5$cells/ml 48 hours prior to infection. To determine the amount of pfu of a given solution of virus, the stock was titrated in serum free (SF) DMEM. MDCK cells were washed once with PBS. Titrated virus was added to the cells and adsorbed for one hour at 37°C. Following adsorption, cells were washed once with PBS. Overlay media containing 2 µg/ml trypsin TPCK and 0.33% agarose was added to each well. Cells were incubated for approximately 72 hours and the amount of plaques counted and used to calculate the titre.

2.2.8 Multi-step growth curve in immortalised cells

Cells were seeded $1x10^5$cells/ml 48 hours prior to infection. Cells were washed with PBS and infected with virus. Virus was allowed to adsorb to cells for one hour at 37°C. Following adsorption, cells were washed once with PBS and replaced with IM. Infected cells were incubated at 37°C. 300 µl of supernatant was removed and replaced with IM at each time point. Viral titres of each time point were determined by plaque assay. Deviations from this protocol are outlined within relevant figures.

2.2.9 Multi-step growth curve of virus in infected HNE cultures

HNE cultures were ordered from Epithelix-Sarl, Switzerland. The basal layers of the cultures were maintained in HNE culture media. The media was changed and cultures washed every two-three days. Cultures were washed by adding 200 µl of SF DMEM to the apical layer of the cultures and incubated for 30 minutes at 37°C. For infection, virus stocks were diluted to the intended MOI. Cultures were washed once prior to infection, then 100 µl of virus was added to each culture and adsorbed for one hour at 32°C. The virus inoculum was removed and washed once with SF DMEM. At each time point, 200 µl of SF DMEM was added to the cultures, incubated for 30 minutes, removed and stored at -80°C. Viral titres were determined by plaque assay. Deviations from this protocol are outlined within relevant figures.

2.2.10 Determining the thermal stability of viruses of viruses

Virus stocks were diluted to $2.5x10^4$ pfu/ml in 0.9% saline. 250 µl of this was aliquoted into tubes, with triplicate tubes per time point being tested. Tubes were incubated in a water bath set to either 20°C or 37°C, depending on the temperature being tested.

Triplicate tubes were stored at -80^{o}C and designated as the 0 hour time point. At indicated times post incubation, tubes were removed and stored at -80^{o}C. Viral titres were determined by plaque assay.

2.2.11 Antiserum plaque reduction assay

Viruses were diluted to 1000 pfu/ml in SF DMEM. Anti-Vic75 HA was diluted 1:4000 in SF DMEM. Antiserum and virus dilutions were mixed 1:1 and incubated for one hour at 37^{o}C. Untreated controls were viruses diluted 1:1 with SF DMEM. 200 µl of the virus/antiserum was added in triplicate to 6 well plates and adsorbed for one hour at 37^{o}C. Cells were washed once with PBS and replaced with overlay media and agarose. Plaques were counted after approximately 72 hours incubation. Results are reported as percentages of the untreated controls. The mean and standard deviations of the percentages of the untreated control are reported as percentage infectivity remaining.

2.2.12 Respiratory mucus plaque reduction assay

Viruses were diluted to 1000 pfu/ml in SF DMEM. Respiratory mucus that had been harvested from HNE cultures was diluted in SF DMEM. Mucus and virus dilutions were mixed 1:1 and incubated for one hour at 4^{o}C. Untreated controls were viruses diluted 1:1 with SF DMEM. 200 µl of the virus/mucus was added in triplicate to 6 well plates and adsorbed for one hour at 37^{o}C. Cells were washed once with PBS and replaced with overlay media and agarose. Plaques were counted after approximately 72 hours incubation. Results are reported as percentages of the untreated controls. The mean and standard deviations of the percentages of the untreated control are reported as percentage infectivity remaining.

2.2.13 pH plaque reduction assay

Virus stocks were diluted to 5000 pfu/100 µl in 0.9% saline. MES buffer for pH plaque reduction assay was prepared as outlined in section 2.1.6. The buffer was aliquoted in to several tubes and the pH of each tube increased to the desired pH using NaOH, and measured using a pH meter. The buffers at different pHs were filter sterilised. 10 µl of virus was added to 90 µl of each buffer and incubated at 37^{o}C for 15 minutes. For the untreated control, 10 µl of virus was added to 90 µl of 0.9% saline. After the 15 minute incubation, SF DMEM was added to each tube. 200 µl of each virus/buffer solution was

added in triplicate to 6 well tissue culture plates and adsorbed for one hour at 37^{o}C. Cells were washed and incubated with overlay media for approximately 72 hours. Plaques were counted and the amount of pfu for each buffer pH was calculated as a percentage of the untreated control. The mean and standard deviation of the percentage infectivity for each pH are reported.

2.2.14 NA activity measurement using MUNANA

Stock viruses were diluted to 2x10^{4} pfu in MES buffer for NA assay. Viruses were incubated with 100 µM of MUNANA in triplicate for one hour at 37^{o}C using a Biotek Synergy H1 hybrid plate reader. The plate reader was set to excite the samples at a wavelength of 355 nanometres (nm) and read emissions at 460 nm every minute for one hour. The gain was set to the lowest setting. The input titre was calculated by back-titration. The rates of signal generation were calculated as the slopes of the curve by plotting the amount of relative fluorescent units against time. Statistical differences were calculated by comparing the rates of signal generation for viruses by a two-tailed student's t-test.

2.2.15 Immunofluorescence Microscopy

Cells on coverslips were infected at an MOI: 1, adsorbed for one hour, washed with PBS and replaced with IM. The supernatant was removed and cells washed with PBS. A 1:200 dilution of anti-Vic75 HA in blocking buffer was added to the cells and incubated at 4^{o}C for one hour. The antibody solution was removed and cells washed with PBS. Cells were fixed with 4% formaldehyde at 4^{o}C for 30 minutes. Cells were washed three times with PBS and incubated with blocking buffer at room temperature for 30 minutes. Cells were counter-stained with a 1:200 dilution of protein A-FITC conjugate diluted in blocking buffer for one hour at room temperature. Coverslips were washed twice with dH_2O and mounted to coverslips using mowiol. Confocal images were taken using a Leica SP8 scanning confocal microscope. Deviations from this protocol are outlined within relevant figures.

2.2.16 Immunofluorescence of infected HNE cultures

A 1:100 of anti-Vic75 ferret antisera was added to the apical layer of infected HNE cultures at either 96 or 120 hours post infection (hpi) and incubated at room

temperature for one hour. Cultures were washed three times with PBS and apical and basal layers were fixed with 4% formaldehyde for 30 minutes at 4^{o}C. Protein A FITC-conjugate was diluted 1:200 in blocking buffer, added to the apical layer of the cultures and incubated for one hour at room temperature. Cells were washed three times with PBS. Cultures were permeabilised for 15 minutes with a 0.1% triton-X solution in PBS and washed three times with PBS. For staining filamentous actin, a 1:100 dilution of Alexa fluor^{TM} Phalloidin was added to cells and incubated at room temperature for one hour. Cells were washed three times in PBS. For anti-β-tubulin staining, the anti-β-tubulin antibody was diluted 1:200 in blocking buffer, added to the apical layer of the cultures and incubated for one hour at room temperature. Cells were washed three times with PBS. A polyclonal goat anti-mouse IgG antibody with an Alexa Fluor^{TM} 594 conjugate was diluted 1:200 and added to the HNE cultures and incubated for one hour at room temperature. Cells were washed three times with PBS. Coverslips were washed twice with dH_2O and mounted to coverslips with mowiol containing 4',6-diamidino-2-phenylindole (DAPI). Confocal images were taken using a Leica SP8 scanning confocal micrsoscope.

2.2.17 Visualisation of released viral particles by transmission electron microscopy (TEM)

Stocks of virus were diluted to 4x10^{7}pfu/ml and inactivated using a UV radiation. A carbon coated 200 mesh copper grid was inverted onto a 20 µl drop of diluted virus. Virus was adsorbed for 15 minutes. The sample was washed by inverting the grid onto three successive drops of TEM phosphate buffer, each wash was incubated for 15 minutes. Samples were fixed for 30 minutes with 3% glutaraldehyde. Samples were washed three more times with dH_2O. The samples were stained using a 1% uranyl acetate solution for 1 minute. Stained samples were air-dried. Samples were imaged using a Jeol 2100 transmission electron microscope. Sample processing and imaging was performed by Neal Leddy.

2.2.18 Spinoculation assay for immunofluorescence

Stocks of virus were diluted to 4x10^{7}pfu/ml. A549 cells on coverslips were washed with cold PBS and 200 µl of virus was added to them. Virus was centrifuged onto cells at 500

RCF for 30 minutes at 4°C. Cells were washed twice with cold PBS and fixed with 4% formaldehyde for 30 minutes at 4°C. Anti-Vic75 HA was diluted 1:100 in blocking buffer, added to the cells and incubated for one hour at room temperature. Cells were washed three times with PBS. Cells were incubated with blocking buffer for 30 minutes at room temperature. Protein-A FITC conjugate was diluted 1:200 in blocking buffer and incubated with cells for one hour at room temperature. The coverslips were washed with dH_2O and mounted to coverslips using mowiol. Stained virus was observed using a Leica SP8 confocal microscope.

2.2.19 Spinoculation assay for flow cytometry

Stocks of virus were diluted to $4x10^7$pfu/ml. A549 cells were washed with cold PBS and 200 µl of virus was added to them. Virus was centrifuged onto cells at 500 RCF for 30 minutes at 4°C. Cells were washed twice with cold PBS, then trypsinised at room temperature. Once cells were in suspension, they were centrifuged for five minutes at 300 RCF. The cell pellet was resuspended in a 1:100 dilution of anti-Vic75 HA and incubated for one hour at room temperature. Cells were vortexed every fifteen minutes. Cells were centrifuged and washed three times with blocking buffer, each time vortexing for ten seconds and centrifuging for five minutes at 300 RCF. The cell pellet was resuspended in a 1:200 dilution of protein-A FITC conjugate and incubated for one hour with vortexing every fifteen minutes. Cells were washed three times in PBS, with vortexing and centrifuging after each wash. Cells were resuspended in PBS. Samples were analysed in triplicate using a BD Accuri C6 flow cytometer. The flow cytometer was set to read 50,000 events and the median fluorescent signal generated was recorded. The mean and standard deviation of the median fluorescent signal was calculated and reported. Negative controls consisted of cells that did not have virus added. The values of the negative control were not deducted from the reported values.

2.2.20 Segment 7 mRNA and vRNA quantification

MDCK cells were infected with viruses at an MOI: 10^{-4}, input titres were confirmed by plaque assay. Viruses were adsorbed for one hour and washed with PBS, replaced with IM and incubated for either 4 or 6 hours. After these times, triplicate wells of infected cells were harvested. Using the QIAGEN RNeasy RNA extraction kit, cells were lysed using pre-chilled lysis buffer with 10% mercaptoethanol and incubated at 4°C for 10

minutes. The lysate was mixed 1:1 with pre-chilled 70% ethanol, added to spin columns, and centrifuged at 4,000 RCF for 15 seconds. The spin-through was discarded and the columns were washed with wash buffer. Columns were spun for 15 seconds at 4,000 RCF. Columns were washed with wash buffer and spun for 15 seconds at 10,000 and the spin-through discarded. Columns were washed again with wash buffer and spun for 1 minute at 4,000 RCF. 20 µl of dH_2O was added to the filter in the column and incubated on ice for 2 minutes, then spun at 4,000 RCF for 15 seconds. RNA was reverse transcribed using a Superscript™ reverse transcriptase (RT) kit. vRNA cDNA was generated using the Universal 1 F primer. mRNA was generated using the M2/M42 R primer. Each reaction had the following: 0.5 µl of 10 µM primer, 2 µl RNA, 2.5 µl 10 mM dNTPs mixture, 2.5 µl dH_2O. This mix was incubated for 5 minutes at 65°C and for 1 minute at 4°C. The following was added to the mixture: 2 µl of buffer, 0.5 µl 0.1 M 1,4-Dithiothreitol (DTT), 0.5 µl RT. Reaction mixtures were incubate at 55°C for 55 minutes and then at 70°C for 15 minutes. For the qPCR reactions the following was used per reaction, the following was added: 1 µl of cDNA, 5 µl of Luna reaction mix, 0.5 µl of Luna RT, 0.8 µl of 10 µM forward and reverse primers, 2.7 µl of dH_2O. The reaction parameters were as follows: 55°C for 10 minutes, 95°C for 1 minute, then 40 cycles of 95°C for 10 seconds and 60°C for 30 seconds using an Applied Biosystems Step one plus™ real-time PCR machine.

2.2.21 Quantification of genetic segments by qPCR

Stocks of virus were diluted to $4x10^7$pfu/ml. 200 µl of the virus dilution was extracted and processed as outlined in section 2.2.11. RT-qPCR was performed using a Luna® universal one-step RT-qPCR kit. Triplicate wells were set up for each genetic segment with the following: 4 µl of reaction mix, 1.6 µl of 10 µM of forward and reverse primers, 3.4 µl dH_2O. Extracted RNA was diluted 1:2. For each virus, triplicate reactions for each segment were run. For the qPCR reactions the following was used per reaction, the following was added: 1 µl of diluted RNA, 5 µl of Luna reaction mix, 0.5 µl of Luna RT, 0.8 µl of 10 µM forward and reverse primers, 2.7 µl of dH_2O. The reaction parameters were as follows: 55°C for 10 minutes, 95°C for 1 minute, then 40 cycles of 95°C for 10 seconds and 60°C for 30 seconds using an Applied Biosystems Step one plus™ real-time PCR machine.

2.2.22 Determining stability of viruses in aerosolised droplets

The *in vitro* transmission (IVT) system was developed to determine the stability of viruses contained in aerosolised droplets that are carried along an airflow. The initial temperature and relative humidity RH was recorded. Airflow was generated using an EMMS AIR 14X series bias flow generator, and set to generate a flow rate of 1 litre/minute. The IVT was initially primed by nebulising 20 µl of PBS using an Aerogen® Pro nebuliser. The airflow was switched-on and once it reached 1 litre/minute the nebuliser was switched-on. PBS was nebulised for 15 seconds and the nebuliser was switched-off. The airflow was stopped after 5 minutes. This was repeated with PBS once. Another run with the buffer in which the viruses were diluted was performed for five minutes. The IVT was then primed with 20 µl of nebulised virus and the airflow run for five minutes. Three six-well plates containing 200 µl of overlay media per well were added to the IVT at specific distances from the nebuliser. 20 µl of virus was nebulised and the airflow run for five minutes. The plates were removed and incubated for 55 minutes at 37^{o}C, cells were then washed with PBS and overlayed with plaque assay media. Three replicate exposures were performed for each virus. Once the triplicate exposures had been performed for the first virus, the IVT was purged twice with nebulised PBS. The IVT was opened and the RH was allowed to drop to match the initial reading within ±5% RH. The procedure was repeated for the second virus being tested.

Chapter 3: Effect of virion morphology on the replication of IAV in immortalised cells.

Our approach to investigate the effect that morphology has on IAV was to generate reassortant and isogenic viruses that had different morphological phenotypes using reverse genetics. A H3N2 strain that produces filamentous viral particles was mutated so that it would only generate spherical particles from infected cells by swapping the M segment of a spherical-producing strain with that of a filamentous-producing one. The amount of mutations to achieve this was kept to a minimum to limit the effects of silent phenotypes that might affect analyses. The relative growth capacities of filamentous- and spherical-producing viruses were investigated to ascertain if the adoption of a spherical-producing phenotype would confer a replication advantage to the virus when replicating in immortalised monoculture cells. Point mutations and their effects on morphology and viral replication were also investigated

3.1 Generation of isogenic Vic75 WT viruses.

To start characterising the biological significance of influenza virus morphology we first needed to create viruses that were genetically similar but differed in their morphology. A twelve-plasmid reverse genetics system (see section 2.2.6) was used to create isogenic viruses of the strain Vic75. Vic75 WT was generated using this system and the original plasmids that were a kind gift from Prof. Wendy Barlcay. The mutant Vic:PR8M was generated in the same way but the segment 7 with the sequence of another virus, PR8 WT, was used. The M1 and M2 proteins of Vic75 WT and PR8 WT differ by 8 and 11 amino acids respectively. Cells infected with Vic75 WT produce extended filamentous bundles of virus particles that can extend in excess of 10 μm in length (Elleman and Barclay, 2004). Conversely, cells infected with PR8 WT produce uniformly spherical virus particles (Liu, Muller and Ye, 2002). Previous reports have shown that by swapping segment 7 of a filament-producing strain with that of a spherical-producing strain, the resulting virus will produce spherical-only virions (Roberts, Lamb and Compans, 1998; Bourmakina and García-Sastre, 2003; Elleman and Barclay, 2004). The predicted virion shapes for these two viruses are illustrated in Figure 3.1.

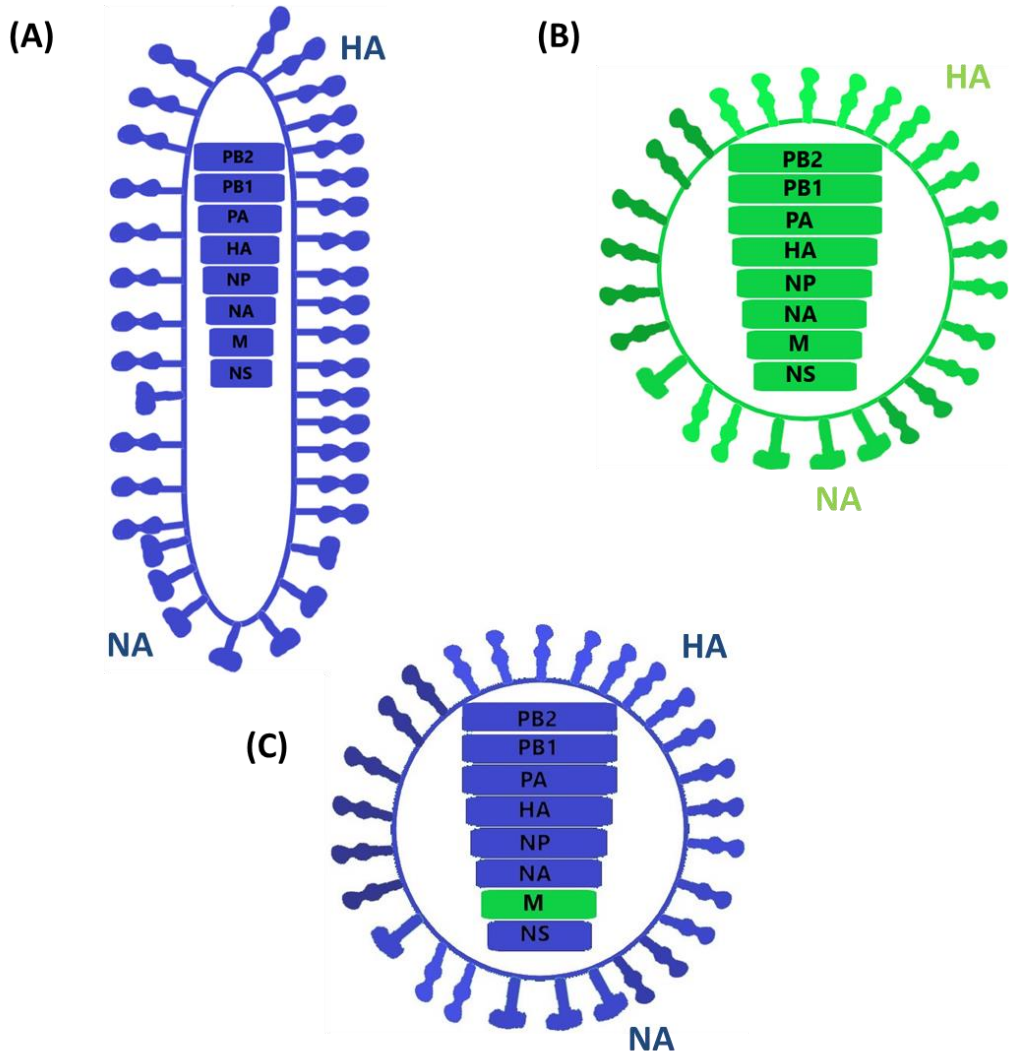

Figure 3.1: Diagram of mutant viruses generated through reverse genetics. (A) Cartoon representation of a filamentous virion with a Vic75 WT genome. (B) A spherical virion with a PR8 WT genome. (C) Mutant virus that has been generated using 7 genetic segments from Vic75 (blue) and the M segment from PR8 WT.

3.2 Segment 7 of the IAV genome is sufficient to determine the morphology of budding virions.

The first task was to confirm the morphology phenotypes of the two viruses. Figure 3.2 shows immunofluorescence microscopy images of two different types of immortalised cell lines, MDCK and A549 cells, that have been infected with either Vic75 WT or Vic:PR8M at an MOI: 1. Infected cells were stained with anti-Vic75 HA antibody at 16 hours post infection, fixed and then counter-stained with a FITC-conjugated secondary antibody. In agreement with previous observations (Roberts, Lamb and Compans, 1998; Bourmakina and García-Sastre, 2003; Elleman and Barclay, 2004), Vic75 WT produced long filamentous virus structures that normally occurred as bundles (see arrows) in both cell types. Conversely, only punctate staining was observed in Vic:PR8M infected cells, which is typical of budding spherical particles.

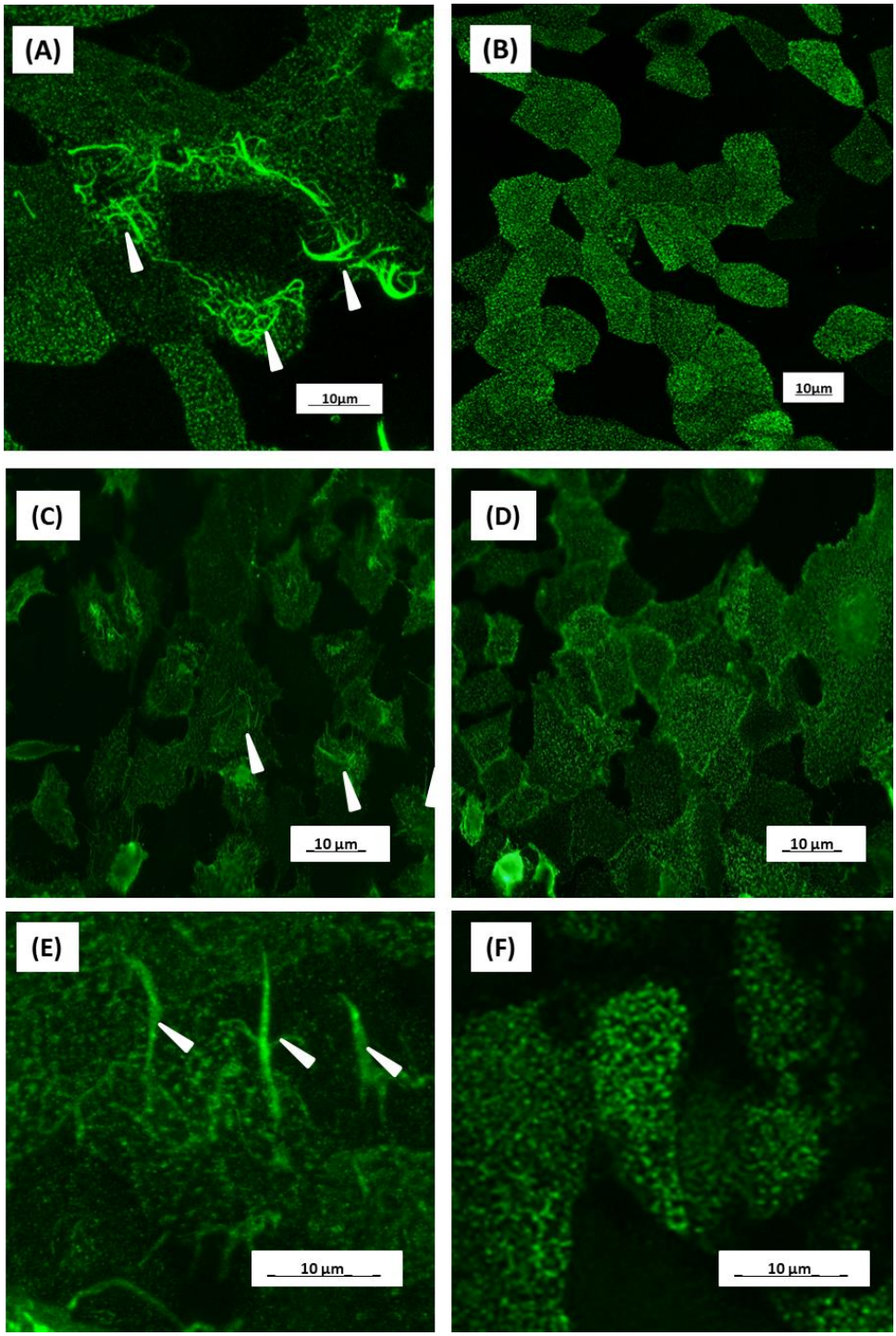

Figure 3.2: Cell associated virion morphology of isogenic Vic75 viruses in MDCK and A549 cells. (A, B, E, F) MDCK and (C, D) A549 cells were infected at an MOI: 1 with (A, C, E) Vic75 WT and (B, D, F) Vic:PR8M. At 16 hours post infection cells were fixed and immunostained using ferret anti-sera raised against Vic75 WT virus. Cells were counter-stained with a protein A conjugated to FITC. (A, B, C, D) 40X magnification. (E, F) 63X magnification. Images were taken using a Leica S8 scanning confocal Microscope. Arrowheads indicate budding filamentous virions N:3

3.3 Spherical morphology correlates with increased replication kinetics in immortalised cell lines.

The loss of a filamentous morphology upon serial passage *in vitro* in eggs or immortalised cells has been commonly observed (Burnet and Lind, 1957; Seladi-Schulman *et al*., 2013). This adoption of a spherical-only phenotype correlates with increased replication of the spherical variant *in vitro* (Bialas *et al*., 2012; Seladi-Schulman *et al*., 2013). As such, we hypothesised that by adopting a spherical morphology, the Vic:PR8M mutant would grow to higher titres in a multi-step growth curve. For figure 3.3, MDCK or A549 cells were infected at an MOI: 0.0001. Supernatant from infected cells was collected at the indicated times post infection and the amount of each virus was determined by plaque assay titration. In both cell types, Vic:PR8M infected cells produced significantly greater levels of infectious viral particles, at all time points, than Vic75 WT. In MDCK cells this difference was the greatest at earlier time points, with the greatest difference between the two viruses at 24 hpi, where there was 1085-fold greater amount of Vic:PR8M virus particles released from infected cells. Vic:PR8M also grew to higher levels in A549, but the difference in the growth profile was not as great as in MDCK cells. The greatest difference in infectious titre in A549 cells was at 48 hpi, where there was 122-fold more Vic:PR8M generated from infected cells. Therefore, as previously published, Vic:PR8M had a replicative advantage over the filamentous Vic75 WT virus. As well as growing to higher titres in a multi-step growth curve, Vic:PR8M generated larger plaques than Vic75 WT in infected MDCK cells. Plaque assay plates were stained 72 hpi. Images of plates with cells that had been infected with either Vic75 WT or Vic:PR8M were visualised using Microsoft paint. Sizes of plaques were calculated by determining the number of pixels that a given plaque was. This was done for thirty plaques for either virus. The mean size and standard deviation were calculated and are shown in figure 3.3 (C).

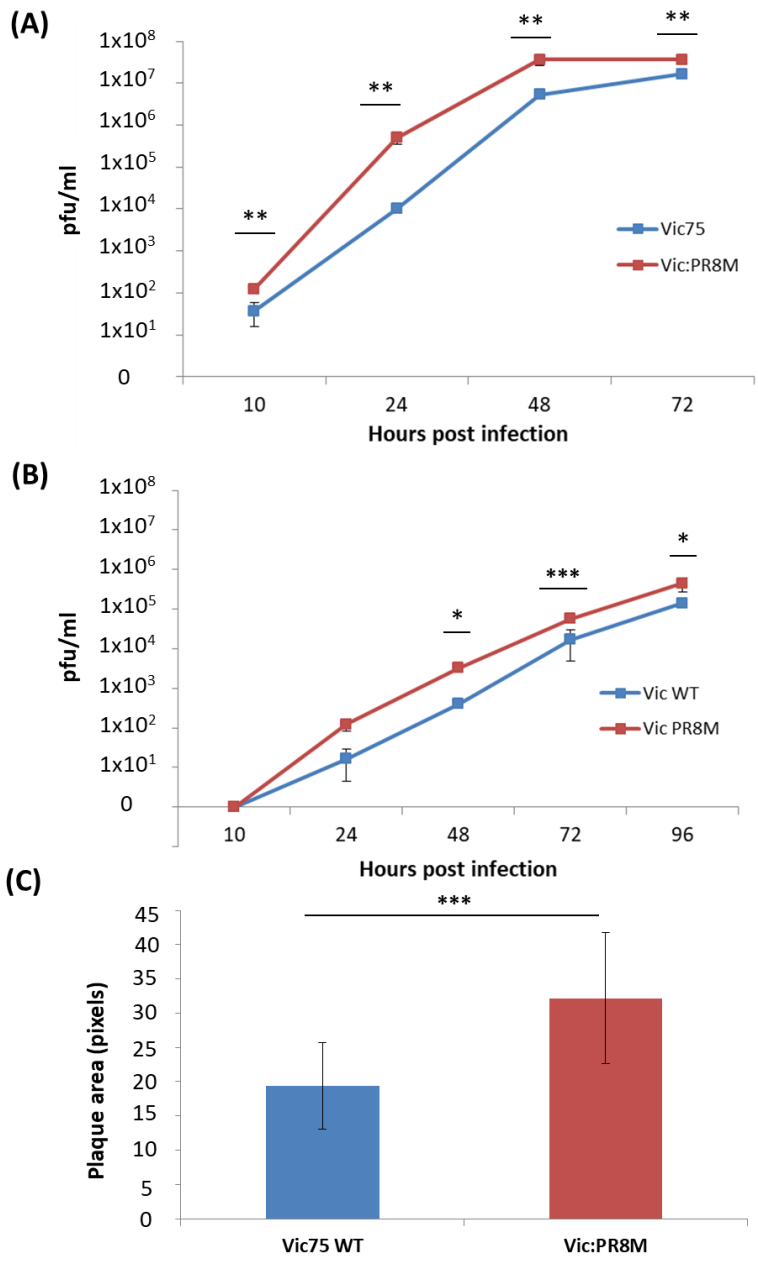

Figure 3.3: Vic:PR8M replicates to higher titres than Vic75 in immortalised cell lines. (A) MDCK or (B) A549 cells were infected at an MOI: 0.0001. Supernatants from infected cells were taken from triplicate wells at the times indicated and viral titres determined by plaque assay. Mean pfu values are plotted and error bars represent standard deviation from the mean. (C) Plaque size. The sizes of plaques from infected MDCK cells were calculated by visualising images of plaque assay plates in Microsoft paint. The size in pixels was calculated for 30 randomly selected plaques for either virus. *, **, and *** represent p. values less than: 0.05, 0.01 and 0.001 respectively as determined by a two-tailed students T test. (A) N:3 (B) N:1 (C) N:3.

3.4 At a low MOI, filamentous particles are produced much later in Vic75 WT-infected cells.

As the greatest difference in the growth profiles between the two viruses in MDCK cells was at 24 hpi, we were interested to repeat the multi-step growth curve and focus on early times post infection. Cells were infected at an MOI: 0.0001 and the titres of released virus and morphology of budding virions was determined at 6, 8, 10, 12 and 24 hpi. Interestingly, at this low MOI, budding filamentous virus particles were not observed until 24 hours post infection (see figure 3.4 A). This suggests that under these conditions, filaments begin to form sometime between 12 and 16 hpi (see figure 3.2 and 3.4 A), which could suggest that filamentous particles are delayed in budding compared to spherical ones. Previous studies have observed this phenotype as early as 9 hours post infection (Roberts, Lamb and Compans, 1998). It should be noted that when the filamentous phenotype was observed at earlier time points, the cells had been infected at high MOIs.

As before, Vic:PR8M grew to higher titres than Vic75 WT at early time points. Figure 3.4 (B) shows the amount of virus released into the supernatant by either virus at 6, 8, 10, 12 and 24 hpi. The typical time frame for a full replication cycle of IAV is 8 hours (Frensing *et al.*, 2016). At 8 hpi there was 4.6-fold more virus released from Vic:PR8M-infected cells than Vic75 WT-infected cells. Thus, in a single round of replication, Vic:PR8M generated 4.6-fold more virus from infected MDCK cells. The titre for both viruses increases at the next time point (10 hpi) and plateaus at this level to the next time point (12 hpi). This shows that the cells that were initially infected release a steadily increasing amount of virus following the initial burst at 8 hours that then plateaus after 2 hours, meaning that the amount of virus being produced by this group of cells reaches a threshold capacity. It is interesting to note that the fold difference at 8 hours is 4.6 but only 2 at 10 and 12 hpi. This suggests that in a single round of replication, the Vic:PR8M is more efficient at immediately releasing virus particles, and that there is a slight delay in release of virus particles from Vic75 WT infected cells. It also suggests that Vic:PR8M generates double the total amount of virus per infected cell in a single round of replication (as measured at 10 and 12 hpi). The lack of filamentous virions seen before 24 hpi suggests that the differences in virus replication are independent of virion

morphology, because there is a difference in viral titre without the generation of filamentous particles.

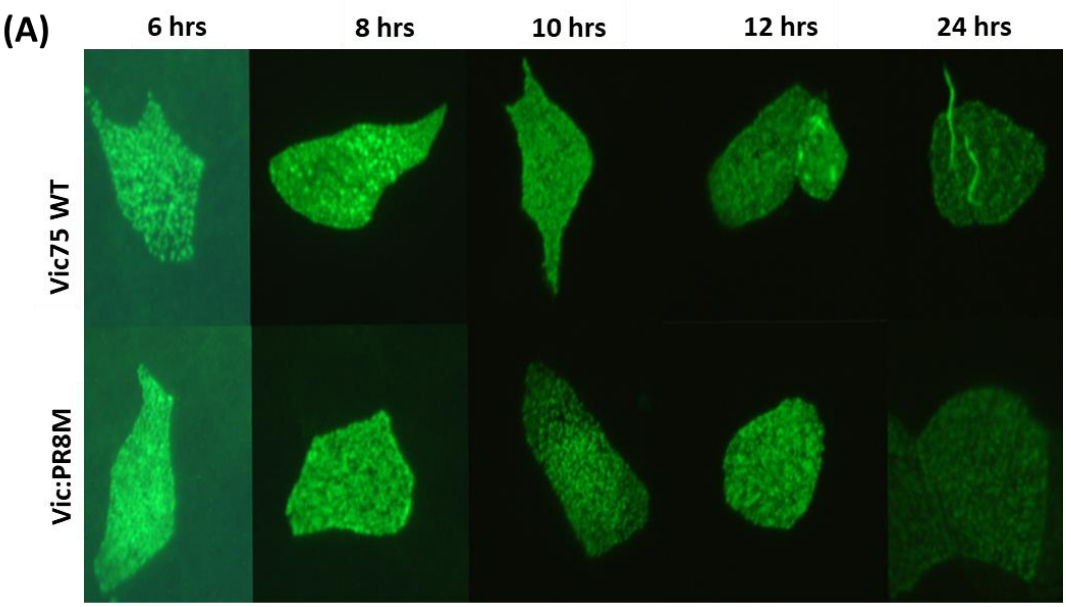

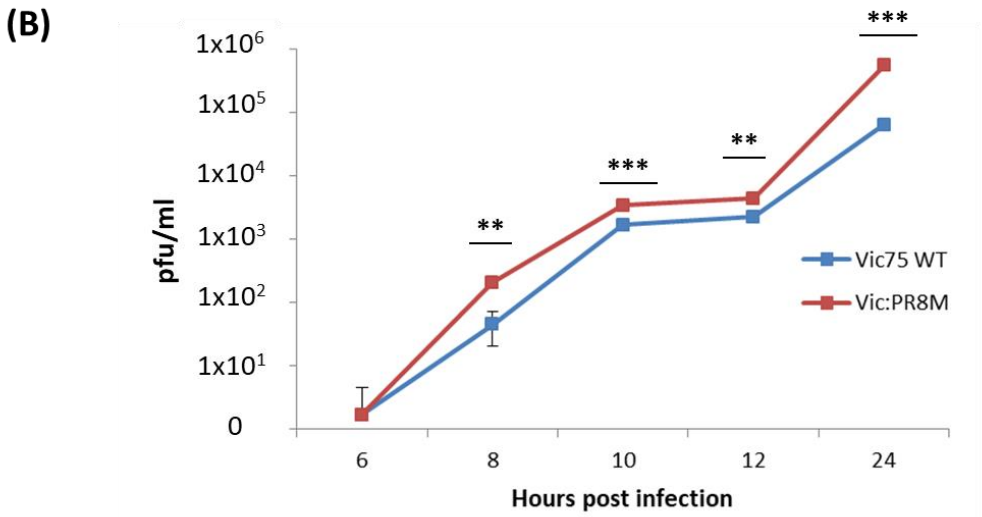

Figure 3.4: Effect of M gene segment on replication kinetics and morphology early in infection. MDCK cells were infected at an MOI: 0.0001. (A) Immunofluorescent images taken of infected cells showing morphology of viral particles budding from them. N:3 (B) Titres of virus generated from infected cells at indicated time points. N:3. *, **, and *** represent p. values less than: 0.05, 0.01 and 0.001 respectively as determined by a two-tailed students T test.

3.5 The difference seen in replication capacity of Vic75 WT and Vic:PR8M is not dependent on morphology of budding virions.

Another interpretation for the difference in titre seen in figure 3.4 (B) is that the production of filamentous particles is delayed and this is why Vic:PR8M grew to higher titres. To confirm that differences in virus replication are independent of differences in virion morphology, growth curves paired with immunofluorescent microscopy of both viruses at low and high MOIs were performed (Figure 3.5). In agreement with the data in figure 3.4, Vic:PR8M grew to higher titres than Vic75 WT at both MOIs. At low MOI, filamentous particles produced by Vic75 WT infected cells were only observed at 24 hpi (Figure 3.5 C). Interestingly, at an MOI: 3, Vic75 WT produces filamentous particles at 8 hpi and at all other time points recorded (Figure 3.5 C). The fold-difference in viral titre between Vic75 WT and Vic:PR8M at 8 hpi in cells infected at an MOI: 3 is similar to the fold difference to that seen in cells infected at an MOI: 0.0001 which were 1.8 and 2.2 respectively (Figure 3.5 A and B). This suggests that the relative difference in replication capacity of Vic75 WT is the same in the absence or presence of filaments and so the production of extended, 10 μm long filamentous bundles is not contributing to the difference in viral titres for the two viruses. The increased difference at 24 hpi compared to 8 hpi in cells infected at an MOI: 0.0001, here Vic:PR8M had a 2.2-fold greater amount of virus at 8 hpi and 15-fold more at 24 hpi infection, is most likely the compounded viral titre accumulated over 3 rounds of replication of Vic:PR8M. The increased amount of virus at 24 hpi most likely results from an increased amount of cells infected after the first round of replication and the fact that Vic:PR8M produces more virions per infected cell. This is underpinned by the differences seen in the growth profiles of Vic75 WT and Vic:PR8M when cells were infected at an MOI:3 where the fold differences at 8, 10, and 24 hpi were 1.8, 1.2 and 2.4 respectively. The titres did not increase as they did when cells were infected at an MOI: 0.0001, where the fold differences at 8, 10, and 24 hpi were 2.2, 1.9 and 15.5 respectively. The fold difference between viruses at an infection of MOI: 3 did not increase because the growth advantage that Vic:PR8M had was not compounded over multiple rounds of replication, because at this MOI, 95% of cells would have been infected at time 0, as described by the Poisson distribution.

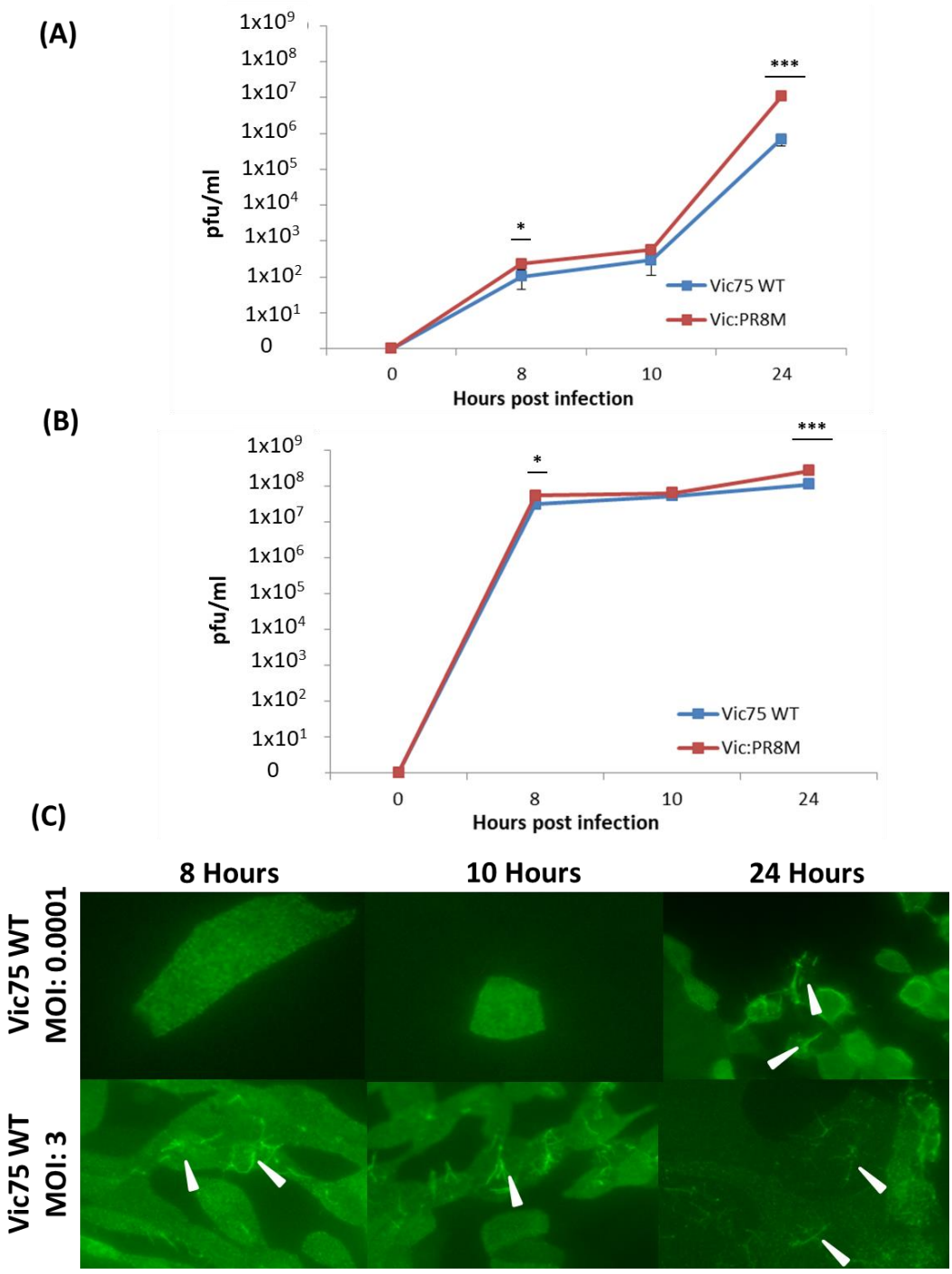

Figure 3.5. Vic 75 WT grows to lower titres compared to Vic:PR8M regardless of budding morphology. (A) MDCK cells were infected at an MOI: 0.0001 and (B) MOI: 3. Supernatants were collected at indicated time points and titrated by plaque assay. (C) MDCK cells were infected at the indicated MOI, and immunofluorescent images taken at the indicated times post infection. *, **, and *** represent p. values less than: 0.05, 0.01 and 0.001 respectively as determined by a two-tailed students T test. Arrowheads indicate budding filamentous virions N:3

3.6 Vic75 WT and Vic:PR8M generate the same amount of segment 7 mRNAs but different amounts of vRNA.

As the morphology of budding virions was not the cause of the increased replication kinetics of Vic:PR8M, or more specifically, the reduced replication kinetics of Vic75 WT, we were interested to investigate what other stages of the viral replication cycle might be affected. Filamentous IAV particles solely utilise macropinocytosis to enter cells (Rossman, Leser and Lamb, 2012), they are too big to enter by endocytosis. It is possible therefore that there might be a delay in the translocation of vRNPs to the nucleus to begin the cycle of replication. As such we were interested to investigate the relative levels of mRNA and vRNA production in infected cells, with the assumption that greater levels of RNA would accumulate quicker if vRNPs translocated sooner. Figure 3.6 shows the amounts of segment 7 mRNA and vRNA in either Vic75 WT- or Vic:PR8M-infected cells at 4 and 6 (hpi). This data shows that there is no difference in the amounts of mRNA produced in cells infected with either virus at either 4 or 6 hours. This suggests that there is no delay in production of mRNA seen for either virus. It also suggests that neither virus has a greater propensity to produce mRNA once RNA replication has begun. Cells infected with Vic75 WT had twice as much vRNA as cells infected with Vic:PR8M at 6 hpi. At 6 hpi, Vic75 WT had 1.7 fold more segment 7 vRNA. While this was a modest difference, it was statistically significant. This difference is interesting when compared to the relative levels of segment 7 mRNA for either virus, where there was no difference in the amount of mRNA generated by either virus. It suggests that more segment 7 vRNA is produced in Vic75 WT-infected cells.

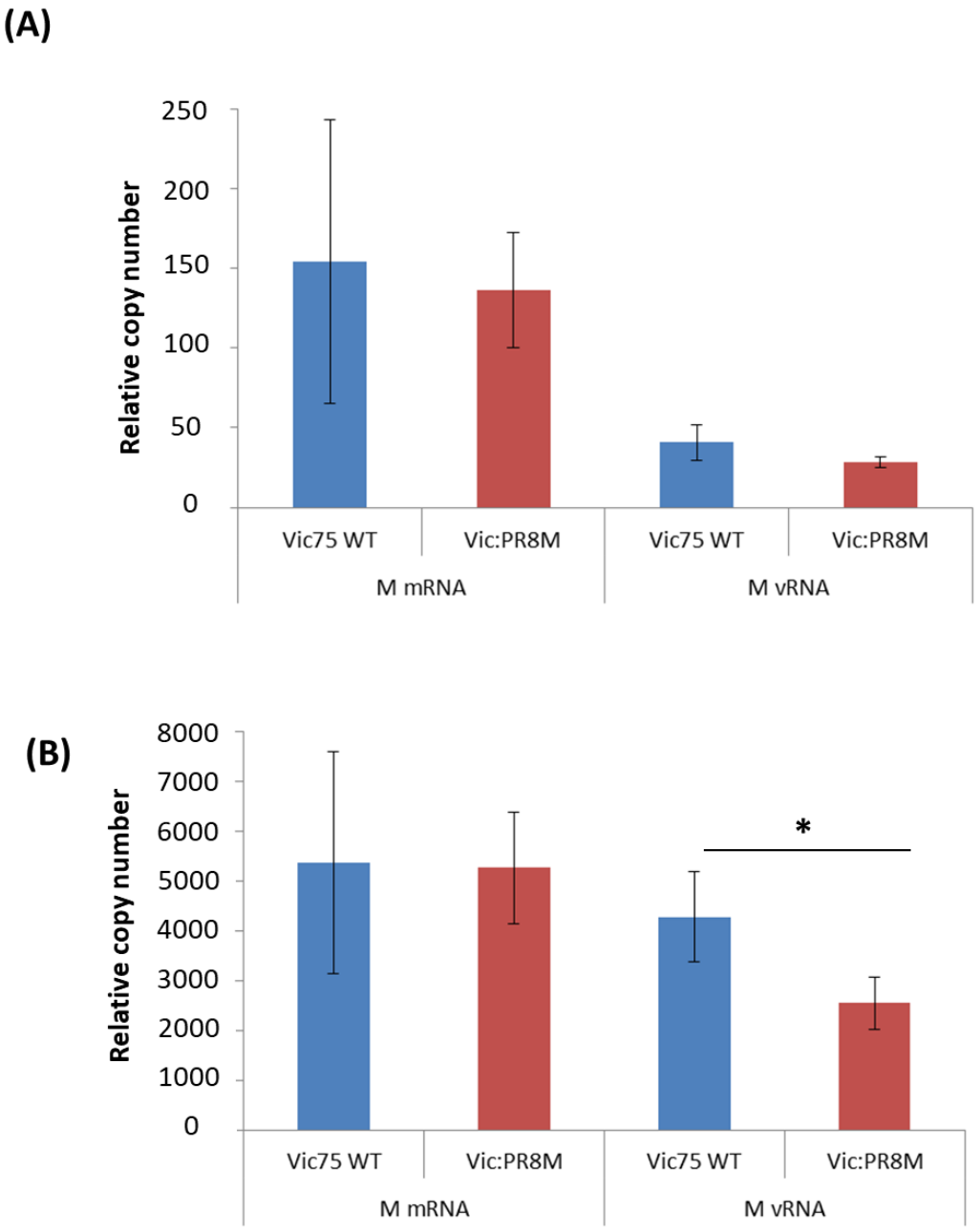

Figure 3.6: Vic75 WT and Vic:PR8M produce the same amount of M mRNA, but Vic75 WT generates two-fold more M vRNA at 6 hpi. MDCK cells were infected at an MOI: 0.0001. Infected cells were lysed and RNA extracted at (A) 4 hours and (B) 6 hours post infection. cDNA was generated from extracted RNA using primers directed against the 3' end of both M segment vRNA or mRNA. Relative levels of cDNA were quantified by qPCR. * represents a p. value > 0.05. N: 3

3.7 Alternative ORFs within segment 7 of the IAV genome

The data presented thus far suggests that the PR8 segment 7 confers a replication advantage in MDCK cells. To begin to understand the cause of this, we decided to introduce single nucleotide mutagenesis to segment 7 of Vic75 WT. One difference between the segment 7 of Vic75 WT and PR8 WT is at residue 41 of the M1 protein. Vic75 WT encodes an alanine at this position while PR8 WT encodes a valine. While this is a relatively innocuous amino acid substitution, it has been shown to be sufficient to induce a spherical-only phenotype in Vic75 WT (Elleman and Barclay, 2004), but interestingly not in a closely related strain A/Udorn/301/72 (Bourmakina and García-Sastre, 2003). Expression of a valine is disproportionally overrepresented for the residue at position 41 of the M1 protein in laboratory-derived strains of IAV when compared to strains isolated from natural hosts (Table 3.1).Therefore, we decided to investigate the effect that this mutation may have on morphology as it is so markedly under-represented in naturally-derived strains and over-represented in laboratory-derived ones. By altering the nucleotides in the codons for residue 41 and the surrounding codons it was found that expression of a novel protein called M42 could be induced (Wise *et al.*, 2012). This protein was found to completely restore replication competence to a mutant virus that was unable to express M2. M2 is closely linked to the budding of IAV, and in some models is postulated to mediate the scission event that releases the viral membrane from the cellular one (Rossman and Lamb, 2011). Thus, we were interested to investigate the effect that this mutation might have on morphology.

Figure 3.7 outlines the rationale for mutagenesis to the Vic75 WT segment 7. Figure 3.7 (A) is a diagram that outlines the negative sense vRNA, the positive sense mRNA, and the predicted and experimentally proven polypeptides generated from the mRNA as a result of RNA splicing. Start codons, splice donor and splice acceptor sites are marked for the relative locations on the mRNA. Figure 3.7 (B) outlines the sequence homology of the intended mutations and their consensus to a canonical eukaryotic splice donor site. M1 41V has the most consensus to the splice donor sequence. The M1 E40E:41V was used to discern whether any observed effects were due to expression of mRNA transcripts, or if it is due the amino acid sequence of the M1 protein. This mutant matches the amino acid profile of the M1 41V mutant, but should not express the M42 mRNA.

	Combined H1N1 and H3N2 M1 data			
	Human (Total: 16,092)	Swine (Total: 4,165)	Avian (Total: 707)	Laboratory (Total: 373)
M1 41V	0.2%	0.2%	0.3%	46.9%

Table 3.1: Percentage expression of a valine residue at position 41 of the M1 protein in different groups of isolates. This table represents the percentage of M1 gene sequences available that express a valine at position 41 of the M1 protein. Representative M1 gene sequences for H1N1 and H3N2 viruses isolated from the indicated sources were analysed for which amino acid was encoded for position 41 of the M1 protein. H1N1 and H3N2 data were pooled and the number of strains that encoded a valine was expressed as a percentage of the total amount of sequences. Sequence data taken from: www.fludb.org.

(A)

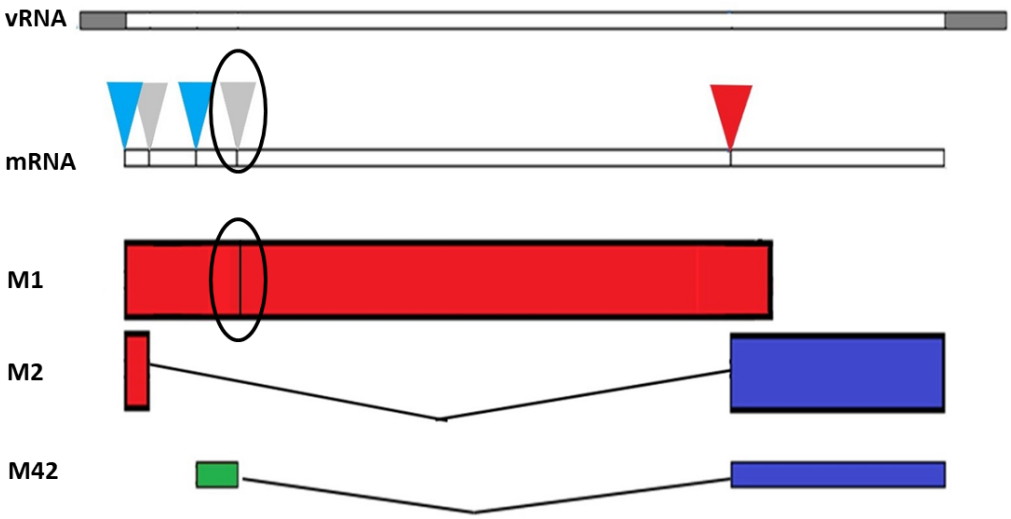

(B)

Eukaryotic splice donor site sequence:	AG/GUA
M1 A41:	AG/Gcu
M1 V41:	AG/GUu
M1 E40E:41V	Aa/GUu

Figure 3.7: Diagram of M segment mRNA transcripts and rationale for mutagenesis. (A) A representation of genomic vRNA, including the noncoding regions (dark grey) is shown. Start codons (blue arrow), splice donor sites (grey arrow) and the splice acceptor site (red arrow) are indicated on the representation of the + sense mRNA. Polypeptides generated from the mRNA are shown, with red indicating a +1 sense reading frame, blue indicating a +2 and green a +3. (B) Mutagenesis design rationale. The relevant nucleotide residues that share consensus with a typical eukaryotic splice donor site are shown, where bold signifies consensus. The location of this residue is shown on both the mRNA and M1 polypeptide by a dark oval. The line between the two guanine residues denotes were the covalent bond in the mRNA backbone is broken. The indicated mutations were introduced into plasmids encoding the Vic75 WT M gene. Mutant viruses were generated by transfection of these plasmids. Viruses were sequenced to confirm that the desired mutation had been introduced**.**

3.8 Expression of M42 transcripts by splice variant isogenic viruses.

To demonstrate that the engineered mutations had the desired effect, we investigated if the putative M42 transcript would be expressed. It was hypothesised that by mutating the splice donor site, expression of the transcript could be switched-on or –off. qPCR primers to detect splice variants were designed in the following manner: M1 primers were directed against the area of the M mRNA that is in the area removed when spliced to form the M2 mRNA. The reverse primer was directed against the 3' end of the + mRNA sequence and the forward against the 5' end of M2. The reverse primer for M42 was the same as for M2, but the forward primer was designed so that half of it bound to the sequence just upstream of the splice donor site and the other half of the primer bound to the nucleotides downstream of the splice acceptor site. MDCK cells were infected at an MOI 1 and cells were harvested at 16 hours post infection and lysed. mRNA was reverse transcribed and then the relative amounts of cDNA was quantified. cDNA was generated using a primer directed against the 3' end of the + mRNA sequence (Section 2.2.20). The relative copy numbers of the cDNA generated are shown in figure 3.8.

For all three viruses, there was 10-fold more M1 mRNA than M2 in all virus samples (Figure 3.8). The same amount of M1 and M2 mRNA species was seen for all three viruses. The level of M42 mRNA generated by the 41V mutant was the same as M2 mRNA. M42 mRNA expression for Vic75 WT and the E40:41V mutant was at the level of the negative control (figure 3.8). Thus, by substituting the nucleotide at position 146 in segment 7 of Vic75 WT, expression of a novel mRNA can be induced. It is interesting to note that by ostensibly doubling the amount of mRNA being produced from the pool of progenitor M mRNA, the relative levels of M1 and M2 do not drop in Vic75 41V infected cells.

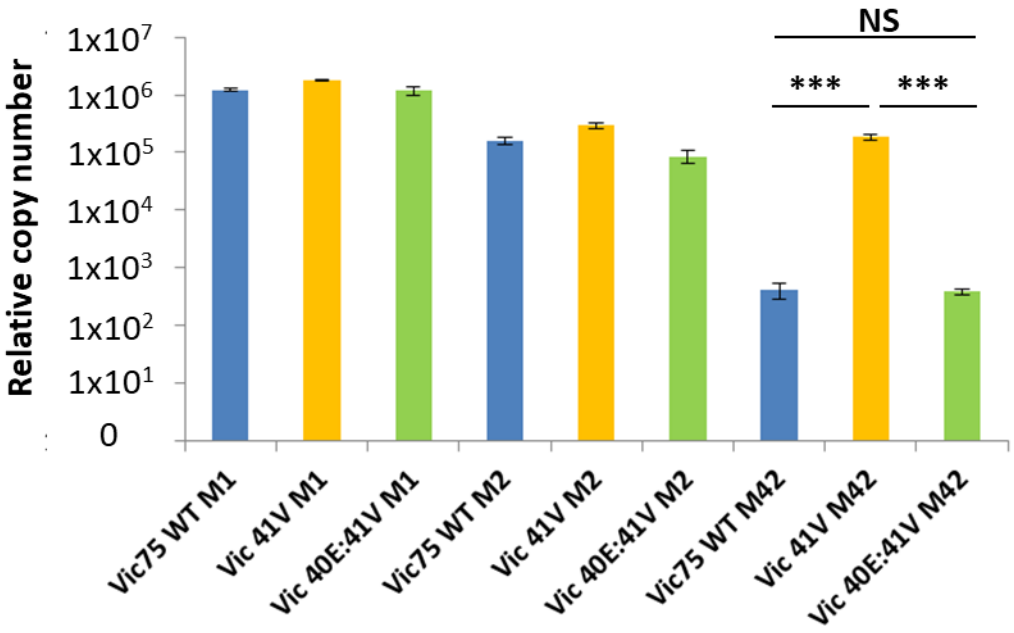

Figure 3.8: Vic 41V has significantly increased levels of M42 expression compared to Vic75 WT or Vic40E:41V. MDCK cells were infected at an MOI: 1. 16 hours post infection cells were harvested, lysed and RNA was extracted. cDNA was generated by targeting a primer against the 3' end of the full length M mRNA. qPCR was performed on this cDNA with primers directed specifically against RNA species containing sequences unique to: M1, M2 or M42. N:3

3.9 Amino acid residue 41 of the M1 protein determines the morphology of budding virus particles.

It was demonstrated that the M1 A41V mutation generated a transcript that was amplified by primers directed specifically against the putative M42 transcript originally described by (Wise *et al.*, 2012). It has been shown previously that this mutation resulted in the switch of a filament-producing virus to a solely spherical-producing one (Elleman and Barclay, 2004). We were interested to determine if this mutation was able to change the morphological phenotype and if this was the result of the expression of the M42 mRNA transcript. MDCK cells were infected at an MOI: 1 with the viruses indicated (Figure 3.9). Infected cells were stained with anti-Vic75 HA antibody at 16 hours post infection, fixed and then counter-stained with a FITC-conjugated secondary antibody (see section 2.2.15). Vic75 WT produced long filamentous virus structures that normally occur as bundles. Cells infected with Vic75 41V produced punctate staining which closely resembles the spherical budding phenotype seen for the Vic:PR8M virus (Figure 3.2). A similar spherical phenotype was seen in Vic75 E40:41V infected cells. Thus, as previously reported (Elleman and Barclay, 2004), expression of a valine at position 41 of the M1 protein in Vic75 is sufficient to confer a spherical-only budding virion phenotype. This appears to be independent of the expression of the M42 open reading frame, because Vic75 41V and Vic75 E40:41V share the same morphological phenotype but Vic75 E40:41V does not express the M42 transcript. It therefore appears that the morphology of budding virus particles can be determined by residue 41 of the M1 protein, and not by expression of the M42 transcript.

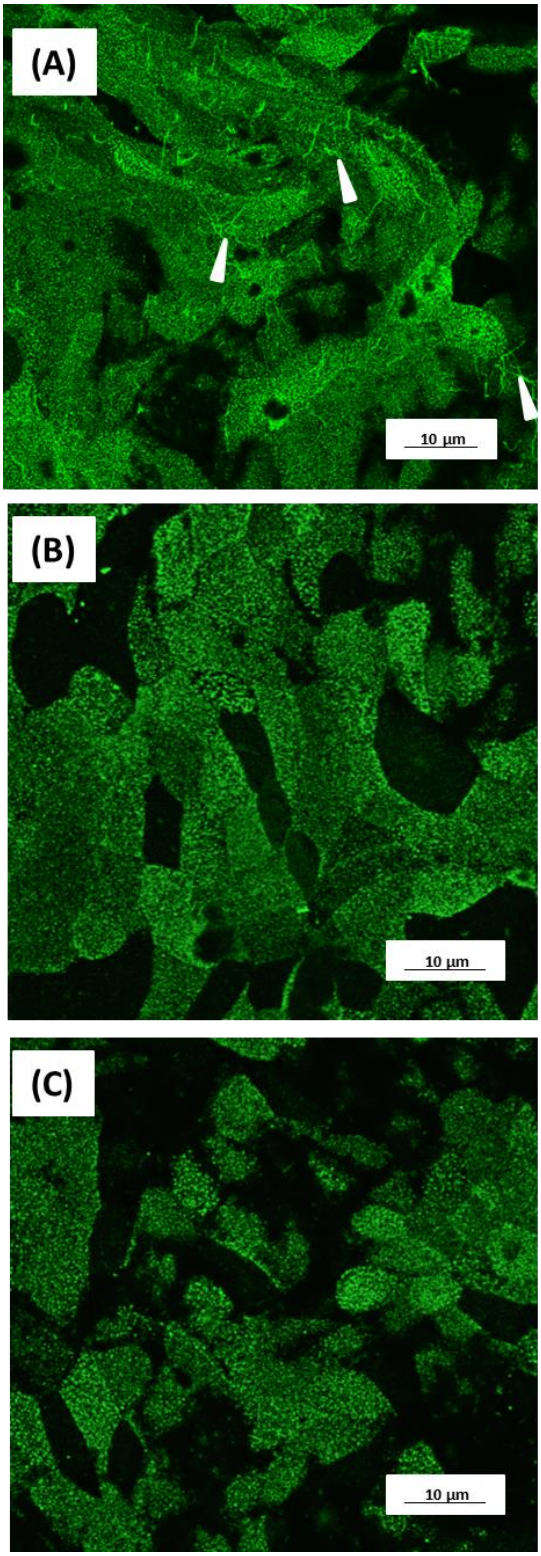

Figure 3.9: Mutagenesis of the M42 splice donor site does not affect cell-associated morphology. MDCK cells were infected at an MOI: 1 with (A) Vic75 WT (B) Vic75 41V (C) Vic75 40E:41V. Cells were fixed and stained using ferret anti-sera at 16 hours post infection. Arrowheads indicate budding filamentous structures. N:3.

3.10 Amino acid residue 41 of the M1 protein is sufficient to confer increased replication kinetics in immortalised cells.

We were interested to investigate if the M1 A41V point mutant was sufficient to confer the increased replication kinetics compared to WT. It has been shown that the difference seen in the replication kinetics of filament- and spherical-producing viruses is independent of the production of extended, 10 µm-long bundles of filamentous particles. We were interested to investigate if M1 A41V was sufficient to increase the replication capacity of the virus and if this was dependent on the expression of the M42 transcript. MDCK and A549 cells were infected at an MOI: 0.0001. Titres of infectious virus were determined at 10, 24, 48 and 72 hpi (Figure 3.10). Both Vic75 41V and Vic75 E40:41V produced significantly greater levels of infectious virus than Vic WT at 24 and 48 hpi in MDCK cells. Similarly, Vic75 41V and Vic75 E40:41V grew to significantly higher titres at 48 and 72 hpi in A549 cells. The relative replication kinetics of viruses with a filamentous phenotype (Vic75 WT) and that displaying a spherical phenotype (Vic75 41V and Vic75 40E:41V) match that seen in figure 3.3. There was no significant difference in the replication kinetics between Vic75 41V and Vic75 E40:41V in MDCK cells. Therefore the expression of the M42 mRNA doesn't increase or decrease the replicative capacity of Vic75. The increased replicative capacity is most likely conferred by the M1 protein and not by expression of the M42 transcript. Figure 3.10 (C) represents the difference the plaque sizes of Vic75 WT- or Vic 41V-infected MDCK cells. Cells were infected with 100 pfu of either virus and incubated for 72 hours with an agarose overlay. Cells were stained with crystal violet and images of the plates were assessed using Microsoft paint. Plaque areas were calculated in total amount of pixels. Vic 41V consistently generated larger plaques. The difference in plaque size is in agreement with the data shown in figure 3.3 (C), where Vic:PR8M generates significantly larger plaques. Plaque size was not calculated for Vic 40E:41V

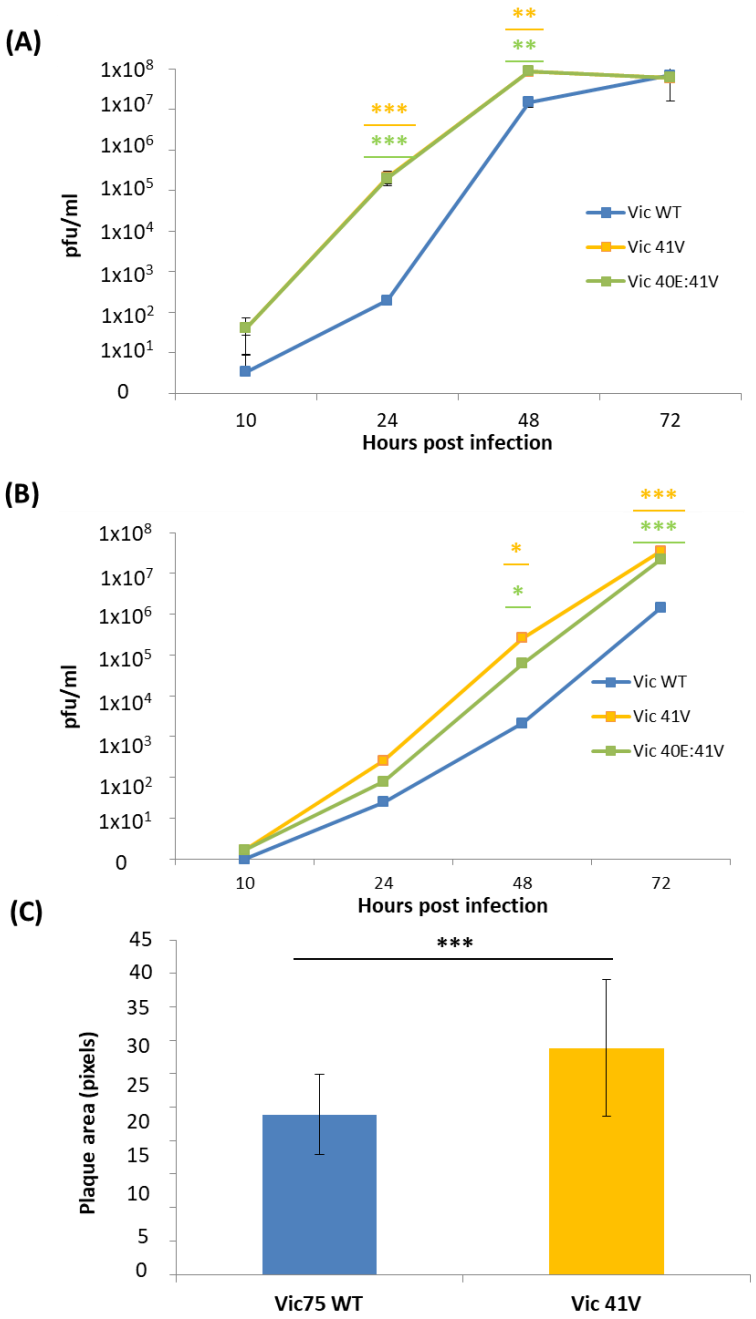

Figure 3.10: Both Vic 41V and Vic 40E:41V grow to higher titres than Vic75 WT in immortalised cells. (A) MDCK and (B) A549 cells were infected at an MOI: 0.0001. Supernatants were collected at indicated time points and titres determined by plaque assay. (C) Plaque size in MDCK cells infected with either Vic75 WT or Vic 41V. The sizes of plaques from infected MDCK cells were calculated by visualising images of plaque assay plates in Microsoft paint. The size in pixels was calculated for 30 randomly selected plaques for either virus. *, **, and *** represent p. values less than: 0.05, 0.01 and 0.001 respectively as determined by a two-tailed student's t-test. N: 3

3.11 Chapter 3 discussion.

We have demonstrated that a budding filamentous morphological phenotype correlates with, but is not solely responsible for reduced replication kinetics in MDCK cells when compared to a spherical-producing variant (Figure 3.5). This agrees with an observation made by Roberts and Compans, 1998, where they found that by treating cells with cytochalasin D they could inhibit the production of filamentous particles and this did not significantly affect the titres of released virus. The data presented here agrees with the replicative capacity seen by Roberts *et al*., 1998. The authors found that there was no difference in titres of viruses from cells infected with a filamentous strain or a mutant harbouring a M1 A41V mutation. While we noted significant differences in the titres of virus at early time points post infection of either Vic75 WT or Vic41V, there was no difference at 72 hpi, in infected MDCK cells (Figure 3.10). This matches the observation made by Roberts *et al*., 1998, as they only investigated an end-point titre. This effect was not seen in A549 cells, but that is presumably due to the fact that viral growth had not yet plateaued at the final time point tested (Figure 3.10 C). The differences in plaque size between a filamentous virus and one harbouring a M1 A41V is in agreement with previous studies (Elleman and Barclay, 2004).

The increased replication capacity seen for Vic:PR8M is most likely determined at the budding stage of the replication cycle and that residue 41 of the M1 protein is involved with this. While the impact of these mutations on budding efficiency has not been directly demonstrated within the work outlined in this thesis, stages leading up to viral transcription and genome replication can potentially be ruled-out as being the reason for increased replicative capacity of either Vic:PR8M or Vic75 41V because similar levels of mRNA are recorded early and midway through an infection cycle for both Vic75 WT and Vic:PR8M. Figure 3.6 shows the amounts of segment 7 mRNA and vRNA that accumulated after 4 and 6 hpi in MDCK cells infected with either virus. There is no difference in the amount of mRNA accumulated for either virus at either time. From this, one can infer that there was no delay in the translocation of vRNPs to the nucleus following endocytosis and macropinocytosis of viral particles. If there were, then it would be expected that the amount of mRNA generated at 4 and 6 hpi would be different. We speculate that the most likely cause of the difference in titre seen for

these viruses would be at the budding stage. It has been noted that the M1 protein of a spherical virion generating strain binds more avidly to vRNPs compared to the M1 protein of a filament-producing strain (Liu, Muller and Ye, 2002). It is therefore possible that by virtue of binding more strongly to vRNPs, budding would be more efficient, such that when vRNPs are transported to the cell surface where M1 is present at the lipid bilayer, a stronger interaction would increase budding efficiency.

Expression of valine at position 41 of the M1 protein is rare in clinical isolates of IAV. Strains isolated from natural hosts predominantly express an alanine at this position (Table 3.1). Interestingly, expression of a valine at this position is a commonly observed adaptation when grown either *in vitro* or in mice (Smeenk and Brown, 1994; Brown and Bailly, 1999). The M1 A41V mutation was observed when Vic75 WT virus was put under selective pressure by incubating virus with an antibody directed against the ectodomain of the M2 protein. As well as noting that the mutation resulted in a switch from filamentous to spherical morphology, the authors found that this mutant effectively grew in the presence of the anti-M2 antibody (Zebedee and Lamb, 1989). We speculate here that the reason for this is most likely that the 41V mutant was able to express the M42 protein, which is a functional homolog of M2 and does not share the same ectodomain (Wise *et al.*, 2012), and is thus unaffected by the presence of antibody while still generating viruses that bear a functional ion channel.

It has been demonstrated that viruses that have been engineered to produce cell-associated spherical-only viral particles are more efficient at growing in immortalised cells compared to a virus that produces cell-associated, extended, 10 µm in length, filamentous bundles of particles. We hypothesise that the difference seen in the replicative capacity of Vic75 WT and Vic:PR8M results from the expression of the respective proteins from either M segment, rather than due to the production of large, resource-demanding, particles. We hypothesise that that the most likely stage of replication where this effect is conferred is the assembly and budding of virus particles from the host membrane.

It has also been demonstrated that a single point mutation in the M1 protein was sufficient to both abrogate the budding filamentous phenotype and to generate the M42 mRNA transcript. Expression of this transcript and morphology of cell-associated

particles were found to be independent of one another. Thus, the mechanism by which the M1 41V mutation confers a spherical-only particle phenotype is most likely mediated by the M1 protein, presumably through self-interaction or interaction with other viral or cellular proteins.

So far, we have examined the morphology of IAV particles in a cell-associated context. Next, we were interested to investigate the effect that virus particle morphology has on virions that have been released from infected cells.

Chapter 4: Filamentous IAV particles are more resistant to inhibition by both innate- and adaptive-mediated effectors of the immune system.

One difficulty when investigating the biological significance of filamentous virions is variation between stocks of the same virus. Although the genetic make-up of the virus did not change, we found stock to stock variation in the results of some of the standard assays. It is understood that cellular factors can affect filamentous virion formation and alter the ratios of filaments to spheres in a pleomorphic stock of virus (see section 1.4.2). However, the impact of cellular growth conditions on virus morphology is not clearly defined. The phenotype difference that we were investigating affects budding of the virus, thus it was possible that the level of NIPs generated by either virus was different, depending on the cellular conditions used to produce the virus stocks. We hypothesised that differences in the results of our standard assays could be due to differences in the proportions NIPs within the stocks.

4.1 Filamentous virus particles are released from Vic75 WT but not Vic PR8M-infected cells.

When characterising the morphology of influenza virions, cell-associated virions (Figure 3.2) are often used as a proxy for released virions (Seladi-Schulman *et al*., 2013; Campbell *et al.*, 2014b). However, when investigating the biological significance of filaments we wanted to confirm that filamentous virions were released from cells and were present in infectious supernant. To do this, TEM was used to characterise the morphological phenotype of released virions. Figure 4.1 (A) and (B) show the morphology of released virus particles from Vic75 WT- or Vic:PR8M-infected MDCK cells respectively. $2x10^5$ pfu was UV-inactivated and added to carbon formvar grids, negatively stained using uranyl-acetate and images taken using a JEOL 1400 transmission electron microscope. Samples were processed and imaged by Noel Leddy. No released or cell-associated filamentous particles were observed in Vic:PR8M-infected cells. Filamentous particles up to lengths of 1-2 µm were observed in the supernatant of Vic75 WT-infected cells. Interestingly, particles that exceeded this size were not observed. When compared to the particles that are still cell-associated (Figure 3.2) one would

expect to observe filamentous particles up to and exceeding 10 µm in size, but none were noted. Similarly, no bundles of filamentous particles were observed in the supernatant sample.

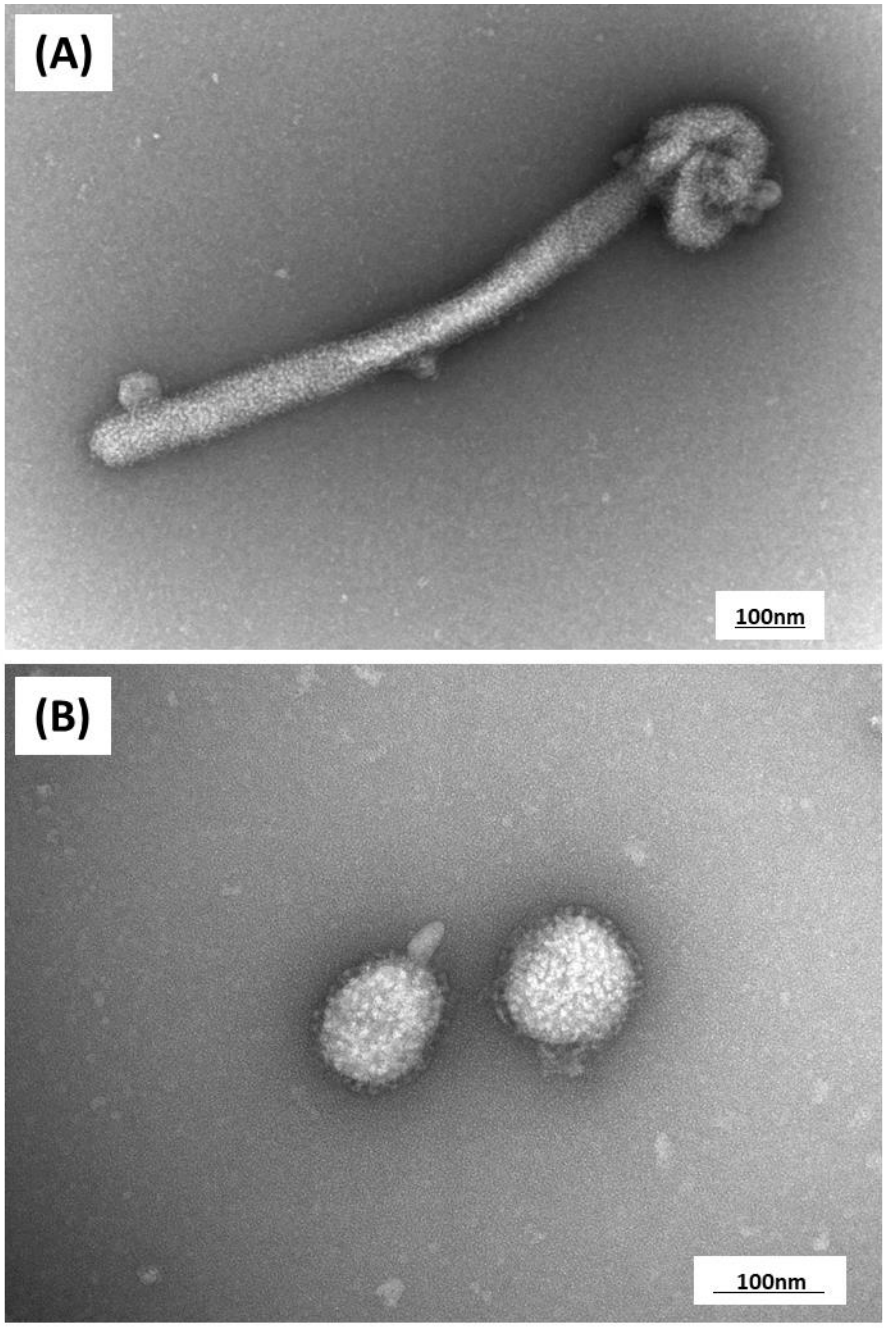

Figure 4.1: Morphology of released IAV particles. Electron micrographs of released virus particles present in viral stocks. $2x10^5$ pfu was added to carbon formvar grids and stained with uranyl acetate. (A) is a typical representation a filamentous particle observed in Vic75 WT stocks. (B) Spherical particles were the only virion type seen in Vic:PR8M stocks. N: 2

4.2 Validation of a spinoculation and flow cytometry assay to determine relative amounts of anti-HA staining could be used to observe virus bound to cells.

Whilst electron microscopy provides high quality visualisation of virions, the volume of stock assessed is relatively small, the process is time consuming, and the data are qualitative and not easily repeated for each new stock of virus produced. In order to determine variation in the proportions of filamentous and spherical virions between viruses and stocks we utilised a spinoculation assay as outlined by Carter *et al.*, (2005).

We were interested to determine if it was possible to quantify the extent of filamentous virus particles in a given stock of Vic75 WT. A known titre of virus was centrifuged onto MDCK cells at 500 RCF for 30 minutes at 4^{o}C, fixed, stained and counter-stained (see section 2.2.18). Virus particles that had bound to cell surfaces but had not yet been endocytosed were readily observed (Figure 4.2 A and B). Interestingly, shapes that closely resembled filamentous particles in morphology and size were seen in cells with Vic75 WT bound to the surface (Figure 4.2 A). We used this assay as a relatively quick way to assess new virus stocks, confirming that filamentous virions were present.

Flow cytometry has been previously shown to be able to quantify virus particles and discern different sizes in a morphologically heterogeneous population (Gaudin and Barteneva, 2015). Thus, we were interested to apply this concept to attempt to define different sizes of virions in a given stock. 1x10^{7} pfu of Vic75 WT or Vic:PR8M was centrifuged onto A549 cells. Cells were trypsinised, fixed and stained using an anti-Vic75 HA antibody, then counter stained with protein A FITC-conjugate. Cells were carried through BD Accuri C6 flow cytometer and the amount of signal that was excited at a wavelength of 488 nm was recorded. Cells were gated based on the relative amount of side scatter (SSC-A) and forward scatter (FSC-A) generated by the flow of cells. The median 488 nm-generated fluorescent signal was recorded (Figure 4.2 C). While the relative difference in sizes of virus particles was unable to be calculated, a significant difference in the amount of anti-Vic75 HA signal was noted (Figure 4.2 D), where a significantly higher median fluorescence signal was detected in samples of Vic75 WT compared to Vic:PR8M. There are two possible reasons for the difference seen in anti-

Vic75 HA signal generated. That stocks of Vic75 WT had greater levels of NIPs, which would contribute to increased levels of anti-HA staining, or the increased amount of anti-HA signal results from the increased amount of HA protein present per infectious unit on a filamentous particle compared to a spherical one (Figure 4.1).

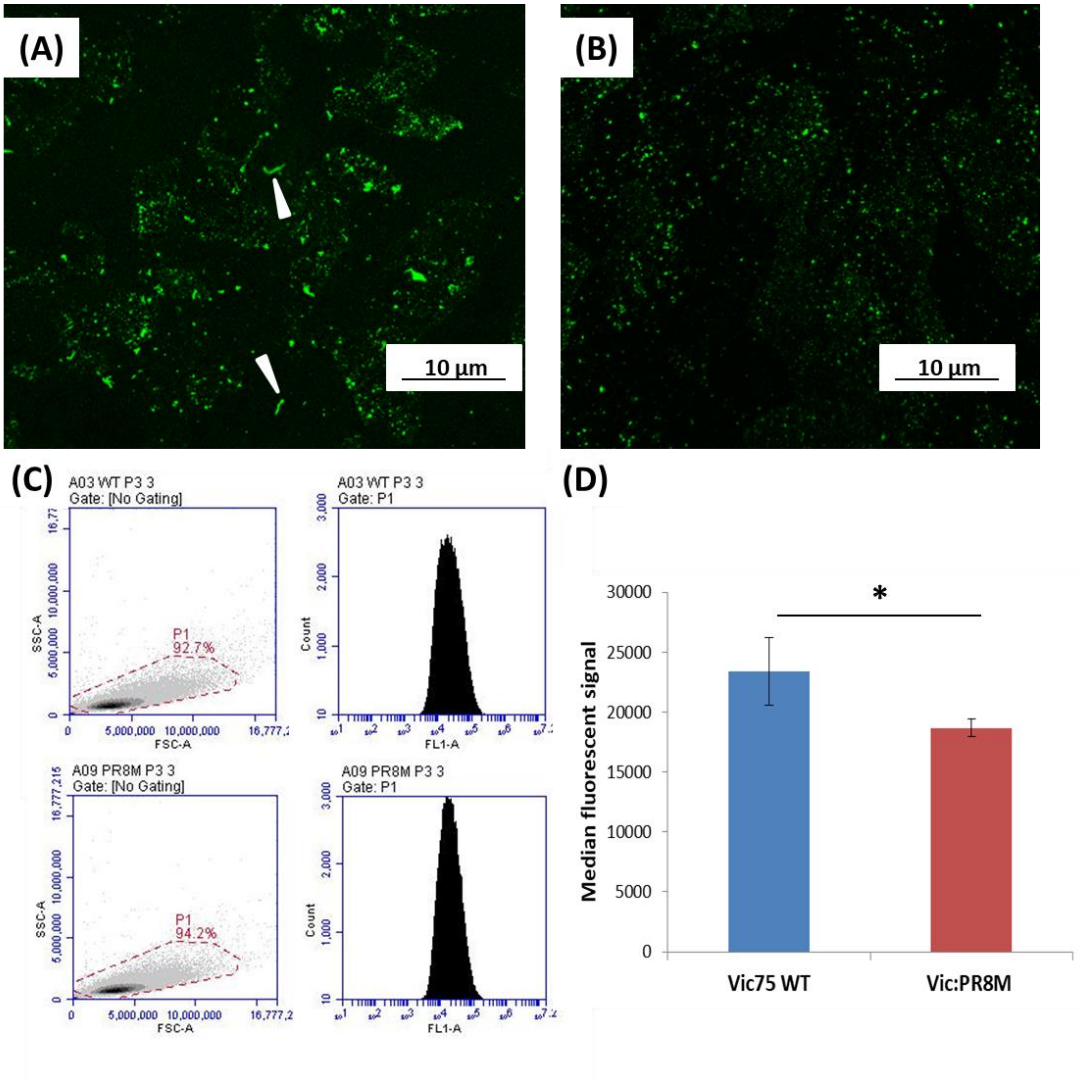

Figure 4.2: Spinoculation assay of virus onto cells and determination of fluorescent signal by flow cytometry. 1x10^{7}pfu of (A) Vic75 WT and (B) Vic:PR8M was centrifuged onto MDCK cells at 500 RCF at 4^{o}C. Cells were fixed and stained with anti-HA anti-sera and counter-stained with a FITC-conjugated protein A. Filamentous particles can be observed in Cells bearing Vic75 WT and are denoted by white circles. N: 3 (C) Flow cytometry analysis of A549 cells bearing fluorescently stained virions on their surface. Representative plots are shown for both Vic75 WT and Vic:PR8M. Cell populations were gated based on side and forward scatter plots (left hand side). The amount of fluorescence for the 488 nm channel was plotted against cell counts (right hand side) N: 3. (D) The median value for fluorescence in the 488 nm channel was recorded for each and the mean and standard deviation calculated. N: 3. * indicates a p value of <0.05 as calculated by two-tailed student's t-test. Error bars represent standard deviation from the mean.

4.3 Vic75 WT virus particles have increased NA activity but have the same amount of genetic segments compared to Vic:PR8M.

Previous studies have shown that filamentous virus particles have increased NA activity when compared to spherical ones (Campbell, Danzy, *et al.*, 2014; Campbell, Kyriakis, *et al.*, 2014), therefore we were interested to investigate if we could replicate that phenotype. $5x10^4$ pfu was incubated in triplicate with 100 µM of MUNANA, incubated at 37^oC. The amount of fluorescent signal generated from the cleaved substrate was recorded every minute for one hour. Per infectious unit, Vic75 WT had a 2.4-fold greater amount of NA activity (Figure 4.3 A).

The data in figure 4.2 (D) and figure 4.3 (A) suggests that Vic75 WT has more protein present per infectious unit. It is possible that the phenotype switch between producing filamentous and spherical particles could affect the relative budding profiles of either virus, which could potentially affect the ratio of NIPs produced by either virus. NIPs are defined as particles which resemble infectious virions, but are non-infectious. Therefore, by normalising to infectious titre, NIPs are not quantified and may give erroneous results in assays that normalise to pfu. One reason as to why a particle might be non-infectious might be that it does not have a full genome. This can occur either from deletions, typically in the larger-sized segments, or if the total requisite 8 segments are not incorporated into virions. Thus, by comparing the ratio of genetic segments between both viruses when normalised to pfu, the presence or absence of NIPs can be discerned. Figure 4.3 (B) shows the ratio of Vic:PR8M to Vic75 WT segments. $1x10^7$ pfu was lysed and the RNA extracted. The amount of RNA was determined in a single-step RT-qPCR reaction. The relative copy number for seven genetic segments was calculated for both viruses. The ratio of the relative copy number for each segment of Vic:PR8M to Vic75 WT was calculated. The RT-qPCR reaction was performed in triplicate and the mean and standard deviation of the amount of Vic:PR8M: Vic75 WT for each segment is reported in figure 4.3 (B). Data presented in figure 4.3 (B) is representative of three sample RNA extractions, each with three replicate RT-qPCR reactions. Vic:PR8M has approximately 1.5-fold more genetic segments for 6 of the 7 segments tested, and 3-fold for the M segment. It is interesting to note that Vic75 WT has significantly higher levels of both HA and NA activity but Vic:PR8 has marginally greater levels of genetic segments. While it

cannot be concluded if there are more NIPs present in the Vic:PR8M stock, it is very likely that the increased amount of HA and NA activity observed for Vic75 WT is due to the presence of filamentous particles. Filamentous and spherical particles are equally infectious and bear only one genomic set (Roberts, Lamb and Compans, 1998; Harris *et al.*, 2006; Calder *et al.*, 2010). Therefore, it was hypothesised that due to their increased size and HA content per infectious unit, filamentous particles would be more resistant to inhibition by inhibitors targeted against the HA.

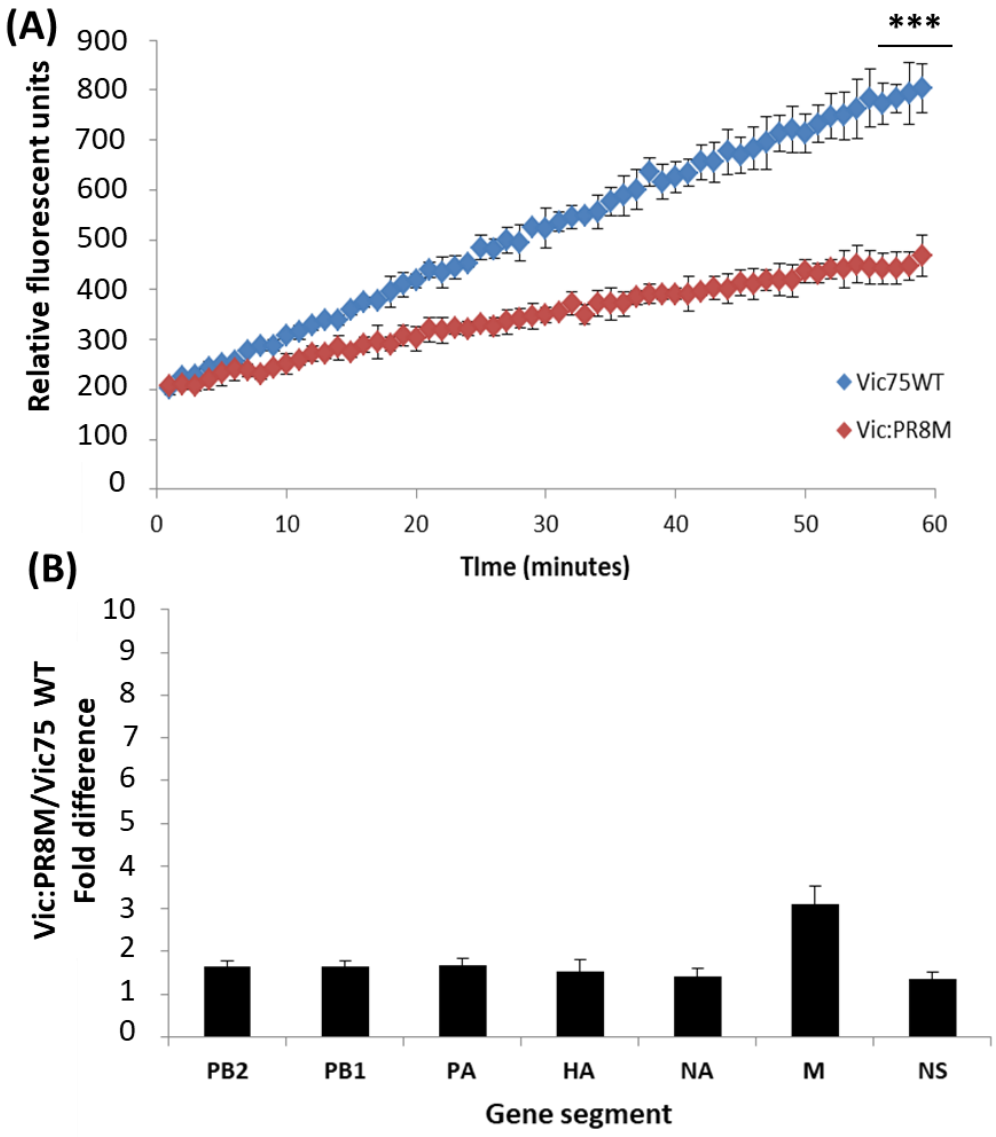

Figure 4.3: Relative NA activities and fold difference of genetic segments of Vic75 WT and Vic:PR8M.(A) NA activity of viruses incubated with MUNANA. $2.5x10^4$ pfu was incubated for one hour with 100 µM MUNANA and the amount of fluorescent signal recorded every minute. The mean and standard deviation of fluorescent signal generated for triplicate wells is reported. (B) Fold difference in amount of vRNA genetic segments. $1x10^7$ pfu was lysed, RNA was extracted and cDNA generated. qPCR was performed in triplicate reactions and the fold difference recorded for each genetic segment. The mean fold difference is represented as the mean of the fold difference recorded for each qPCR reaction. N: 3 for all. * and **indicate a p value of <0.05 or <0.01 as calculated by two-tailed students t-test comparing the rates of fluorescent signal generation. Error bars represent standard deviation from the mean.

4.4 Stocks of IAV that have been generated from high MOIs have significantly greater levels of NA activity, anti-Vic75 HA staining and levels of genetic segments.

The relative amount of increased anti-Vic75 HA staining and NA activity conferred by increased protein content per infectious unit for filamentous particles could not be determined accurately. Similarly, the exact level of NIPs present in either Vic75 WT or Vic:PR8M stocks was not determined. Thus, it was unclear precisely how much anti-Vic75 HA staining and NA activity was conferred by increased particle length or if it was due to increased amounts of NIPs. To address this, stocks of both viruses that contained increased amounts of NIPs were generated. Stocks of IAV that were generated by infection of cells at a high MOI generated increased levels of NIPs, in agreement with previous findings (Marcus, Ngunjiri and Sekellick, 2009; Isken, Genzel and Reichl, 2012). This approach was used to generate stocks of Vic75 WT and Vic:PR8M, where MDCK cells were infected at an MOI: 0.3, which was approximately $1x10^6$-fold higher than the MOI used to generate to other, non-NIP stocks. Vic75 WT and Vic:PR8M generated in this manner were designated: Vic75 WT NIP and Vic:PR8M NIP. Because we were interested in comparing the activities of Vic75 WT and Vic:PR8M in assays in which NIPs could give erroneous results, this approach was undertaken. The rationale being, that if we could control for the effect of NIPs per virus, then more accurate conclusions could be drawn when comparing between viruses, and specifically could be attributed to differences in morphology.

Vic75 WT and Vic:PR8M that were generated from low MOI infections were compared to respective stocks that were grown to contain increased levels of NIPs (Figure 4.4). All assays were normalised to pfu, and there was no difference in the amount of infectious virus for each assay. While the same amount of infectious virus was used for each virus stock being tested, the stocks that had been generated with high MOIs had significantly greater: levels of anti-Vic75 HA staining, NA activity and amounts of genetic segments (Figure 4.4 A-F). This strongly suggests that there is a significant increase in the amount of NIPs present in the NIP stocks. Otherwise we would expect the protein content (HA) and enzyme activity (NA) to be the same between the low MOI and NIP stocks, as well as the ratios of genetic segments being 1:1 with the amount of infectious units.

Table 4.1 summarises the relative fold differences between stocks generated from high MOIs and stocks generated from low MOIs. It is clear that the high MOI, NIP stocks have greater levels of protein content, NA activity and more genetic segments present compared to stocks that were generated from low MOIs. Thus, these stocks could be used to control for the presence of NIPs in assays that would be sensitive to increased levels of NIPs, such as virus inhibition assays. For instance, the presence of NIPs could interfere with and give erroneous results in plaque reduction assays. These assays are normalised to the amount of input infectious virus, so if an inhibitor directed against the viral HA were being tested, the increased amount of NIPs in a stock could give false positive results by the binding of inhibitor to already-non-infectious virus. This would deplete the amount of inhibitor available to inhibit infectious virus, which would increase the infectivity seen for that stock.

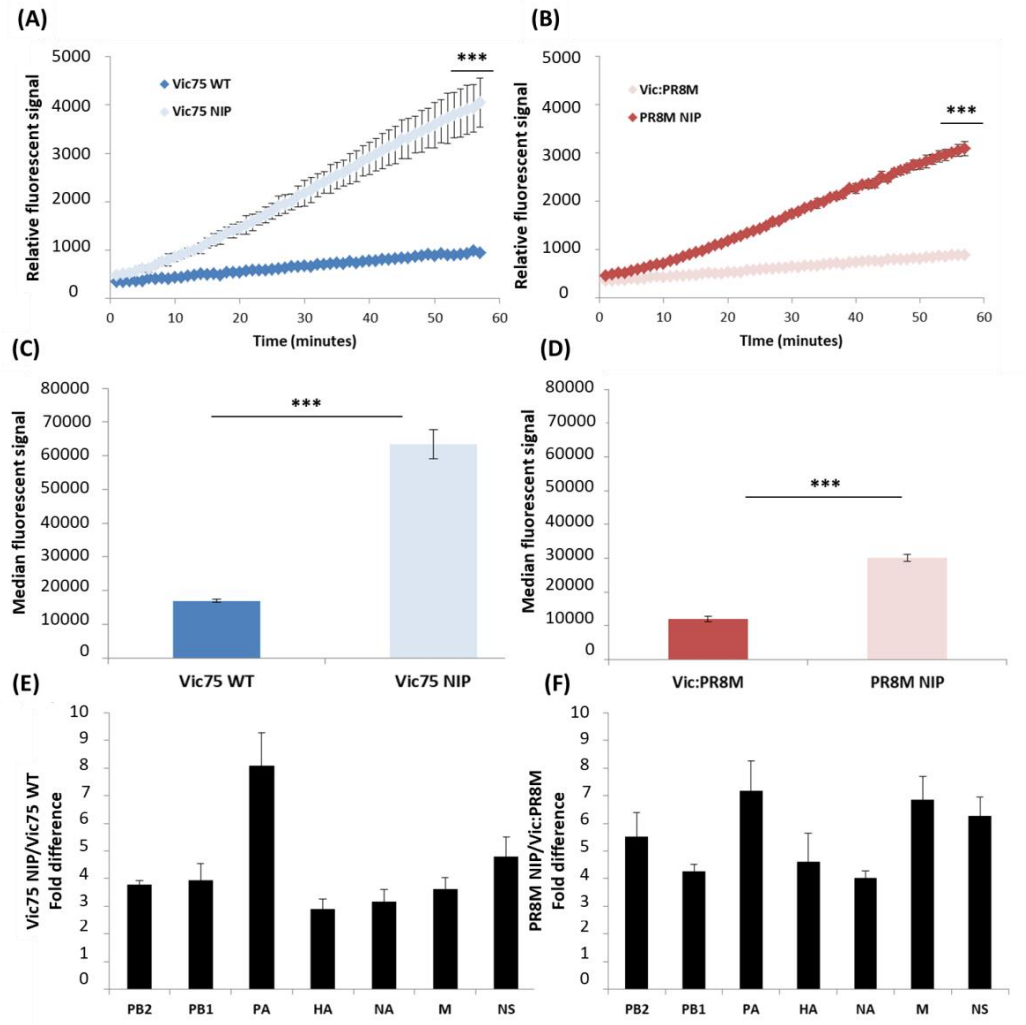

Figure 4.4: Characterisation of NIP stocks. Relative NA activities of (A) Vic75 WT and NIP and (B) Vic:PR8M and stocks. $2.5x10^4$pfu were incubated with 100 µM of MUNANA and amount of fluorescence generated was recorded every minute. P values were calculated by two-tailed students T test of the rates of each replicate. The median amount of anti-HA antibody fluorescence was recorded by a flow cytometer for (C) Vic75 WT and NIP and (D) Vic:PR8M and NIP stocks. $1x10^7$pfu was centrifuged onto A549 cells. Cells were fixed and stained with anti-HA anti-sera and counter-stained with a FITC-conjugated protein A. Fold difference in amount of genetic segments of (E) Vic75 WT and NIP and (F) Vic:PR8M and NIP stocks. $1x10^7$pfu was lysed, RNA was extracted and cDNA generated. QPCR was performed in triplicate reactions and the fold difference recorded for each. The mean fold difference is represented as the mean of those three replicate runs. *, ** and *** indicates a p value of <0.05, <0.01 and <0.001 as calculated by two-tailed students t-test. Error bars represent standard deviation from the mean.

	Fold Difference		
	Vic75 NIP/ Vic75 WT	PR8M NIP/Vic:PR8M	Vic75 WT/ Vic:PR8M
Anti-HA fluorescence	4.0	2.5	1.4
NA activity	3.8	3.5	2.4
Mean amount of genetic segments	4.3±1.8	5.3±0.9	1.8±0.6

Table 4.1: Summary of the fold differences between stocks grown at high and low MOIs. This table summarises the fold differences between virus stocks that have increased levels of NIP and those which do not as measured by relative amounts of: anti-HA fluorescence, NA activity, or genetic segments. Data presented in this table is a summary of the data presented in Figs. 4.1-4.3.

4.5 The presence of NIPs does not affect resistance to inhibition by either respiratory mucus or by anti-Vic75 HA anti-sera.

One possible explanation for the retention of a filamentous phenotype *in vivo* but not *in vitro* would be that filamentous virions are more resistant to inhibition of effectors of the immune system. We hypothesised that due to increased NA activity, filamentous virions would be more resistant to inhibition by the binding of sialic acid-bearing mucins within respiratory mucus to the viral receptor binding protein, HA. The NA achieves this by being able to cleave the bonds made more effectively than the few NA proteins found on spherical virions. Similarly, by virtue of having increased surface area, a greater amount of antibody would be required to inactivate the virus by binding to the HA protein and subsequently halt attachment to host cells. The increased surface area and increased amount of HA per infectious unit would be a viable reason as to why a filamentous phenotype would be retained *in vivo* compared to *in vitro* as it would aid in evasion of host antibodies directed against virus particles.

Thus, we were interested to see if there was a difference in the capacity of Vic75 WT and Vic:PR8M to retain infectivity when treated with either respiratory mucus or anti-Vic75 HA antibodies. However, due to the two viruses possessing two unique budding phenotypes, it is possible that there is a difference in the amount of NIPs generated from infected cells by either virus. Because of this, the influence of NIPs on a plaque reduction assay had to be determined. Thus, the stocks outlined in section 4.4 and table 4.1 were compared for their relative capacities for retaining infectivity when treated with either anti-HA or HNE-derived respiratory mucus. Figure 4.5 shows the amount of infectivity remaining when virus stocks that were grown at low and high MOIs were treated with these inhibitors. As seen in figure 4.5 (A) (Vic75 WT) and (B) (Vic:PR8M) when treated with anti-Vic75 HA antibodies there was no difference in infectivity remaining for low or high MOI stocks. Vic75 NIP virus had consistently higher levels of infectivity than Vic75 WT when treated with anti-sera, but this was not statistically significant. Figure 4.6 (C) (Vic75 WT) and (D) (Vic:PR8M) similarly shows there was no difference in infectivity remaining when high and low MOI stocks were treated with respiratory mucus. Interestingly, Vic75 WT always had marginally, but not statistically significant, higher amounts of infectivity than Vic75 NIP. This is counterintuitive as one

would expect that increased amounts of HA present and NA activity (Figure 4.4) would contribute to resistance to inhibition by respiratory mucus. Vic:PR8M and Vic:PR8M NIP consistently demonstrated the same levels of inhibition by respiratory mucus. Taken together these data suggest that at the levels being tested, NIPs are not having a significant effect on inhibition of infectivity by HA neutralising antibodies or respiratory mucus.

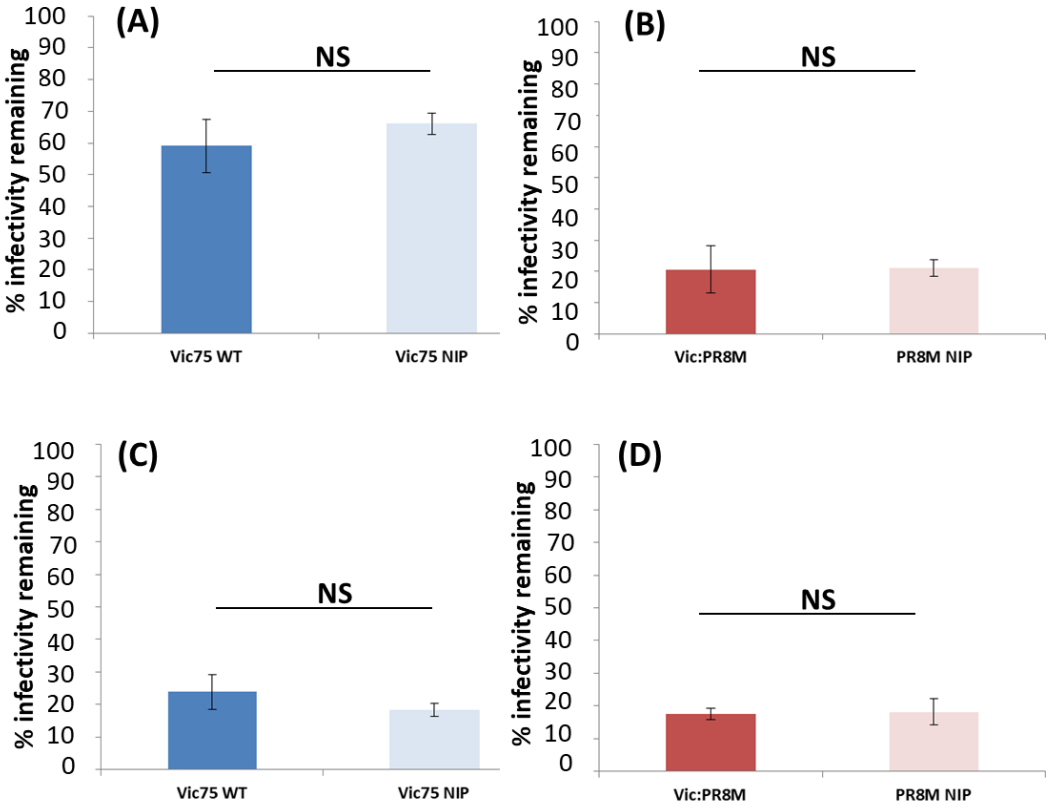

Figure 4.5: Presence of NIP in stocks do not affect resistance to inhibition by effectors of the immune system. (A) Vic75 WT and NIP stocks and (B) Vic:PR8M and NIP stocks were treated with polyclonal goat anti-sera raised against Vic75 HA. The antibody was diluted 1:4000 from stock. 100 pfu of indicated virus was treated with this dilution and incubated for one hour at 37^{o}C. Antibody and virus mixture were adsorbed to MDCK cells. Plaques were counted 72 hours post infection. Results are reported as the amount of plaques counted expressed as a percentage of an untreated control. (C) Vic75 WT and NIP stocks and (D) Vic:PR8M and NIP stocks were treated with respiratory mucus. The mucus was diluted 1:20 from Stock. 100 pfu of indicated virus was treated with this dilution and incubated for one hour at 4^{o}C. The mucus and virus mixture were adsorbed to MDCK cells. Plaques were counted 72 hours post infection. Results are reported as the amount of plaques counted expressed as a percentage of an untreated control. N: 3 for all. NS: p value >0.05 as measured by two-tailed students t-test. Error bars represent standard deviation from the mean.

4.6 Stocks that contain filamentous particles are more resistant to inhibition by respiratory mucus.

NA activity is necessary for resistance to inhibition for IAV (Yang *et al.*, 2014), we were interested to determine if the significant increase in NA activity of the Vic75 NIP stock (Figure 4.4) increased the resistance of Vic75 WT to inhibition by respiratory mucus. Surprisingly, compared to Vic75 WT, Vic75 NIP had a reduced amount of infectivity when treated with respiratory mucus (Figure 4.6 A). While the difference in infectivity between Vic75 WT and Vic75 NIP when treated with respiratory mucus was not statistically significant, neither was the difference between Vic75 NIP and Vic:PR8M. There was a significant difference in infectivity seen between Vic75 WT and Vic:PR8M (Figure 4.6 A). Despite having a greater level of NA activity, Vic75 NIP had diminished resistance to inhibition by respiratory mucus. To investigate this, TEM was performed on Vic75 WT and Vic75 NIP stocks (Figure 4.6 B and C). Filamentous particles were routinely observed in Vic75 WT but very few were seen for the Vic75 NIP stock. Thus, the presence of filamentous particles confers increased resistance to inhibition by respiratory mucus and also NA activity as measured by the MUNANA assay is not necessarily a determinant of increased resistance to inhibition by respiratory mucus.

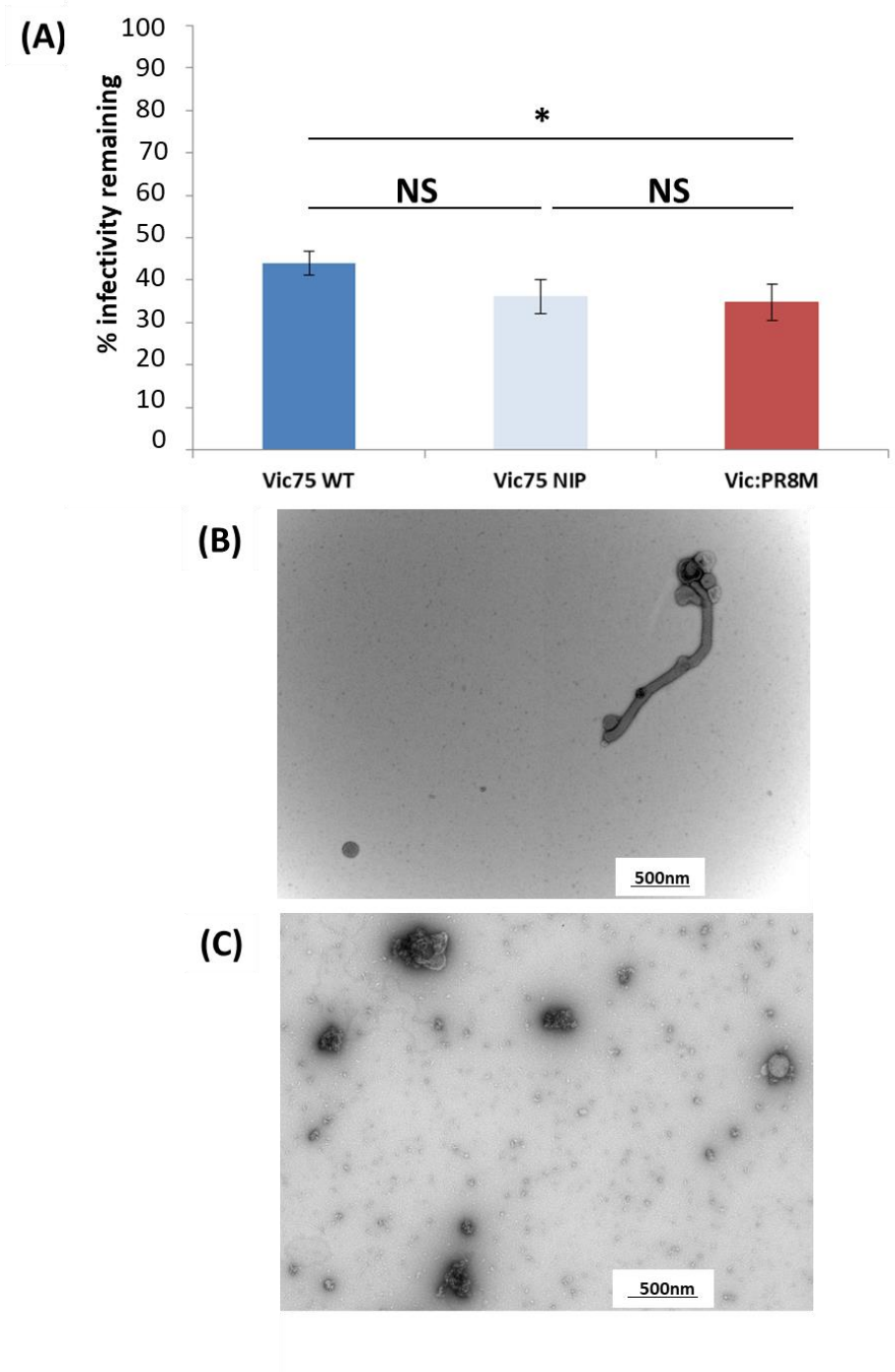

Figure 4.6: Presence of filamentous particles in a stock correlates with increased resistance to Inhibition by respiratory mucus. (A) 100 pfu was treated with a 1:20 dilution of respiratory mucus, incubated for one hour at 4^{o}C and adsorbed onto MDCK cells for one hour at 37^{o}C N:3. Electron micrographs of (B) Vic75 WT and (C) Vic75 NIP stocks. 2x10^{5} pfu was added to carbon formvar grids and stained with uranyl acetate. N: 1. *indicates a p value of <0.05 as calculated by two-tailed students t-test. Error bars represent standard deviation from the mean.

4.7 Chapter 4 discussion.

From the data presented, it cannot be claimed that the presence of NIPs do not increase resistance to inhibition by effectors of the immune system. Stocks grown at high MOIs have greater levels of HA staining, NA activity and greater amounts of genetic segments. We inferred from this that these stocks had increased levels of NIPs. It has only been demonstrated that at the levels being tested, that the presence of NIPs do not increase the resistance of infectious particles to inhibition by inhibitors targeted against the receptor binding protein. The fold difference seen for anti-Vic75 HA staining and NA activity between Vic75 WT and Vic:PR8M is lower and within the limits shown to be inconsequential for the NIP stocks. Thus, we would argue that any difference seen in the capacity of these viruses to resist inhibition would not be due to the presence of NIPs.

It was interesting to note that increased NA activity, as measured by the MUNANA cleavage assay, did not correlate with increased resistance to inhibition by respiratory mucus (Figures 4.4 and 4.5 C), which seemingly disagrees with previous observations (Zanin *et al.*, 2015; Ruangrung *et al.*, 2016). However, these studies compared viruses with different NA proteins, while the data presented here describes increased levels of NIPs without altering NA proteins. It has also been demonstrated that the presence of filamentous particles correlates with greater levels of infectivity when treated with respiratory mucus. It was initially hypothesised that filamentous particles would be more resistant to inhibition by mucus by virtue of having increased NA activities. However, it has been demonstrated that the NA activity of a stock of virus is not a predictor of greater infectivity when treated with mucus. Thus, the mechanism by which filamentous particles could confer increased resistance to inhibition is still unclear.

Chapter 5: Replication and morphology of isogenic Vic75 viruses in differentiated human nasal epithelial (HNE) cultures.

We have demonstrated that the presence of filamentous particles in a stock correlated with greater levels of infectivity when the virus was treated with respiratory mucus (Figure 4.6). We were interested to further investigate what effect NA activity had on the relative capacities of filamentous and spherical particles to resist inhibition by respiratory mucus. We were also interested to investigate if filamentous particles would be less inhibited by antiviral antisera compared to spherical particles.

Due to the increased levels of infectivity observed for filamentous viral particles, we were interested to investigate if filamentous particles were more efficient at replicating in HNE cultures. These cultures were primary cells that were isolated from a pool of human donors. The cells were fully differentiated with stratified architecture and composed of a heterogeneous population of cell types, including ciliated, non-ciliated and goblet cells. At the apical surface of the cultures a layer of respiratory mucus accumulates due to mucus producing goblet cells. We hypothesised that Vic75 WT would be more capable of replicating in these cultures by virtue of retaining more infectivity when treated with respiratory mucus that had been derived from HNE cultures

5.1 Stocks that contain filamentous particles are more resistant to inhibition by anti-HA anti-sera.

It has already been demonstrated that filamentous particles retain greater levels of infectivity when treated with an effector of the innate immune system. We were interested to investigate if a similar observation would be made when viruses were treated with another effector of the immune system, antiserum. Figure 5.1 shows the percentage infectivity remaining when Vic75 WT and Vic:PR8M were treated with polyclonal anti-Vic75 HA anti-sera diluted 1:4000. Vic75 WT retained significantly higher levels of infectivity, where Vic75 WT produced 20% more plaques. Similar to the observation seen in figure 4.6, where the presence of filamentous particles correlated

with increased infectivity when treated with mucus, figure 5.1 shows that Vic75 WT is more resistant to inhibition by anti-Vic75 HA antisera. This suggests that Vic:PR8M is more inhibited by neutralising HA antibodies that Vic75 WT.

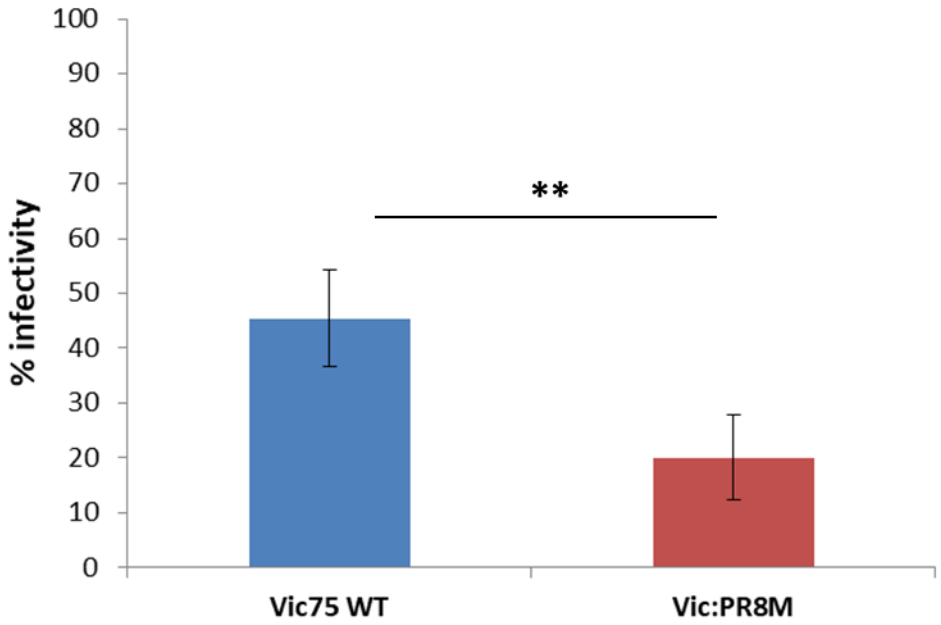

Figure 5.1: Stocks containing filamentous particles are more resistant to inhibition by anti-HA IgG. Vic75 WT and Vic:PR8M were treated with polyclonal goat anti-sera raised against Vic75 HA. The antibody was diluted 1:4000 from stock. 100 pfu of virus was treated with this dilution and incubated for one hour at 37^{o}C. Antibody and virus mixture were adsorbed to MDCK cells. Plaques were counted 72 hours post infection. Results are reported as the amount of plaques counted expressed as a percentage of an untreated control. N: 3. ** indicates a p value of <0.01 as calculated by two-tailed students t-test.

5.2 The increased retention of infectivity by filamentous viruses is dependent on the action of NA.

It has been hypothesised that due to the increased NA activity, pleomorphic populations of virions may be less inhibited by respiratory mucus than spherical-only populations. To test this hypothesis, Vic75 WT and Vic:PR8M viruses were treated with HNE-derived respiratory mucus and the remaining infectivity was compared to untreated virus. Figure 5.2 (A) shows that when treated with respiratory mucus the infectivity remaining of Vic75 WT was 39.8% compared to 17.9% for Vic:PR8M, a difference that was statistically significant. This suggests that Vic:PR8M is more inhibited by respiratory mucus than Vic75 WT.

To determine if the increased NA activity found in Vic75 WT compared to VicPR8M (see figure 4.3 A) contributes to this difference the experiment was repeated but this time was pre-incubated with the NA inhibitor oseltamivir. When NA activity was inhibited there was no significant difference in infectivity remaining between the two viruses, which was 20.8% and 23.2% for Vic75 WT and Vic:PR8M respectively (Figure 5.2 B). This supports the idea that the increased NA activity seen for filamentous virions is important for releasing virions from inhibitory respiratory mucus.

In order to demonstrate that sialic acid containing mucins within respiratory mucus are contributing to the inhibition of infection, the mucus was pre-treated with exogenous NA derived from *Vibrio cholera*. The exogenous NA cleaved the sialic acids decoy receptors present in the mucus and the inhibition of infection was dramatically reduced. The infectivity remaining went up to 72.3% and 60.1% for Vic75 WT and Vic:PR8M respectively (Figure 4.8 C) but the difference seen for remaining infectivity for either virus was not statistically significant. This suggests that filamentous particles are more capable of overcoming the innate barrier to infection presented by decoy receptors present in respiratory mucus, and that the mechanism by which this occurs is dependent on NA activity.

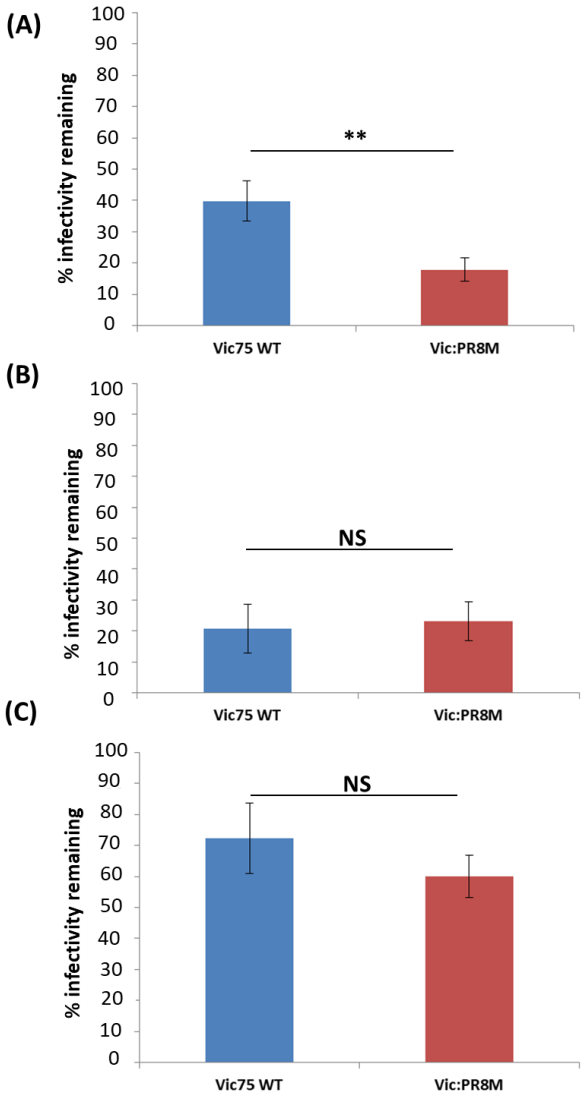

Figure 5.2: Stocks with filamentous particles are more resistant to inhibition by respiratory mucus and this is dependent on NA activity. (A) Vic75 WT and Vic:PR8M were treated with respiratory mucus at a 1:20 dilution from stock. 100 pfu was treated with this dilution and incubated for one hour at 4^{o}C. The mucus and virus mixture were adsorbed to MDCK cells at 37^{o}C. Plaques were counted 72 hours post infection. Results are reported as the amount of plaques counted expressed as a percentage of an untreated control. (B) outlines the percentage infectivity remaining when virus was pre-incubated with 55 nM of oseltamivir for 30 minutes at 37^{o}C. (C) represents data when respiratory mucus was pre-treated with NA from *Vibrio cholerae*. Mucus was incubated with 5 mU of NA for one hour at 37^{o}C. N:3 for all. ** indicates a p value of <0.01 as calculated by two-tailed students t-test. Error bars represent standard deviation from the mean.

5.3 Vic75 WT and Vic75 41V possess the same replicative capacities in HNE cultures and this is independent of input MOI.

One hypothesis that would account for the retention of a filamentous phenotype *in vivo* is that strains of IAV that generate filamentous particles are better suited to replication in the complex environment of the respiratory tract (see section 1.5.1). Filamentous stocks of IAV were more resistant to inhibition by respiratory mucus (Figures 4.6 and 5.2 A). We therefore hypothesised that Vic75 WT would replicate to higher titres than Vic:PR8M in fully differentiated HNE cultures. HNE cultures provide a complex environment of a mixture of cell types, such as ciliated cells and goblet cells, as well as respiratory mucus. These cultures more closely model the human respiratory tract than simple, undifferentiated, monocellular MDCK cells.

To test this hypothesis, HNE cultures were infected with either Vic75 WT or Vic75 41V and a multi-step growth curve was performed (Figure 5.3 A). Vic75 41V was initially used as the spherical-producing virus as it was the most similar to Vic75 WT while still presenting a spherical viral particle phenotype (Figure 3.9). Figure 5.3 (A) illustrates the replication kinetics of both viruses in HNE cells when infected at an MOI: 0.02. There was no significant difference seen in the replication capacity of either virus at any time point investigated. This suggests that at this MOI, filamentous particles do not confer any replication advantage in HNE cultures.

As the Vic75 WT virus stock is pleomorphic and the filamentous portion is in the minority, it was possible that the input MOI was too high to feasibly see any difference in the replication capacity of either virus. For instance, Roberts *et al.*, (2011) found that at high MOIs, a receptor binding mutant replicated and transmitted in ferrets with similar efficiencies to WT virus. However, the authors found that transmission was abrogated and replication significantly reduced when ferrets were inoculated at low MOIs. Thus, viral fitness is crucial when the infecting MOI is comparatively low, where the infecting virus will need to be as well suited to infect the sentinel host as possible. It has been noted that the infectious dose required to initiate infection can be as few as <10 pfu (Alford *et al.*, 1966; Gustin *et al.*, 2011; Roberts *et al.*, 2011). We therefore thought that by reducing the infecting MOI, any replicative advantage conferred by possessing a filamentous phenotype might be more apparent. To test this, HNE cultures

were infected at a ten-fold lower MOI (MOI: 0.002, Figure 5.3 B) which equated to 500 pfu. As before, the same replication kinetics were observed for both viruses, matching those seen in Figure 5.3 (A). This suggests that there is no difference in the capacity of Vic75 WT or Vic75 41V to replicate in HNE cultures, even at low MOIs. This strongly suggests that a filamentous phenotype doesn't aid infection of HNE cultures. An even lower input MOI was not investigated as there was concern that infection would not have been initiated.

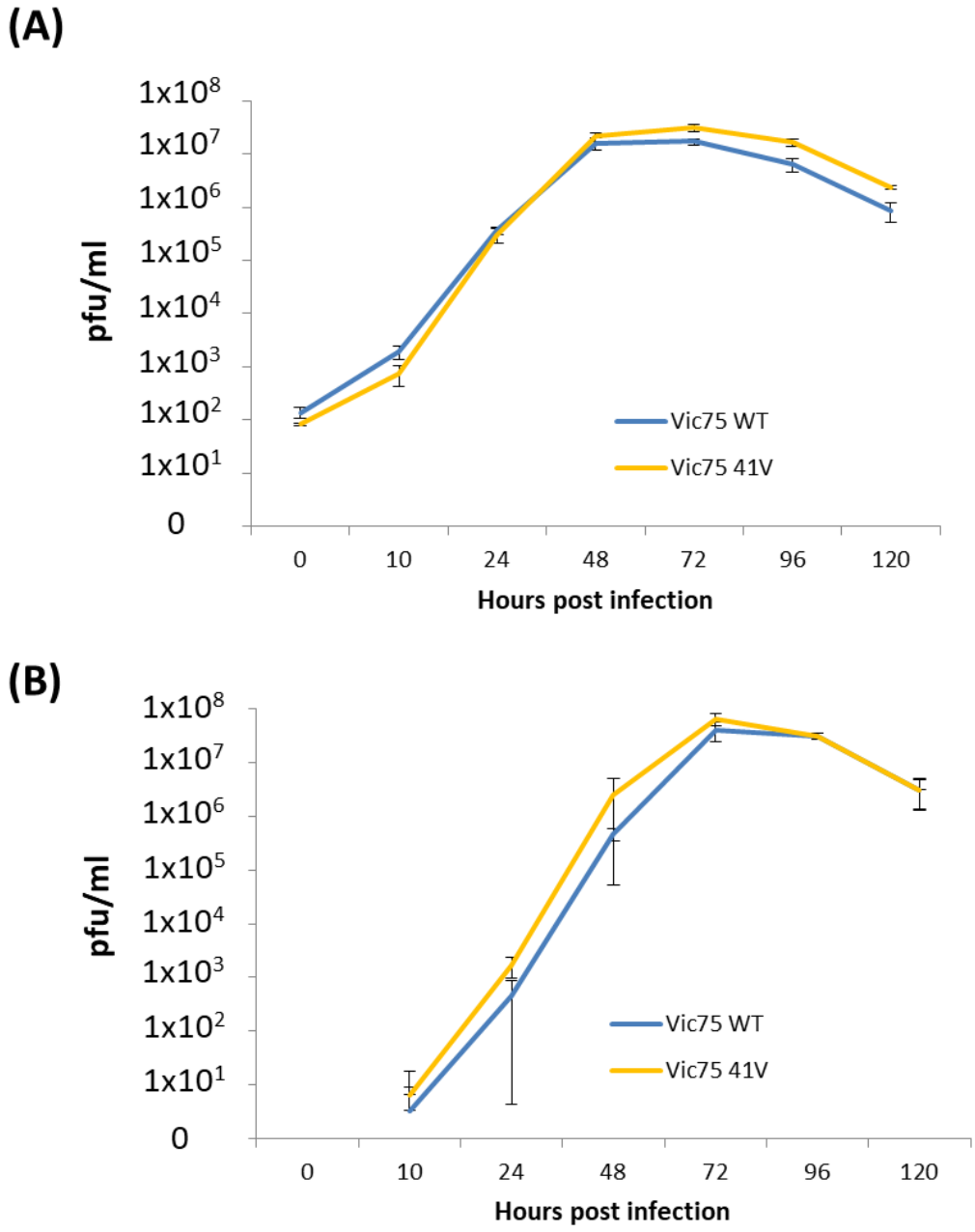

Figure 5.3: Virion morphology and MOI do not affect viral replication in HNE cultures. HNE cultures were washed and infected at an MOI (A) 0.02 and (B) 0.002 and incubated at 32°C. At indicated times post infection SF media was added to the apical surface, incubated for 30 minutes at 32°C and then the apical wash was collected. Viral titres of the apical washes were determined by plaque assay. The mean titre of four replicates is shown for each virus at each time point. Error bars represent standard deviation from the mean. N: 1

5.4 Vic75 WT and Vic75 41V both produce cell-associated filamentous particles in infected HNE cells.

The lack of a difference in replicative capacity between Vic75 WT and Vic75 41V was surprising. It was expected that Vic75 WT would have replicated to higher titres than Vic75 41V. To investigate this, the morphology of virus particles budding from infected HNE cultures was visualised. At 120 hpi, infected HNE cultures were fixed and imunostained with anti-Vic75 HA and counterstained with protein A FITC-conjugate (green colour) and cellular filamentous actin with Alexa Fluor™ phalloidin (red) and double stranded deoxyribonucleic acid (dsDNA) with 4',6-diamidino-2-phenylindole (DAPI) in the nucleus (blue). Immunostained HNE sections were imaged using a Leica SP8 confocal microscope. Interestingly, filamentous viral particles were routinely observed in HNE cultures infected with either Vic75 WT or Vic75 41V viruses (Figure 5.4), with no apparent difference in the abundance of filamentous particles between the two viruses. This could potentially explain why there was no difference in the replicative capacity of the two viruses in HNE cultures.

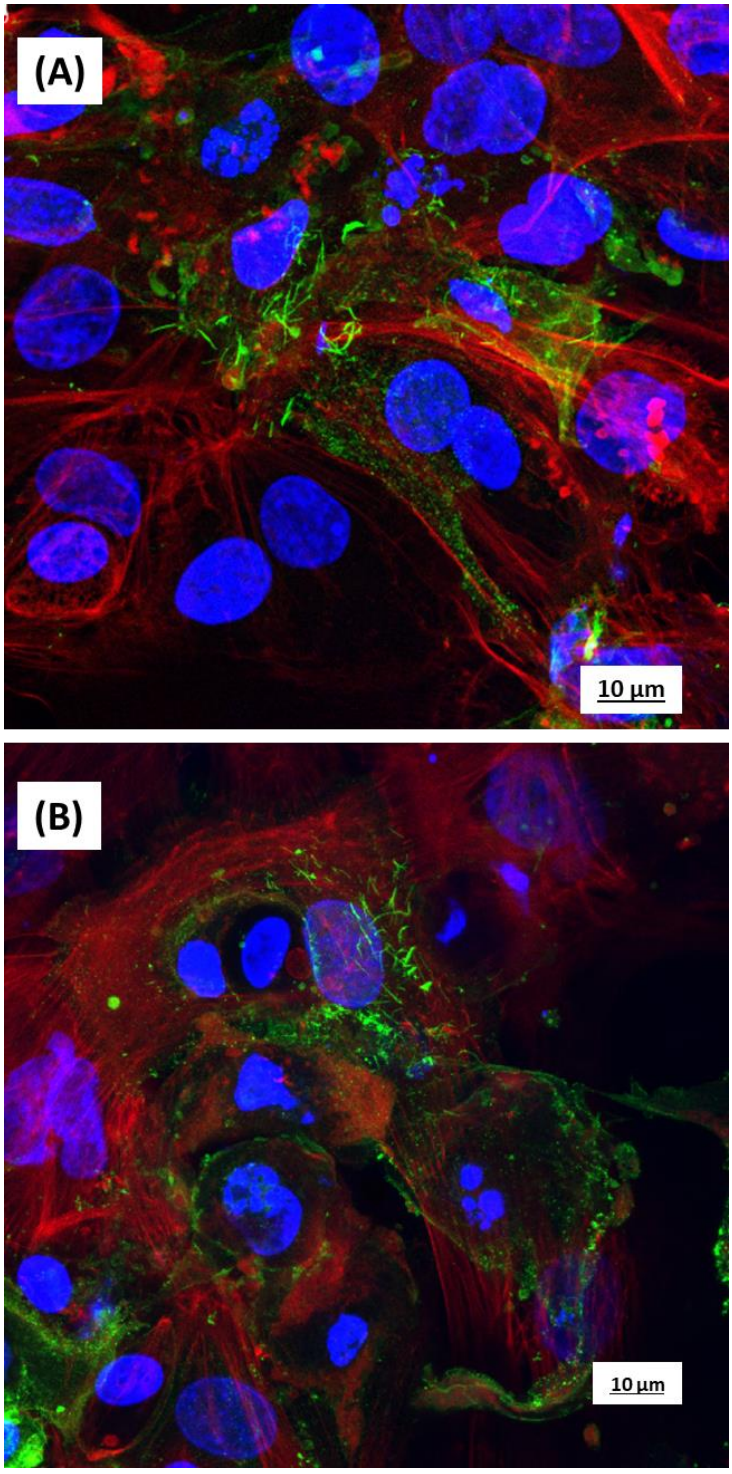

Figure 5.4: Vic75 WT and Vic75 41V produce cell-associated filamentous viral particles from infected HNE cultures. HNE cultures infected with (A) Vic75 WT and (B) Vic75 41V were fixed at 120 hpi. Cultures were stained with polyclonal ferret anti-HA anti-sera (green) and phalloidin to stain filamentous actin (red). DAPI (blue) was used to visualise DNA. Images were obtained using a Leica SP8 scanning confocal microscope. N: 2.

5.5 Vic75 WT and Vic:PR8M generate the same amount of infectious virus from infected HNE cultures.

Despite conferring a spherical-only phenotype in MDCK cells, it was possible that the M1 A41V mutation was insufficient to confer the same phenotype in HNE cultures and produce spherical-only viral particles. It was hypothesised that while a single amino acid substitution was sufficient to confer a spherical-only morphology in immortalised cells, it might be insufficient to induce the same phenotype in HNE cultures. Thus, the full segment 7 reassortant virus, Vic:PR8M, was used as the spherical-only producing viral phenotype.

HNE cultures were infected at an MOI: 0.01 with either Vic75 WT or Vic:PR8M. Similar to the results in figure 5.3 (A), there was no difference in replication capacity of either virus in HNE cultures at all recorded time points (Figure 5.5). These results show that either: substitution of a single amino acid in the M1 protein or replacement of the entire M segment to match those of a spherical virus had no observable effect on replication in HNE cultures. It is interesting to note that in immortalised cells, both the segment 7 swap and M1 41V amino acid substitution are sufficient to increase replication compared to Vic75 WT (Figures 3.3 and 3.10), but not in HNE cultures (Figures 5.3 and 5.5).

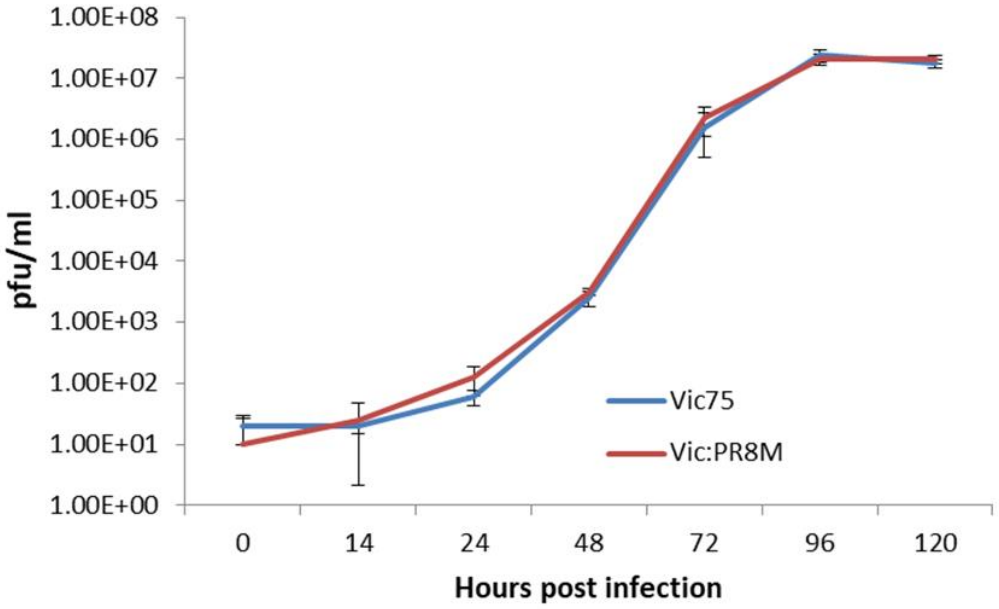

Figure 5.5: Vic75 WT and Vic:PR8M replicate to the same titres in infected HNE cultures. HNE cultures were washed and infected at an MOI: 0.01. HNE cultures were washed and infected at an MOI 0.01 and incubated at 32^{o}C. Four replicate cultures per virus were infected. At indicated times post infection SF media was added to the apical layer of HNE cells and incubated for 30 minutes at 32^{o}C. Viral titres of the apical washes were determined by plaque assay. The mean titre of four replicates is shown for each virus at each time point. Error bars represent standard deviation from the mean. N: 1

5.6 Vic:PR8M produces cell-associated filamentous particles from infected HNE cultures.

Similar to the results in figure 5.6, Vic:PR8M produced filamentous particles from infected HNE cultures similar in morphology to those generated by Vic75 WT (Figure 5.6). Both Vic:PR8M and Vic75 41V solely produced spherical viral particles in immortalised cell lines (Figures 3.2 and 3.9). This shows that the M segment of PR8 is insufficient to confer a spherical virion budding phenotype from infected HNE cultures. It is possible that the filamentous particles seen in Vic:PR8M infected HNE cultures are the result of spherical particles budding from cilia on ciliated cells, where cilia covered in spherical particles and subsequently stained with an anti-Vic75 HA antibody could be similar in morphology and size to a filamentous viral particle. This is unlikely as there was no co-localisation seen between β-tubulin (a marker for cilia) staining and anti-HA staining.

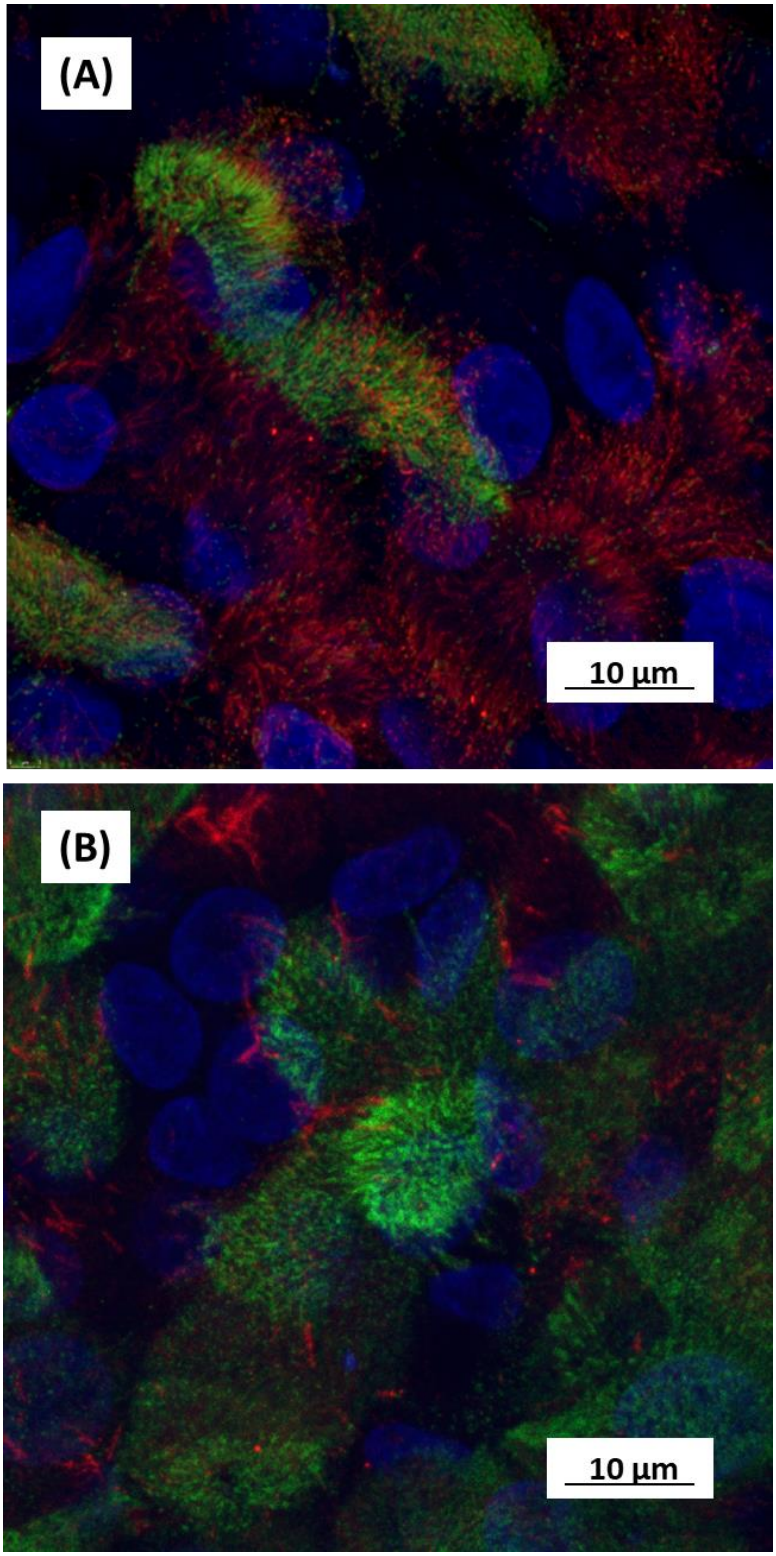

Figure 5.6: Vic75 WT and Vic:PR8M produce cell-associated filamentous viral particles from infected HNE cultures. Infected HNE cultures were fixed at 120 hours post infection. Cells were stained with polyclonal ferret anti-HA anti-sera (green) and anti-β-tubulin (red). DAPI (blue) was used to visualise DNA. Images were obtained using a Leica SP8 scanning confocal microscope. N:3

5.7 HNE-grown viruses revert to distinct morphological phenotypes when used to infect MDCK cells.

The images of infected HNE cultures shown in figures 5.4 and 5.6 were taken at 120 hpi. There was a possibility that in this time, Vic:PR8M could have reverted from a spherical morphological phenotype by virtue of mutation by selective pressure. The M segment of Vic:PR8M from the 120 hour time point was sequenced and no mutations were recorded (data not shown).To further test this, samples from the 120 hour time point were used to infect MDCK cells at an MOI: 1. Cells were fixed and immunostained at 16 hours post infection. Budding morphologies of MDCK cells infected with HNE derived Vic75 WT and Vic:PR8M are illustrated in figure 5.7. Similar to MDCK-grown stocks of virus, HNE Vic75 WT produced extended filamentous structures. HNE-produced-Vic:PR8M virus infected MDCK cells and generated punctate staining in all infected cells. Thus, the production of filamentous viral particles from infected HNE cultures was not the result of accrued mutations from Vic:PR8M undergoing multiple rounds of replication in cells.

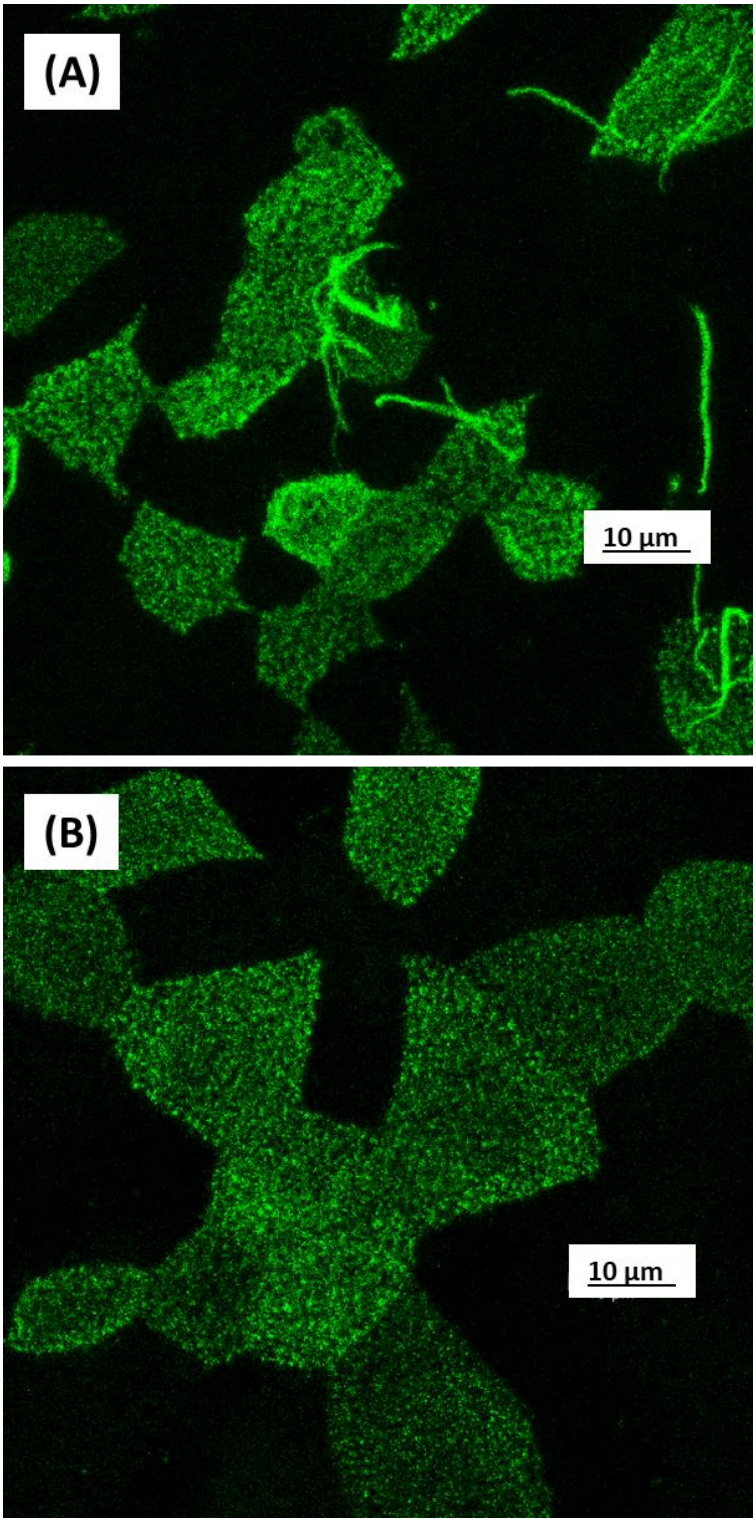

Figure 5.7: MDCK cells determine morphological phenotype of infecting parental virus. MDCK cells were infected at an MOI: 1 with virus generated from infected cells. (A) HNE Vic75 WT produced filamentous particles in infected cells. (B) HNE Vic:PR8M. Cells were fixed and stained 16 hours post infection and imaged using a Leica SP8 confocal microscope. Scale bars represent 10 µm. N: 2

5.8 Only spherical viral particles are visualised by TEM from infected HNE cultures.

The replication kinetics and cell-associated morphology observed for viruses generated from infected HNE cultures led to the hypothesis that only filamentous viral particles are produced from these cells. This hypothesis assumes that the viral genotype, which would otherwise lead to the production of spherical particles, is superseded by cellular machinery which causes the sole-production of filamentous particles. As it is possible that cell-associated morphology can be different to released virion morphology (see chapter 3), TEM was performed on the 120 hpi apical wash samples. Figure 5.8 shows representative images of virus particles release by either (Figure 5.8 A) Vic75 WT- or (Figure 5.8 B) Vic:PR8M-infected HNE cultures. Only spherical virus particles were observed in both of these samples. No filamentous virions were observed in samples collected from two replicate experiments, using different batches of HNE cultures. This suggests a significant difference in the morphology of cell-associated virions and those that are successfully released from infected HNE cultures. In addition, from this data it appears that a filament-producing strain of virus does not produce released filamentous particles in HNE cultures, which are far more representative of the natural tropism than immortalised MDCK cells. This is particularly surprising as the dogma within the field is that filamentous particles are generated *in vivo*. While HNE cultures are not holistically representative of a natural infection, one would assume that the cellular factors that govern virion morphology would be at the cell-level. Assuming this, HNE cultures should be representative of an *in vivo* infection. However, it should be noted that samples that were analysed by TEM were taken at 120 hours post infection so may not be representative of other stages of infection.

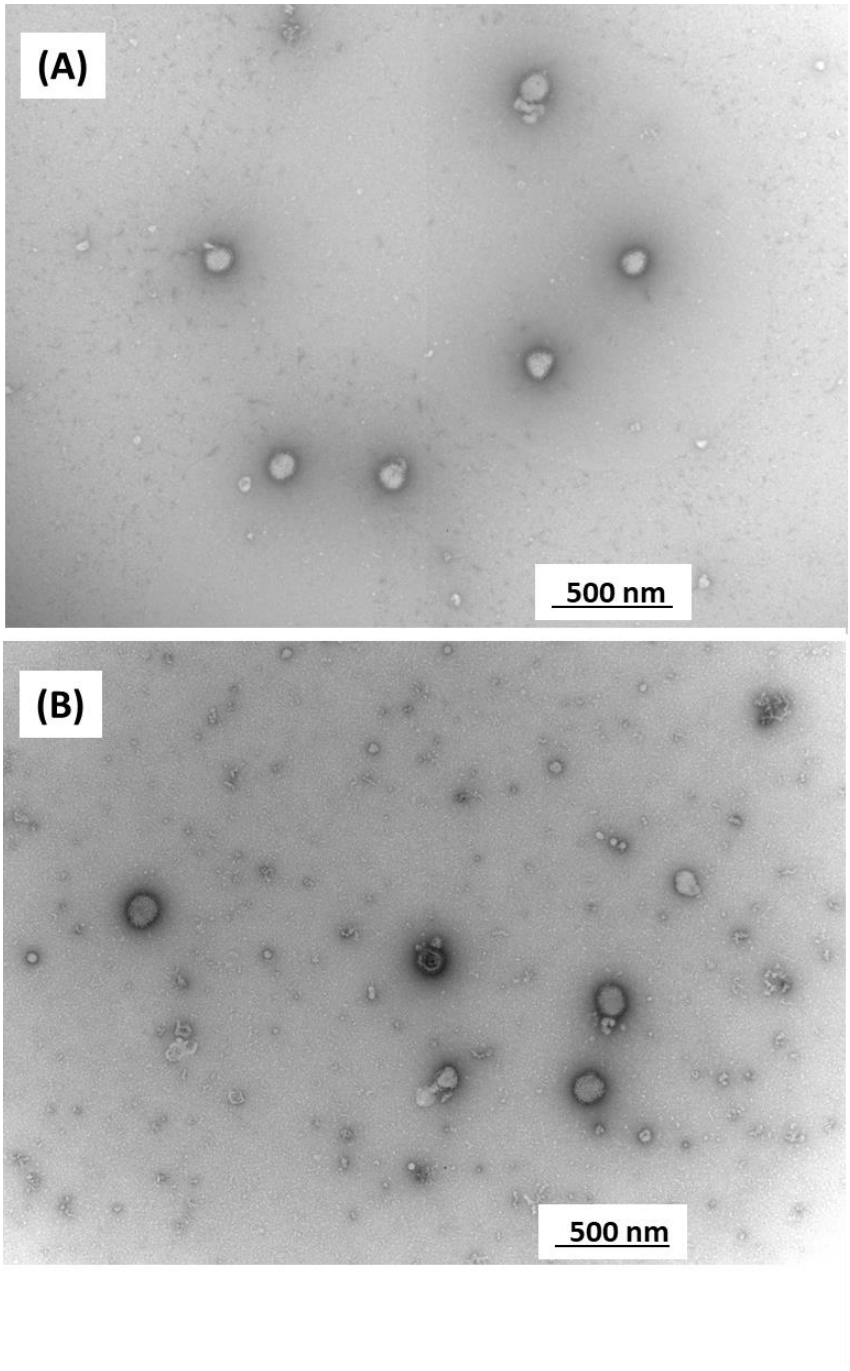

Figure 5.8: Only spherical particles were observed as released virons from infected HNE cells. Samples from (A) Vic75 WT and (B) Vic:PR8M infected HNE cells at 120 hpi are shown. Viruses were inactivated by treating with UV radiation. $5x10^5$ pfu was added to a carbon formvar grid using the inverse drop method. Samples were washed and stained using uranyl acetate. Images were taken using a JEOL TEM. Scale bars represent 500 nm. N: 2. Samples were processed and imaged by Neal Leddy.

5.9 Vic75 WT and Vic:PR8M viruses generated from HNE cultures have the same NA activities.

We were interested to characterise the virus released from the HNE cultures as we did not record any difference in the morphology of released particles of Vic75 WT or Vic:PR8M from infected HNE cultures. Firstly, we compared the relative NA activities of viruses that had been produced from these cultures. It has been demonstrated that when these viruses are generated from MDCK cells, the filamentous Vic75 WT virus had higher NA activities than the spherical only mutant (Figure 4.3 A). This agrees with published data that morphologically distinct viruses that express the same NA enzyme have different NA activities (Campbell *et al.*, 2014b; Seladi-Schulman *et al.*, 2014). Figure 5.9 shows the NA activities of both Vic75 WT and Vic:PR8M viruses collected from infected HNE culture at 120 hpi. There is no difference in the NA activities of these two viruses when they have been produced from HNE cultures (P value: 0.11). Back-titrations confirmed that the same number of infectious units were used for either virus in the assay. This directly contrasts to results presented in Figure 4.3 (A), where Vic75 WT viruses produced from MDCK cells had a 2.5-fold higher rate of reaction compared to Vic:PR8M. This suggests that when HNE cultures are infected, both Vic75 WT and Vic:PR8M produce morphologically similar virus particles (Figure 5.6) that have the same NA activities (Figure 5.9).

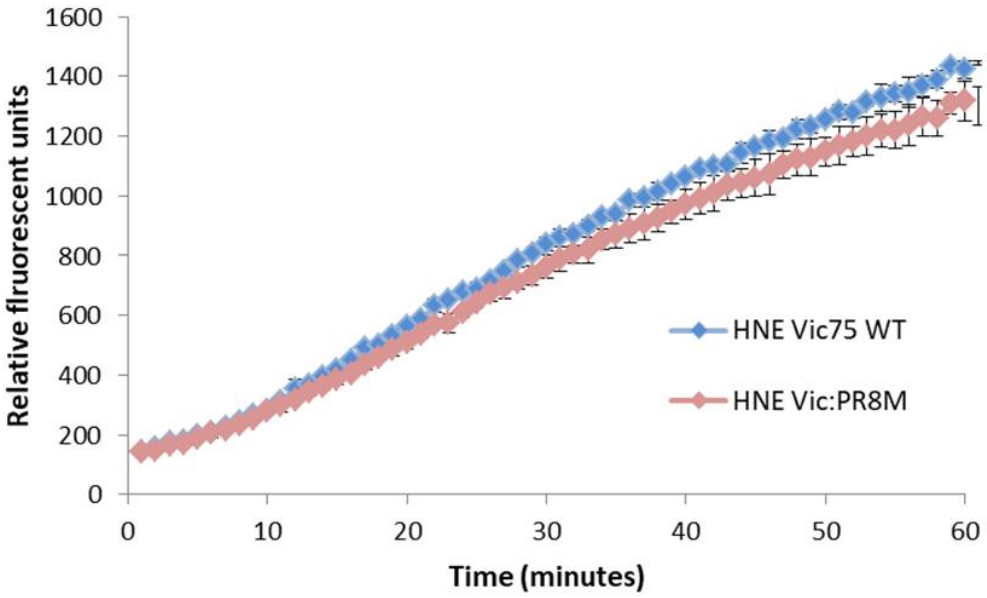

Figure 5.9: There is no difference in NA activity of Vic75 WT and Vic:PR8M viruses produced from HNE cells. 2.5x10^4 pfu was incubated with 100 µM of MUNANA at 37^{o}C and the amount of fluorescence generated from the cleavage of MUNANA by either HNE-grown virus stock was recorded every minute for one hour. The rates of reaction for each replicate were calculated and P values were calculated by a two-tailed student's t-test of the rates of signal generation by both viruses. P=. N:3.

5.10 Vic75 WT and Vic:PR8M virus particles produced from infected HNE culutres are equally inhibited by respiratory mucus.

We were interested to investigate the capacity of HNE-grown viruses to resist inhibition by respiratory mucus due to the HNE-grown viruses having the same released particle morphologies and NA activities. Resistance to inhibition by respiratory mucus is influenced by both NA activity and viral morphology (Figure 5.2). Virus samples from infected HNE cultures at 120 hpi were diluted to 100 pfu and treated with the indicated dilutions of respiratory mucus. Accordingly, no difference was seen when HNE Vic75 WT and HNE Vic:PR8M were treated with respiratory mucus, as neither virus demonstrated any difference in morphology or NA activity. Figure 5.10 illustrates that there is no difference in the amount of infectivity remaining when either HNE-grown sample of virus was used, and that this is independent of mucus concentration.

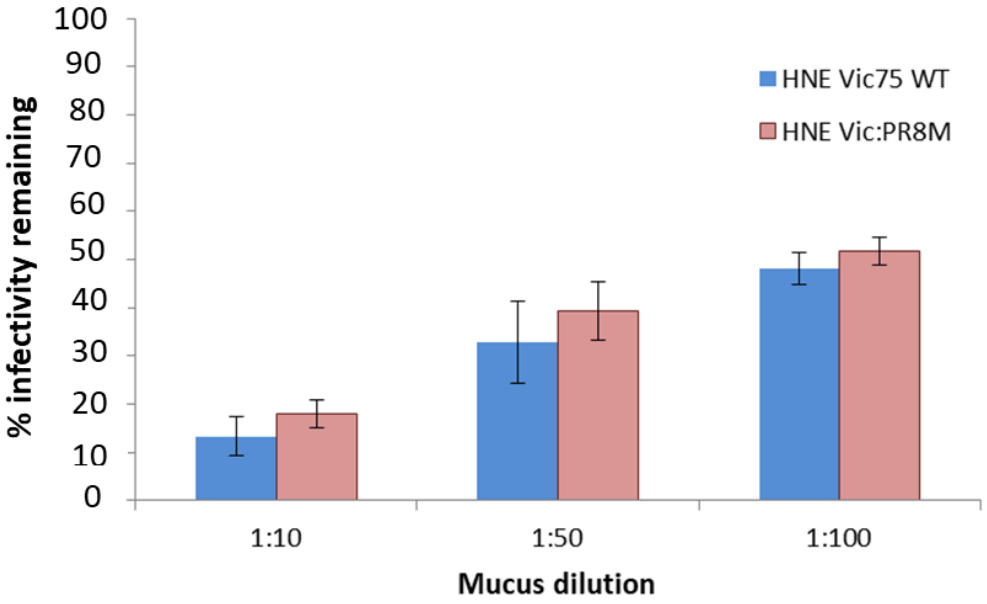

Figure 5.10: Vic75 WT and Vic:PR8M retain the same level of infectivity when produced from HNE cells. Virus produced from infected HNE cells were treated with respiratory mucus. Virus and mucus mixtures were incubated for one hour at 4^{o}C and adsorbed onto MDCK cells. Results are reported as the amount of plaques counted expressed as a percentage of an untreated control. N: 3.

5.11 Respiratory mucus present during initial infection does not convey an environment in which Vic75 WT can replicate to higher levels than Vic:PR8M.

In morphological terms, virions produced from HNE cultures infected with either Vic75 WT or Vic:PR8M are indistinguishable. Similarly, no difference was seen in the capacity of either to resist inhibition by respiratory mucus. Thus, it was hypothesised that if it were to convey any importance, then the initial establishment of infection is the stage at which a filamentous morphology might confer a replication advantage. It has been reported that viruses with lowered NA activities are less efficient at infecting human bronchial epithelial cells if the cultures have not been washed to remove mucus before infection (Zanin *et al.*, 2015). Whereas viruses with increased levels of NA activity were not as significantly affected by the lack of an initial wash prior to infection. Thus, it was hypothesised that by virtue of increased resistance to inhibition by respiratory mucus, filamentous particles might be more efficient at establishing infection in HNE cells with an unwashed mucus layer.

To test this, HNE cultures were washed 24 hours prior to infection, while previously they had been washed immediately prior to infection. To diminish the effect of diluting any mucus layer that was present on the cells, a 20 µl inoculum volume was used (when 100 µl had previously been used). Figure 5.11 shows the replication kinetics of Vic75 WT and Vic:PR8M in unwashed HNE cultures. As previously noted, there was no difference in the capacity of either virus to replicate in these cells. Even at the early time points, the same amount of virus was produced from cells infected with either virus. Thus, even with the initial innate barrier presented by the unwashed mucus layer, filamentous particles present in the MDCK-grown stock of Vic75 WT were insufficient to confer a growth advantage in this cell type.

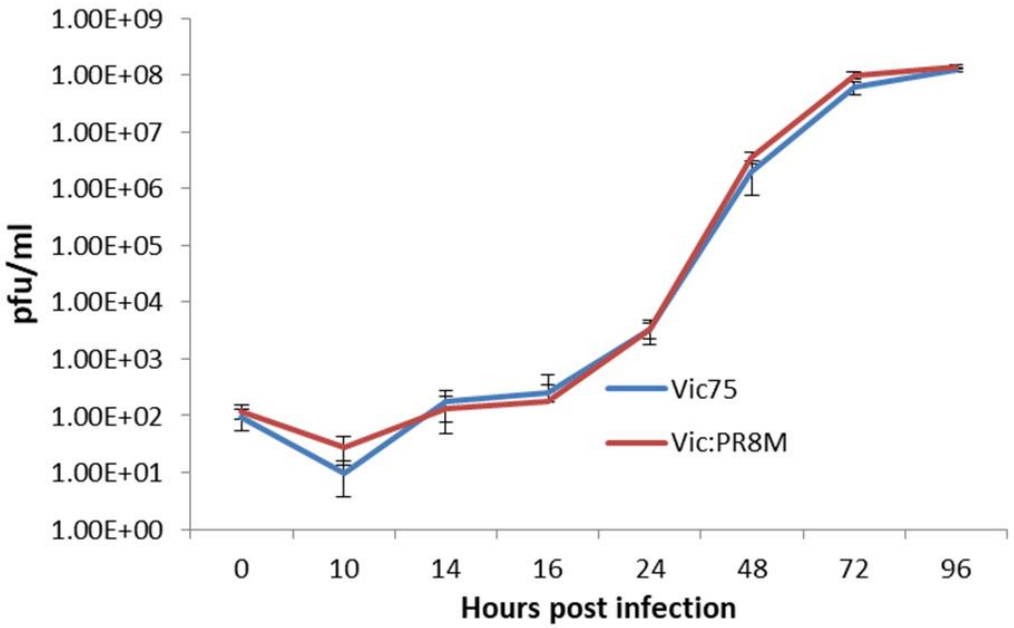

Figure 5.11: Virion morphology doesn't contribute to infectivity in unwashed HNE cells. HNE cells were washed 24 hours prior to infection. Six replicate sections containing HNE cells were infected at indicated MOI. Cells were incubated at 32°C. At indicated times post infection SF media was added to the apical layer of HNE cells and incubated for 30 minutes at 32°C. Viral titres of the apical washes were determined by plaque assay. The mean titre of four replicates is shown for each virus at each time point. Error bars represent standard deviation from the mean. N:1

5.12 Chapter 5 discussion

As stated in section 1.8, the primary focus of the work undertaken for this project was to attempt to discern the biological significance of filamentous particles. There is strong evidence to suggest that a filamentous phenotype influences transmission (Lakdawala *et al.*, 2011; Campbell, Danzy, *et al.*, 2014), but the mechanism by how this is achieved is unknown. To investigate this, the individual steps involved in a successful transmission event were considered. The experiments outlined in this section were designed to investigate whether a filamentous phenotype could confer a replication advantage in HNE cultures, an environment that is more representative of the natural tropism of IAV.

In agreement with section 4, it is demonstrated that stocks containing filamentous particles retain greater levels of infectivity when treated with respiratory mucus. We demonstrate here that this phenotype is dependent on NA activity, where this phenotype is not seen when viruses have been treated with oseltamivir, which blocks NA activity, or if the mucus is pre-treated with exogenous NA. We infer that the difference seen infectivity for either virus is dependent on their relative capacities to clear sialic acid receptors that are present in the respiratory mucus, which is dependent on NA activity. Interestingly, total NA activity as determined by the MUNAN assay is not a predictor of how resistant a virus will be to inhibition by respiratory mucus as demonstrated in figures 4.4 and 4.6.

No difference was seen in the capacity of virus stocks containing either filamentous or spherical-only virus particles to replicate in HNE cultures. This was independent of infecting MOI (Figure 5.3). The observation that cell-associated filamentous particles were generated from HNE cultures infected with Vic:PR8M was unexpected (Figure 5.6). Even more unexpected was the observation that only spherical particles were observed as released virions regardless of the infecting, parental virus (Figure 5.8). This strongly suggests that the cellular machinery that is involved with the assembly, budding and release of viral particles in HNE cells is different to that in immortalised cells. It also suggests that the viral genetic characteristics that influence morphology in immortalised cells are not as relevant in HNE cultures, most likely through interaction with cellular factors.

It is interesting to note that no released filamentous particles were observed from Vic75 WT infected HNE cells. Only spherical viral particles were observed as released virions as determined by TEM (Figure 5.8). This is surprising as a filamentous phenotype is considered to be associated with *in vivo* infections. HNE cultures are composed of primary cells that have originated from a humans nose, thus should be representative of infection *in vivo* at the cellular level. Despite this, only spherical particles were observed as released virions. Thus, assuming that HNE cultures can be considered as a surrogate for infection *in vivo*, the relevance and incidence of filamentous particles *in vivo* should be reconsidered.

Initially it was hypothesised that no difference was seen in replication of Vic75 WT and Vic:PR8M (Figure 5.5) because there was no difference in the morphological phenotype of either virus generated from infected HNE cells (Figures 5.6 and 5.8). It was then hypothesised that if a filamentous morphology were to confer any advantage it would be at the initial infection event; where filamentous particles would be more efficient at resisting inhibition by respiratory mucus present in the layer above the cells. When the mucus layer above the HNE cultures was washed 24 hour prior to infection, no difference was seen in the capacity of either Vic75 WT or Vic:PR8M to establish infection (Figure 5.11). It is possible that if the mucus layer were unwashed for several days prior to infection, the increased amounts of mucus might present an adequate barrier to infection by spherical viral particles. However, this warrants further testing to be able to rule this out with certainty.

Chapter 6: Effect of morphology on the infectivity of virus particles contained in respiratory droplets.

We have investigated two stages of a transmission event, establishment of infection in respiratory epithelium and virus replication in respiratory epithelium. No difference was seen for the replication capacities of either filamentous or spherical viruses in infected HNE cultures (Figure 5.5). From this we infer that if a filamentous phenotype were to affect transmissibility of IAV, it would not due to the titre shed by infected donors. Similarly, our data suggests that morphology would not affect the establishment of infection (Figure 5.11). Therefore, we were interested to investigate the environmental effects on viral particles, and if a filamentous morphology could contribute to increased stability of virions.

6.1 The IVT system

The IVT system is a unique piece of equipment that was designed by Prof. Wendy Barclay's research group at Imperial College London and validated by Dr. Ruth Elderfield. The system was designed to simulate respiratory transmission to aid investigation of the very early stages of infection. The system is illustrated in figure 6.1 and works by blowing aerosolised virus through a chamber, over cell monolayers. Virus stocks were aerosolised using a nebuliser which generated droplets with the range of 1-5 µm in size. The airflow within the system is unidirectional, carrying the droplets through the system, from the nebulisation chamber into the main IVT chamber. Within the main chamber there are three 6 well plates at increasing distances from the nebulisation chamber. As virus-containing droplets are carried along the airflow, some are deposited onto the 6 well plates that contain MDCK cells covered by a minimum volume of media. After exposure, the plates are treated in the same manner as plaque assay plates and incubated until plaques develop. By comparing the amount of pfu of one virus versus another, interpretations can be made about the relative stability of a given virus in aerosolised droplets and conclusions regarding aerosol transmissibility can be made. In collaboration with Prof. Wendy Barclay we used the IVT system to investigate the aerosol stability and transmission of filamentous Vic75 WT and spherical-only Vic:PR8M viruses. A similar system has been developed by Creager *et al*., (2017). This system does

not consider the effect that distance travelled by aerosolised droplets may have on the infectivity of virus particles carried within those droplets. The system described by Creager *et al*., (2017) aerosolises virus and directly inoculates cells. The authors demonstrated robust reproducibility and effectiveness of the system. They were also able to record differences in infectivities of different viral strains (Creager *et al.*, 2017). It is unknown what effect that nebulisation might have on the relative integrity of different virion morphologies and this caveat will have to be considered when interpreting any data.

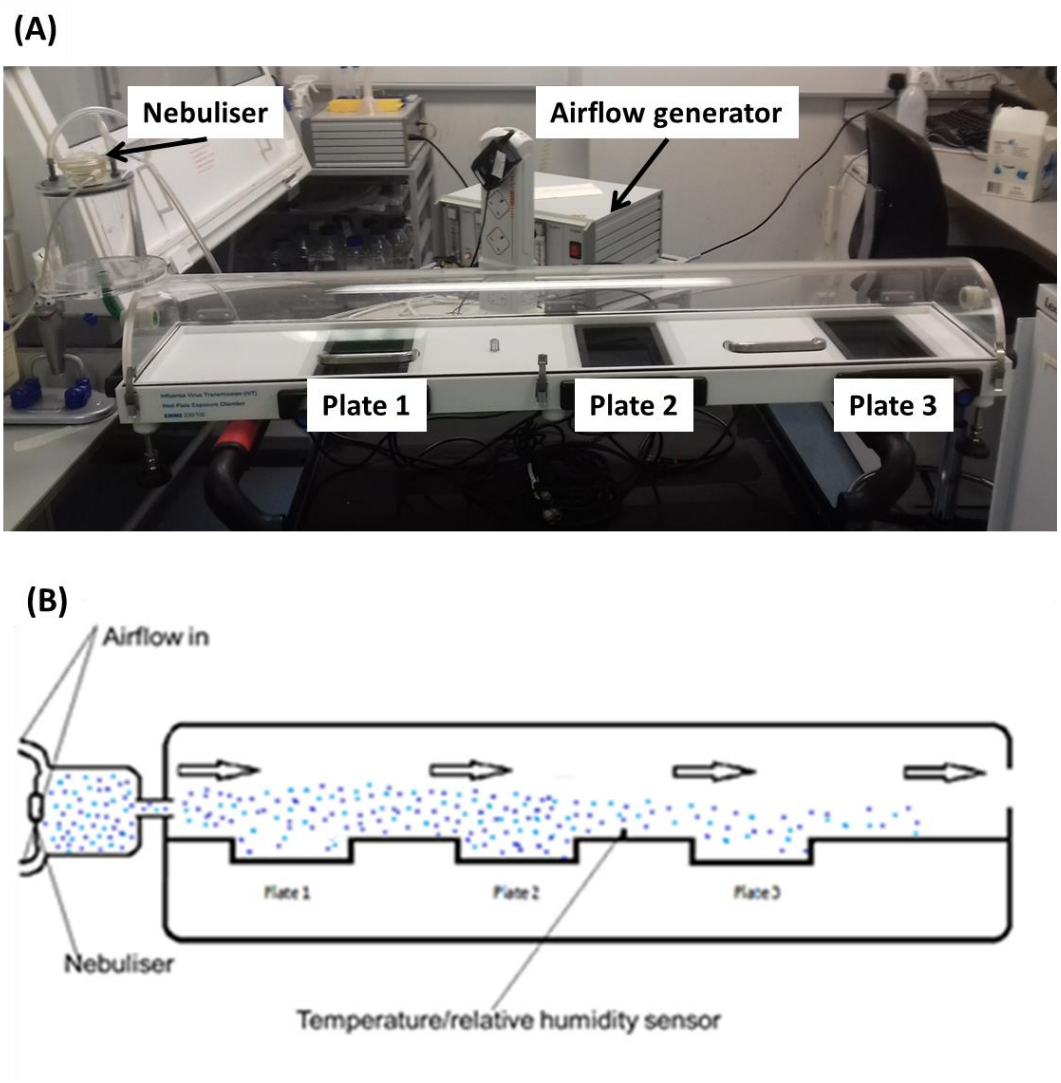

Figure 6.1: The IVT system. (A) A photograph of the IVT system. On the left is the nebulisation chamber with the tubes connected to the airflow generator (middle background). Slots for the tissue culture plates are shown with Plate 1 being closest to the source of virus and plate 3 being the farthest. (B) cartoon diagram of the IVT system. It shows a representation of nebulised virus being carried through the IVT system in a current of air generated from the flow generator. Arrows indicate the direction of airflow.

6.2 In vitro transmission of nebulised Vic75 WT and Vic:PR8M was not affected by a mucus overlay covering MDCK cells

In chapter 4, figure 4.7 we observed that in a plaque reduction assay, Vic75 WT was more resistant to inhibition by respiratory mucus compared to Vic:PR8M, and that this was dependent on a filamentous phenotype and the activity of the NA enzyme (Figure5.2). However we also observed that mucus was not a significant factor during infection of HNE cultures (Figure 5.9). We were therefore interested to test the effect that a mucus barrier had in a setting that was more similar to an aerosolised transmission event, where we measured respiratory droplets containing viral particles settling out of an airflow onto cells beneath a mucus barrier. The aim of this experiment was to model a transmission event and measure the effect of the mucus barrier on infection of the sentinel animal or person. We did not previously see a difference in infectivity in infected HNE cultures, thus it was hypothesised that by reducing the inoculum titre and diluting the concentration of virus per unit volume (i.e. virus-containing droplets in a vapour versus virus in SF media) the effect of filamentous particles to resist inhibition by respiratory mucus would be more apparent than when HNE cultures were infected.

Plates containing MDCK cells were washed and had a 1:20 dilution of respiratory mucus added to each well. Three plates, each at increasing distance from the source of nebulised virus were added to the IVT (Figure 6.1). The viruses were diluted in 0.9% saline, nebulised and carried along an airflow through the IVT over the cells containing a mucus overlay. Triplicate exposure events of $2.5x10^4$ pfu were performed and the mean and standard deviation for each plate calculated and reported. Figure 6.2 (A) shows the mean number of pfu for either virus from a representative experiment of three experiments. There was no significant difference in the number of pfu/plate for either virus. However, it is interesting to note that of the three experiments performed, the mean pfu/plate for Vic75 WT over three individual experiments was 0.6 pfu/plate (Table 6.1). While Vic:PR8M never generated any plaques on the plate the farthest away from the source of nebulised virus. Figure 6.1 (B) shows a positive control that was performed concurrently with the IVT experiment. The inoculum stock was incubated with the same dilution of respiratory mucus used for the IVT for 30 minutes. This was then titrated and

added to confluent MDCK cells. Figure 6.1 (B) shows the percentage of pfu in the treated inoculum versus the untreated. For the mucus inhibition control, Vic75 WT had approximately a 15% greater amount of pfu when treated with respiratory mucus compared to Vic:PR8M, but this was not statistically significant, but the level of difference between Vic75 WT and Vic:PR8M is comparable with previous results (Figure 4.8). This data shows that Vic75 WT does not have a significantly increased capacity to resist inhibition by respiratory mucus when carried in aerosolised droplets.

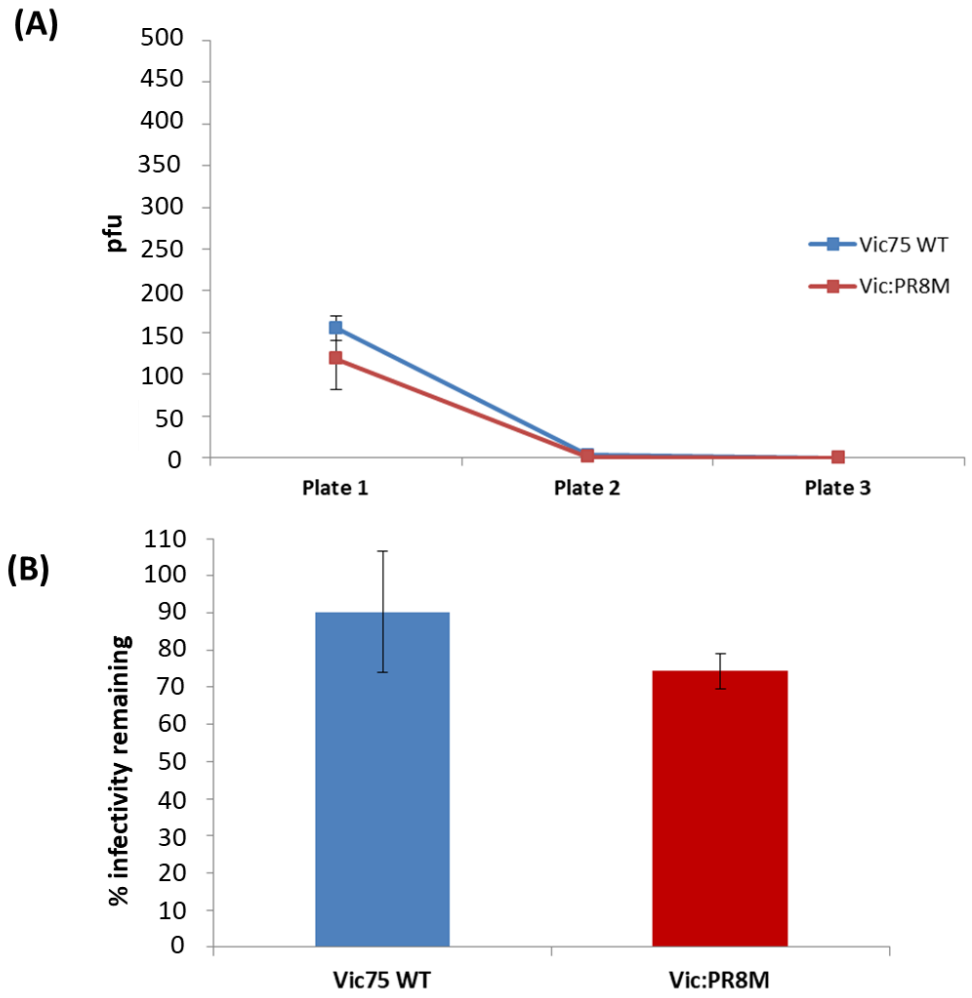

Figure 6.2: There is no difference in infectivity between nebulised Vic75 WT and Vic:PR8M when there is a mucus overlay covering MDCK cells. Viruses were diluted to 2.5 x 10^4 pfu in 0.9% saline solution. Respiratory mucus was diluted 1:20 and added to 6 well plates. The airflow was set to 1 litre/minute. 20 µl of virus was nebulised for 15 seconds and airflow switched-off after 5 minutes of exposure. Cells were overlayed and incubated until plaques developed and the number of pfu per plate was recorded. The mean for each plate for three replicate exposure events for each virus are shown. Error bars represent the standard deviation of the mean of the three replicate exposure events. (B) Mucus plaque reduction assay. The virus stocks used for the IVT experiment were incubated with a 1:20 dilution of respiratory mucus. The virus:mucus mixture was incubated for 30 minutes at 4^{o}C then adsorbed to MDCK cells for one hour at 37^{o}C. The mean % pfu as calculated from an untreated control are shown. N:3. Data is representative of three individual experiments.

6.3 Resistance to mucus inhibition is not affected by immediate incubation at 37^{o}C

We were surprised to see that there was no difference seen in the amount of pfu observed by either Vic75 WT or Vic:PR8M when a mucus overlay was placed over MDCK cells and viruses were passed through the IVT. This was unexpected as it has been previously observed that Vic75 WT is more resistant to inhibition by respiratory mucus (Figure 5.2). One potential cause for this discrepancy was in the protocol for either assay. The previous protocol involved incubation of the virus:mucus for one hour at 4^{o}C and then adsorption onto MDCK cells for one hour at 37^{o}C. For the IVT protocol, there was no incubation step at 4^{o}C. Aerosolised virus was added directly to mucus and then allowed to adsorb to cells at 37^{o}C. To address if this was the cause of the lack of difference in resistance to inhibition by respiratory mucus seen for both viruses, an assay was set up where virus was mixed with respiratory mucus and added directly to cells. Figure 6.3 shows the percentage infectivity remaining of Vic75 WT and Vic:PR8M when the virus was mixed with respiratory mucus and added directly to cells and adsorbed for one hour at 37^{o}C. Vic75 WT had a significantly greater amount of infectivity remaining compared to Vic:PR8M (Figure 6.3) and the difference in infectivity was similar to that seen when there was an initial 4^{o}C incubation (Figure 5.2). Thus, the lack of a 4^{o}C pre-incubation step was not the cause for the lack of difference seen when the viruses were passed through the IVT (Figure 6.2).

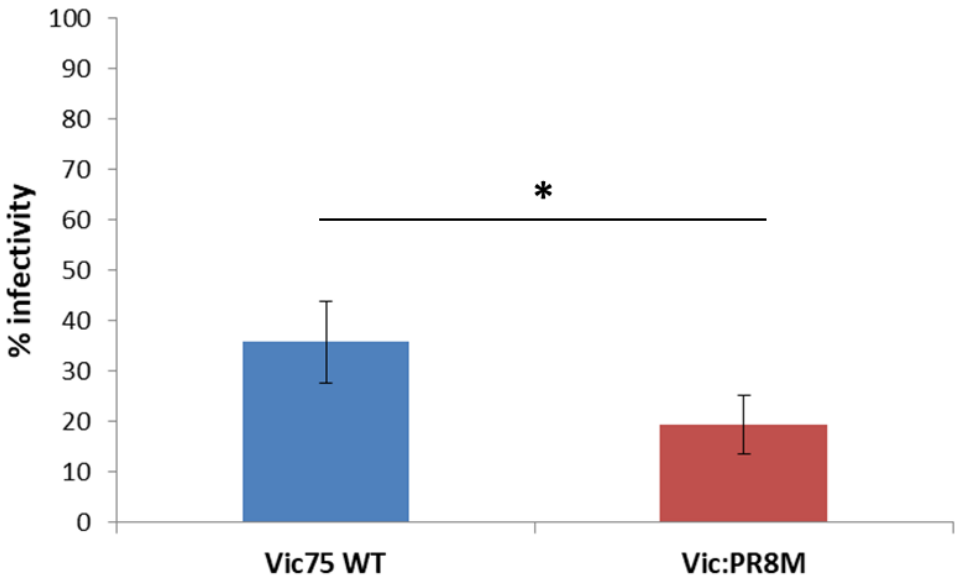

Figure 6.3: Resistance to mucus inhibition is not affected by immediate incubation at 37°C. 100 pfu of either virus was treated with a 1:20 dilution of respiratory mucus. Virus:mucus mixtures were added to MDCK cells and incubated for one hour at 37°C. Cells were washed with PBS, overlayed and incubated for 72 hours. Plaques were counted and expressed as a percentage of the mucus-untreated control. Error bars representthe standard deviation of the mean of the three replicate exposure events. * represents a p value of <0.05. N: 3. Data is representative of three individual experiments.

6.4 Vic75 WT retains higher levels of infectivity in the IVT when pre-treated with respiratory mucus.

As no effect was seen when respiratory mucus was used as a barrier to infection as an overlay over MDCK cells, we were interested to investigate any potential effects that pre-treating virus with mucus may play in levels of infectivity in this system. We were interested to investigate the effect that the presence of mucus in donor respiratory droplets might have. It was hypothesised that if respiratory mucus were present in the respiratory droplets alongside the viral particles, it would confer an inhibitory effect.

Vic75 WT and Vic:PR8M were diluted to $5x10^4$ pfu and mixed 1:1 with a 1:10 dilution of respiratory mucus in quadruplicate. Each replicate was incubated at 4^oC for 30±5 minutes. Tissue culture plates containing MDCK cells were washed and replaced with 200 µl of overlay media. Plates were added to the IVT and the virus:mucus mixture was nebulised and passed over the cells for 5 minutes. Figure 6.4 (A) shows the mean number of pfu/plate recorded for triplicate exposure events. A greater amount of pfu was observed for Vic75 WT on all three plates. There was significantly greater numbers of plaques on the two plates closest to the source of virus, with Vic75 WT having 2- and 4-fold greater pfu on the closest and second closest plates respectively. Over the course of three stand-alone experiments, the mean pfu/plate for the farthest plate was 1.7 for Vic75 WT and 0 for Vic:PR8M (Table 6.1). Therefore during transmission respiratory mucus presented a barrier to infection that was more difficult for Vic:PR8M to surmount than Vic75 WT. Figure 6.4 (B) shows a positive control that was performed concurrently with the IVT experiment. The inoculum virus:mucus stock was incubated at 4^oC for 30 minutes, titrated and adsorbed to MDCK cells for one hour at 37^oC. In agreement with previous data (Figure 5.2), Vic75 WT retained significantly greater levels of infectivity when treated with respiratory mucus.

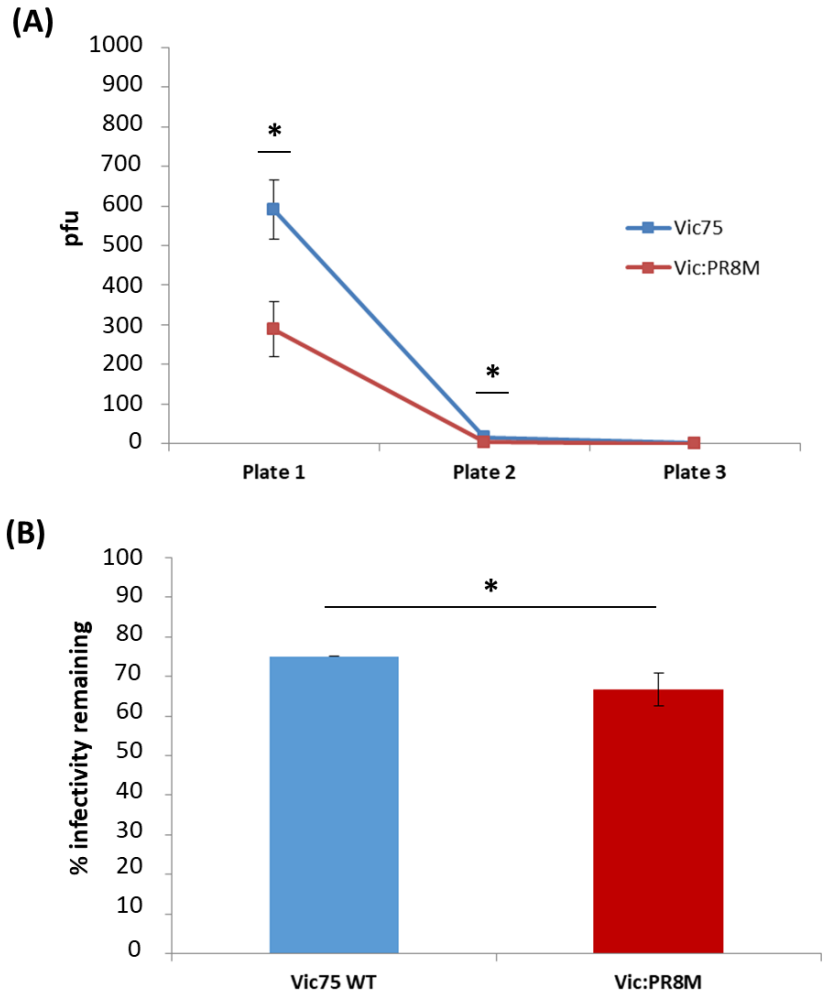

Figure 6.4: Vic75 WT retains higher levels of infectivity when pre-treated with respiratory mucus and passed through the IVT. Viruses were diluted in 0.9% saline solution. Respiratory mucus was diluted 1:10, mixed with diluted virus in triplicate and incubated for 30 minutes at 4^{o}C before nebulisation. The airflow was set to 1 litre/minute. The virus/mucus mixture containing 2.5x10^{4} pfu was nebulised for 15 seconds and cells were exposed for 5 minutes. The mean for each plate for three replicate exposure events for each virus are shown. (B) Mucus plaque reduction assay. The virus stocks used for the IVT experiment were incubated with diluted respiratory mucus. The virus:mucus mixture was incubated for 30 minutes at 4^{o}C then adsorbed to MDCK cells for one hour at 37^{o}C. The mean % pfu as calculated from an untreated control are shown. Error bars represent the standard deviation of the mean of the three replicate exposure events. * represents a p value of <0.05 as determined by a two-tailed students t-test.N:3.Data is representative of three individual experiments.

6.5 Buffer in which viruses are diluted determines infectivity of viruses carried through the IVT.

Initial validations for the IVT was carried out using a stabilisation buffer that consisted of 0.375% BSA diluted in PBS as the diluent in which viruses were prepared. The purpose of this was to make the system as conducive as possible to the retention of infectivity of the viruses that were passed through the IVT. Figure 6.5 (A) shows the mean pfu/plate for each plate when either virus stock was diluted in the stabilisation buffer and passed through the IVT. When this buffer was used, there were no significant differences in the amount of pfu/plate seen for either virus. This data is representative of three replicate experiments.

We were interested to investigate if the conditions could be made to be less conducive for viruses. We were interested to investigate what effect that diluting the viruses in an un-buffered solution might have. It was decided to investigate the effect that diluting the viruses in 0.9% saline, which is more physiologically relevant than PBS with BSA. It was considered that by using a 0.9% saline buffer the pH of the nebulised droplets would be less stable and more prone to a reduced pH due to evaporation of water from the microscopic droplets. It was hypothesised that by containing greater amounts of HA per infectious unit, filamentous particles would be more resistant to inhibition by lowered pHs and premature adoption of a fusion conformation, because the chance that a filamentous particle would have a HA with a receptor-binding conformation would be greater than that for a spherical particle. Figure 6.5 B shows the mean pfu/plate for Vic75 WT and Vic:PR8M when 0.9% saline was used as a diluent buffer. When $2.5x10^4$ pfu of either virus was passed through the IVT, Vic75 WT had significantly greater levels of pfu for each plate. Therefore when the viruses were diluted in 0.9% saline, Vic75 WT retained greater levels of infectivity when passed through the IVT than Vic:PR8M. Similar to observations made in Figures 6.2 and 6.4, Vic75 WT plaques formed on the most distal plate while Vic:PR8M did not. This strongly suggests that filamentous particles are more stable when carried in aerosolised droplets.

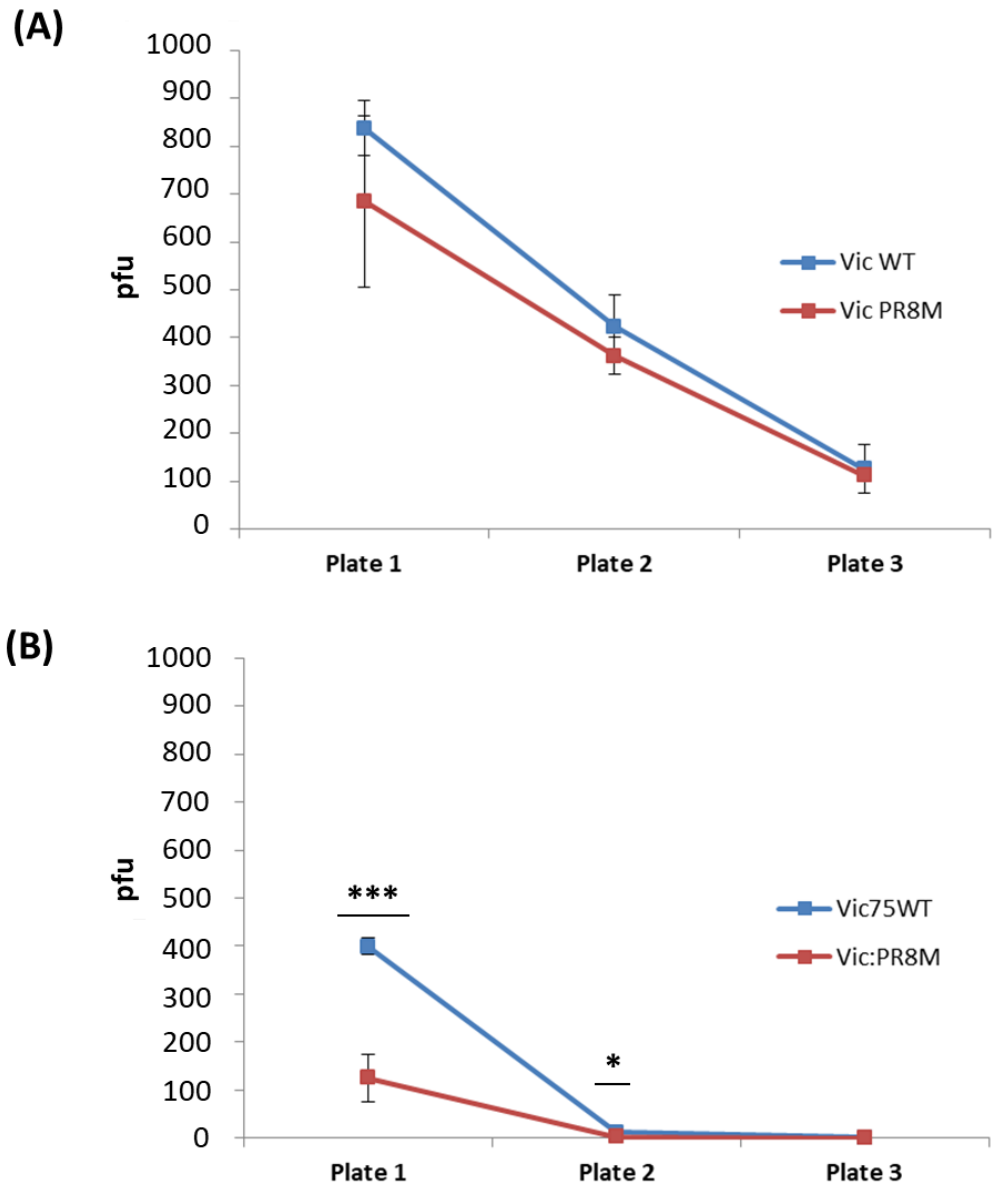

Figure 6.5: The buffer in which viruses are diluted affects infectivity and Vic75 WT is less significantly affected. Viruses were diluted in (A) a stabilisation buffer or (B) 0.9% saline. Plates were exposed to 2.5 x 10^4 pfu for five minutes, adsorbed to cells for one hour then incubated at 37^{o}C for approximately 72 hours. The number of pfu per plate was recorded. The mean for each plate for three replicate exposure events for each virus are shown. Figures show representative data from one of three replicate experiments. Error bars represent the standard deviation of the mean of the three replicate exposure events in the course of a single experiment. *** and * represent a p value of <0.001 and <0.05 as determined by a two-tailed students t-test. N:3. Data is representative of three individual experiments.

		Mean pfu count of three individual experimental runs			
		Mucus Overlay	0.9% Saline + Respiratory Mucus	Stabilisation Buffer	0.9% Saline
Vic75 WT	Plate 1	155.8±51.0	495.4±127.0	1027±244.6	447.7±124.2
	Plate 2	1.9±1.5	14.4±6.0	358.8±236.9	18.1±6.0
	Plate 3	0.6±0.4	1.7±0.8	119.2±101.4	1.4±0.8
Vic:PR8M	Plate 1	140.2±15.1	312.8±42.8	969±259.2	239.3±129.7
	Plate 2	1.3±0.6	5.4±1.7	439.9±288.6	6.6±3.1
	Plate 3	0±0	0.3±0.3	118.2±95.6	0±0

Table 6.1: Summary of IVT experiments. Each treatment investigated using the IVT was performed three separate times, on individual days. This table gives a summary of the mean of the combined pfu count per plate for the three replicate experiments for each experimental condition. Standard deviation from the mean for combined experimental data is also represented.

6.6 Vic75 WT virions are more stable at 37^{o}C and lowered pHs.

We were next interested in comparing the relative thermal and pH stabilities of Vic75 WT and Vic:PR8M virus particles. One previous study compared the temperature stability of filamentous and spherical viruses, and found no differences between the two (Seladi-Schulman *et al.*, 2014). Another study demonstrated that viruses that had a diminished capacity to produce extended, cell-associated, filamentous bundles were significantly less stable when incubated at room temperature (Beale *et al.*, 2014). First we investigated the relative stability of virus particles at room temperature, which would be relevant for fomite transmission. Figure 6.6 (A) shows the stability of either Vic75 WT or Vic:PR8M virus diluted to a starting titre of 2.5x10^{4} pfu/ml when incubated for the indicated times at 20^{o}C. It is clear that virions of both viruses are quite stable at this temperature, as no reduction in titre was observed.

Next, we were interested to investigate if the virions were as stable at the higher, but still physiologically relevant, temperature of 37^{o}C. Figure 6.6 (B) shows the relative stability of Vic75 WT and Vic:PR8M when diluted in 0.9% saline and incubated at 37^{o}C for the indicated times. Vic75 WT and Vic:PR8M were unstable for extended periods of time at 37^{o}C and the titres had dropped to 401.7 and 3.33 pfu/ml respectively by 8 hours.Vic75 WT virions retained significantly greater levels of infectivity after 8 hours incubation at 37^{o}C than Vic:PR8M.

Due to the observation made in figure 6.4 that the buffer in which viruses were diluted significantly affected the relative infectivity of either Vic75 WT or Vic:PR8M when passed through the IVT, it was hypothesised that filamentous particles are more resistant to inhibition by lowered pH. To investigate this, Vic75 WT and Vic:PR8M were treated with buffers at different pHs. Viruses were diluted in 0.9% saline and 500 pfu were treated with buffers at the pHs indicated in figure 6.5 (C) for 15 minutes at 37^{o}C. Untreated controls were diluted in 0.9% saline, and the amount of pfu for each pH buffer was expressed as a percentage of the untreated pfu control. Vic75 WT retained significantly higher levels of infectivity at pH 5.6, 5.5 and 5.4 than Vic:PR8M. This agrees with the hypothesis that filamentous virus particles are more resistant to inhibition by lowered pHs.

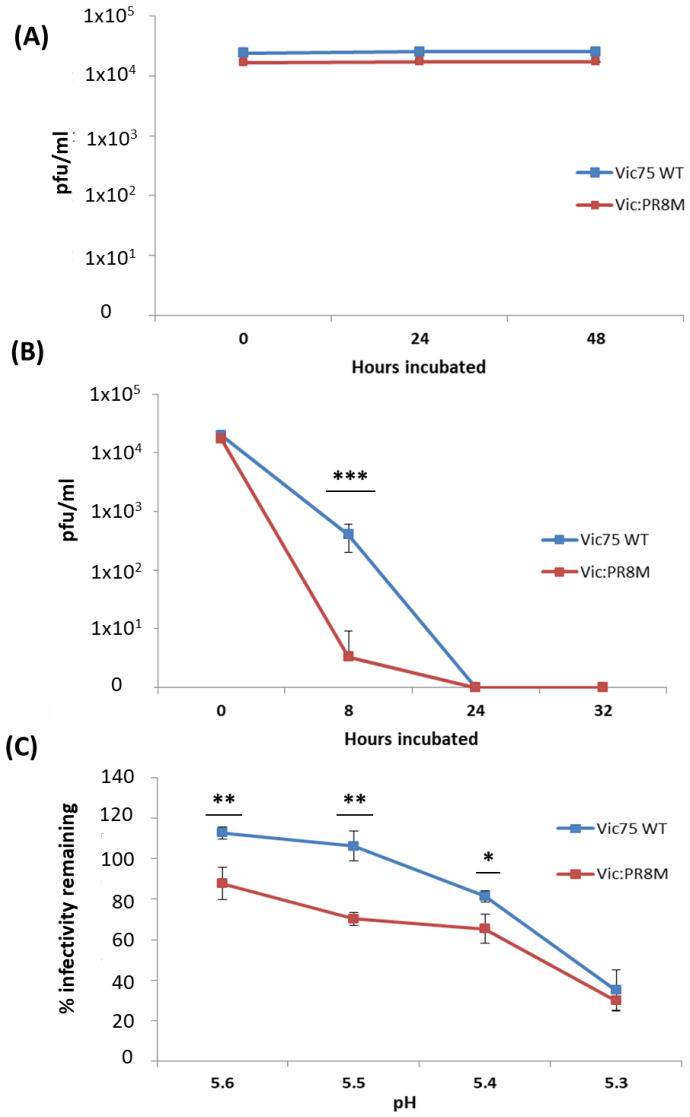

Figure 6.6: Vic75 WT virions are more stable at 37°C and at lowered pHs than Vic:PR8M. 2.5x10^4 pfu/ml of Vic75 WT and Vic:PR8M were diluted in 0.9% saline and incubated at either (A) 20°C or (B) 37°C for the indicated times. Collected samples were stored at -80°C and viral titre determined by plaque assay. N:3. (C) Vic75 is more stable at low pHs. Vic75 WT and Vic:PR8M were diluted in 0.9% saline. 500 pfu was incubated with buffers at the indicated pHs at 37°C for 15 minutes. Untreated controls were incubated with 0.9% saline. Following incubation, SF media was added to each tube to buffer the solution and added to MDCK cells. Infectivity remaining is represented as a percentage of the untreated 0.9% control. Error bars represent standard deviation of the mean % pfu. ***, ** and * represent a p value of <0.001, <0.01 and <0.05 respectively as determined by a two-tailed students t-test. N: 3. Data is representative of three individual experiments.

6.7 Viruses that express the same segment 7 have the same stability at lowered pH.

We were interested to investigate the mechanism by which filamentous viral particles confer increased temperature and pH stability. It has been previously recorded that there was no difference in the relative stability of the viruses that were spherical or filamentous (Beale *et al.*, 2014). The authors found that a motif in the M2 protein significantly altered the stability of both filamentous and spherical viruses when they were incubated at room temperature. Because of this, we were interested to investigate if the different polypeptide products of the segment 7 generated by either Vic75 WT or Vic:PR8M could influence stability. The generation and characterisation of stocks with increased amount of NIPs was outlined in section 4. A surprising phenotype of the Vic75 NIP stock was that it did not have significantly greater levels of infectivity compared to Vic:PR8M when treated with respiratory mucus (Figure 4.7). Fewer filamentous particles were qualitatively observed when this stock was visualised by TEM, compared to the common observation of filamentous particles in the Vic75 WT stock. Thus, it was hypothesised that by comparing the stability of the two Vic75 stocks, the effect that filaments had on relative stability could be ascertained while controlling for different products expressed from either segment 7.

Figure 6.7 (A) shows the thermal stability of the different standard and NIP stocks of Vic75 WT and Vic:PR8M. Both stocks of Vic75 WT retain significantly greater levels of infectivity when compared to the two stocks of Vic:PR8M when incubated at 37^{o}C. We have previously noted that the Vic75 NIP stock has far fewer filamentous virions compared to the Vic75 WT stock (Figure 4.9). Despite having fewer filamentous particles, the Vic75 NIP samples retained the same level of infectivity as Vic75 WT samples. Similarly, no difference in infectivity was seen between either the Vic:PR8M or PR8M NIP stocks. Importantly, both stocks of Vic75 viruses retained greater levels of infectivity compared to both stocks of viruses that express the PR8 segment 7. Therefore, the increased thermal stability of Vic75 WT is most likely mediated by the proteins expressed from the Vic75 WT segment 7, or possibly by altered RNA-RNA interactions.

Similar to investigating the stability of these viruses at 37^{o}C, we were interested to ascertain the relative pH stability of these viruses. We have reported that Vic75 WT is more stable than Vic:PR8M at lowered pHs (Figure 6.6). Similar to the results recorded for the stability of viruses at 37^{o}C, viruses that expressed the proteins encoded by Vic75 WT segment 7 were more stable at lower pHs than viruses that expressed PR8 segment 7 proteins (Figure 6.7 B) and that this is independent of virion morphology (Figure 4.9). Where both stocks of Vic75 WT viruses had significantly greater levels of infectivity compared to both stocks of Vic:PR8M. This strongly suggests that the difference seen in pH stability for Vic75 WT and Vic:PR8M is due to virion composition and not virion morphology.

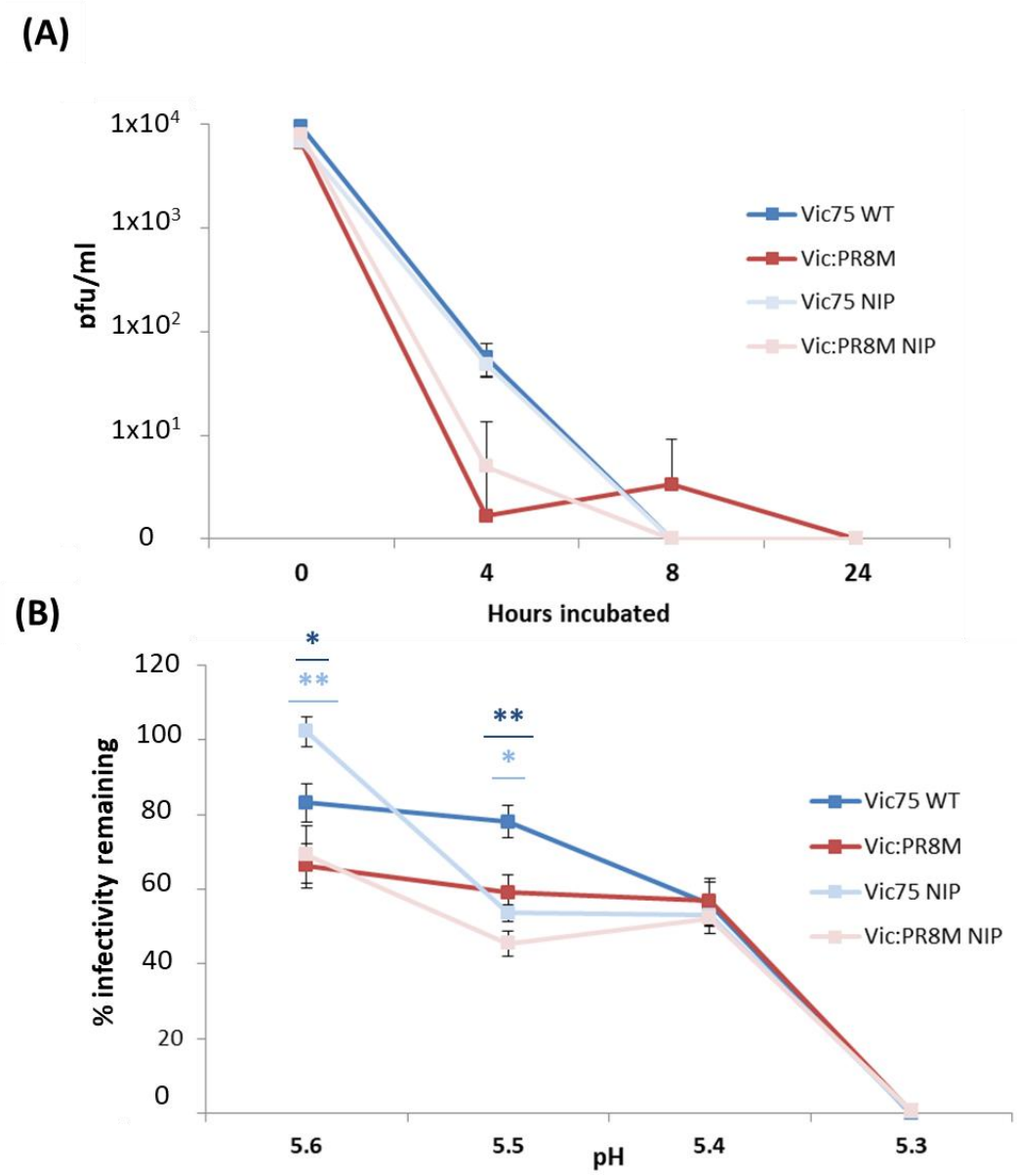

Figure 6.7: Vic75 NIP and Vic:PR8M NIP stocks have the same stability profiles as the Vic75 WT and Vic:PR8M stocks. (A) Virus stability at 37°C. 2.5x10^{4}pfu/ml of virus was diluted in 0.9% saline and incubated at 37°C for the indicated times. Samples were stored at -80°C and viral titre determined by plaque assay. N:3. (B) pH stability. Viruses were diluted in 0.9% saline. 500 pfu was incubated with buffers at the indicated pHs at 37°C for 15 minutes. Untreated controls were incubated with 0.9% saline. Pfu were counted and are represented as a percentage of the untreated 0.9% control. *** and * represent a p value of <0.001 and <0.05 respectively as determined by a two-tailed students t-test. N: 3. Data is representative of three individual experiments

6.8 HNE-grown Vic75 WT has greater pH stability compared to HNE-grown Vic:PR8M

To further control for the effect of virion morphology versus expression of different M1 and M2 proteins, the pH stability of HNE-grown virus stocks was investigated. In section 5 it was shown that when HNE cultures were infected with either Vic75 WT or Vic:PR8M no difference was seen in the morphology of the virions, NA activity or resistance to mucus (Figures: 5.7, 5.8, 5.10), whilst differences had been observed in MDCK grown stocks (Figures: 4.1, 4.3, 5.2). Therefore, in the assays tested the Vic75 WT and Vic:PR8M virions produced from HNE cells are indistinct apart from the different M1 and M2 proteins.

Virus stocks that were generated from HNE cultures infected with either Vic75 WT or Vic:PR8M were treated with buffers at a range of pHs. Figure 6.8 shows the percentage infectivity remaining when both HNE stocks were treated with acidic buffers. HNE Vic75 retained significantly greater amounts of infectivity at a pH of 5.5 and 5.4. This data matches the observation made in figure 6.7 (B), where viruses that have the Vic75 WT segment 7 are more resistant to inhibition by lowered pHs. This observation coupled with the data presented in figures: 5.7, 5.8 and 5.10, strongly suggests that virion protein composition, not morphology, is the arbiter of increased pH stability. We had previously hypothesised that the difference seen in pH stability of Vic75 WT and Vic:PR8M was due to increased amounts of HA on a filamentous virion. This is unlikely to be the mechanism by which Vic75 WT retained greater levels of infectivity but is more likely due to increased stability conferred by the Vic75 WT M1 and M2 proteins present in virions.

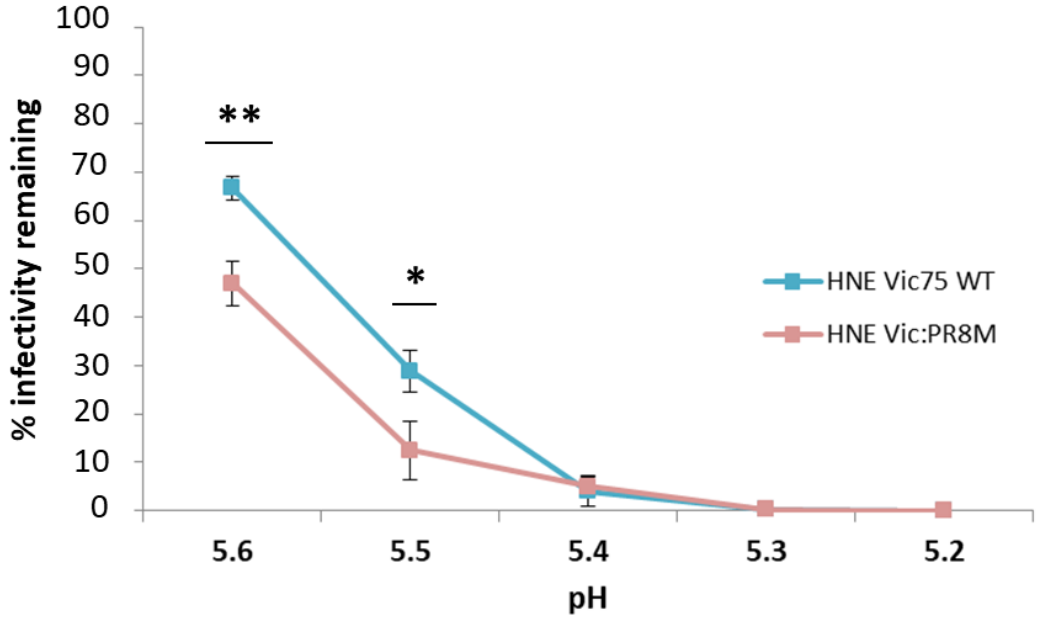

Figure 6.8: Vic75 and Vic:PR8M grown in HNE cultures have different pH stabilities. Vic75 WT and Vic:PR8M that were grown from HNE cultures were diluted in 0.9% saline. 500 pfu was incubated with buffers at the indicated pHs at 37^{o}C for 15 minutes. Untreated controls were incubated with 0.9% saline. Following incubation, SF media was added to each tube to buffer the solution. 200 µl of this was added to confluent MDCK cells. Plaques were counted and Infectivity remaining represented as a percentage of the untreated 0.9% control. ** and * represent a p value of <0.01 and <0.05 respectively as determined by a two-tailed students t-test. N:3. Data is representative of three individual experiments

6.9 Chapter 6 discussion

Traditional animal-based aerosol transmission studies typically address two questions regarding IAV transmission: Quantification of viral titres shed by donor animals and quantification of transmission events leading to infection or seroconversion of exposed sentinel animals. Animal models are and will remain the gold standard when assessing the transmission potential of IAV, however, they are expensive and lack certain measurable and controllable factors. There are several benefits to using the IVT system to investigate aerosol transmission. It can provide a direct comparison between input titre and the amount of infectious virus carried through an airflow. There is also the capacity for the direct comparison of the infectivity of different viruses when carried within aerosolised droplets.

As discussed in the section 1.6.5, there is strong evidence that correlates transmissibility with morphology (Lakdawala *et al.*, 2011; Campbell, Danzy, *et al.*, 2014). We decided to use the IVT system to investigate the infectivity and stability of morphologically distinct virions within aerosolised droplets. Firstly, the inhibitory effect of respiratory mucus as a barrier against infection was investigated. Cells with a mucus overlay were exposed to aerosolised virus (Figure 6.2) and we found that there was no difference observed in the infectivity of either virus under these conditions. In section 4 we demonstrated that filamentous particles confer increased resistance to inhibition by respiratory mucus (Figure 4.7). It is therefore tempting to speculate that filamentous particles are maintained in aerosolised droplets, and that this is the reason why Vic75 WT generates plaques on the farthest plate from the source of aerosolised virus. On three separate experimental runs Vic:PR8M failed to generate any plaques on the this plate (Table 6.1). If the experiment outlined in figure 6.2 was to represent the effect that respiratory mucus may have *in vivo*, it would be the effect that it presents to incoming viral particles in a naïve sentinel. However, this conclusion is undermined by the infectivities recorded for either virus on the first and second closest plates to the source of nebulised virus (Figure 6.2 and Table 6.1). No difference in infectivity was seen for Vic75 WT and Vic:PR8M for plate 1 or 2 when there was a mucus overlay, when Vic75 WT has retains significantly greater infectivity when neither virus are nebulised (Figures 4.6, 5.2 and

6.3). This suggests that filamentous particles may not be maintained when passed through the IVT.

To investigate if there was any effect that the donor respiratory mucus might have in an aerosol transmission event, virus was pre-incubated with mucus and then exposed to cells. Figure 6.3 shows that when pre-treated with respiratory mucus, Vic75 WT retained significantly greater levels of infectious virus. This suggests that filamentous particles are more capable of retaining infectivity when respiratory mucus is present in the aerosolised droplets, and thus could potentially more transmissible.

The buffer in which IAV are diluted affects their stability and infectivity when moving through the IVT (Figure 6.5), and this effect is more pronounced for Vic:PR8M than for Vic75 WT. The farther away the source of susceptible cells is from the aerosolised virus, the less infection events were observed. This suggests that as the droplets pass through the air, water evaporates causing the droplets to shrink and the ion concentration within the droplets to change, lowering the pH of each droplet and causing premature conformational changes in HA proteins, from the receptor binding conformation to the fusion conformation, thereby decreasing infectivity.

Viruses with HA molecules that have decreased pH and temperature stability display reduced transmissibility, infectivity and pathogenicity (DuBois *et al.*, 2011; Imai *et al.*, 2012; Zaraket *et al.*, 2013; Linster *et al.*, 2014). Here, we provide initial data to suggest that susceptibility to lowered pHs and temperature sensitivity can be mediated by proteins expressed from segment 7. A difference in temperature stability was seen at 37^{o}C. It would have been useful to investigate the relative stability of either virus at the slightly lower temperature of 32^{o}C as this is closer to the temperature of the URT, however this was not done. We have demonstrated that Vic75 WT has greater temperature and pH stability compared to Vic:PR8M. Initially, it was hypothesised that this was conferred by filamentous particles. However, when a stock of Vic75 WT was used that had greatly reduced amounts of filamentous particles, the stability was unchanged compared to a Vic75 WT stock with filamentous particles. This suggested that filamentous virions do not confer the increased stability seen for Vic75 WT, and therefore the most likely effector of increased stability was not virion morphology, but rather M1 and/or M2 proteins within the virions. Similarly, it was found that viruses

grown in HNE cells, which did not have observable amounts of filaments by TEM, had similar pH stability properties as virus stocks grown in MDCKs, which were morphologically different. Unlike the MDCK stocks, the HNE stocks of Vic75 WT and Vic:PR8M were indistinct in terms of morphology, NA activity and resistance to inhibition by respiratory mucus. Yet, HNE grown Vic75 WT viruses still demonstrated greater pH stability. Thus the most likely arbiter of pH stability seen between these viruses is due to virion composition and not morphology.

Unfortunately, due to time constraints it was not possible to use either the NIP or HNE viral stocks with the IVT system. The most likely effector of the difference seen in infectivity between Vic75 WT and Vic:PR8M when passed through the IVT was differences in pH stability. This is based on the observation that by altering the buffer in which the viruses were diluted, the relative difference seen in infectivity was altered (Figure 6.5). It has been demonstrated that the cause of the difference in pH stability between these two viruses is most likely due to virion composition and not morphology. Thus, it would confirm our hypothesis if the NIP or HNE stocks could be tested using the IVT system, where virions that possess PR8 M1 and M2 proteins in their virions are less stable in aerosolised droplets. Similarly, it would be interesting to investigate the difference in infectivity between Vic75 WT and Vic75 41V in the IVT as well as relative pH stabilities. This would investigate any potential effects that M42 expression may have on virion stability.

Chapter 7: Discussion

Viral particles from low passage clinical strains of IAV typically have a filamentous morphology (Choppin *et al*., 1960; Itoh *et al.*, 2009a; Elton *et al.*, 2013; Seladi-Schulman *et al*., 2013). This phenotype is typically lost when the viruses undergo multiple passages in laboratory substrates, such as immortalised cells or ECEs (Choppin *et al*., 1960; Seladi-Schulman *et al*., 2013). The inverse has also been recorded, where an IAV strain has been shown to switch from a spherical phenotype to a filamentous one after passage *in vivo* (Seladi-Schulman *et al*., 2013). Thus, there is strong evidence to support the hypothesis that a filamentous phenotype is advantageous *in vivo*, although how it is advantageous is unclear. The main question that I have attempted to address within the scope of this thesis has been: what is the biological significance of IAV filamentous particles?

7.1 The morphologies of cell-associated and released viral particles do not necessarily correlate with one another

Often within the literature, cell-associated filamentous virions produced in MDCK cells are used as a surrogate marker for a filamentous phenotype assumed to include filamentous released virions (Campbell *et al.*, 2014b; Seladi-Schulman *et al.*, 2014). It has been suggested that depending on which genetic constellations are used, a difference in the relative amounts of different morphologies have been recorded between cell-associated and released virus particles, and that some viruses could have 3-fold less released filamentous particles than those still attached to cells (Campbell, Danzy, *et al.*, 2014). This suggests that by altering the budding morphological phenotype, the ratio of released versus cell-associated viruses can be altered.

We also found differences in the morphologies of virions produced in HNE cultures versus MDCK cells. In this study, cell-associated filamentous virions were observed in infected HNE cultures regardless of infecting virus genotype and morphology in infected MDCK cells (Figure 5.4 and 5.6). Surprisingly however, only spherical virions were observed as released particles from infected HNE cultures irrespective of virus used (Figure 5.10). This observation agrees with one made by Thompson *et al.*, (2006) when

primary respiratory epithelial cells were infected with a different strain of IAV, and the authors noted that spherical particles were predominantly observed to be released from infected human airway epithelium (HAE) cultures (Thompson *et al.*, 2006). Similarly, in another study, filamentous particles were observed in infected human tracheobronchial epithelial (HTBE) cultures but only cell-associated particles were investigated (Kolesnikova *et al.*, 2013). From the data presented in this thesis, there was a discrepancy between the cell-associated morphologies and the morphologies of released particles of the filamentous virus-producing Vic75 WT in HNE cultures, as examined by TEM.

It is clear that the cell-associated filamentous particles present a far greater level of antigen which can be bound by antibodies directed against the HA (Figures 3.2 and 4.1). Yet when the level of anti-HA staining for released virions was tested, Vic75 WT only had 1.3 fold higher measured fluorescence compared to Vic:PR8M (Figure 4.3 B and Table 4.1). This fold difference seems too low and incongruent with the very obvious, qualitative, visual differences seen for the staining of cell-associated spherical particles and ≥ 10 µm long filaments (Figures 3.2 and 4.1). The lack of released ≥ 10 µm long filaments has also been recorded by cryoelectron microscopy, but the authors conclude that this was due to inherent fragility of particles of this length and that they might have been disrupted during processing (Vijayakrishnan *et al.*, 2013). It has been noted that fragmentation of filamentous particles increases the haemagglutination titre without affecting infectious titre (Donald and Isaacs, 1954), so one might expect that if the ≥ 10 µm long filaments were released but broken-up, that this would be observable by a greater difference in anti-HA fluorescence, which we did not observe. The fold difference in anti-HA staining matches an observation made by Roberts, Lamb and Compans, (1998), where the authors found that when normalised to the total amount of NP, there was 2.2-fold more HA in the filamentous fraction of a sucrose gradient while there was only a 1.3-fold difference in the same fraction for a spherical-producing variant. The presumption was that NP should remain constant as only one genome set is incorporated into virions and this is independent of morphology (Harris *et al.*, 2006; Calder *et al.*, 2010; Noda *et al.*, 2012). However, this may be a false correlation as the authors of this study fractionated the viral stocks into distinct spherical and filamentous

populations, while the data presented in Chapter 4 was not fractionated. It is possible that the ≥ 10 µm long filaments are produced through a defective budding pathway, and remain tethered to the cell surface, but further work will have to be done to determine this with certainty. In disagreement with this, 10 µm long filamentous particles have been observed as released viral particles (Roberts, Lamb and Compans, 1998). A similar observation was made in a different study, where filaments 5-7 µm in length were observed (Roberts and Compans, 1998). Clearly further work is required to understand the relationship between cell-associated and released virions, and that careful attention need to be made to: stock generation, strain and host cell type used and sample handling.

7.2 Stocks containing filamentous viral particles are more resistant to inhibition by antibodies

The haemagglutination inhibition (HAI) titre of serum antibodies correlates with susceptibility of the individual to infection by IAV (DiazGranados *et al.*, 2014). Viruses with increased resistance to inhibition by antibodies will have increased fitness *in vivo*. Because of their increased size, and therefore, increased number of HA molecules per virion, we were interested to investigate if filamentous particles were more resistant to inhibition by anti-sera raised against the HA of the virus. Stocks containing filamentous or spherical virions were treated with the same dilution of polyclonal goat anti-Vic75 HA sera. Stocks with filamentous viruses retained 25% more infectivity compared to stocks with just spherical particles (Figure 5.1). Presumably this is caused by the increased number of HA molecules on filamentous particles that have not been bound by antibodies and therefore still have the capacity to attach to and enter cells. Fewer spherical particles were able to achieve this because at the same antibody dilution, they were saturated by inhibiting antibodies. While increased resistance to antibodies would be an adequate method for selection and persistence *in vivo*, it does not explain the observations made in animal models where transmission was found to correlate with morphology (Lakdawala *et al.*, 2011; Campbell, Danzy, *et al.*, 2014), as the animals used in these studies were seronegative to the inoculum virus.

7.3 The presence of filamentous particles of a given stock is a predictor of a mucus-resistant phenotype and this is dependent on NA activity.

It has been previously hypothesised and observed that filamentous particles would have a greater capacity to infect *in vivo* by virtue of having increased NA activities (Campbell, Danzy, *et al.*, 2014; Campbell, Kyriakis, *et al.*, 2014). Viruses that have low NA activities are generally less transmissible and more readily inhibited by mucus (M. Kesimer *et al.*, 2009; Zanin *et al.*, 2015). In agreement with previous findings (Campbell *et al.*, 2014; Seladi-Schulman *et al.*, 2014), we have demonstrated that filamentous particles of a different strain of IAV also have increased NA activities compared to spherical counterparts (Figure 4.3). It is assumed that this is due to the increased amount of NA proteins incorporated into filamentous viral particles, but this has not been quantified. We have also demonstrated that virus stocks which contain filamentous particles are more resistant to inhibition by respiratory mucus in an *in vitro* assay, than virus stocks that only contain spherical particles (Figures 5.2) and that this was dependent on NA activity. This suggested that filamentous virions may be better at navigating through respiratory mucus during the initial infection phase of transmission.

NA enzyme activity is necessary for resistance to inhibition by respiratory mucus (Mikhail N Matrosovich *et al.*, 2004; Thompson *et al.*, 2006; Cohen *et al.*, 2013; Yang *et al.*, 2014). However, NA activity as a single metric is not the sole predictor of how resistant a given stock will be to inhibition by respiratory mucus. Blumenkrantz *et al.*, 2013 investigated truncation of the NA protein and the effects that this had on transmissibility, for example. They found that viruses that had a normal-sized NA, was more transmissible in a respiratory droplet model than a virus with a truncated NA. The authors also noted that the virus with a truncated NA was more susceptible to inhibition by respiratory mucus. Interestingly, there was no difference in the NA activity of two viruses in this study, as measured by the cleavage of the MUNANA substrate, yet there was a significant difference in the inhibition by mucus (Blumenkrantz *et al.*, 2013). In this report, we offer the inverse observation but with the same conclusion. In Chapter 4, it was reported that stocks of viruses with increased amounts of NIPs had significantly increased NA activity as measured by the MUNANA assay (Figure 4.4). It was also reported that stocks that contained increased levels of NIPs did not have significantly

higher levels of infectivity when treated with respiratory mucus (Figure 4.6), where this phenotype was seen for both Vic75 WT and Vic:PR8M stocks. It could be argued that the MUNANA substrate does not accurately reflect the natural presentation of sialic acid ligands that would typically be found in respiratory mucus (Amaya *et al.*, 2004; Jia *et al.*, 2014). However, NA activity as measured by the cleavage of the MUNANA substrate was found to correlate with the binding capacity of NA to a glycan array of differentially presented, terminally linked sialic acids (Xu *et al.*, 2012), which suggest that the MUNANA read out is adequate for this purpose. Therefore, we argue that NA activity, as measured by the cleavage of MUNANA, is not a sole predictor of resistance to inhibition by respiratory mucus.

Interestingly, it was observed that not only did a stock of virus with increased NA activity not increase the capacity for resisting mucus inhibition, it had marginally lower levels of infectivity when compared with a stock that had increased amounts of filamentous particles (Figure 4.6). When the capacity to resist mucus inhibition was compared between a virus that only contained spherical particles, and a filamentous stock, the virus with filamentous particles had significantly greater levels of infectivity (p value: 0.011) while the stock with reduced levels of filaments did not (p value: 0.61). Thus we would argue that filamentous virions are more capable of resisting inhibition by respiratory mucus, and that while NA activity is necessary, there is a mechanism of resistance that is unique to virion morphology.

One possible model to explain this observation could be the dynamic interactions of filamentous particles with the sialic acid-bearing molecules or exogenous vesicles that are present in the mucus. Recent studies have been able to track the movement of viral particles on glass surfaces coated with sialic acid-bearing glycans (fetuin) (Sakai, Nishimura, *et al.*, 2017) and they found that HA and NA can function as machinery for viral motility. This was achieved by the process of HA receptor exchange, where HA initially bound to receptors and then this interaction was subsequently broken due to the action of the NA enzyme. The freed HA molecules were then able to bind to adjacent sialic acid-bearing molecules and these bonds were in-turn broken. This mechanism of HA-receptor binding, then breaking, then binding to new ligands was repeated and could act as a motor to move virions along the surface. The authors also noted that this HA-

and NA-mediated directional movement increased the entry of viruses into A549 cells. The mechanism that they offer for this is that virions will move along a cell surface until an area is reached that is more conducive to virus entry. Another study utilising this technique was used to investigate the effect that a filamentous morphology might have. Glass covers were coated with bovine mucin and virus movements were analysed. The authors found that filamentous particles of influenza C virus were able to move in a directed, unidirectional motion, compared to the random movement seen for spherical viruses. They also noted that this process was quicker than that seen for spherical viruses (Sakai, Takagi, *et al.*, 2017).

It is interesting to consider this motility mechanism when analysing the data presented within this thesis. The increased resistance to inhibition by respiratory mucus in our *in vitro* assay, demonstrated in figures 4.6 and 5.2, suggests that there is a benefit for the filamentous morphology to move through a matrix consisting of sialic acid decoy receptors, possibly in a unidirectional and quick-paced fashion similar to that described Sakai *et al* (2017). One key difference being that the experiments produced by Sakai *et al* (2017) were performed on a 2-dimensional plane and the assays outlined in this thesis would have occurred in a 3 dimensional one. In addition, while a mucus resistant phenotype was noted for Vic75 WT when infecting MDCK cells, this was not observed when used to infect HNE cultures, with or without the cultures being washed prior to infection (Figures 5 .11), so it is still unclear precisely how this may relate to infectivity *in vivo*.

7.4 Vic75 WT virus particles are more stable in aerosolised droplets, and this is most likely pH-mediated.

Compared to Vic:PR8M, Vic75 WT generates significantly greater levels of infectious virus, as measured by pfu, when nebulised and passed through the IVT system. This difference is dependent on the buffer in which the viruses are diluted (Figure 6.5). This, coupled with the pH stability data presented in figure 6.6, leads us to hypothesise that the difference seen in infectivity in aerosolised droplets is due to differential pH stabilities of the two viruses. This difference is lessened by the addition of respiratory mucus either as an overlay on cells or as being present in the aerosolised droplets. Therefore, as tested by the IVT system, susceptibility to lowered pHs has a more

significant bearing on the infectivity of Vic75 WT or Vic:PR8M virions than resistance to inhibition by respiratory mucus.

Treatment of virus particles with low pH causes loss of filamentous morphology as well as increasing the sizes of spherical particles (Shangguan *et al.*, 1998; Calder *et al.*, 2010). It is possible for virions to be affected morphologically at lowered pHs without inducing the fusogenic conformation of the HA trimer (Shangguan *et al.*, 1998; Calder *et al.*, 2010). These studies found that when virions were incubated at low pHs, the morphologies of virions became distorted. The distortion of the virion structures was observed concomitantly with the disruption of the M1 layer in viral particles. We hypothesise that the changes in the morphology noted in these studies are indicative of the mechanism of inhibition proposed within this thesis. We have demonstrated that virions composed of proteins from Vic75 WT virus have greater stability compared to viruses that express segment 7 from PR8 WT in a Vic75 WT background (Figures 6.7 and 6.8). It is unclear what the mechanism of this is, and due to time constraints it was unable to be investigated in the scope of this thesis.

7.5 The stability of Vic75 WT viruses is independent of viral morphology

From the IVT data presented in figure 6.5, Vic75 WT retains greater levels of infectivity when carried in aerosolised droplet and that this is dependent on the buffer in which the viruses are diluted. It was initially hypothesised that Vic75 WT retained greater levels of infectivity in a HA-mediated mechanism that was dependent on pH stability (Figure 6.6). However, subsequent experiments demonstrated that pH stability was independent of the presence of filamentous particles, and instead correlated with viruses that expressed a Vic75 WT segment 7 (Figures 6.7 and 6.8). We demonstrated that stocks of virus that had indistinguishable virion morphologies (Figure 5.8) had the same differences in pH stability as stocks which did have morphological differences (Figures 4.1 and 6.6 C). Of three separate sets of stocks that were tested, viruses bearing a Vic75 WT segment 7 correlated with increased pH stability (Figures 6.7 and 6.8). We hypothesise that the increased infectivity displayed by Vic75 WT in the IVT (Figure 6.5) was due to better pH stability and that this was dependent on virion composition. However, due to time constraints, it was not possible to test this hypothesis using the IVT, but we would

predict that greater infectivity in the IVT would correlate with segment 7 expression and not filamentous particles.

The incompatibility of genetic segments and their influence on viral fitness is reviewed in (White and Lowen, 2018). This review outlines available data that shows how the incompatibility of certain constellations of genetic segments from disparate evolutionary backgrounds can affect viral fitness. However, the review does not include information regarding incompatibility of segment 7. There is available data to suggest that segments 5 and 7 from the same strain, which have co-evolved, are preferentially reassorted with one another (Schrauwen *et al.*, 2013). Similarly, a study found that in a swine transmission model, segment 7 alone was insufficient to confer a transmission phenotype, but when both segments 5 and 7 from the same strain were used, transmission occurred (Ma *et al.*, 2012).

Another study found a link between palmitoylation of the cytoplasmic tail of the HA molecule, segment 7 expression and their effect on viral fitness. The authors found that by altering the palymitolation of the HA cytoplasmic tail of a filamentous-producing strain, viral titres were significantly reduced. They also found that by expressing segment 7 of a spherical-producing strain in an otherwise filamentous-producing strain that viral fitness could be rescued despite the HA palmitoylation mutations, and that this difference couldn't be attributed to one single amino acid, but rather numerous ones (Chen, Takeda and Lamb, 2005). Thus, expression of segment 7 in a virus constellation in which it has separately evolved can affect the functionality of the reassortant virus in the context of an altered HA cytoplasmic tail.

Acidification of the virion interior prior to endocytosis has been found to affect infectivity of IAV (Zhirnov *et al.*, 2016). This study found that acidification of virion interiors affected virion morphology where virions with acidified interiors had localised blebs in their membranes. They determined that this was dependent on whether or not the HA molecules were in the HA_0 or receptor binding conformations, where virions with HA molecules in the HA_0 conformation were susceptible to acidification-driven morphological changes. Similarly, they found that the effect that acidity had on morphology was dependent on M2 ion channel activity. They also found that acidification resulted in disrupted cohesion of M1-vRNP complexes and that acidification

resulted in a loss of 10,000-fold in infectivity with only a loss of two-fold the haemagluttinating capacity, suggesting that only a marginal loss of infectivity was due to loss of receptor binding capacity. Taken together, this study shows that acidification of virions prior to endocytosis can affect infectivity in an M1-vRNP association manner.

The mechanism by which products of segment 7 might confer increased pH stability is unclear. The most likely effectors are either: decreased M1-vRNP binding avidity; altered vRNP-vRNP interactions; a more active M2 ion channel activity; greater levels of incorporation of M1; or a combination of all four. It has been speculated that a reassortment event started a new genotypic lineage of a H9N2 subtype virus circulating among poultry populations which enhanced infectivity and nationwide outbreaks in China during 2010 to 2013, that then went on to be one of the progenitors of a novel H7N9 subtype virus (Pu *et al.*, 2015). The segment 7 from this hypothesised reassortment event was demonstrated to impact viral fitness of the H9N2 subtype in chickens (Pu *et al.*, 2017). The authors correlate a spherical morphology with increased mRNA, vRNA and protein expression in infected CEF cells. The replication capacities reported for filamentous- and spherical-generating viruses match the trends reported in section 3. The authors went on to demonstrate a correlation between a spherical morphology and increased replication *in vivo* in infected chickens. They also reported a correlation with extrapulmonary spread and virulence with a spherical phenotype. Pu *et al* were able to map the amino acids related to this phenotype. Two of which were in a putative M1-vRNP binding site (Baudin *et al.*, 2001) and another was in the transmembrane domain of M2 (Takeda *et al.*, 2002) which could possibly affect the ion channel activity.

The pH of fusion for avian strains is higher, and therefore the virions are less stable than for mammalian strains at lowered pHs (Reed *et al.*, 2009; Galloway *et al.*, 2013). It is therefore interesting to speculate that the increased pathogenesis conferred by segment 7 as recorded by Pu *et al*. could be due to altering pH stability. Further circumstantial evidence to support this hypothesis is the observation that segment 7 gene products have also been implicated in limitation of avian influenza viruses to growth in the respiratory tract of primates (Tian *et al.*, 1985; Buckler-White, Naeve and Murphy, 1986).

The mechanism by which the expressed products of segment 7 may affect virulence is unclear. From our data (Figure 6.7 and 6.8), we hypothesise that it may have to do with virion composition and stability, where weakened M1-vRNP binding or increased ion channel activity could affect virion pH stability, in a mechanism similar to that seen by Zhirnov *et al*., 2016, where acidification of the virion interior significantly reduced infectivity. Lui, Muller and Ye investigated the effect of salt and low pH on the disassociation of M1 and NP. The authors compared the relative disassociation of M1 and NP of spherical- and filamentous-producing strains, and they found that the M1-NP interaction was more readily broken for the filamentous strain than for the spherical one at low pHs (Liu, Muller and Ye, 2002), which disagrees with our hypothesis that an M1 associated with a spherical morphology would have weaker associations with vRNPs. The authors did not however, investigate the effect of a protein "mismatch", i.e. the interaction of a "spherical" segment 7 with a "filamentous" vRNP. The mechanism by which Vic:PR8M has reduced pH stability is unclear and warrants further investigation. However, this remains untested and could be due to other factors.

7.6 Viral morphology could be a false correlate of transmission

It is interesting to consider the IVT data (Figure 6.5) and the pH stability data (Figures 6.7 and 6.8) in the context of an aerosol transmission event. It can only be speculated that the infectivity seen for Vic75 WT and Vic:PR8M in the IVT would match what would be seen *in vivo*, but Vic75 WT viruses were more stable in aerosolised droplets and this was most likely pH-mediated (Figure 6.5). It has also been demonstrated that the pH stability is independent of virion morphology (Figures 6.7 and 6.8). This is interesting to consider in the context of the previous studies that have shown a correlation between morphology and transmissibility.

Only studies that have done full segment 7 swaps have reliably demonstrated a correlation between transmission and filamentous morphology (Lakdawala *et al.*, 2011; Campbell, Danzy, *et al.*, 2014). While other studies have demonstrated that segment 7, or a combination of segment 5 and 7 swaps, are sufficient to confer transmissibility without investigating morphology (Chou *et al.*, 2011; Ma *et al.*, 2012). When single point mutations have been investigated, the transmissibility phenotype did not correlate with a filamentous phenotype. Campbell, Kyriakis, *et al.*, 2014 investigated the effects of a

novel amino acid substitution of a proline for an alanine at position 41 of the M1 protein. The authors found that expression of a proline in the context of different genetic constellations increased the frequency and length of cell-associated filamentous viral particles. The authors also noted that compared to viruses with an alanine at position 41 of M1, the proline viruses had greatly reduced transmissibility, despite having greater levels of cell-associated filamentous particles. Therefore, a filamentous morphology is not necessarily a correlate of transmission.

Another study investigated the mutations that are accrued during serial passage of a filamentous strain in MDCK cells as well as ECEs, and also failed to demonstrate a correlation between transmissibility and a filamentous morphology. It was noted that there was a delay in shedding of virus from sentinel hosts, as well as reduced shedding of virus in donor animals for the spherical viruses. However, there was no difference in the total number of successful transmission events (Seladi-Schulman *et al*., 2013). Similarly, the authors noted that when a spherical-producing virus was mutated by a single amino acid in the M1 protein, it significantly increased the number of cell-associated filamentous particles in MDCK cells, but did not affect transmissibility compared to the spherical WT. Taken together, the transmission phenotype is only correlated with a filamentous phenotype when full segment 7 reassortant viruses are tested. This is interesting to consider with the observation that segment 7 expression correlated with increased infectivity of viruses in aerosolised droplets.

7.7 Conclusion

We conclude that the morphology of cell-associated virus particles does not necessarily match the morphology of released particles. We also conclude that expression of segment 7 of PR8 WT in a Vic75 background results in increased replicative capacity in MDCK cells and that this is independent of the production of Vic75 WT cell-associated, extended ≥10 μm long filamentous particles.

It has been demonstrated that compared to spherical particles, filamentous virions are more resistant to inhibition by respiratory mucus and that this is dependent on NA activity and an undefined characteristic of a filamentous morphology. However, we were unable to demonstrate the effectiveness of this phenotype when infecting HNE cultures.

We demonstrate that there is no difference in the growth capacities of morphologically distinct viruses in differentiated HNE cultures. We also demonstrate that despite having distinct morphological phenotypes in immortalised cells, viruses display indistinguishable morphologies in infected HNE cultures both as cell-associated and released viral particles.

We offer initial evidence that virion morphology may be a false correlate of transmission because infectivity of viruses in aerosolised droplets is dependent on pH stability, which can be traced to segment 7 expression, and increased pH stability is independent of virion morphology. It has been demonstrated that viruses that possess a transgenic segment 7 from a lab adapted spherical-only strain are less infectious when carried in aerosolised droplet, and that this is most likely dependent on pH stability. We also demonstrate those viruses carrying a transgenic segment 7 are less resistant to inhibition by lowered pHs and incubation at 37^{o}C. Thermal and pH stability are significant determinants of transmissibility, thus we argue that expression of an inadequate segment 7 will result in unstable virions. Without identifying the mechanism of decreased stability and then subsequently testing in an animal model, it cannot be claimed that segment 7 affects transmissibility in a pH-dependent manner.

Finally, we have provided evidence that filamentous viral particles are more resistant to inhibition by effectors of the immune system which would be an adequate explanation for their role *in vivo*. We also speculate that virion morphology may not be involved in aerosol transmission, but rather virion composition is.

Bibliography

Al-Mubarak, F. *et al.* (2015) 'Identification of morphological differences between avian influenza A viruses grown in chicken and duck cells', *Virus Research*. Elsevier B.V., 199, pp. 9–19. doi: 10.1016/j.virusres.2015.01.005.

Alford, R. H. *et al.* (1966) 'Human Influenza Resulting from Aerosol Inhalation', *Proceedings of the Society for Experimental Biology and Medicine*. SAGE Publications, 122(3), pp. 800–804. doi: 10.3181/00379727-122-31255.

Amaya, M. F. *et al.* (2004) 'Structural insights into the catalytic mechanism of Trypanosoma cruzi trans-sialidase', *Structure*, 12(5), pp. 775–784. doi: 10.1016/j.str.2004.02.036.

Amorim, M. J. *et al.* (2011) 'A Rab11- and Microtubule-Dependent Mechanism for Cytoplasmic Transport of Influenza A Virus Viral RNA', *Journal of Virology*, 85(9), pp. 4143–4156. doi: 10.1128/JVI.02606-10.

Antunes, M. B. and Cohen, N. A. (2007) 'Mucociliary clearance – a critical upper airway host defense mechanism and methods of assessment', *Current Opinion in Allergy and Clinical Immunology*, 7(1). Available at: https://journals.lww.com/co-allergy/Fulltext/2007/02000/Mucociliary_clearance___a_critical_upper_airway.3.aspx.

Arzt, S. *et al.* (2001) 'Combined Results from Solution Studies on Intact Influenza Virus M1 Protein and from a New Crystal Form of Its N-Terminal Domain Show That M1 Is an Elongated Monomer', *Virology*, 279(2), pp. 439–446. doi: 10.1006/viro.2000.0727.

Barman, S. *et al.* (2001) 'Transport of viral proteins to the apical membranes and interaction of matrix protein with glycoproteins in the assembly of influenza viruses', *Virus Research*, 77(1), pp. 61–69. doi: 10.1016/S0168-1702(01)00266-0.

Barman, S. and Nayak, D. P. (2007) 'Lipid Raft Disruption by Cholesterol Depletion Enhances Influenza A Virus Budding from MDCK Cells', *Journal of Virology*, 81(22), pp. 12169–12178. doi: 10.1128/JVI.00835-07.

Baudin, F. *et al.* (2001) 'In vitro dissection of the membrane and RNP binding activities of influenza virus M1 protein.', *Virology*, 281(1), pp. 102–108. doi: 10.1006/viro.2000.0804.

Beale, R. *et al.* (2014) 'A LC3-interacting motif in the influenza A virus M2 protein is required to subvert autophagy and maintain virion stability', *Cell Host and Microbe*. Elsevier Inc., 15(2), pp. 239–247. doi: 10.1016/j.chom.2014.01.006.

Berri, F. *et al.* (2014) 'Annexin V Incorporated into Influenza Virus Particles Inhibits Gamma Interferon Signaling and Promotes Viral Replication', *Journal of Virology*, 88(19), pp. 11215–11228. doi: 10.1128/JVI.01405-14.

Bialas, K. M. *et al.* (2014) 'Specific Nucleoprotein Residues Affect Influenza Virus Morphology', *Journal of Virology*, 88(4), pp. 2227–2234. doi: 10.1128/JVI.03354-13.

Bialas, K. M., Desmet, E. A. and Takimoto, T. (2012) 'Specific Residues in the 2009 H1N1 Swine-Origin Influenza Matrix Protein Influence Virion Morphology and Efficiency of Viral Spread In Vitro', *PLoS ONE*, 7(11). doi: 10.1371/journal.pone.0050595.

Blumenkrantz, D. *et al.* (2013) 'The short stalk length of highly pathogenic avian influenza H5N1 virus neuraminidase limits transmission of pandemic H1N1 virus in ferrets.', *Journal of virology*, 87(19), pp. 10539–51. doi: 10.1128/JVI.00967-13.

Bottcher-Friebertshauser, E. *et al.* (2010) 'Cleavage of Influenza Virus Hemagglutinin by Airway Proteases TMPRSS2 and HAT Differs in Subcellular Localization and Susceptibility to Protease Inhibitors', *Journal of Virology*, 84(11), pp. 5605–5614. doi: 10.1128/JVI.00140-10.

Boulo, S. *et al.* (2007) 'Nuclear traffic of influenza virus proteins and ribonucleoprotein complexes', *Virus Research*, 124(1–2), pp. 12–21. doi: 10.1016/j.virusres.2006.09.013.

Bourmakina, S. V. and García-Sastre, A. (2003) 'Reverse genetics studies on the filamentous morphology of influenza A virus', *Journal of General Virology*, 84(3), pp. 517–527. doi: 10.1099/vir.0.18803-0.

Bouvier, N. M. (2015) 'Animal models for influenza virus transmission studies: A historical perspective', *Current Opinion in Virology*. Elsevier B.V., 13, pp. 101–108. doi: 10.1016/j.coviro.2015.06.002.

Brass, A. L. *et al.* (2009) 'The IFITM Proteins Mediate Cellular Resistance to Influenza A H1N1 Virus, West Nile Virus, and Dengue Virus', *Cell*. Elsevier Ltd, 139(7), pp. 1243–

1254. doi: 10.1016/j.cell.2009.12.017.

Brooke, C. B. *et al.* (2013) 'Most Influenza A Virions Fail To Express at Least One Essential Viral Protein', *Journal of Virology*, 87(6), pp. 3155–3162. doi: 10.1128/JVI.02284-12.

Brown, E. G. *et al.* (2001) 'Pattern of mutation in the genome of influenza A virus on adaptation to increased virulence in the mouse lung: identification of functional themes', *Proc Natl Acad Sci U S A*, 98(12), pp. 6883–6888. doi: 10.1073/pnas.111165798.

Brown, E. G. and Bailly, J. E. (1999) 'Genetic analysis of mouse-adapted influenza A virus identifies roles for the NA, PB1, and PB2 genes in virulence', *Virus Research*, 61(1), pp. 63–76. doi: 10.1016/S0168-1702(99)00027-1.

Bruce, E. A. *et al.* (2012) 'Release of filamentous and spherical influenza a virus is not restricted by tetherin', *Journal of General Virology*, 93(5), pp. 963–969. doi: 10.1099/vir.0.038778-0.

Bruce, E. A., Digard, P. and Stuart, A. D. (2010) 'The Rab11 Pathway Is Required for Influenza A Virus Budding and Filament Formation', *Journal of Virology*, 84(12), pp. 5848–5859. doi: 10.1128/JVI.00307-10.

Buckler-White, A. J., Naeve, C. W. and Murphy, B. R. (1986) 'Characterization of a gene coding for M proteins which is involved in host range restriction of an avian influenza A virus in monkeys.', *J. Virol.*, 57(2), pp. 697–700. Available at: http://jvi.asm.org/cgi/content/long/57/2/697.

Bui, M., Whittaker, G. and Helenius, a (1996) 'Effect of M1 protein and low pH on nuclear transport of influenza virus ribonucleoproteins.', *Journal of virology*, 70(12), pp. 8391–401. Available at: http://www.pubmedcentral.nih.gov/articlerender.fcgi?artid=190928&tool=pmcentrez&rendertype=abstract.

Burleigh, L. M. *et al.* (2005) 'Influenza a viruses with mutations in the m1 helix six domain display a wide variety of morphological phenotypes.', *Journal of virology*, 79(2), pp. 1262–70. doi: 10.1128/JVI.79.2.1262-1270.2005.

Burnet, F. M. and Lind, P. E. (1957) 'Studies on filamentary forms of influenza virus with

special reference to the use of dark-ground-microscopy', *Archiv für die gesamte Virusforschung*, 7(5), pp. 413–428. doi: 10.1007/BF01241959.

Cai, H., Reinisch, K. and Ferro-Novick, S. (2007) 'Coats, Tethers, Rabs, and SNAREs Work Together to Mediate the Intracellular Destination of a Transport Vesicle', *Developmental Cell*, 12(5), pp. 671–682. doi: 10.1016/j.devcel.2007.04.005.

Calder, L. J. *et al.* (2010) 'Structural organization of a filamentous influenza A virus', *Proceedings of the National Academy of Sciences*, 107(23), pp. 10685–10690. doi: 10.1073/pnas.1002123107.

Campbell, P. J., Kyriakis, C. S., *et al.* (2014) 'Residue 41 of the Eurasian Avian-Like Swine Influenza A Virus Matrix Protein Modulates Virion Filament Length and Efficiency of Contact Transmission', *Journal of Virology*, 88(13), pp. 7569–7577. doi: 10.1128/JVI.00119-14.

Campbell, P. J., Danzy, S., *et al.* (2014) 'The M Segment of the 2009 Pandemic Influenza Virus Confers Increased Neuraminidase Activity, Filamentous Morphology, and Efficient Contact Transmissibility to A/Puerto Rico/8/1934-Based Reassortant Viruses', *Journal of Virology*, 88(7), pp. 3802–3814. doi: 10.1128/JVI.03607-13.

Carrat, F. and Flahault, A. (2007) 'Influenza vaccine: The challenge of antigenic drift', *Vaccine*, 25(39–40), pp. 6852–6862. doi: 10.1016/j.vaccine.2007.07.027.

Carter, G. C. *et al.* (2005) 'Entry of the vaccinia virus intracellular mature virion and its interactions with glycosaminoglycans', *Journal of General Virology*, 86(5), pp. 1279–1290. doi: 10.1099/vir.0.80831-0.

Chang, W. K. (1969) 'National influenza experience in Hong Kong, 1968.', *Bulletin of the World Health Organization*, 41(3), pp. 349–351.

Chen, W.; Feng, Y.; Chen, D. and Wandinger-Ness, A. (1998) 'Rab11 is required for trans-golgi network-to-plasma membrane transport and a preferential target for GDP dissociation inhibitor.', *Molecular biology of the cell*, 9(11), pp. 3241–3257. doi: 10.1091/mbc.9.11.3241.

Chen, B. J. *et al.* (2007) 'Influenza Virus Hemagglutinin and Neuraminidase, but Not the

Matrix Protein, Are Required for Assembly and Budding of Plasmid-Derived Virus-Like Particles', *Journal of Virology*, 81(13), pp. 7111–7123. doi: 10.1128/JVI.00361-07.

Chen, B. J. *et al.* (2008) 'The Influenza Virus M2 Protein Cytoplasmic Tail Interacts with the M1 Protein and Influences Virus Assembly at the Site of Virus Budding', *Journal of Virology*, 82(20), pp. 10059–10070. doi: 10.1128/JVI.01184-08.

Chen, B. J. and Lamb, R. A. (2008) 'Mechanisms for enveloped virus budding: Can some viruses do without an ESCRT?', *Virology*, 372(2), pp. 221–232. doi: 10.1016/j.virol.2007.11.008.

Chen, B. J., Takeda, M. and Lamb, R. A. (2005) 'Influenza virus hemagglutinin (H3 subtype) requires palmitoylation of its cytoplasmic tail for assembly: M1 proteins of two subtypes differ in their ability to support assembly.', *Journal of virology*, 79(21), pp. 13673–13684. doi: 10.1128/JVI.79.21.13673-13684.2005.

Chen, W. *et al.* (2001) 'A novel influenza A virus mitochondrial protein that induces cell death', *Nature Medicine*, 7(12), pp. 1306–1312. doi: 10.1038/nm1201-1306.

Chen, Y. *et al.* (2013) 'Human infections with the emerging avian influenza A H7N9 virus from wet market poultry: Clinical analysis and characterisation of viral genome', *The Lancet*. Elsevier Ltd, 381(9881), pp. 1916–1925. doi: 10.1016/S0140-6736(13)60903-4.

Chin, K.-C. and Cresswell, P. (2001) 'Viperin (cig5), an IFN-inducible antiviral protein directly induced by human cytomegalovirus', *Proceedings of the National Academy of Sciences*, 98(26), pp. 15125–15130. doi: 10.1073/pnas.011593298.

Chlanda, P. *et al.* (2015) 'Structural Analysis of the Roles of Influenza A Virus Membrane-Associated Proteins in Assembly and Morphology', *Journal of Virology*, 89(17), pp. 8957–8966. doi: 10.1128/JVI.00592-15.

Choppin, P. W. (1960) 'Studies of Two Kinds of Virus Particles Which Comprise Influenza a2 Virus Strains: Iii. Morphological Characteristics: Independence of Morphological and Functional Traits', *Journal of Experimental Medicine*, 112(5), pp. 945–952. doi: 10.1084/jem.112.5.945.

Choppin, P. W., Murphy, J. S. and Tamm, I. (1960) 'STUDIES OF TWO KINDS OF VIRUS

PARTICLES WHICH COMPRISE INFLUENZA A2 VIRUS STRAINS', *The Journal of Experimental Medicine*, 112(5), p. 945 LP-952. Available at: http://jem.rupress.org/content/112/5/945.abstract.

Chou, Y. -y. *et al.* (2011) 'The M Segment of the 2009 New Pandemic H1N1 Influenza Virus Is Critical for Its High Transmission Efficiency in the Guinea Pig Model', *Journal of Virology*, 85(21), pp. 11235–11241. doi: 10.1128/JVI.05794-11.

Chou, Y. ying *et al.* (2013) 'Colocalization of Different Influenza Viral RNA Segments in the Cytoplasm before Viral Budding as Shown by Single-molecule Sensitivity FISH Analysis', *PLoS Pathogens*, 9(5). doi: 10.1371/journal.ppat.1003358.

Cohen, M. *et al.* (2013) 'Influenza A penetrates host mucus by cleaving sialic acids with neuraminidase', *Virology Journal*. Virology Journal, 10(1), p. 321. doi: 10.1186/1743-422X-10-321.

Cowling, B. J. *et al.* (2013) 'Aerosol transmission is an important mode of influenza A virus spread', *Nature Communications*. Nature Publishing Group, 4, pp. 1935–1936. doi: 10.1038/ncomms2922.

Creager, H. M. *et al.* (2017) 'In vitro exposure system for study of aerosolized influenza virus', *Virology*. Elsevier, 500(October 2016), pp. 62–70. doi: 10.1016/j.virol.2016.10.007.

Cros, J. F., García-Sastre, A. and Palese, P. (2005) 'An unconventional NLS is critical for the nuclear import of the influenza A virus nucleoprotein and ribonucleoprotein', *Traffic*, 6(3), pp. 205–213. doi: 10.1111/j.1600-0854.2005.00263.x.

Dadonaite, B. *et al.* (2016) 'Filamentous influenza viruses', *Journal of General Virology*, 97(8), pp. 1755–1764. doi: 10.1099/jgv.0.000535.

Dawood, F. S. *et al.* (2012) 'Estimated global mortality associated with the first 12 months of 2009 pandemic influenza A H1N1 virus circulation: A modelling study', *The Lancet Infectious Diseases*. Elsevier Ltd, 12(9), pp. 687–695. doi: 10.1016/S1473-3099(12)70121-4.

Dias, A. *et al.* (2009) 'The cap-snatching endonuclease of influenza virus polymerase

resides in the PA subunit', *Nature*, 458(7240), pp. 914–918. doi: 10.1038/nature07745.

DiazGranados, C. A. *et al.* (2014) 'Efficacy of High-Dose versus Standard-Dose Influenza Vaccine in Older Adults', *New England Journal of Medicine*, 371(7), pp. 635–645. doi: 10.1056/NEJMoa1315727.

Donald, H. B. and Isaacs, a (1954) 'Some properties of influenza virus filaments shown by electron microscopic particle counts.', *Journal of general microbiology*, 11(2), pp. 325–31. doi: 10.1099/00221287-11-2-325.

Dubois, J. *et al.* (2014) 'Influenza Viruses and mRNA Splicing : Doing More with Less', 5(3), pp. 1–13. doi: 10.1128/mBio.00070-14.Invited.

DuBois, R. M. *et al.* (2011) 'Acid stability of the hemagglutinin protein regulates H5N1 influenza virus pathogenicity', *PLoS Pathogens*, 7(12), pp. 1–11. doi: 10.1371/journal.ppat.1002398.

Edenborough, K. M., Gilbertson, B. P. and Brown, L. E. (2012) 'A Mouse Model for the Study of Contact-Dependent Transmission of Influenza A Virus and the Factors That Govern Transmissibility', *Journal of Virology*, 86(23), pp. 12544–12551. doi: 10.1128/JVI.00859-12.

Ehre, C. *et al.* (2012) 'Overexpressing mouse model demonstrates the protective role of Muc5ac in the lungs', *Proceedings of the National Academy of Sciences*, 109(41), pp. 16528–16533. doi: 10.1073/pnas.1206552109.

Eisfeld, A. J. *et al.* (2011) 'RAB11A Is Essential for Transport of the Influenza Virus Genome to the Plasma Membrane', *Journal of Virology*, 85(13), pp. 6117–6126. doi: 10.1128/JVI.00378-11.

Elleman, C. J. and Barclay, W. S. (2004) 'The M1 matrix protein controls the filamentous phenotype of influenza A virus', *Virology*, 321(1), pp. 144–153. doi: 10.1016/j.virol.2003.12.009.

Elton, D. *et al.* (2013) 'The genetics of virus particle shape in equine influenza A virus', *Influenza and other Respiratory Viruses*, 7(SUPPL.4), pp. 81–89. doi: 10.1111/irv.12197.

England, R. J. A. *et al.* (1999) 'Nasal pH measurement: A reliable and repeatable

parameter', *Clinical Otolaryngology and Allied Sciences*, 24(1), pp. 67–68. doi: 10.1046/j.1365-2273.1999.00223.x.

Fabian, P. *et al.* (2008) 'Influenza virus in human exhaled breath: an observational study', *PLoS ONE*, 3(7), p. e2691. doi: 10.1371/journal.pone.0002691.

Falcon, A. M. *et al.* (2004) 'Defective RNA replication and late gene expression in temperature-sensitive influenza viruses expressing deleted forms of the NS1 protein', *J Virol*, 78(8), pp. 3880–3888. doi: 10.1128/JVI.78.8.3880-3888.2004.

Fontana, J. *et al.* (2012) 'Structural Changes in Influenza Virus at Low pH Characterized by Cryo-Electron Tomography', *Journal of Virology*, 86(6), pp. 2919–2929. doi: 10.1128/JVI.06698-11.

Forrest, H. L. and Webster, R. G. (2010) 'Perspectives on influenza evolution and the role of research.', *Animal health research reviews / Conference of Research Workers in Animal Diseases*, 11(1), pp. 3–18. doi: 10.1017/S1466252310000071.

Frensing, T. *et al.* (2014) 'Impact of defective interfering particles on virus replication and antiviral host response in cell culture-based influenza vaccine production', *Applied Microbiology and Biotechnology*, 98(21), pp. 8999–9008. doi: 10.1007/s00253-014-5933-y.

Frensing, T. *et al.* (2016) 'Influenza virus intracellular replication dynamics, release kinetics, and particle morphology during propagation in MDCK cells', *Applied Microbiology and Biotechnology*. Applied Microbiology and Biotechnology, 100(16), pp. 7181–7192. doi: 10.1007/s00253-016-7542-4.

Frise, R. *et al.* (2016) 'Contact transmission of influenza virus between ferrets imposes a looser bottleneck than respiratory droplet transmission allowing propagation of antiviral resistance', *Scientific Reports*. Nature Publishing Group, 6(July), pp. 1–14. doi: 10.1038/srep29793.

Fuchs, R., Schmid, S. and Mellman, I. (1989) 'A possible role for Na+,K+-ATPase in regulating ATP-dependent endosome acidification.', *Proceedings of the National Academy of Sciences*, 86(2), pp. 539–543. doi: 10.1073/pnas.86.2.539.

Gabriel, G. *et al.* (2011) 'Differential use of importin-α isoforms governs cell tropism and host adaptation of influenza virus', *Nature Communications*, 2(1). doi: 10.1038/ncomms1158.

Gabriel, G., Herwig, A. and Klenk, H. D. (2008) 'Interaction of polymerase subunit PB2 and NP with importin α1 is a determinant of host range of influenza A virus', *PLoS Pathogens*, 4(2). doi: 10.1371/journal.ppat.0040011.

Galloway, S. E. *et al.* (2013) 'Influenza HA Subtypes Demonstrate Divergent Phenotypes for Cleavage Activation and pH of Fusion: Implications for Host Range and Adaptation', *PLoS Pathogens*, 9(2). doi: 10.1371/journal.ppat.1003151.

Gamblin, S. J. and Skehel, J. J. (2010) 'Influenza hemagglutinin and neuraminidase membrane glycoproteins', *Journal of Biological Chemistry*, 285(37), pp. 28403–28409. doi: 10.1074/jbc.R110.129809.

García-Sastre, A. (2011) 'Induction and evasion of type I interferon responses by influenza viruses', *Virus Research*, 162(1–2), pp. 12–18. doi: 10.1016/j.virusres.2011.10.017.

Garten, R. J. *et al.* (2009) 'Antigenic and Genetic Characteristics Influenza Viruses Circulating in Humans', *Science*, 325(July), pp. 197–201. doi: 10.1126/science.1176225.

Gaudin, R. and Barteneva, N. S. (2015) 'Sorting of small infectious virus particles by flow virometry reveals distinct infectivity profiles', *Nature communications*, 6, p. 6022. doi: 10.1038/ncomms7022.

Gnirß, K. *et al.* (2015) 'Tetherin Sensitivity of Influenza A Viruses Is Strain Specific: Role of Hemagglutinin and Neuraminidase', *Journal of Virology*, 89(18), pp. 9178–9188. doi: 10.1128/JVI.00615-15.

Gómez-Puertas, P. *et al.* (2000) 'Influenza virus matrix protein is the major driving force in virus budding.', *Journal of virology*, 74(24), pp. 11538–11547. doi: 10.1128/JVI.74.24.11538-11547.2000.

Govorkova, E. a *et al.* (2005) 'Lethality to Ferrets of H5N1 Influenza Viruses Isolated from Humans and Poultry in 2004 Lethality to Ferrets of', *Journal of Virology*, 79(4), pp. 2191–

6195. doi: 10.1128/JVI.79.4.2191.

Grantham, M. L. *et al.* (2010) 'Tyrosines in the influenza A virus M2 protein cytoplasmic tail are critical for production of infectious virus particles', *J Virol*, 84(17), pp. 8765–8776. doi: 10.1128/JVI.00853-10.

Gustin, K. M. *et al.* (2011) 'Influenza virus aerosol exposure and analytical system for ferrets', *Proceedings of the National Academy of Sciences*, 108(20), pp. 8432–8437. doi: 10.1073/pnas.1100768108.

Gustin, K. M. *et al.* (2013) 'Comparison of the Levels of Infectious Virus in Respirable Aerosols Exhaled by Ferrets Infected with Influenza Viruses Exhibiting Diverse Transmissibility Phenotypes', *Journal of Virology*, 87(14), pp. 7864–7873. doi: 10.1128/JVI.00719-13.

Gustin, K. M. *et al.* (2015) 'Environmental conditions affect exhalation of H3N2 seasonal and variant influenza viruses and respiratory droplet transmission in ferrets', *PLoS ONE*, 10(5), pp. 1–19. doi: 10.1371/journal.pone.0125874.

Han, X. *et al.* (2012) 'Influenza Virus A/Beijing/501/2009(H1N1) NS1 Interacts with β-Tubulin and Induces Disruption of the Microtubule Network and Apoptosis on A549 Cells', *PLoS ONE*, 7(11), p. e48340. doi: 10.1371/journal.pone.0048340.

Hancock, K. *et al.* (2009) 'Cross-reactive antibody responses to the 2009 pandemic H1N1 influenza virus', *The New England journal of medicine*, 361(20), pp. 1945–1952. doi: 10.1056/NEJMoa0906453.

Harris, A. *et al.* (2006) 'Influenza virus pleiomorphy characterized by cryoelectron tomography', *Proceedings of the National Academy of Sciences*, 103(50), pp. 19123–19127. doi: 10.1073/pnas.0607614103.

Harrison, S. C. (2009) 'Viral membrane fusionHarrison, S. C. (2009). Viral membrane fusion, 15(7), 690–698.', *National Structure Molecular Biology*, 15(7), pp. 690–698. doi: 10.1038/nsmb.1456.Viral.

Harvey, R. *et al.* (2004) 'Restrictions to the adaptation of influenza a virus h5 hemagglutinin to the human host.', *Journal of virology*, 78(1), pp. 502–7. doi:

10.1128/JVI.78.1.502.

Herfst, S. *et al.* (2012) 'Airborne Transmission of Influenza A/H5N1 Virus Between Ferrets', *Science*, 336(6088), pp. 1534–1541. doi: 10.1126/science.1213362.

Hilsch, M. *et al.* (2014) 'Influenza a matrix protein m1 multimerizes upon binding to lipid membranes', *Biophysical Journal*, 107(4), pp. 912–923. doi: 10.1016/j.bpj.2014.06.042.

Van Hoeven, N. *et al.* (2009) 'Pathogenesis of 1918 Pandemic and H5N1 Influenza Virus Infections in a Guinea Pig Model: Antiviral Potential of Exogenous Alpha Interferon To Reduce Virus Shedding', *Journal of Virology*, 83(7), pp. 2851–2861. doi: 10.1128/JVI.02174-08.

Hornung, V. *et al.* (2006) '{5'-Triphosphate} {RNA} Is the Ligand for {RIG-I}', 314(5801), pp. 994–997. doi: 10.1126/science.1132505.

Hovenberg, H. W., Davies, J. R. and Carlstedt, I. (1996) 'Different mucins are produced by the surface epithelium and the submucosa in human trachea: identification of MUC5AC as a major mucin from the goblet cells.', *The Biochemical journal*, 318 (Pt 1, pp. 319–324.

Huang, Q. *et al.* (2002) 'Protonation and stability of the globular domain of influenza virus hemagglutinin', *Biophysical Journal*. Elsevier, 82(2), pp. 1050–1058. doi: 10.1016/S0006-3495(02)75464-7.

Hui, D. S. C., Lee, N. and Chan, P. K. S. (2017) 'Avian influenza A (H7N9) virus infections in humans across five epidemics in mainland China, 2013–2017', *Journal of Thoracic Disease*, 9(12), pp. 4808–4811. doi: 10.21037/jtd.2017.11.17.

Hutchinson, E. C. *et al.* (2014) 'Conserved and host-specific features of influenza virion architecture', *Nature Communications*, 5(May), p. 4816. doi: 10.1038/ncomms5816.

Hutchinson, E. C. and Fodor, E. (2013) 'Transport of the influenza virus genome from nucleus to nucleus', *Viruses*, 5(10), pp. 2424–2446. doi: 10.3390/v5102424.

Ilyushina, N. A. *et al.* (2010) 'Adaptation of pandemic H1N1 influenza viruses in mice', *J Virol*, 84(17), pp. 8607–8616. doi: 10.1128/JVI.00159-10.

Imai, M. *et al.* (2012) 'Experimental adaptation of an influenza H5 HA confers respiratory

droplet transmission to a reassortant H5 HA/H1N1 virus in ferrets', *Nature*. Nature Publishing Group, 486(7403), pp. 420–428. doi: 10.1038/nature10831.

Isken, B., Genzel, Y. and Reichl, U. (2012) 'Productivity, apoptosis, and infection dynamics of influenza A/PR/8 strains and A/PR/8-based reassortants', *Vaccine*. Elsevier Ltd, 30(35), pp. 5253–5261. doi: 10.1016/j.vaccine.2012.05.065.

Ito, T. and Kawaoka, Y. (2000) 'Host-range barrier of influenza A viruses', *Veterinary Microbiology*, 74(1–2), pp. 71–75. doi: 10.1016/S0378-1135(00)00167-X.

Itoh, Y. *et al.* (2009a) 'In vitro and in vivo characterization of new swine-origin H1N1 influenza viruses', *Nature*, pp. 1–24. doi: 10.1038/nature08260.

Itoh, Y. *et al.* (2009b) 'In vitro and in vivo characterization of new swine-origin H1N1 influenza viruses', *Nature*. Nature Publishing Group, 460(7258), pp. 1021–1025. doi: 10.1038/nature08260.

Iwatsuki-horimoto, K. *et al.* (2004) 'Generation of In uenza A Virus NS2 (NEP) Mutants with an Altered Nuclear Export Signal Sequence', *Society*, 78(18), pp. 10149–10155. doi: 10.1128/JVI.78.18.10149.

Iwatsuki-Horimoto, K. *et al.* (2006) 'The cytoplasmic tail of the influenza A virus M2 protein plays a role in viral assembly.', *Journal of virology*, 80(11), pp. 5233–40. doi: 10.1128/JVI.00049-06.

Jagger, B. W. *et al.* (2012) 'An overlapping protein-coding region in influenza A virus segment 3 modulates the host response', *Science*, 337(6091), pp. 199–204. doi: 10.1126/science.1222213.

Jia, N. *et al.* (2014) 'Glycomic characterization of respiratory tract tissues of ferrets: Implications for its use in influenza virus infection studies', *Journal of Biological Chemistry*, 289(41), pp. 28489–28504. doi: 10.1074/jbc.M114.588541.

Jin, H. *et al.* (1997) 'Influenza virus hemagglutinin and neuraminidase cytoplasmic tails control particle shape', *EMBO Journal*, 16(6), pp. 1236–1247. doi: 10.1093/emboj/16.6.1236.

Job, E. R. *et al.* (2016) 'Neutralizing inhibitors in the airways of naïve ferrets do not play a

major role in modulating the virulence of H3 subtype influenza A viruses', *Virology*. Elsevier, 494, pp. 143–157. doi: 10.1016/j.virol.2016.01.024.

Jorba, N., Coloma, R. and Ortín, J. (2009) 'Genetic trans-complementation establishes a new model for influenza virus RNA transcription and replication', *PLoS Pathogens*, 5(5). doi: 10.1371/journal.ppat.1000462.

Kato, H. *et al.* (2006) 'Differential roles of MDA5 and RIG-I helicases in the recognition of RNA viruses', *Nature*, 441(1), pp. 101–105. doi: 10.1038/nature04734.

Kesimer, M. *et al.* (2009) 'Characterization of exosome-like vesicles released from human tracheobronchial ciliated epithelium: a possible role in innate defense', *Faseb J*, 23(6), pp. 1858–1868. doi: fj.08-119131 [pii]10.1096/fj.08-119131.

Kesimer, M. *et al.* (2009) 'Characterization of exosome-like vesicles released from human tracheobronchial ciliated epithelium: a possible role in innate defense', *The FASEB Journal*, 23(6), pp. 1858–1868. doi: 10.1096/fj.08-119131.

Kielian, M. and Rey, F. A. (2006) 'Virus membrane-fusion proteins: More than one way to make a hairpin', *Nature Reviews Microbiology*, 4(1), pp. 67–76. doi: 10.1038/nrmicro1326.

Kolesnikova, L. *et al.* (2013) 'Influenza virus budding from the tips of cellular microvilli in differentiated human airway epithelial cells', *Journal of General Virology*, 94(PART 5), pp. 971–976. doi: 10.1099/vir.0.049239-0.

Koren, C. W. R. and Nylund, A. (1997) 'Morphology and morphogenesis of infectious salmon anaemia virus replicating in the endothelium of Atlantic salmon Salmo salar', *Diseases Of Aquatic Organisms*, 29, pp. 99–109. doi: 10.3354/dao029099.

Kundu, A. *et al.* (1996) 'Transmembrane domain of influenza virus neuraminidase, a type II protein, possesses an apical sorting signal in polarized MDCK cells.', *Journal of virology*, 70(9), pp. 6508–15. Available at: http://www.pubmedcentral.nih.gov/articlerender.fcgi?artid=190689&tool=pmcentrez&rendertype=abstract.

Lakdawala, S. S. *et al.* (2011) 'Eurasian-origin gene segments contribute to the

transmissibility, aerosol release, and morphology of the 2009 pandemic H1N1 influenza virus', *PLoS Pathogens*, 7(12). doi: 10.1371/journal.ppat.1002443.

Lamb, R. A., Lai, C. J. and Choppin, P. W. (1981) 'Sequences of mRNAs derived from genome RNA segment 7 of influenza virus: colinear and interrupted mRNAs code for overlapping proteins.', *Proceedings of the National Academy of Sciences*, 78(7), pp. 4170–4174. doi: 10.1073/pnas.78.7.4170.

Leser, G. P. and Lamb, R. A. (2005) 'Influenza virus assembly and budding in raft-derived microdomains: A quantitative analysis of the surface distribution of HA, NA and M2 proteins', *Virology*, 342(2), pp. 215–227. doi: 10.1016/j.virol.2005.09.049.

Lin, S. *et al.* (1998) 'Mutations in the middle of the transmembrane domain reverse the polarity of transport of the influenza virus hemagglutinin in MDCK epithelial cells', *Journal of Cell Biology*, 142(1), pp. 51–57. doi: 10.1083/jcb.142.1.51.

Linster, M. *et al.* (2014) 'Identification, characterization, and natural selection of mutations driving airborne transmission of A/H5N1 virus', *Cell*, 157(2), pp. 329–339. doi: 10.1016/j.cell.2014.02.040.

Liu, T., Muller, J. and Ye, Z. (2002) 'Association of influenza virus matrix protein with ribonucleoproteins may control viral growth and morphology.', *Virology*, 304(1), pp. 89–96. doi: 10.1006/viro.2002.1669.

Lowen, A. C. *et al.* (2006) 'The guinea pig as a transmission model for human influenza viruses.', *Proceedings of the National Academy of Sciences of the United States of America*, 103(26), pp. 9988–92. doi: 10.1073/pnas.0604157103.

Lowen, A. C. *et al.* (2007) 'Influenza virus transmission is dependent on relative humidity and temperature', *PLoS Pathogens*, 3(10), pp. 1470–1476. doi: 10.1371/journal.ppat.0030151.

Lu, C. *et al.* (2010) 'The structural basis of 5' triphosphate double-stranded RNA recognition by RIG-I C-terminal domain', *Structure*. Elsevier Ltd, 18(8), pp. 1032–1043. doi: 10.1016/j.str.2010.05.007.

Ma, W. *et al.* (2012) 'The neuraminidase and matrix genes of the 2009 pandemic

influenza H1N1 virus cooperate functionally to facilitate efficient replication and transmissibility in pigs', *Journal of General Virology*, 93(6), pp. 1261–1268. doi: 10.1099/vir.0.040535-0.

Madsen, J. *et al.* (2000) 'Localization of Lung Surfactant Protein D on Mucosal Surfaces in Human Tissues', *The Journal of Immunology*, 164(11), pp. 5866–5870. doi: 10.4049/jimmunol.164.11.5866.

Maines, T. R. *et al.* (2005) 'Avian Influenza (H5N1) Viruses Isolated from Humans in Asia in 2004 Exhibit Increased Virulence in Mammals', *Journal of Virology*, 79(18), pp. 11788–11800. doi: 10.1128/JVI.79.18.11788.

Maines, T. R. *et al.* (2009) 'Transmission and Pathogenesis of Swine-Origin 2009 A(H1N1) Influenza Viruses in Ferrets and Mice', *Science*, 325(July), pp. 484–487. doi: 10.1126/science.1177238.

Mänz, B. *et al.* (2012) 'Adaptive mutations in NEP compensate for defective H5N1 RNA replication in cultured human cells.', *Nature communications*, 3(May), p. 802. doi: 10.1038/ncomms1804.

Marcus, P. I., Ngunjiri, J. M. and Sekellick, M. J. (2009) 'Dynamics of biologically active subpopulations of influenza virus: plaque-forming, noninfectious cell-killing, and defective interfering particles', *J Virol*, 83(16), pp. 8122–8130. doi: 10.1128/JVI.02680-08.

Martin, K. and Heleniust, A. (1991) 'Nuclear transport of influenza virus ribonucleoproteins: The viral matrix protein (M1) promotes export and inhibits import', *Cell*, 67(1), pp. 117–130. doi: 10.1016/0092-8674(91)90576-K.

Matrosovich, M. *et al.* (2000) 'Early Alterations of the Receptor-Binding Properties of H1, H2, and H3 Avian Influenza Virus Hemagglutinins after Their Introduction into Mammals', *Journal of Virology*, 74(18), pp. 8502–8512. doi: 10.1128/JVI.74.18.8502-8512.2000.

Matrosovich, M. N. *et al.* (2004) 'Human and avian influenza viruses target different cell types in cultures of human airway epithelium', *Proceedings of the National Academy of Sciences*, 101(13), pp. 4620–4624. doi: 10.1073/pnas.0308001101.

Matrosovich, M. N. *et al.* (2004) 'Neuraminidase Is Important for the Initiation of Influenza Virus Infection in Human Airway Epithelium', *Society*, 78(22), pp. 12665–12667. doi: 10.1128/JVI.78.22.12665.

Matsuoka, Y. *et al.* (2009) 'Neuraminidase stalk length and additional glycosylation of the hemagglutinin influence the virulence of influenza H5N1 viruses for mice', *J Virol*, 83(9), pp. 4704–4708. doi: 10.1128/JVI.01987-08.

McCown, M. F. and Pekosz, A. (2006) 'Distinct domains of the influenza a virus M2 protein cytoplasmic tail mediate binding to the M1 protein and facilitate infectious virus production.', *Journal of virology*, 80(16), pp. 8178–89. doi: 10.1128/JVI.00627-06.

Mercer, J. and Helenius, A. (2009) 'Virus entry by macropinocytosis', *Nature Cell Biology*, 11(5), pp. 510–520. doi: 10.1038/ncb0509-510.

Mibayashi, M. *et al.* (2007) 'Inhibition of Retinoic Acid-Inducible Gene I-Mediated Induction of Beta Interferon by the NS1 Protein of Influenza A Virus', *Journal of Virology*, 81(2), pp. 514–524. doi: 10.1128/JVI.01265-06.

Mikhail Matrosovich and Klenk, H.-D. (2003) 'Natural and synthetic sialic acid-containing inhibitors of influenza virus receptor binding.pdf', *Rev. Med. Virol.*, pp. 85–97. doi: 10.1002/rmv.372.

Milton, D. K. *et al.* (2013) 'Influenza Virus Aerosols in Human Exhaled Breath: Particle Size, Culturability, and Effect of Surgical Masks', *PLoS Pathogens*, 9(3). doi: 10.1371/journal.ppat.1003205.

Mitnaul, L. J. *et al.* (1996) 'The Cytoplasmic Tail of Influenza A Virus Neuraminidase (NA) Affects NA Incorporation into Virions, Virion Morphology, and Virulence in Mice but Is Not Essential for Virus Replication', *Journal of Virology*, 70(2), pp. 873–879.

Mitnaul, L. J. *et al.* (2000) 'Balanced hemagglutinin and neuraminidase activities are critical for efficient replication of influenza A virus.', *Journal of virology*, 74(13), pp. 6015–20. doi: 10.1128/JVI.74.13.6015-6020.2000.

Moeller, A. *et al.* (2012) 'Organization of the Influenza Virus Replication Machinery TL - 338', *Science*, 338 VN-(6114), pp. 1631–1634. doi: 10.1126/science.1227270.

Molinari, N. A. M. *et al.* (2007) 'The annual impact of seasonal influenza in the US: Measuring disease burden and costs', *Vaccine*, 25(27), pp. 5086–5096. doi: 10.1016/j.vaccine.2007.03.046.

Momose, F. *et al.* (2007) 'Visualization of microtubule-mediated transport of influenza viral progeny ribonucleoprotein', *Microbes and Infection*, 9(12–13), pp. 1422–1433. doi: 10.1016/j.micinf.2007.07.007.

Mubareka, S. *et al.* (2009) 'Transmission of Influenza Virus via Aerosols and Fomites in the Guinea Pig Model', *The Journal of Infectious Diseases*, 199(6), pp. 858–865. doi: 10.1086/597073.

Munster, V. J. *et al.* (2007) 'Spatial, temporal, and species variation in prevalence of influenza a viruses in wild migratory birds', *PLoS Pathogens*, 3(5), pp. 0630–0638. doi: 10.1371/journal.ppat.0030061.

Munster, V. J. *et al.* (2009) 'Virus in Ferrets', 503(2003), pp. 481–483. doi: 10.1126/science.1177127.Pathogenesis.

Muramoto, Y. *et al.* (2006) 'Hierarchy among viral RNA (vRNA) segments in their role in vRNA incorporation into influenza A virions.', *Journal of virology*, 80(5), pp. 2318–25. doi: 10.1128/JVI.80.5.2318-2325.2006.

Muramoto, Y. *et al.* (2013) 'Identification of Novel Influenza A Virus Proteins Translated from PA mRNA', *Journal of Virology*, 87(5), pp. 2455–2462. doi: 10.1128/JVI.02656-12.

Nakatsu, S. *et al.* (2018) 'Influenza C and D viruses package eight organized ribonucleoprotein complexes', *Journal of Virology*, (January), p. JVI.02084-17. doi: 10.1128/JVI.02084-17.

Nayak, D. P., Hui, E. K. W. and Barman, S. (2004) 'Assembly and budding of influenza virus', *Virus Research*, 106(2 SPEC.ISS.), pp. 147–165. doi: 10.1016/j.virusres.2004.08.012.

Neil, S. J. D., Zang, T. and Bieniasz, P. D. (2008) 'Tetherin inhibits retrovirus release and is antagonized by HIV-1 Vpu', *Nature*, 451(7177), pp. 425–430. doi: 10.1038/nature06553.

Neumann, G. *et al.* (2000) 'Influenza A virus NS2 protein mediates vRNP nuclear export

through NES-independent interaction with hCRM1', *The EMBO Journal*, 19(24), pp. 6751–6758. doi: 10.1093/emboj/19.24.6751.

Neumann, G. and Kawaoka, Y. (2015) 'Transmission of influenza A viruses', *Virology*, 479–480, pp. 234–246. doi: 10.1016/j.virol.2015.03.009.

Nguyen-Van-Tam, J. S. and Hampson, A. W. (2003) 'The epidemiology and clinical impact of pandemic influenza', *Vaccine*, 21(16), pp. 1762–1768. doi: 10.1016/S0264-410X(03)00069-0.

Nicholls, J. M. *et al.* (2007) 'Sialic acid receptor detection in the human respiratory tract: evidence for widespread distribution of potential binding sites for human and avian influenza viruses', *Respiratory Research*, 8(1), p. 73. doi: 10.1186/1465-9921-8-73.

Noda, T. *et al.* (2006) 'Architecture of ribonucleoprotein complexes in influenza A virus particles', *Nature*, 439(7075), pp. 490–492. doi: 10.1038/nature04378.

Noda, T. *et al.* (2012) 'Three-dimensional analysis of ribonucleoprotein complexes in influenza A virus', *Nature Communications*. Nature Publishing Group, 3, p. 639. doi: 10.1038/ncomms1647.

Pleschka, S. *et al.* (1996) 'A plasmid-based reverse genetics system for influenza A virus.', *Journal of virology*, 70(6), pp. 4188–92. Available at: http://www.ncbi.nlm.nih.gov/pubmed/8648766%5Cnhttp://www.pubmedcentral.nih.gov/articlerender.fcgi?artid=PMC190316.

Pritlove, D. C. *et al.* (1998) 'Polyadenylation of influenza virus mRNA transcribed in vitro from model virion RNA templates: requirement for 5' conserved sequences.', *Journal of virology*, 72(2), pp. 1280–6. Available at: http://www.ncbi.nlm.nih.gov/pubmed/9445028%0Ahttp://www.pubmedcentral.nih.gov/articlerender.fcgi?artid=PMC124606.

Pu, J. *et al.* (2015) 'Evolution of the H9N2 influenza genotype that facilitated the genesis of the novel H7N9 virus', *Proceedings of the National Academy of Sciences*, 112(2), pp. 548–553. doi: 10.1073/pnas.1422456112.

Pu, J. *et al.* (2017) 'M Gene Reassortment in H9N2 Influenza Virus Promotes Early

Infection and Replication: Contribution to Rising Virus Prevalence in Chickens in China.', *Journal of virology*, 91(8), pp. e02055-16. doi: 10.1128/JVI.02055-16.

Read, E. K. C. and Digard, P. (2010) 'Individual influenza A virus mRNAs show differential dependence on cellular NXF1/TAP for their nuclear export', *Journal of General Virology*, 91(5), pp. 1290–1301. doi: 10.1099/vir.0.018564-0.

Reed, M. L. *et al.* (2009) 'Amino acid residues in the fusion peptide pocket regulate the pH of activation of the H5N1 influenza virus hemagglutinin protein.', *Journal of virology*, 83(8), pp. 3568–3580. doi: 10.1128/JVI.02238-08.

Reed, M. L. *et al.* (2010) 'The pH of Activation of the Hemagglutinin Protein Regulates H5N1 Influenza Virus Pathogenicity and Transmissibility in Ducks', *Journal of Virology*, 84(3), pp. 1527–1535. doi: 10.1128/JVI.02069-09.

Rehwinkel, J. *et al.* (2010) 'RIG-I Detects Viral Genomic RNA during Negative-Strand RNA Virus Infection', *Cell*. Elsevier Ltd, 140(3), pp. 397–408. doi: 10.1016/j.cell.2010.01.020.

Reich, S. *et al.* (2014) 'Structural insight into cap-snatching and RNA synthesis by influenza polymerase', *Nature*, 516(7531), pp. 361–366. doi: 10.1038/nature14009.

Riggs, B. *et al.* (2003) 'Actin cytoskeleton remodeling during early Drosophila furrow formation requires recycling endosomal components Nuclear-fallout and Rab11', *Journal of Cell Biology*, 163(1), pp. 143–154. doi: 10.1083/jcb.200305115.

Roberts, C., Lamb, R. A. and Compans, R. W. (1998) 'The M1 and M2 Proteins of Influenza A Virus Are Important Determinantsin Filamentous Particle Formation', *Virology*, 240, pp. 127–137.

Roberts, K. L. *et al.* (2011) 'Lack of transmission of a human influenza virus with avian receptor specificity between ferrets is not due to decreased virus shedding but rather a lower infectivity in vivo', *Journal of General Virology*, 92(8), pp. 1822–1831. doi: 10.1099/vir.0.031203-0.

Roberts, K. L. *et al.* (2012) 'Transmission of a 2009 H1N1 Pandemic Influenza Virus Occurs before Fever Is Detected, in the Ferret Model', *PLoS ONE*, 7(8), pp. 1–8. doi: 10.1371/journal.pone.0043303.

Roberts, K. L. *et al.* (2013) 'The amphipathic helix of influenza A virus M2 protein is required for filamentous bud formation and scission of filamentous and spherical particles.', *Journal of virology*, 87(18), pp. 9973–82. doi: 10.1128/JVI.01363-13.

Roberts, P. C. and Compans, R. W. (1998) 'Host cell dependence of viral morphology', *Proceedings of the National Academy of Sciences of the United States of America*, 95(10), pp. 5746–5751. doi: 10.1073/pnas.95.10.5746.

Rossman, J. S. *et al.* (2010) 'Influenza Virus M2 Ion Channel Protein Is Necessary for Filamentous Virion Formation', *Journal of Virology*, 84(10), pp. 5078–5088. doi: 10.1128/JVI.00119-10.

Rossman, J. S. *et al.* (2010) 'Influenza Virus M2 Protein Mediates ESCRT-Independent Membrane Scission', *Cell*. Elsevier Ltd, 142(6), pp. 902–913. doi: 10.1016/j.cell.2010.08.029.

Rossman, J. S. and Lamb, R. A. (2011) 'Influenza virus assembly and budding', *Virology*, 411(2), pp. 229–236. doi: 10.1016/j.virol.2010.12.003.

Rossman, J. S., Leser, G. P. and Lamb, R. A. (2012) 'Filamentous Influenza Virus Enters Cells via Macropinocytosis', *Journal of Virology*, 86(20), pp. 10950–10960. doi: 10.1128/JVI.05992-11.

Ruangrung, K. *et al.* (2016) 'Neuraminidase Activity and Resistance of 2009 Pandemic H1N1 Influenza Virus to Antiviral Activity in Bronchoalveolar Fluid', *Journal of Virology*, 90(9), pp. 4637–4646. doi: 10.1128/JVI.00013-16.

Sakabe, S. *et al.* (2011) 'Mutations in PA, NP, and HA of a pandemic (H1N1) 2009 influenza virus contribute to its adaptation to mice', *Virus Research*. Elsevier B.V., 158(1–2), pp. 124–129. doi: 10.1016/j.virusres.2011.03.022.

Sakaguchi, A. *et al.* (2003) 'Nuclear export of influenza viral ribonucleoprotein is temperature-dependently inhibited by dissociation of viral matrix protein', *Virology*, 306(2), pp. 244–253. doi: 10.1016/S0042-6822(02)00013-2.

Sakai, T., Nishimura, S. I., *et al.* (2017) 'Influenza A virus hemagglutinin and neuraminidase act as novel motile machinery', *Scientific Reports*. Nature Publishing

Group, 7(March), p. 45043. doi: 10.1038/srep45043.

Sakai, T., Takagi, H., *et al.* (2017) 'Unique directional motility of influenza C virus controlled by its filamentous morphology and short-range motions', *Journal of Virology*, (November), p. JVI.01522-17. doi: 10.1128/JVI.01522-17.

Salomon, R. and Webster, R. G. (2009) 'The Influenza Virus Enigma', *Cell*, 136(3), pp. 402–410. doi: 10.1016/j.cell.2009.01.029.

Samuel, C. E. (2001) 'Antiviral Actions of Interferons.pdf', 14(4), pp. 778–809. doi: 10.1128/CMR.14.4.778.

Sasaki, S. *et al.* (2008) 'Influence of prior influenza vaccination on antibody and B-cell responses', *PLoS ONE*, 3(8). doi: 10.1371/journal.pone.0002975.

Schrauwen, E. J. A. *et al.* (2013) 'Reassortment between Avian H5N1 and Human Influenza Viruses Is Mainly Restricted to the Matrix and Neuraminidase Gene Segments', *PLoS ONE*, 8(3), pp. 1–8. doi: 10.1371/journal.pone.0059889.

Schulman, J. L. and Kilbourne, E. D. (1963) 'Experimental Transmission of Influenza Virus Infection in Mice. I. the Period of Transmissibility.', *The Journal of experimental medicine*, 118, pp. 257–66. Available at: http://www.pubmedcentral.nih.gov/articlerender.fcgi?artid=2137713&tool=pmcentrez&rendertype=abstract.

Scull, M. A. *et al.* (2009) 'Avian influenza virus glycoproteins restrict virus replication and spread through human airway epithelium at temperatures of the proximal airways', *PLoS Pathogens*, 5(5). doi: 10.1371/journal.ppat.1000424.

Seladi-Schulman, J. *et al.* (2014) 'Filament-producing mutants of influenza A/Puerto Rico/ 8/1934 (H1N1) virus have higher neuraminidase activities than the spherical wild-type', *PLoS ONE*, 9(11), pp. 1–10. doi: 10.1371/journal.pone.0112462.

Seladi-Schulman, J., Steel, J. and Lowen, A. C. (2013) 'Spherical Influenza Viruses Have a Fitness Advantage in Embryonated Eggs, while Filament-Producing Strains Are Selected In Vivo', *Journal of Virology*, 87(24), pp. 13343–13353. doi: 10.1128/JVI.02004-13.

Sha, B. and Luo, M. (1997) 'Structure of a bifunctional membrane-RNA binding protein,

influenza virus matrix protein M1.', *Nature structural biology*, 4(3), pp. 239–44. doi: 10.1038/nsb0397-239.

Shangguan, T. *et al.* (1998) 'Morphological changes and fusogenic activity of influenza virus hemagglutinin', *Biophysical Journal*. Elsevier, 74(1), pp. 54–62. doi: 10.1016/S0006-3495(98)77766-5.

Shanks, G. D. (2015) 'Insights from unusual aspects of the 1918 influenza pandemic', *Travel Medicine and Infectious Disease*. Elsevier Ltd, 13(3), pp. 217–222. doi: 10.1016/j.tmaid.2015.05.001.

Shapiro, G. I. and Krug, R. M. (1988) 'Influenza virus RNA replication in vitro : synthesis of viral template RNAs and virion RNAs in the absence of an added primer . Influenza Virus RNA Replication In Vitro : Synthesis of Viral Template RNAs and Virion RNAs in the Absence of an Added Primer', 62(7), pp. 2285–2290.

Shaw, M. L. *et al.* (2008) 'Cellular proteins in influenza virus particles', *PLoS Pathogens*, 4(6), pp. 1–13. doi: 10.1371/journal.ppat.1000085.

Shelton, H. *et al.* (2013) 'Mutations in haemagglutinin that affect receptor binding and pH stability increase replication of a PR8 influenza virus with H5 HA in the upper respiratory tract of ferrets and may contribute to transmissibility', *Journal of General Virology*, 94(PART 6), pp. 1220–1229. doi: 10.1099/vir.0.050526-0.

Shinya, K. *et al.* (2006) 'Influenza virus receptors in the human airway', *Nature*, 440(7083), pp. 435–436. doi: 10.1038/440435a.

Shortridge, K. F. *et al.* (1998) 'Characterization of avian H5N1 influenza viruses from poultry in Hong Kong.', *Virology*, 252(2), pp. 331–342. doi: 10.1006/viro.1998.9488.

Sieczkarski, S. B. and Whittaker, G. R. (2005) 'Characterization of the host cell entry of filamentous influenza virus', *Archives of Virology*, 150(9), pp. 1783–1796. doi: 10.1007/s00705-005-0558-1.

de Silva, T. I. *et al.* (2017) 'Comparison of mucosal lining fluid sampling methods and influenza-specific IgA detection assays for use in human studies of influenza immunity', *Journal of Immunological Methods*, 449, pp. 1–6. doi: 10.1016/j.jim.2017.06.008.

Simpson-Holley, M. *et al.* (2002) 'A Functional Link between the Actin Cytoskeleton and Lipid Rafts during Budding of Filamentous Influenza Virions', *Virology*, 301(2), pp. 212–225. doi: 10.1006/viro.2002.1595.

Skehel, J. J. and Wiley, D. C. (2000) 'Receptor Binding and Membrane Fusion in Virus Entry: The Influenza Hemagglutinin', *Annual Review of Biochemistry*. Annual Reviews, 69(1), pp. 531–569. doi: 10.1146/annurev.biochem.69.1.531.

Smeenk, C. A. *et al.* (1996) 'Mutations in the hemagglutinin and matrix genes of a virulent influenza virus variant, A/FM/1/47-MA, control different stages in pathogenesis', *Virus Research*, 44(2), pp. 79–95. doi: 10.1016/0168-1702(96)01329-9.

Smeenk, C. a and Brown, E. G. (1994) 'The influenza virus variant A/FM/1/47-MA possesses single amino acid replacements in the hemagglutinin, controlling virulence, and in the matrix protein, controlling virulence as well as growth.', *Journal of virology*, 68(1), pp. 530–4. Available at: http://www.pubmedcentral.nih.gov/articlerender.fcgi?artid=236317&tool=pmcentrez&rendertype=abstract.

Smirnov, Y. A., Kuznetsova, M. A. and Kaverin, N. V. (1991) 'The genetic aspects of influenza virus filamentous particle formation', *Archives of Virology*, 118(3–4), pp. 279–284. doi: 10.1007/BF01314038.

Stegmann, T., White, J. M. and Helenius, a (1990) 'Intermediates in influenza induced membrane fusion.', *The EMBO journal*, 9(13), pp. 4231–4241. doi: 10.1002/j.1460-2075.1990.tb07871.x.

Steinhauer, D. A. (1999) 'Role of heamagglutinin cleavage for the pathogenicity of influenza virus.', *Virology*, 258, pp. 1–20.

Stieneke-Gröber, A. *et al.* (1992) 'Influenza virus hemagglutinin with multibasic cleavage site is activated by furin, a subtilisin-like endoprotease.', *The EMBO journal*, 11(7), pp. 2407–14. Available at: http://www.ncbi.nlm.nih.gov/pubmed/1628614%5Cnhttp://www.pubmedcentral.nih.gov/articlerender.fcgi?artid=PMC556715.

Suzuki, Y. *et al.* (2000) 'Sialic Acid Species as a Determinant of the Host Range of

Influenza A Viruses', *Journal of Virology*, 74(24), pp. 11825–11831. doi: 10.1128/JVI.74.24.11825-11831.2000.

Tafesse, F. G. *et al.* (2013) 'Intact sphingomyelin biosynthetic pathway is essential for intracellular transport of influenza virus glycoproteins.', *Proceedings of the National Academy of Sciences of the United States of America*, 110(16), pp. 6406–11. doi: 10.1073/pnas.1219909110.

Takahasi, K. *et al.* (2008) 'Nonself RNA-Sensing Mechanism of RIG-I Helicase and Activation of Antiviral Immune Responses', *Molecular Cell*, 29(4), pp. 428–440. doi: 10.1016/j.molcel.2007.11.028.

Takeda, M. *et al.* (2002) 'Influenza A Virus M 2 Ion Channel Activity Is Essential for Efficient Replication in Tissue Culture', *Society*, 76(3), pp. 1391–1399. doi: 10.1128/JVI.76.3.1391.

Takeuchi, K. and Lamb, R. A. (1994) 'Influenza virus M2 protein ion channel activity stabilizes the native form of fowl plague virus hemagglutinin during intracellular transport.', *Journal of virology*, 68(2), pp. 911–9. doi: 10.1006/viro.1994.1428.

Tan, K. Sen *et al.* (2012) 'In vivo and in vitro studies on the antiviral activities of viperin against influenza H1N1 virus infection', *Journal of General Virology*, 93(6), pp. 1269–1277. doi: 10.1099/vir.0.040824-0.

Taubenberger, J. K. *et al.* (2012) 'Initial Genetic Characterization of the 1918 ' ' Spanish ' ' Influenza Virus Initial Genetic Characterization of the 1918 " Spanish " Influenza Virus', 1793(1997). doi: 10.1126/science.275.5307.1793.

Thompson, C. I. *et al.* (2006) 'Infection of Human Airway Epithelium by Human and Avian Strains of Influenza A Virus', *Journal of Virology*, 80(16), pp. 8060–8068. doi: 10.1128/JVI.00384-06.

Thompson, W. W. *et al.* (2004) 'in the United States', 292(11), pp. 1333–1340.

Thornton, D. J., Rousseau, K. and McGuckin, M. A. (2008) 'Structure and Function of the Polymeric Mucins in Airways Mucus', *Annual Review of Physiology*, 70(1), pp. 459–486. doi: 10.1146/annurev.physiol.70.113006.100702.

Tian, S. F. *et al.* (1985) 'Nucleoprotein and membrane protein genes are associated with restriction of replication of influenza A/Mallard/NY/78 virus and its reassortants in squirrel monkey respiratory tract', *J Virol*, 53(3), pp. 771–775. Available at: http://www.ncbi.nlm.nih.gov/pubmed/3973966.

Tong, S. *et al.* (2012) 'A distinct lineage of influenza A virus from bats', *Proceedings of the National Academy of Sciences*, 109(11), pp. 4269–4274. doi: 10.1073/pnas.1116200109.

Tsfasman, T. *et al.* (2015) 'Amphipathic alpha-helices and putative cholesterol binding domains of the influenza virus matrix M1 protein are crucial for virion structure organisation', *Virus Research*. Elsevier B.V., 210, pp. 114–118. doi: 10.1016/j.virusres.2015.07.017.

Ullrich, O. and Molecular, E. (1996) 'Rabl 1 Regulates Recycling through the Pericentriolar Recycling Endosome', 135(4), pp. 913–924.

Urbé, S.; Huber, L. A.; Zerial, M.; Tooze, S. A. and Parton, R. G. (1993) 'Rab 11, a small GTPase associated with both constitutive and regulatory secretory pathwyas in PC12 cells', *FEBS lett.*, 334, pp. 175–182.

Vasin, A. V. *et al.* (2014) 'Molecular mechanisms enhancing the proteome of influenza A viruses: An overview of recently discovered proteins', *Virus Research*. Elsevier B.V., 185, pp. 53–63. doi: 10.1016/j.virusres.2014.03.015.

Vigerust, D. J. *et al.* (2007) 'N-Linked Glycosylation Attenuates H3N2 Influenza Viruses', *Journal of Virology*, 81(16), pp. 8593–8600. doi: 10.1128/JVI.00769-07.

Vijayakrishnan, S. *et al.* (2013) 'Cryotomography of Budding Influenza A Virus Reveals Filaments with Diverse Morphologies that Mostly Do Not Bear a Genome at Their Distal End', *PLoS Pathogens*, 9(6). doi: 10.1371/journal.ppat.1003413.

Vreede, F. T., Gifford, H. and Brownlee, G. G. (2008) 'Role of initiating nucleoside triphosphate concentrations in the regulation of influenza virus replication and transcription', *J Virol*, 82(14), pp. 6902–6910. doi: 10.1128/JVI.00627-08.

de Vries, R. P. *et al.* (2014) 'Hemagglutinin Receptor Specificity and Structural Analyses

of Respiratory Droplet-Transmissible H5N1 Viruses', *Journal of Virology*, 88(1), pp. 768–773. doi: 10.1128/JVI.02690-13.

Wang, C., Lamb, R. A. and Pinto, L. H. (1995) 'Activation of the M2 ion channel of influenza virus: a role for the transmembrane domain histidine residue', *Biophysical Journal*. Elsevier, 69(4), pp. 1363–1371. doi: 10.1016/S0006-3495(95)80003-2.

Wang, X., Hinson, E. R. and Cresswell, P. (2007) 'The Interferon-Inducible Protein Viperin Inhibits Influenza Virus Release by Perturbing Lipid Rafts', *Cell Host and Microbe*, 2(2), pp. 96–105. doi: 10.1016/j.chom.2007.06.009.

Wang, Z. *et al.* (2010) 'NS Reassortment of an H7-Type Highly Pathogenic Avian Influenza Virus Affects Its Propagation by Altering the Regulation of Viral RNA Production and Antiviral Host Response', *Journal of Virology*, 84(21), pp. 11323–11335. doi: 10.1128/JVI.01034-10.

Watanabe, K. *et al.* (2014) 'Nuclear export of the influenza virus ribonucleoprotein complex: Interaction of Hsc70 with viral proteins M1 and NS2', *FEBS Open Bio*. Federation of European Biochemical Societies, 4, pp. 683–688. doi: 10.1016/j.fob.2014.07.004.

Webster, R. G. *et al.* (1992) 'Evolution and Ecology of Influenza A Viruses', *Microbiol. Rev.*, 56(1), pp. 152–177.

White, J. M. *et al.* (2008) 'Structures and Mechanisms of Viral Membrane Fusion Proteins', *Critical Reviews in Biochemistry and Molecular Biology*, 43(3), pp. 189–219. doi: 10.1080/10409230802058320.Structures.

White, M. C. and Lowen, A. C. (2018) 'Implications of segment mismatch for influenza A virus evolution', *Journal of General Virology*, 99(1), pp. 3–16. doi: 10.1099/jgv.0.000989.

Wilkinson, T. M. *et al.* (2012) 'Preexisting influenza-specific CD4+T cells correlate with disease protection against influenza challenge in humans', *Nature Medicine*. Nature Publishing Group, 18(2), pp. 274–280. doi: 10.1038/nm.2612.

Wilson, R. L. *et al.* (2015) 'Hemagglutinin clusters in the plasma membrane are not enriched with cholesterol and sphingolipids', *Biophysical Journal*. Biophysical Society,

108(7), pp. 1652–1659. doi: 10.1016/j.bpj.2015.02.026.

Wise, H. M. *et al.* (2009) 'A Complicated Message: Identification of a Novel PB1-Related Protein Translated from Influenza A Virus Segment 2 mRNA', *Journal of Virology*, 83(16), pp. 8021–8031. doi: 10.1128/JVI.00826-09.

Wise, H. M. *et al.* (2012) 'Identification of a Novel Splice Variant Form of the Influenza A Virus M2 Ion Channel with an Antigenically Distinct Ectodomain', *PLoS Pathogens*, 8(11). doi: 10.1371/journal.ppat.1002998.

Wrammert, J. *et al.* (2011) 'Broadly cross-reactive antibodies dominate the human B cell response against 2009 pandemic H1N1 influenza virus infection', *The Journal of Experimental Medicine*, 208(1), pp. 181–193. doi: 10.1084/jem.20101352.

Xu, R. *et al.* (2012) 'Functional Balance of the Hemagglutinin and Neuraminidase Activities Accompanies the Emergence of the 2009 H1N1 Influenza Pandemic', *Journal of Virology*, 86(17), pp. 9221–9232. doi: 10.1128/JVI.00697-12.

Yang, W., Elankumaran, S. and Marr, L. C. (2011) 'Concentrations and size distributions of airborne influenza A viruses measured indoors at a health centre, a day-care centre and on aeroplanes.', *Journal of the Royal Society, Interface / the Royal Society*, 8(61), pp. 1176–84. doi: 10.1098/rsif.2010.0686.

Yang, X. *et al.* (2014) 'A beneficiary role for neuraminidase in influenza virus penetration through the respiratory mucus', *PLoS ONE*, 9(10), pp. 1–11. doi: 10.1371/journal.pone.0110026.

Yasuda, J., Bucher, D. J. and Ishihama, A. (1994) 'Growth control of influenza A virus by M1 protein: analysis of transfectant viruses carrying the chimeric M gene.', *J. Virol.*, 68(12), pp. 8141–8146. Available at: http://jvi.asm.org/cgi/content/long/68/12/8141.

Ye, Z. *et al.* (1999) 'Association of influenza virus matrix protein with ribonucleoproteins', *J Virol*, 73(9), pp. 7467–7473. doi: 10.1006/viro.2002.1669.

Ye, Z. P. *et al.* (1987) 'Functional and antigenic domains of the matrix (M1) protein of influenza A virus.', *Journal of virology*, 61(2), pp. 239–46. Available at: http://www.pubmedcentral.nih.gov/articlerender.fcgi?artid=253942&tool=pmcentrez&r

endertype=abstract%5Cnhttp://www.ncbi.nlm.nih.gov/pubmed/2433462%5Cnhttp://www.pubmedcentral.nih.gov/articlerender.fcgi?artid=PMC253942.

Yen, H.-L. *et al.* (2011) 'Hemagglutinin-neuraminidase balance confers respiratory-droplet transmissibility of the pandemic H1N1 influenza virus in ferrets.', *Proceedings of the National Academy of Sciences of the United States of America*, 108(34), pp. 14264–14269. doi: 10.1073/pnas.1111000108.

Zamarin, D., Ortigoza, M. B. and Palese, P. (2006) 'Influenza A Virus PB1-F2 Protein Contributes to Viral Pathogenesis in Mice', *Journal of Virology*, 80(16), pp. 7976–7983. doi: 10.1128/JVI.00415-06.

Zanin, M. *et al.* (2015) 'Pandemic Swine H1N1 Influenza Viruses with Almost Undetectable Neuraminidase Activity Are Not Transmitted via Aerosols in Ferrets and Are Inhibited by Human Mucus but Not Swine Mucus', *Journal of Virology*, 89(11), pp. 5935–5948. doi: 10.1128/JVI.02537-14.

Zanin, M. *et al.* (2016) 'The Interaction between Respiratory Pathogens and Mucus', *Cell Host and Microbe*. Elsevier Inc., 19(2), pp. 159–168. doi: 10.1016/j.chom.2016.01.001.

Zaraket, H. *et al.* (2013) 'Increased Acid Stability of the Hemagglutinin Protein Enhances H5N1 Influenza Virus Growth in the Upper Respiratory Tract but Is Insufficient for Transmission in Ferrets', *Journal of Virology*, 87(17), pp. 9911–9922. doi: 10.1128/JVI.01175-13.

Zebedee, S. L. and Lamb, R. A. (1989) 'Growth restriction of influenza A virus by M2 protein antibody is genetically linked to the M1 protein (genetic reassortants/second-site mutations/viral assembly/protein-protein interactions)', *Microbiology*, 86(February), pp. 1061–1065. doi: 10.1073/pnas.86.3.1061.

Zhang, J. *et al.* (2000) 'The cytoplasmic tails of the influenza virus spike glycoproteins are required for normal genome packaging', *Virology*, 269(2), pp. 325–334. doi: 10.1006/viro.2000.0228.

Zhang, K. *et al.* (2015) 'Two polar residues within C-terminal domain of M1 are critical for the formation of influenza A Virions', *Cellular Microbiology*, 17(11), pp. 1583–1593. doi: 10.1111/cmi.12457.

Zhang, W. *et al.* (2017) 'Crystal structure of an orthomyxovirus matrix protein reveals mechanisms for self-polymerization and membrane association', *Proceedings of the National Academy of Sciences*, 114(32), pp. 8550–8555. doi: 10.1073/pnas.1701747114.

Zheng, M. *et al.* (2015) 'An A14U Substitution in the 3' Noncoding Region of the M Segment of Viral RNA Supports Replication of Influenza Virus with an NS1 Deletion by Modulating Alternative Splicing of M Segment mRNAs.', *Journal of virology*, 89(20), pp. 10273–85. doi: 10.1128/JVI.00919-15.

Zhirnov, O. P. (1992) 'Isolation of matrix protein M1 from influenza viruses by acid-dependent extraction with nonionic detergent', *Virology*, 186(1), pp. 324–330. doi: 10.1016/0042-6822(92)90090-C.

Zhirnov, O. P. *et al.* (2016) 'Intravirion cohesion of matrix protein M1 with ribonucleocapsid is a prerequisite of influenza virus infectivity', *Virology*. Elsevier, 492, pp. 187–196. doi: 10.1016/j.virol.2016.02.021.